

**Interactome Mapping with Enzyme-Mediated Proximity
Labeling and Establishment of DHFR* Reporter Dependent
Protein Fragment Complementation Assay for Plant
Research**

Dissertation

Zur Erlangung des Doktorgrades der Naturwissenschaften

(Dr. rer. nat.)

der Fakultät für Biologie

der Ludwig-Maximilians-Universität München

vorgelegt von

Şebnem Akbaş

aus Eregli/Türkei

München, August 2022

First Reviewer: Prof. Dr. Wolfgang Frank

Second Reviewer: Prof. Dr. Herwig Stibor

Date of Submission: 09.08.2022

Date of Defense: 16.01.2023

Eidesstattliche Erklärung

Ich versichere hiermit an Eides statt, dass die vorgelegte Dissertation von mir selbständig und ohne unerlaubte Hilfe angefertigt ist.

I declare that I have authored this thesis independently and that I have not used other than the declared sources.

München, den 09.08.2022

.....

(Şebnem Akbaş)

Erklärung

Hiermit erkläre ich, dass ich zuvor nicht versucht habe, anderweitig eine Dissertation einzureichen oder mich einer Doktorprüfung zu unterziehen. Die vorliegende Dissertation wurde keiner weiteren Prüfungskommission weder in Teilen noch als Ganzes vorgelegt.

I declare that I have not submitted or defended a dissertation previously without success. The present dissertation has not been presented to another examination board, neither entirely nor in parts.

München, den 09.08.2022

.....

(Şebnem Akbaş)

*"The only good is knowledge and
the only evil is ignorance."*

Socrates

Contents

Summary	1
Zusammenfassung	2
Abbreviations	3
1 Introduction	7
1.1 The Origin of Modern Plant Cell	7
1.2 Protein Translocation Across the Membranes and Its Regulatory Components.....	8
1.2.1 <i>AtToc75</i>	10
1.2.2 <i>AtTic40</i>	12
1.2.2 <i>AtTrxM2</i>	13
1.2.3 <i>AtPic1/AtTic21</i>	14
1.3 Proximity Labeling Techniques	15
1.4 Protein Fragment Complementation Assays	18
1.5 Aim of the Current Work	19
2 Materials and Methods	20
2.1 Materials	20
2.1.1 Chemicals and Supplies.....	20
2.1.2 Oligonucleotides	20
2.1.2.1 DNA Oligonucleotides for Golden Gate Cloning	20
2.1.2.2 DNA Oligonucleotides for Genotyping.....	22
2.1.3 Backbone Plasmids	22
2.1.4 <i>Escherichia coli</i> Strains	23
2.1.5 <i>Agrobacterium tumefaciens</i> Strains	23
2.1.6 Medium Compositions, General Antibiotics and Herbicide	23
2.1.7 General Buffers and Stock Solutions	24
2.1.8 Gene Accession Numbers	24
2.2 Methods.....	25
2.2.1 Molecular Biological Methods	25
2.2.1.1 Cloning Strategy	25
2.2.1.2 Polymerase chain reaction (PCR)	25
2.2.1.3 Sequencing.....	26
2.2.1.4 Plasmid DNA Isolation from <i>Escherichia coli</i>	27
2.2.1.5 Genomic DNA Isolation from <i>Arabidopsis thaliana</i>	27
2.2.1.6 RNA Isolation from <i>Arabidopsis thaliana</i>	27

2.2.1.7 cDNA Synthesis.....	27
2.2.1.8 Site-Directed Mutagenesis.....	27
2.2.2 Biochemical Methods.....	28
2.2.2.1 Agarose gel electrophoresis.....	28
2.2.2.2 Protein Overexpression from <i>Escherichia coli</i>	28
2.2.2.3 Protein Purification from Plants.....	28
2.2.2.4 Protein Purification from Inclusion Bodies.....	28
2.2.2.5 SDS polyacrylamide gel electrophoresis (SDS-PAGE).....	29
2.2.2.6 Wet Western Blot and Immunodetection of Proteins.....	29
2.2.2.7 Protein Extraction for LS-MS/MS Analysis.....	29
2.2.2.8 Redox State Analysis and TCA Precipitation of Proteins.....	30
2.2.2.9 AMS Labeling (Gel Shift Assay).....	30
2.2.2.10 PEGylation of Proteins.....	30
2.2.2.11 Affinity Purification of Biotinylated Proteins.....	30
2.2.2.12 Sample Preparation for Mass Spectrometry Analysis.....	31
2.2.2.13 LC-MS/MS.....	31
2.2.3 Plant Biological Methods.....	32
2.2.3.1 Plant Growth Conditions.....	32
2.2.3.2 <i>Agrobacterium tumefaciens</i> Transformation by the Freeze-Thaw Method.....	32
2.2.3.3 Transient Transformation of <i>Nicotiana benthamiana</i>	32
2.2.3.4 Stable Transformation of <i>Arabidopsis thaliana</i>	33
2.2.3.5 Protoplast Isolation from <i>Nicotiana benthamiana</i>	33
2.2.3.6 EMS Mutagenesis.....	34
2.2.4 Computational Analysis.....	34
2.2.4.1 General Computational Tools.....	34
2.2.4.2 Data Analysis and Protein Enrichment of Mass Spectrometry Datasets.....	35
3 Results.....	36
3.1 Golden Gate Cloning Validation.....	36
3.2 <i>In silico</i> Protein Interaction Partner Analysis of Candidate Proteins.....	36
3.3 <i>In silico</i> Secondary Structure Analysis of Candidate Proteins.....	38
3.4 Establishment of the Proximity Dependent Labeling in Plant Systems.....	39
3.4.1 Transient Protein Expression in <i>Nicotiana benthamiana</i> and Determination of Biotinylation Reaction Parameters.....	42
3.4.2 Generation of <i>Arabidopsis thaliana</i> Plant Lines Suitable for Proximity Dependent Labeling.....	45

3.4.3 Determination of Biotinylation Reaction Parameters for Stable Transformed <i>Arabidopsis thaliana</i> Plant Lines.....	50
3.4.4 Identification of Interaction Partners by TurboID Mediated Proximity Labeling.....	54
3.5 Establishment of the Survival Selection DHFR* Reporter Protein-Fragment Complementation Assay in Plant Species.....	60
3.5.1 Generation of <i>Arabidopsis thaliana</i> Plant Lines Suitable for DHFR* Dependent PCA..	64
3.5.2 Insertion Line Selection for EMS Mutagenesis and MTX Plate-Based Screening	68
3.6 Analysis of Regulatory Cysteines	71
3.6.1 <i>In silico</i> Remodeling of AtToc75-III POTRA Domain.....	71
3.6.2 Overexpression Profile of Native and Mutated AtToc75-III POTRA Domains.....	73
3.6.3 <i>In vitro</i> Examination of the Regulatory Function of the Cysteines-Oxidation and Reduction Reactions.....	75
3.6.4 <i>In vivo</i> Examination of the Regulatory Cysteines in the POTRA Domain.....	78
4 Discussion	80
4.1 Analysis of Interaction Partners Using Proximity Labeling.....	80
4.1.1 Interactome of AtTic40	81
4.1.2 Interactome of AtTrxM2	84
4.1.3 Interactome of AtPic1	86
4.2 DHFR* Reporter Based Protein Fragment Complementation Assay	87
4.3 Regulatory Cysteine Analysis.....	89
4.4 Conclusion & Future Perspectives.....	90
5 Supplemental Figures.....	92
6 Supplemental Tables	97
7 Appendices	126
7.1 Gene Expression Profile, Protein Interaction Network and Sequence Similarity Across Plant Species.....	126
8 References	134
9 Acknowledgment.....	148

Summary

Chloroplasts evolved from cyanobacterial ancestors about 1.5 billion years ago because of an endosymbiotic event that culminated in extensive gene transfer to the host cell. Only few genes remained, constituting the genome of the chloroplasts found today. As a result, chloroplast biogenesis requires the expression of the genes encoded both in the nucleus and chloroplast, thus, demanding proper trafficking of the translated proteins to the organelle and through the chloroplast envelopes. Highly regulated quality control and transportation systems are required to maintain cellular homeostasis. The main pathways and essential protein components were characterized long ago. Although the intermediate associating proteins are still missing, the conventional biochemical methods limit the investigation of transient protein-protein interactions *in vivo*. Here, we provide a detailed optimization procedure for the biotin ligase mediated proximity labeling approach, enabling the detection of transitory protein interactions *in vivo*. Furthermore, we generated an interaction network map for the *AtTrxM2*, *AtTic40* and *AtPic1*, using the optimized proximity labeling procedure. The protein-interaction network revealed that the *AtTic40* interacts with the stromal chaperones Hsp70 and Hsp90 precisely. *Stic2* was also reported to associate with the proteins TrxM2, Tic40, and Pic1, referring to the involvement in a common molecular pathway.

Method development is crucial for addressing unsolved scientific debates; thus, we developed an approach for enabling organelle-specific mutation selection. For this reason, we have combined the split enzyme technology with EMS-mediated chemical mutagenesis to create a DHFR* reporter-based protein fragment complementation assay. Here, we describe the procedure and provide evidence for the reconstitution of split proteins, demonstrating the applicability of the platform for forward genetic studies.

The potential chemical reactivity and the tertiary structure of the protein also influence the regulatory properties of the metabolic pathways, leading amino acids to be the targets for biochemical characterization. *AtToc75-III* is an essential protein for translocation of chloroplast destined peptides, functioning as a molecular pore within the TOC complex. Its unique POTRA domain comprises five cysteines, three of which are close to constituting disulfide bridges. Here, we biochemically analyze the bonding potentials of the three cysteines and further investigate their significance by creating complementation lines. As a result, we demonstrated that intermolecular disulfide bonding is not essential for the proper function of POTRA domain.

Zusammenfassung

Chloroplasten entwickelten sich vor etwa 1,5 Milliarden Jahren aus cyanobakteriellen Vorfahren durch ein endosymbiotisches Ereignis, das in einem umfangreichen Gentransfer auf die Wirtszelle gipfelte. Es blieben nur wenige Gene übrig, aus denen das Genom der heutigen Chloroplasten besteht. Infolgedessen erfordert die Chloroplastenbiogenese die Expression von Genen, die sowohl im Zellkern als auch im Chloroplasten kodiert werden, was wiederum einen ordnungsgemäßen Transport der Proteine in die Organelle und durch die Chloroplastenhüllen erfordert. Zur Aufrechterhaltung der zellulären Homöostase sind hochregulierte Qualitätskontroll- und Transportsysteme erforderlich. Daher wurden die Hauptwege und ihre wesentlichen Proteinkomponenten schon vor langer Zeit charakterisiert. Obwohl die zwischengeschalteten assoziierten Proteine noch fehlen, schränken die konventionellen biochemischen Methoden die Untersuchung transienter Protein-Protein-Wechselwirkungen *in vivo* ein. Hier stellen wir ein detailliertes Optimierungsverfahren für den Biotin-Ligase-vermittelten Proximity-Labeling-Ansatz vor, mit dem vorübergehende Proteininteraktionen *in vivo* nachgewiesen werden können. Darüber hinaus haben wir für jedes *AtTrxM2*-, *AtTic40*- und *AtPic1*-Protein mit Hilfe des optimierten Proximity-Labeling-Verfahrens eine Interaktionsnetzwerkkarte erstellt. Das Protein-Interaktions-Netzwerk zeigte, dass *AtTic40* mit den stromalen Chaperonen Hsp70 und Hsp90 interagiert. Es wurde auch berichtet, dass *Stic2* mit den Proteinen *TrxM2*, *Tic40* und *Pic1* assoziiert ist, was auf eine Beteiligung an einem gemeinsamen molekularen Signalweg hindeutet.

Die Entwicklung von Methoden ist für die Lösung ungelöster wissenschaftlicher Probleme von entscheidender Bedeutung; daher haben wir einen Ansatz entwickelt, der eine organellenspezifische Mutationsauswahl ermöglicht. Aus diesem Grund haben wir die Split-Enzym-Technologie mit der EMS-vermittelten chemischen Mutagenese kombiniert, um einen DHFR*-Reporter-basierten Proteinfragment-Komplementierungstest zu entwickeln. Hier beschreiben wir das Verfahren und erbringen den Nachweis für die Rekonstitution aufgespaltener Proteine, wodurch die Anwendbarkeit der Plattform für vorwärtsgerichtete genetische Studien demonstriert wird.

Die potenzielle chemische Reaktivität und die Tertiärstruktur des Proteins beeinflussen auch die regulatorischen Eigenschaften der Stoffwechselwege, was dazu führt, dass Aminosäuren die Ziele für die biochemische Charakterisierung sind. *AtToc75-III* ist ein wesentliches Protein für die Translokation von für den Chloroplasten bestimmten Peptiden und fungiert als molekulare Pore innerhalb des TOC-Komplexes. Seine einzigartige POTRA-Domäne besteht aus fünf Cysteinen, von denen drei kurz davor stehen, Disulfidbrücken zu bilden. Hier analysieren wir biochemisch die Bindungspotenziale der drei Cysteine und untersuchen ihre Bedeutung weiter, indem wir Komplementationslinien erzeugen. Damit konnten wir nachweisen, dass die intermolekulare Disulfidbindung für die ordnungsgemäße Funktion der POTRA-Domäne nicht wesentlich ist.

Abbreviations

μM	mikromolar
airID	ancestral BirA for proximity-dependent biotin identification
Alb	albino
AMP	adenosine monophosphate
AMS	4-acetamido-4'-maleimidylstilbene-2,2'-disulfonic acid
APEX	ascorbate peroxidase
AT/At	<i>Arabidopsis thaliana</i>
ATP	adenosine triphosphate
BASU	<i>Bacillus subtilis</i> BirA
BAT	biotin acceptor sequence
BiFC	bimolecular fluorescence complementation
BioID	proximity-dependent biotin identification
BirA	biotin retention A
BRET	bioluminescence resonance energy transfer
BSA	bovine serum albumin
CaCl ₂	calcium chloride
C-DHFR	C-terminal part of the DHFR protein
cDNA	complementary DNA
CDS	coding sequence
CFP	cyan fluorescent protein
CIA5	chloroplast import apparatus 5
Cim/Com44	chloroplast outer/inner membrane protein 44
Clp	caseinolytic protease
Col-0	<i>Arabidopsis thaliana</i> ecotype Columbia
Cpn	chaperonin
CuCl ₂	copper (II) chloride
Cys/C	cysteine
DHFR	dihydrofolate reductase
DMSO	dimethylsulfoxide
DNA	deoxyribonucleic acid
dNTP	deoxynucleoside triphosphate
DTT	dithiothreitol
EDTA	ethylene-diamine-tetra-acetic acid
EGTA	ethylene glycol bis (aminoethyl ether) -N, N, N', N'-tetraacetic acid
EMS	ethyl methanesulfonate
FC1	ferrochelataase-1
FCCS	fluorescence cross-correlation spectroscopy
FDR	false discovery rate
Fe	iron
Fe-S	iron-sulfur
FL	full length
FLuc	firefly luciferase
FNR	ferredoxin:NADP(H) oxidoreductase
FRET	Förster resonance energy transfer

g/RCF	relative centrifugal force
G6PD	glucose-6-phosphate dehydrogenase
gDNA	genomic DNA
GFP	green fluorescent protein
GLuc	<i>Gaussia</i> luciferase
GOI	gene of interest
GTP	guanosine triphosphate
H ₂ O ₂	hydrogen peroxide
HCl	hydrogen chloride
Hip	Hsp70 interacting protein
His	histidine
Hop	Hsp70 and Hsp90 organizing protein
HRP	horseradish peroxidase
Hsp	heat shock protein
IMS	intermembrane space
IPTG	isopropyl-β-D-thiogalactopyranoside
KCl	potassium chloride
kDa	kilo Dalton
KH ₂ PO ₄	monopotassium phosphate
KNO ₃	potassium nitrate
LB	left border
LB medium	Luria-Bertani medium
LC-MS/MS	liquid chromatography with tandem mass spectrometry
LDS	lithium dodecyl sulfate
LFQ	label-free quantitation
LHCA1	photosystem I light harvesting complex gene 1
LHCP	light-harvesting complex I chlorophyll a/b binding protein
LP	left primer
LTD	LHCP targeting deficient
Lys	lysine
M	molarity
mA	milliampere
MES	2-ethanesulfonic acid
MgCl ₂	magnesium chloride
MgSO ₄	magnesium sulfate
M-MLV	Moloney Murine Leukemia Virus
mPEG	methoxy polyethylene glycol
mRNA	messenger RNA
MS	mass spectrometry
MS medium	Murashige and Skoog medium
MTX	methotrexate
Myb3	myb domain protein 3
Na ₂ CO ₃	sodium carbonate
NAA	α-naphthalene acetic acid
NaCl	sodium chloride

NAD(P)H	nicotinamide adenine dinucleotide phosphate
NanoLuc	NanoLuc® luciferase
NaOAc	sodium acetate
NaOH	sodium hydroxide
N-DHFR	N-terminal part of the DHFR protein
NH ₄	ammonium
NiCo	nickel-cobalt transporter
nm	nanometer
nM	nanomolar
NPQ	non-photochemical quenching
<i>Nt</i>	<i>Nicotiana benthamiana</i>
OD ₆₀₀	optical density at a wavelength of 600 nm
OEP80	outer envelope protein 80
Omp85	outer membrane protein 85
PAGE	polyacrylamide gel electrophoresis
PBS	phosphate-buffered saline
PCA	protein-fragment complementation assay
PCR	polymerase chain reaction
PEG	polyethylene glycol
PEG	polyethylene glycol
Pic1	permease in chloroplasts 1
PL	proximity labeling
PMSF	phenylmethylsulfonyl fluoride
POTRA	polypeptide-transport-associated
PPI	protein-protein interaction
<i>Ps</i>	<i>Pisum sativum</i>
PSII	photosystem II
pSSU	small subunit of ribulose-1,5-bisphosphate carboxylase
PVDF	polyvinylidene fluoride
PVP	polyvinylpyrrolidone
RbCL	large subunit of the ribulose-bisphosphate carboxylase
RLuc	<i>Renilla</i> luciferase
RNA	ribonucleic acid
RP	right primer
rpm	revolutions per minute
RuBisCo	ribulose-1,5-bisphosphate carboxylase-oxygenase
saGFP	self-assembling split GFP
saGFP11	saGFP β-strand 11
saGFP1-10	saGFP β-strands 1-10
SDS	sodium dodecyl sulfate
Ser/S	serine
SPP	stromal processing peptidase
Sti1	stress inducible 1
Stic	suppressor of Tic40
<i>Syn</i>	<i>Synechocystis</i> sp. PCC6803
TAE	tris-acetate-EDTA

TBS	tris-buffered saline
TCA	trichloroacetic acid
T-DNA	transferred DNA
TIC	translocase of the inner membrane of chloroplasts
TOC	translocase of the outer membrane of chloroplasts
TP	transit peptide
TPR	tetratricopeptide repeat
Trp	tryptophane
Trx	thioredoxin
Tyr	tyrosine
V	volt
VDAC	voltage dependent anion channel
WT	wild type
Y2H	yeast-2-hybrid
ZE	zeaxanthin epoxidase
Δ	delta

1 Introduction

1.1 The Origin of Modern Plant Cell

Today's life on earth depends on oxygen production, which breaks down metabolic substrates and it is mainly constructed with a series of chemical reactions termed photosynthesis. This is a biological process where the Sun's energy is captured and stored by various chemical reactions, which converts the light energy into chemical energy to drive cellular processes (Sánchez-Baracaldo & Cardona, 2020). Plants can enable photosynthesis reactions within the organelle called chloroplast which are found to be derived from a cyanobacterial ancestor. This phenomenon is best explained by the endosymbiotic theory (Figure 1), claiming that chloroplast and mitochondria were once free-living prokaryotes and became functional organelles of eukaryotic cells (Gray, 2017).

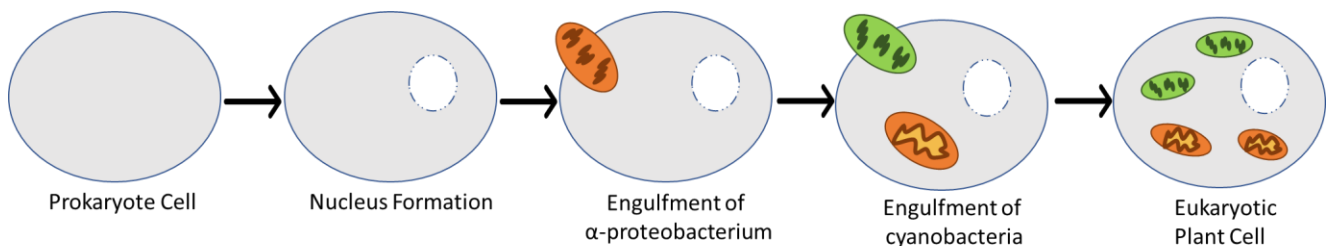


Figure 1: The endosymbiotic theory states that the origin of the mitochondria and chloroplasts were prokaryotes. The nucleus is formed around the genetic information, creating an enclosed compartment. Later, the α -proteobacterium, the ancestor of the mitochondria, was engulfed and became internalized. The engulfment of a cyanobacterium by a eukaryote already containing mitochondria gave rise to today's plant cells. Scheme based on Zimorski et al. (2014).

Approximately 1.5 billion years ago, cyanobacteria were engulfed by a prokaryote which already contained mitochondria (de Vries & Archibald, 2017). The bacterial genome size has dramatically reduced during its evolution due to the massive genetic material transfer from photosynthetic cyanobacterial endosymbiont to the emerging host nucleus, thus, the host nucleus took over the cyanobacteria control (Gross & Bhattacharya, 2009a; Dyall et al., 2004). Accordingly, the chloroplast genome encodes only ~ 200 of the 3500-4000 plastidial proteins, whereas the remaining are nuclear-encoded (Richly & Leister, 2004; Timmis et al., 2004; Martin & Herrmann, 1998). As a result, nuclear encoded chloroplast proteins are synthesized in the cytosol and translocated post translationally to the relevant organelle (Dyall et al., 2004).

1.2 Protein Translocation Across the Membranes and Its Regulatory Components

As a result of the massive gene transfer to the nucleus, the return of the chloroplast-destined proteins requires a well-established protein transport system, termed TOC and TIC (Gross & Bhattacharya, 2009b) (Figure 2). Therefore, nuclear-encoded proteins targeted to the chloroplast contain a transit peptide, by which the recognition of TOC components is mediated and translocation through the membranes is maintained (Bruce, 2000). The transit peptide sequence mostly resides in the N-terminal region of the protein and will be cleaved off once the protein reaches the final destination (Bruce, 2000; Richter & Lamppa, 1998). Although only limited research was available about transit peptides, some general properties were obtained, such as unstructured behavior in aqueous solutions (Wienk et al., 1999; Endo et al., 1992), high serine and proline abundancy (Karlín-Neumann & Tobin, 1986), absence of acidic residues (von Heijne et al., 1989), having lengths of 10-150 amino acids (Teixeira & Glaser, 2013).

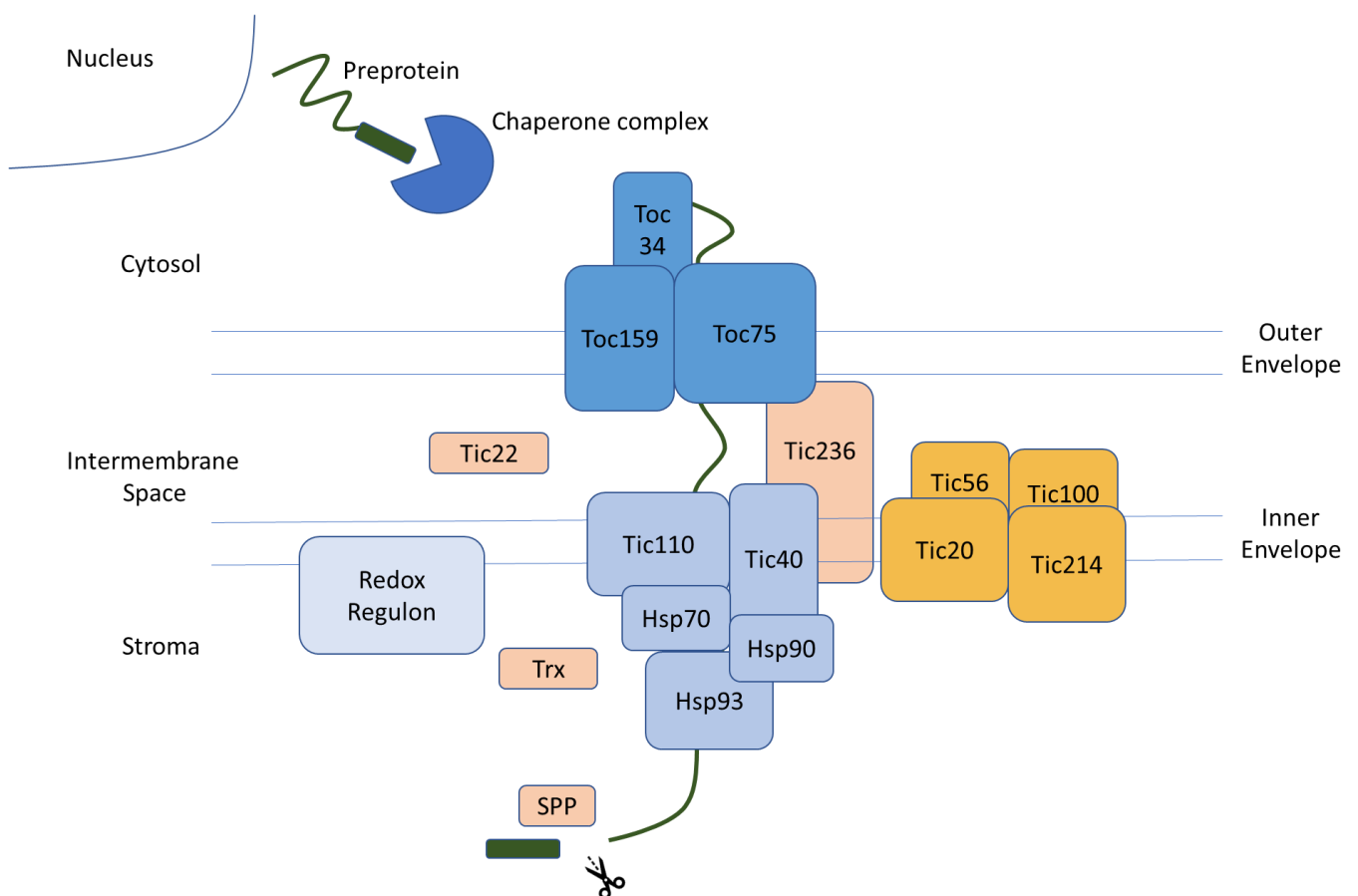


Figure 2: General representation of protein translocation system and its regulatory components. Nucleus encoded chloroplast destined proteins should pass through a double membrane system consisting of the outer and inner envelopes of the chloroplast. Firstly, preproteins are recognized by GTP-dependent receptor proteins Toc159 and Toc34, then delivered to the channel protein Toc75. Later, Tic22 assists the preprotein passage across intermembrane space. The inner envelope harbors

two translocation channels, Tic110 and Tic20, hypothesizing two independent pathways for the preprotein's way to the stroma. Moreover, Tic110 is proposed to be involved in post translocational events by recruiting stromal chaperones associated with Tic40. The redox regulon of inner envelope may enable the import regulation in close association with thioredoxins. Scheme based on (Chen et al., 2018; Balsera et al., 2009b; Kikuchi et al., 2006; Chen et al., 2002; Heins et al., 2002; Kuchler et al., 2002; Stahl et al., 1999; Kouranov & Schnell, 1997; Kessler et al., 1994).

Along the way to the organelle, preproteins are assisted by the chaperones, specifically cytosolic Hsp90 (Qbadou et al., 2006) or guidance complex consisting of Hsp70 and 14-3-3 proteins (May & Soll, 2000), to prevent their aggregation. Once the preprotein-chaperone complex reaches the surface of the chloroplast, the transit peptide is recognized by the components of TOC, consisting of one channel (Toc75) and two GTPase (Toc159, Toc34) proteins (Becker et al., 2004; Hinnah et al., 2002). The chaperones bound to the preprotein determine which receptor to interact with, either Toc159 or Toc34 in a GTP-dependent manner (Qbadou et al., 2006; Becker et al., 2004; Hirsch et al., 1994; Kessler et al., 1994). Afterward, the preprotein passes through the Toc75, the main import channel embedded in the outer envelope membrane, and reaches the intermembrane space (IMS) (Hinnah et al., 2002). The transition from IMS to TIC is facilitated by Tic22, the only protein in IMS involved in protein translocation (Rudolf et al., 2013; Glaser et al., 2012; Kouranov et al., 1998). Although there are several theories concerning the components of the TIC apparatus, Tic110 was identified a few decades ago as the first contact of incoming preproteins at the inner envelope membrane (Schnell et al., 1994). Thus, the Tic110 has been proposed to be the major channel in the TIC complex (Balsera et al., 2009a; Kovacheva et al., 2005; Heins et al., 2002), however, Tic20 was also found to possess channel-forming characteristics (Kikuchi et al., 2009; Kouranov et al., 1998). Purification of a 1 mega Dalton TIC complex revealed that the proposed TIC translocon with Tic20 as the main channel is composed of the further three proteins: Tic56, Tic100, and Tic214 (Kikuchi et al., 2013). Although more research into their separate functions in protein import is required, it is important to note that Tic214 is chloroplast encoded, whilst Tic56 and Tic100 are nuclear encoded (Kikuchi et al., 2013). The preprotein import from the Tic110 is mediated by the Tic40 (Chou et al., 2003) and Hsp93 (Chou et al., 2006), followed by the interaction of Hsp70 (Chou et al., 2006) and Hsp90 (Inoue et al., 2013). Upon reaching the stroma, the preprotein's transit peptide is cleaved off by a soluble stromal processing peptidase (SPP) (Trösch & Jarvis, 2011) and subsequently folded into native form with the assistance of stromal chaperones (Goloubinoff et al., 1989). Recently, another potential TIC component termed Tic236 was identified as an integral membrane protein associated with

Toc75, Tic110, Tic20, and Tic40; thus, providing a physical link between TOC and TIC complexes (Chen et al., 2018).

The import process has been reported to be regulated by the reciprocal action between Tic110 and the redox regulon, which is composed of Tic62, Tic55, and Tic32 (Stengel et al., 2009). Tic32 and Tic62, are classified as dehydrogenases, interacting with Tic110 in a NADP⁺/NADPH dependent manner (Benz et al., 2009; Chigri et al., 2006). Additionally, Tic55 is a Rieske protein and identified as a potential thioredoxin target (Hsu et al., 2022; Bartsch et al., 2008). In principle, the redox system is connected to the protein translocation system, which modulates the efficiency of the protein import in response to cellular stimuli and allows the entire organism to acquire about the physiological prerequisites.

1.2.1 *AtToc75*

Toc75 was first identified in pea (*Pisum sativum*) as one of the components of the protein translocation system (Waegemann & Soll, 1991), forming the import channel across the membranes (Tranel et al., 1995; Schnell et al., 1994). Its function in the import process was discovered via cross-linking of Toc75 to the small subunit of ribulose-1,5-bisphosphate carboxylase (pSSU) (Ma et al., 1996; Perry & Keegstra, 1994). The structure information was obtained through the topology studies, demonstrating a pore with 16 membrane-spanning β -sheets (Hinnah et al., 2002; Sveshnikova et al., 2000). The pore size of the channel was measured as 14-26 Å by reconstitution of *PsToc75* into liposomes (Hinnah et al., 2002).

A homolog of Toc75 was identified in the cyanobacterium *Synechocystis* sp. PCC6803 (Reumann et al., 1999; Bölter et al., 1998), indicating a prokaryotic origin of a central component of the protein import machinery in chloroplasts. After this discovery, further homologs to the cyanobacterial *SynToc75* were found in gram-negative bacteria, specified in protein assembly in the outer membrane (Voulhoux et al., 2003). Toc75 belongs to the protein family of Omp85, consisting of proteins involved in passive diffusion, import of nutrients and proteins, and outer envelope biogenesis (Wu et al., 2005; Genevrois et al., 2003; Voulhoux et al., 2003). The characteristics of this family of proteins are associated with a C-terminal β -barrel domain (Schulz, 2002; Buchanan, 1999) and an N-terminal polypeptide transport-associated (POTRA) domain (Sánchez-Pulido et al., 2003). The POTRA domain is suggested to act as a chaperone (Sánchez-Pulido et al., 2003), involved in preprotein recognition and translocation complex assembly (Ertel et al., 2005). Although the POTRA domain is necessary for the proper

function of Toc75, the orientation remains ambiguous. It has been shown that the POTRA domain faces the cytoplasm by self-assembly GFP based *in vivo* approaches and *in situ* topology studies (Sommer et al., 2011). However, another study has proposed that the POTRA domain resides in the intermembrane space by BiFC and immunogold labeling (Chen et al., 2016). The structural evidence has supported the intermembrane space localization of the POTRA domain and the chaperone-like function (O'Neil et al., 2017); accordingly, the C-terminal β -barrel domain forms a channel, while the POTRA domain facilitates protein transportation (O'Neil et al., 2017; Paila et al., 2016). The mature form of Toc75-III harbors three POTRA domains, each of which is essential for protein function since the expression of Toc75-III lacking one or more POTRA domains is insufficient to complement the embryo-lethal phenotype of the *toc75* null mutants (O'Neil et al., 2017).

Arabidopsis thaliana encodes three Toc75-related proteins in its genome, among which is *AtToc75-III*, is an essential gene, demonstrated with the embryo lethality of the null mutants (Baldwin et al., 2005). Moreover, *AtToc75-III* exhibits the most sequence similarity in silico (%73) to *PsToc75* (Baldwin et al., 2005). With these two shreds of evidence, it can be suggested that *AtToc75-III* is the main channel protein concerning import apparatus. The second protein, *AtToc75-IV*, shows 60% sequence similarity with *PsToc75* (Baldwin et al., 2005). It also does not contain a large N-terminal domain which causes the lack of transit peptides and shows a low expression profile (Baldwin et al., 2005). In addition, *AtToc75-IV* null mutants are inefficient for de-etiolation (Baldwin et al., 2005), suggesting that the *AtToc75-IV* has an essential role in etioplast development, a transitional stage of mature plastid development. Bioinformatic analysis has revealed that the *Arabidopsis* genome has another gene, *AtToc75-I*, from the *AtToc75* family (Baldwin et al., 2005). However, the lack of gene expression led to the conclusion that *AtToc75-I* is a pseudogene that contains a transposon insertion and several mutations (Baldwin et al., 2005). Another gene, *AtToc75-V*, was first thought to be a *PsToc75* homolog due to the phylogenetic analysis (Eckart et al., 2002). However, it has been renamed Outer Envelope Protein 80 (OEP80) after identifying the mature size of the protein as 80 kDa (Inoue & Potter, 2004). Although the role of the OEP80 remains elusive, null mutants have a deficiency in early plastid development (Patel et al., 2008). Recent studies reported that OEP80 is responsible for β -barrel protein insertion in the outer envelope (Gross et al., 2021), whereas Toc75 is the main import channel for proteins due to gene duplication and functional function separation through evolution (Knopp et al., 2020).

1.2.2 *AtTic40*

Tic40 was previously identified as Toc36 (Pang et al., 1997) and Cim/Com44 (Ko et al., 1995; Wu et al., 1994), located in the stromal site of the inner envelope (Stahl et al., 1999). The large soluble portion of the Tic40 resides in the stroma, whereas a single transmembrane domain anchors the protein into the inner envelope (Chou et al., 2003). The stromal part consists of a tetratricopeptide repeat (TPR) motif followed by a Sti/Hip/Hop domain, serving as binding sites for associating proteins. Thus, it is proposed that the TPR domain interacts with Tic110 (Chou et al., 2006) while Sti/Hip/Hop binds to stromal chaperones, Hsp70/Hsp90/Hsp93 (Chou et al., 2003). However, it was suggested that Tic40 consists of two Sti1 domains by amino acid sequence-based domain prediction algorithms, and the previously predicted TPR motif is largely degenerated (Balsera et al., 2009a).

Tic40 has a eukaryotic origin and is encoded by one single gene in *Arabidopsis thaliana* (Kalanon & McFadden, 2008). The phenotype of *tic40* null mutant was characterized by pale green leaves, reduced grana stacks in chloroplasts and growth retardation compared to WT implying abnormalities in chloroplast biogenesis (Kovacheva et al., 2005). Besides, *tic40* null mutants exhibited reduced protein import capacity into chloroplasts, independent of non-photosynthetic or photosynthetic precursor proteins (Kovacheva et al., 2005). The complementation studies of *tic40* null mutants with *AtTic40* constructs lacking either TPR or Sti1/Hip/Hop domain were unsuccessful, indicating that each part is essential for proper molecular function (Bédard et al., 2007).

The molecular involvement of Tic40 in protein translocation procedure was first confirmed *in vitro* (Chou et al., 2003, 2006). Based on the interaction between preprotein and translocation complexes, precursor import was thought to be mediated through Tic110-Tic40 communication on the TPR domain and followed by the release of the preprotein from Tic110 for stromal processing (Chou et al., 2006). Subsequently, either Hsp93 or Hsp70 binds to the precursor through the Sti1/Hip/Hop domain of Tic40 (Flores-Pérez et al., 2016; Huang et al., 2016; Chou et al., 2006). In addition, Tic40 was proposed to facilitate protein reinsertion into the inner envelope membrane from stroma, particularly itself (Tripp et al., 2007), and Tic110, Pic1/Tic21 (Chiu & Li, 2008). Surprisingly, a genetic screen of *tic40* mutants revealed two proteins, Stic1/Alb4 and Stic2, as suppressors of Tic40, thus, introducing a new molecular function to Tic40 in thylakoid biogenesis (Bédard et al., 2017). Recently, it was shown that preproteins could be imported into chloroplasts with or without Tic40 based on the amino acid

composition of transit peptides, hypothesizing two distinct import pathways; Tic40-dependent and Tic40-independent (Lee & Hwang, 2019). Together, these data refer that the exact molecular function of Tic40 remains elusive and might have a dual function in chaperoning the actual import process and mediating post-import processes.

1.2.2 *AtTrxM2*

Thioredoxin (Trx) is a small group of proteins with a molecular weight of 12-14 kDa, involved in redox signaling pathways by adding post-translational modifications to target proteins depending on the environmental stimuli (Jacquot et al., 2002). Trx consists of a highly conserved redox-active site containing two reactive cysteines, through which oxidation and reduction reactions occur (Capitani et al., 2000) and contributes to maintaining cellular homeostasis in all living cells (Meyer et al., 2009). Comprehensive genomic analysis in *Arabidopsis thaliana* has revealed that 41 genes encode Trx and could be divided into seven subfamilies (h, f, m, z, x, y and o) based on subcellular localizations (e.g., cytosol, mitochondria, chloroplast) (Chibani et al., 2021). Trx-m family consists of 4 isoforms; TrxM1, M2, M3 and M4 are the most abundant proteins among chloroplast Trx enzymes (f, m, x, y, z) (Okegawa & Motohashi, 2015). It was shown that TrxM3 acts in the interplay between symplastic trafficking and meristem development in non-photosynthetic tissues (Benitez-Alfonso et al., 2009), whereas TrxM1, M2 and M4 regulate photosynthesis-related reactions in chloroplasts (Nikkanen & Rintamäki, 2019; Nikkanen et al., 2016; Okegawa & Motohashi, 2015; Wang et al., 2013).

The triple mutants of *trxm1m2m4* resulted in impaired leaf development and reduced PSII accumulation by fifty percent (Wang et al., 2013), whereas single mutants exhibited no visible phenotype under normal growth conditions, however *trxm4* null mutants had altered cyclic electron transport (Courteille et al., 2013). On the other hand, double mutants of *trxm1m2* exhibited similar growth rate to wild type under fluctuating light (4 min low light, 1 min high light) but improved photosynthetic activity during high light periods (Thormählen et al., 2017). As light and redox signaling are closely linked, a recent study investigated the growth stages of single, double, and triple mutants of *trxm1*, *trxm2* and *trxm4* under the high light conditions ($700 \mu\text{mol photons m}^{-2} \text{sec}^{-1}$), revealing that they might interact pathways in stomatal biogenesis, stomatal conductance and mesophyll structure (Serrato et al., 2021). Hence, it can be concluded that Trx-m family proteins could regulate proteins involved in plant acclimation/response to changing light conditions.

Comprehensive proteomics research has shown that TrxM1, M2 and M4 proteins are loosely associated with the stromal site of the thylakoid membrane in chloroplasts (Friso et al., 2004); therefore, enabling flexible movement through the cell. Dual functionality is associated with TrxM2 by interacting proteins in both mitochondria (Zhang et al., 2015) and chloroplast (Meyer et al., 2011). Moreover, it was shown that TrxM2, together with TrxM1 and M4, interacts with zeaxanthin epoxidase (ZE) to regulate NPQ-dependent photoprotection under low light conditions ($56 \mu\text{mol photons m}^{-2} \text{s}^{-1}$) (Da et al., 2018). Taken together, it is possible that each Trx-m family protein might have an individual role and still compensate for each other's function, yet more research would lead to a broad understanding of redox regulation and involved proteins.

1.2.3 *AtPic1/AtTic21*

Initially, Pic1/Tic21 was identified as a component of the translocon system within the inner envelope of the chloroplast, named CIA5 and later Tic21 (Teng et al., 2006). Another study proposed that Pic1/Tic21 acts as a permease in iron transport and cellular metal homeostasis (Duy et al., 2011; Duy et al., 2007). The mature form of Pic1/Tic21 is located in the inner envelope of the chloroplast, spanning the membrane with four transmembrane domains (Duy et al., 2007; Teng et al., 2006) and associated with other components of the translocon system, Tic110 and Toc75 (Teng et al., 2006).

Two independent research groups reported different functions for Pic1/Tic21 by analyzing plants with similar mutant phenotype; *Pic1/tic21* knock out mutants resulting in albino plants (Duy et al., 2007; Teng et al., 2006). The first study demonstrates that the null mutants have defects in the protein translocation system leading to precursor protein accumulation *in vitro* (Teng et al., 2006). The second group observed increasing ferritin clusters and differential gene regulation in pathways of photosynthesis, Fe-S cluster biogenesis, iron stress response, metal homeostasis, and abnormal chloroplast development in *Pic1/tic21* null mutants (Duy et al., 2011; Duy et al., 2007). The overexpression of Pic1/Tic21 in plants lacking Pic1/Tic21 resulted in chlorosis and oxidative damage induced by increased iron levels, thus, supporting its role as a metal transporter (Duy et al., 2011). Additionally, the expression levels of Pic1/Tic21 and proteins to deal with iron overload was greatly increased in Pic1/Tic21 overexpressing plants (Duy et al., 2011) as complementary to the study that displayed elevated Pic1/Tic21 mRNA level in response to the iron stress caused by loss of ferritin (Ravet et al., 2009).

The detection of Pic1/Tic21 within the one megadalton translocation complex via blue native PAGE, deepened the conflict about the function of Pic1/Tic21 (Kikuchi et al., 2009). Furthermore, a distinct group of proteins (size of ~100 kDa), including Pic1/Tic21, was found not to be interacting with one mega-dalton complex, suggesting a regulatory role for Pic1/Tic21 in the proper assembly of translocation complex in the inner membrane (Kikuchi et al., 2009). Interestingly, it was reported that *Pic1/tic21* mutants had an impaired ability to import photosynthetic precursor proteins rather than housekeeping and non-photosynthetic proteins (Kikuchi et al., 2009). The research also exhibited that the upregulation of iron deficiency-related gene expressions is not peculiar to *Pic1/tic21* mutants but a similar response occurs in *tic20* and *albino3* mutants (Kikuchi et al., 2009). Although the exact role of the protein is still under debate, the *Nicotiana benthamiana* homolog of Pic1/Tic21 (*NtPic1*) was characterized as the major component of iron homeostasis by allowing iron transportation into chloroplasts (Gong et al., 2015). A comprehensive bioinformatic analysis revealed putative orthologous of *AtPic1/AtTic21* and associating partners in tomato (*Solanum lycopersicum*), maize (*Zea mays*) and sorghum (*Sorghum bicolor*), reporting sensitivity in expression patterns under salt and drought stresses (Filiz & Akbudak, 2020).

1.3 Proximity Labeling Techniques

Each cellular process within the cell requires several interactions, including protein-protein, protein-RNA and protein-DNA interactions. These interactions are crucial for the proper function of the cell; therefore, understanding interaction networks will eventually improve our knowledge about cellular growth and development. Over the years, many methods have been developed to screen for protein-protein interactions, such as yeast-2-hybrid (Y2H) (Brückner et al., 2009) or affinity complex purification coupled with mass spectrometry (Dunham et al., 2012). The major disadvantage of the conventional techniques is detecting the high-affinity protein-protein interactions (PPI) (Mair & Bergmann, 2022). Additionally, the probability of generating false results is high due to the failures in expression, localization, and interaction (Mair & Bergmann, 2022). Therefore, recent technological advancements have enabled researchers to develop more efficient ways to overcome the disadvantages of traditional techniques. Enzyme catalyzed proximity labeling (PL) was established as a complementary approach for identifying PPIs, proteomes and transcriptomes. PL uses genetically engineered enzymes such as peroxidases, and biotin ligases (Table 1), tagged with the protein of interest. The overall PL reaction involves the covalent attachment of the short-lived reactive species,

converted from an inert molecule by the PL enzyme to the neighboring proteins or nucleotides (Chapman-Smith & Cronan, 1999). The characteristics of the PL enzymes determine the labeling conditions and radius, therefore, affecting the applicability to various systems and organisms (Mair & Bergmann, 2022).

Table 1: An overview of the characteristics of different enzymes used in protein labeling

Enzyme	Origin	Size (kDa)	Labeling Time	Modification Sites	References
APEX	Pea or soybean APEX	28	1 min	Tyr, Trp, Cys, His	(Hung et al., 2014; Martell et al., 2012)
APEX2	Soybean APEX	28	1 min	Tyr, Trp, Cys, His	(Lam et al., 2014)
HRP	Horseradish Peroxidase	44	5 min- 2 h	Tyr, Trp, Cys, His	(Kotani et al., 2008)
BioID	<i>Escherichia coli</i> BirA	35	16-24 h	Lys	(Roux et al., 2012)
BioID2	<i>Aquifex aeolicus</i> BirA	27	16-24 h	Lys	(Kim et al., 2016)
BASU	<i>Bacillus subtilis</i> BirA	29	16-18 h	Lys	(Ramanathan et al., 2018)
TurboID	<i>Escherichia coli</i> BirA	35	≥10 min	Lys	(Branon et al., 2018)
miniTurboID	<i>Escherichia coli</i> BirA	28	≥10 min	Lys	(Branon et al., 2018)

Plant-derived peroxidases (APEX, APEX2 and HRP) were adapted for proximity labeling applications. The reaction depends on the enzyme activation by hydrogen peroxide and the subsequent release of the free radicals of biotin phenol. The addition of biotin occurs on surface-exposed electron-rich amino acid residues (frequently on Tyr, sporadically on Trp, His, Cys) of the adjacent proteins (Kalocsay, 2019). Among peroxidases, the HRP enzyme favors oxidizing environments and cell surfaces (Martell et al., 2012), while APEX is primarily active in reducing conditions such as cytosol (Rhee et al., 2013). APEX2 originated from a yeast display-based evolution of APEX, enabling interactome mapping of low-abundance proteins by improved activity and sensitivity (Lam et al., 2014). Peroxidase-mediated proximity labeling enables timely control of the biotinylation reaction by the presence of hydrogen peroxide and

facilitates an extremely fast labeling process. However, the applicability of the peroxidase method is limited due to the high cellular toxicity of hydrogen peroxide and the low membrane permeability of the biotin-phenol (Kalocsay, 2019).

The most extensively studied bifunctional enzyme for labeling purposes is bacterial biotin ligase biotin retention A (BirA), originating from *Escherichia coli* (Barker & Campbell, 1981). BirA is a 35 kDa enzyme that mediates biotinylation of a specific lysine residue of the biotin accepting protein, a two-step reaction. The first step of the reaction aims to create reactive biotinyl-AMP from biotin and ATP. That is followed by attaching that biotinyl-AMP (bioAMP) to a specific lysine on the protein's active side as the second step (Barker & Campbell, 1981; Chapman-Smith & Cronan, 1999). Additionally, biotin transfer from the BirA enzyme depends explicitly on the presence of biotin acceptor sequence (BAT) within the protein, hindering the erroneous biotinylation (Chapman-Smith & Cronan, 1999). Therefore, many biotin ligase versions were identified and adapted for proximity labeling purposes (Table 1 and Supplemental Table 1). A single point mutation (R118G) was introduced within the wild type BirA has promoted the enzyme to become more promiscuous, naming the new enzyme BirA* or BioID (Roux et al., 2012). The labeling radius of BioID was estimated as ~10 nm (Roux et al., 2012) and was proposed to be increased by flexible linker addition between the PL enzyme and the bait protein (Kim et al., 2014). Two years later, another BirA variant was engineered from *Aquifex aeolicus*, which was known to be the smallest by lacking the DNA binding domain of the original BirA from *Escherichia coli* (Kim et al., 2016). The promiscuous enzymatic activity was given with the R40G mutation to the catalytic domain of the enzyme, and later it was called BioID2 (Kim et al., 2016). In addition to having a small size, BioID2 requires less biotin and promotes biotinylation at high temperatures up to 50°C (Kim et al., 2016). Another BirA variant was modified from *Bacillus subtilis*: BASU, having a size of 29 kDa and displaying faster reaction kinetics (Ramanathan et al., 2018). Compared to peroxidases, biotin ligases' labeling speed was significantly slower in creating non-specific biotinylation. Thus, two highly active BirA versions were engineered by yeast-based directed evolution, TurboID and miniTurboID (Branon et al., 2018). The involvement of the new TurboID enzymes has reduced the labeling time to a minimum of 10 mins and facilitated biotin reaction occurring at room temperature (25°C) (Branon et al., 2018). Along with the advancements in the PL enzymes, the applicability of the PL techniques is extended beyond mammalian cells to various model organisms such as plants, worms, flies and yeast (Mair et al., 2019; Zhang et al., 2019; Branon et al., 2018).

Several other enzymes and procedures are developed for PL applications (Supplemental Table 1). A synthetic ancestral BirA variant, airID, exhibited more specific tagging and less cellular toxicity over the long incubation periods than TurboID (Kido et al., 2020). The smallest BirA variants are microID and ultraID, showing the similar labeling kinetics as TurboID and creating less background from endogenous biotin (Zhao et al., 2021). Split versions of the PL enzymes provide a basis for identifying context-specific PPI and temporal control of biotinylation (Kwak et al., 2020). However, their activity is much lower than their native forms, resulting in an increasing labeling time (Cho et al., 2020). The length of the linker may influence contact-dependent reconstitution of the split PL enzymes, therefore, requiring in-depth prior research. In short, PL has developed into a powerful tool to detect PPI *in vivo* without disturbing the cell's integrity and gaining attention over the past years.

1.4 Protein Fragment Complementation Assays

As discussed in the previous section, there are several methodologies to detect PPIs, however, most of them disturb numerous physical interactions by separating proteins from their native environments. In contrast, many others enable to monitor PPIs in the intact cells with minimal cellular perturbation, these are depending on Förster resonance energy transfer (FRET) (Förster, 1948), bioluminescence resonance energy transfer (BRET) (Pfleger et al., 2006), fluorescence cross-correlation spectroscopy (FCCS) (Bacia et al., 2006), proximity labeling (Roux et al., 2012) and protein-fragment complementation assay (PCA) (Remy & Michnick, 2007). In the PCA strategy, two proteins of interest are fused as complementary fragments to a reporter protein, which is engineered to be divided into two inactive but integral parts. The interaction of complementary proteins brings together the split fragments of the reporter protein, facilitating the reconstitution of the reporter and subsequent detection of its activity (Michnick et al., 2007). Many reporter proteins can be utilized for PCA and thus provide several readouts depending on the applicability, in fact, PCA serves as a toolkit from which an appropriate assay can be developed for specific purposes. PCA reporter proteins are classified into four categories concerning detection signals, such as survival (DHFR, cytosine deaminase), colorimetric (β -lactamase), fluorescent (GFP, CFP, Venus, mCherry), and luminescent (RLuc, FLuc, GLuc, NanoLuc) assays (Blaszczak et al., 2021).

The crucial feature of the PCA is that it mainly depends on protein folding and topology. Thus, the spatial distance and the mobility of individual fragments determine the reconstitution efficiency of the reporter protein. Furthermore, N- terminal, C- terminal or internal fusions, and

also the presence of linker sequences can influence the strength of the signal (Chrétien et al., 2018). However, fusing reporter fragments can alter the protein's activity, interaction, stabilization, or even localization (Ohmuro-Matsuyama et al., 2013). For this reason, small reporter proteins (~19 kDa) are engineered for optimal size and stability of the split fragments (Dixon et al., 2016). Another critical parameter for PCA is the dynamics of the reporter reconstitution, which should be contact-dependent, reversible, and have a low intrinsic affinity. Among the PCA reporters, GFP-family proteins are reported to have irreversible nature (Romei & Boxer, 2019; Lindman et al., 2010). The availability of multiple PCA reporters with complementary features and various outcomes enables researchers to select the best-suited approach concerning the research needs. Moreover, the reconcilability of PCAs with other biochemical and molecular approaches grants it the method of choice to build high-quality protein-interaction networks. Hence, comprehensive PCA studies can unveil the genotype-phenotype relationship by resolving molecular interactions at the proteomics level.

1.5 Aim of the Current Work

The ultimate goal of this thesis was to investigate the regulatory properties of the protein translocation system and identify novel proteins that acted as mediators. In addition, we wanted to know how the translocation system influences the downstream metabolic pathways involved in chloroplast biogenesis. To accomplish this goal, cutting-edge molecular biology techniques such as proximity labeling and protein fragmentation complementation assays were used. Therefore, the project was divided into three subsections: Firstly, optimization of the enzyme-mediated proximity labeling procedure and application for the creation of the interaction map for the selected proteins should be carried out. Secondly, by combining split enzyme technology with protein fragmentation complementation, a new approach for organelle-specific mutation-selection should be implemented. Thirdly, to better understand the regulatory system in the outer chloroplast envelope, the kinetics of chemical reactivity of cysteines in the POTRA domain of *AtToc75-III* should be studied.

2 Materials and Methods

2.1 Materials

2.1.1 Chemicals and Supplies

All common chemicals used during experimental procedures were purchased from Serva (Heidelberg, Germany), Roth (Karlsruhe, Germany), Merck (Darmstadt, Germany) and Sigma (Taufkirchen, Germany) unless stated otherwise. Enzymes were obtained from New England Biolabs, NEB (Frankfurt am Main, Germany), Bioron (Ludwigshafen, Germany) and Thermo Fisher Scientific (Braunschweig, Germany), protein molecular weight marker was ordered from peQLab (VWR, Ismaning, Germany). DNA oligonucleotides were purchased from Metabion AG (Martinsried, Germany).

2.1.2 Oligonucleotides

2.1.2.1 DNA Oligonucleotides for Golden Gate Cloning

Table 2: DNA Oligonucleotides for Cloning. Red letters indicate the mutated nucleotide in the plasmid.

Name	Sequence from 5' to 3'
<i>Proximity Labeling</i>	
AtTic40 C-D F1	ATG AAG ACT TTA CGG GTC TCA CAC CAT GGA GAA CCT TAC CCT AGT T
AtTic40 C-D R1	TAG AAG ACA ACG TTT TCA TAG CTG TTT GCA TTG CAT
AtTic40 C-D F2	TAG AAG ACA AAA CGA TGA TGA ACC AAA TGA ATA C
AtTic40 C-D R2	TAG AAG ACA ATG ACG ACT GGG ATT GAG ATT GG
AtTic40 C-D F3	TAG AAG ACA AGT CAG GTG CTA CCG TTG A
AtTic40 C-D R3	TAG AAG ACA AAA TAT CTT CAA AGG CAT AGT TCT TTT C
AtTic40 C-D F4	TAG AAG ACA ATA TTT CAC CCG AGG AAA CC
AtTic40 C-D R4	ATG AAG ACT TCA GAG GTC TCA CCT TAC CCG TCA TTC CTG GGA AGA
AtTrxF1 C-D F	ATG AAG ACT TTA CGG GTC TCA CAC CAT GCC TCT TTC TCT CCG TCT
AtTrxF1 C-D R	ATG AAG ACT TCA GAG GTC TCA CCT TAG CTG GAT CTC CGG AAG CAG
AtTrxM2 C-D F	ATG AAG ACT TTA CGG GTC TCA CAC CAT GGC TGC TTT CAC TTG TAC C
AtTrxM2 C-D R	ATG AAG ACT TCA GAG GTC TCA CCT TTG GCA AGA ACT TGT CGA GGC
Pic1 CDS C-D F1	ATG AAG ACT TTA CGG GTC TCA CAC CAT GCA ATC ACT ACT CTT GCC G
Pic1 CDS C-D R1	TAG AAG ACA AGG ACG ACG GAG AAG TCG GAT AT
Pic1 CDS C-D F2	TAG AAG ACA AGT CCG TTC CCG GTG ATA A
Pic1 CDS C-D R2	TAG AAG ACA AAG TTT TCT CCA ATC TCT TTG CAA CC
Pic1 CDS C-D F3	TAG AAG ACA AAA CTT CAA GGT ACT TTA AGA GAC
Pic1 CDS C-D R3	TAG AAG ACA ATA GAA AGA CAT CAA GAG CAA GAA C
Pic1 CDS C-D F4	TAG AAG ACA ATC TAG TTC AGG CAT CGG C

Pic1 CDS C-D R4	ATG AAG ACT TCA GAG GTC TCA CCT TAG CAA CCT TAG GAA CTA CGA C
BioID2 D-E F	ATG AAG ACT TTA CGG GTC TCA AAG GGA GGA GGA GGA GGA TCG GGA GGA GGA GGA TCG TTC AAA AAC TTA ATT TGG TTA AAA GAA
BioID2 D-E R	ATG AAG ACT TCA GAG GTC TCA GAT TCT AGC TTC GAC GCA AGG AGA
TurboID D-E F	ATG AAG ACT TTA CGG GTC TCA AAG GGA GGA GGA GGA GGA TCG GGA GGA GGA GGA TCG AAG GAC AAT ACT GTG CCT TTG
TurboID D-E R	ATG AAG ACT TCA GAG GTC TCA GAT TTT ACT TTT CGG CCG ATC TCA AGC
LI-AtTrxM2 Mutation F	GCT CCG AGA CAA GAA TCG TAT C
LI-AtTrxM2 Mutation R	GGA GAG AAA TCG GAG GAC
<i>DHFR* Dependent Protein Fragment Complementation Assay</i>	
NDHFR* C-D F	ATG AAG ACT TTA CGG GTC TCA CAC CAT GGT TCG ACC ATT GAA CTG CA
NDHFR* C-D R	ATG AAG ACT TCA GAG GTC TCA CCT TGG TAC CCA ATT CCG GTT GTT
CDHFR C-D F	ATG AAG ACT TTA CGG GTC TCA CAC CAT GAG TAA AGT AGA CAT GGT
CDHFR* C-D R	ATG AAG ACT TCA GAG GTC TCA CCT TGT CTT TCT TCT CGT AGA CTT
saGFP1-10 D-E F	ATG AAG ACT TTA CGG GTC TCA AAG GGA GGA GGA GGA GGA TCG GGA GGA GGA GGA TCG ATG GGT GGC ACC AGT AGC AA
saGFP1-10 D-E R	ATG AAG ACT TCA GAG GTC TCA GAT TTT AGG TAC CCT TTT CGT TGG GAT
saGFP1-10 B-C F	ATG AAG ACT TTA CGG GTC TCA TCT GAA CAA TGG GTG GCA CCA GTA GCA A
saGFP1-10 B-C R	ATG AAG ACT TCA GAG GTC TCA GGT GCC CGA TCC TCC TCC TCC CGA TCC TCC TCC TCC GGT ACC CTT TTC GTT GGG AT
saGFP11C D-E F	ATG AAG ACT TTA CGG GTC TCA AAG GGA GGA GGA GGA GGA TCG GGA GGA GGA GGA TCG ATG ACT AGT GGA TCC GAT GG
saGFP11C D-E R	ATG AAG ACT TCA GAG GTC TCA GAT TTT ATG TAA TCC CAG CAG CAT TTA
saGFP11N B-C F	ATG AAG ACT TTA CGG GTC TCA TCT GAA CAA TGC GTG ACC ACA TGG TCC TTC
saGFP11N B-C R	ATG AAG ACT TCA GAG GTC TCA GGT GCC CGA TCC TCC TCC TCC CGA TCC TCC TCC TCC TCC GCC ACC AGA CCC TCC AC
LHCA1 TP B-C F	ATG AAG ACT TTA CGG GTC TCA TCT GAA CAA TGG CGT CGA ACT CGC TTA T
LHCA1 TP B-C R	ATG AAG ACT TCA GAG GTC TCA GGT GCC AGG CAT CCA GTG AGC AGC CA
<i>TOC75 POTRA Domain-Regulatory Cysteines</i>	
Potra C256S F	CCG TTT TCG TAG CAT CAA CGT GGG C
Potra C256S R	TCC GCG CTC TGC CAG GTG
Potra C300S F	TGC GCG TCC GAG CCT GCT GCC
Potra C300S R	CGA TCG ATA CGA CGT TTG TAG TCC TTT TCC AGG
Potra C359S F	AGA AGT GGT TAG CGA GGT GGT
Potra C359S R	TTG GTG TTC AGG TTG CCG
AtToc75III Promoter A-C F1	ATG AAG ACT TTA CGG GTC TCA GCG GTC ATT GAT ACG CCT TTG TCC C
AtToc75III Promoter A-C R1	TAG AAG ACA ATG AAA AGA CAA GGA AAG AGT GCA C
AtToc75III Promoter A-C F2	TAG AAG ACA ATT CAG ACG ATT CTG TTA CTA TTG

AtToc75III Promoter A-C R2	TAG AAG ACA AAA GCG ACC ATG ACT ATT TTA AGC
AtToc75III Promoter A-C F3	TAG AAG ACA AGC TTA TTG GAG AAG CAT GAA GGG AAG ATA AAG TCT TG
AtToc75III Promoter A-C R3	ATG AAG ACT TCA GAG GTC TCA GGT GCC GGG CGG AGA AGA TAA GGT TT
AtToc75III CDS C-D F1	ATG AAG ACT TTA CGG GTC TCA CAC CAT GGC CGC CTT CTC CGT CAA
AtToc75III CDS C-D R1	TAG AAG ACA ACG ATA CCA TCT CGA AGA AGG AAT C
AtToc75III CDS C-D F2	TAG AAG ACA AAT CGA TTC GTC CTG GTG G
AtToc75III CDS C-D R2	TAG AAG ACA AGA GCG ACC TAT TAA GAC CCT GG
AtToc75III CDS C-D F3	TAG AAG ACA AGC TCA TGG GTT CAG TGA C
AtToc75III CDS C-D R3	ATG AAG ACT TCA GAG GTC TCA CCT TAT ACC TCT CTC CAA ATC GGA A
LI-AtToc75 CDS C256S CD-F	TAG GTT TAG AAG TAT TAA CGT TGG G
LI-AtToc75 CDS C256S CD-R	TCA GCA GAT TGC CAT GTA C
LI-AtToc75 CDS C300S CD-F	GGC ACG GCC TAG TTT GTT GCC
LI-AtToc75 CDS C300S CD-R	CTA TCA ATT CTC CTC TTG TAA TCC TTC TCC

2.1.2.2 DNA Oligonucleotides for Genotyping

Table 3: DNA Oligonucleotides for Genotyping

Name	Sequence from 5' to 3'
Tic40 SALK-057111 LP	CTT TTT GGG CAA TGG AGA AGT G
Tic40 SALK-057111 RP	GGT GAT AAA GAG GAA TGA GTT GG
AtToc75III SALK-015928 LP	CCT TCA ACC ACA TTA CCA AGC
AtToc75III SALK-015928 RP	CTC GCA TCT CCA CTC AAT CTC
AtToc75III Genotype F	GCC TAA GCA GGT ATG TTT CT
AtToc75III Genotype R	TTC TCA CAT TAC CTT AAT AC
SALK LB	ATT TTG CCG ATT TCG GAA C
RbCL F	ATG TCA CCA CAA ACA GAG ACT AAA GC
RbCL R	GAA ACG GTC TCT CCA ACG CAT
NDHFR* F	ATG AAG ACT TTA CGG GTC TCA CAC CAT GGT TCG ACC ATT GAA CTG CA
NDHFR* R	ATG AAG ACT TCA GAG GTC TCA CCT TGG TAC CCA ATT CCG GTT GTT

2.1.3 Backbone Plasmids

Table 4: Backbone Plasmids

Name	Application	Antibiotic Resistance	Source
BB02-pUC57	LI Plasmid Construction	Gentamycin	BB01-pUC57
BB20-LIIβ F 1-2	LII Plasmid Construction	Spectinomycin	Xpre2-S (pCAMBIA)
BB53-LIIIβ A-B	LIII Plasmid Construction	Kanamycin	Xpre2-K (pCAMBIA)

2.1.4 *Escherichia coli* Strains

Table 5: *Escherichia coli* Strains

Name	Genotype	Application
TOP10	F- mcrA Δ(mrr-hsdRMS-mcrBC) Φ80lacZΔM15 Δ lacX74 recA1 araD139 Δ(araleu)7697 galU galK rpsL (StrR) endA1 nupG	Cloning
BL21 (DE3)	fhuA2 [lon] ompT gal (λ DE3) [dcm] Δhsd λ DE3 = λ sBamHIo ΔEcoRI-B int::(lacI::PlacUV5::T7 gene1) i21 Δnin5	Protein Expression

2.1.5 *Agrobacterium tumefaciens* Strains

Table 6: *Agrobacterium tumefaciens* Strains

Name	Genotype	Application
AGL1	C58 RecA (rif R/carbR) Ti pTiBo542DT-DNA (strepR) Succinamopine	Transient Plant Transformation
GV3101	C58 (rif R) Ti pMP90 (pTiC58DT-DNA) (gentR/strepR) Nopaline	Stable Plant Transformation

2.1.6 Medium Compositions, General Antibiotics and Herbicide

Table 7: Medium Compositions

Medium	Composition	Application
LB (Luria-Bertani medium)	1 % (w/v) bacto tryptone, 0.5 % (w/v) bacto yeast extract, 0.5 % (w/v) NaCl, add 1.5 % (w/v) agar for plates	Bacterial Cell Culture
MS (Murashige and Skoog medium)	0.5% (w/v) MES, 0.226% (w/v) Murashige and Skoog (MS) salt and vitamin mixture, 3% (w/v) sucrose, pH 5.8 with KOH add 0.75 % (w/v) agar for plates	Plant Growth Culture

Table 8: General Antibiotics

Antibiotics	Abbreviation	Final Concentration
Ampicillin	Amp	100 µg/ml
Kanamycin	Kan	50 µg/ml
Gentamycin	Gent	10 µg/ml
Spectinomycin	Spec	100 µg/ml
Rifamycin	Rif	50 µg/ml
Carbenicillin	Carb	100 µg/ml
Cefotaxime	Cef	50 µg/ml

Table 9: General Herbicide

Herbicide	Abbreviation	Final Concentration
Glufosinat-Ammonium	BASTA	5 µg/ml

2.1.7 General Buffers and Stock Solutions

Table 10: General Buffers and Stock Solutions

Name	Composition	Application
50x TAE	2 M Tris-base, 5.71 % (v/v) Acetic acid, 50 mM EDTA (pH 8.0)	Agarose gel electrophoresis
10x DNA loading buffer	30% (v/v) Glycerol, 0.25% (w/v) Bromophenol blue, 0.25% (w/v) Xylene Cyanol FF, 0.35% (w/v) Orange G	Agarose gel electrophoresis
10x SDS running buffer	250 mM Tris, 1.92 M Glycine, 1% (w/v) SDS	SDS PAGE
2x SDS loading buffer	100 mM Tris/HCl pH 6.8, 20 % (v/v) Glycerol, 0.2 % (w/v) Bromophenol blue, 2 % (w/v) SDS, 80 mM Betamercaptoethanol	SDS PAGE
Non-reducing 2x SDS loading buffer	100 mM Tris/HCl pH 6.8, 20 % (v/v) Glycerol, 0.2 % (w/v) Bromophenol blue, 2 % (w/v) SDS	SDS PAGE
Coomassie staining solution	50 % (v/v) Ethanol, 7 % (v/v) Acetic acid, 0.18 % (w/v) Coomassie Brilliant blue R-250	SDS PAGE
1x Towbin Buffer	25 mM Tris, 192 mM Glycine, 0.1% (w/v) SDS, 20% Methanol	Western Blot
Ponceau Solution	5% Acetic acid, 0.3% Ponceau S	Western Blot
10x TBS	1 M Tris, 1.5 M NaCl	Immunodetection

2.1.8 Gene Accession Numbers

The gene accession numbers of the proteins used in this project are listed in Table 11.

Table 11: Gene Accession Numbers

Gene Name	Accession Number
Tic40	AT5g16620
Pic1	AT2g15290
TrxM2	AT4g03520
Toc75-III	AT3g46740

2.2 Methods

2.2.1 Molecular Biological Methods

2.2.1.1 Cloning Strategy

The Golden Gate modular assembly system was used to construct plasmids as described in (Binder et al., 2014). The gene of interest for the respective cloning module was amplified with the primers (Table 2). More than one primer pair was used in order to eliminate the endogenous type IIS restriction enzyme cutting sites. The overall scheme can be seen in Table 12,13,14. LI, LII and LIII plasmids were constructed via enzyme digestion by BsaI and BpiI, and subsequent ligation as depicted in Binder et al, 2014.

Table 12: LII Plasmid Assembly Overall Scheme for Proximity Labeling Constructs

Promoter	N-tag	GOI	C-tag	Terminator	Misc
p35S	LI-dy-B-C	LI-TrxF1	LI-BioID2*	T35S	BASTA
p35S	LI-dy-B-C	LI-TrxM2	LI-BioID2*	T35S	BASTA
p35S	LI-dy-B-C	LI-Tic40	LI-BioID2*	T35S	BASTA
p35S	LI-dy-B-C	LI-Pic1	LI-BioID2*	T35S	BASTA
p35S	LI-dy-B-C	LI-TrxF1	LI-TurboID	T35S	BASTA
p35S	LI-dy-B-C	LI-TrxM2	LI-TurboID	T35S	BASTA
p35S	LI-dy-B-C	LI-Tic40	LI-TurboID	T35S	BASTA
p35S	LI-dy-B-C	LI-Pic1	LI-TurboID	T35S	BASTA

Table 13: LII Plasmid Assembly Overall Scheme for EMS Constructs

Promoter	N-tag	GOI	C-tag	Terminator	Misc
p35S	LI-dy-B-C	NDHFR*	saGFP1-10	T35S	LI-dy-F-G
p35S	LI-dy-B-C	saGFP11	CDHFR*	T35S	LI-dy-F-G
p35S	LI-dy-B-C	saGFP1-10	NDHFR*	T35S	LI-dy-F-G
p35S	LI-dy-B-C	CDHFR*	saGFP11	T35S	LI-dy-F-G

Table 14: LIII Plasmid Assembly Overall Scheme for EMS Constructs

LII 1-2	LII 2-3	LII 3-4	LII 4-5	LII 5-6
LII-NDHFR*-saGFP1-10	LII-ins-2-3	LII-saGFP11-CDHFR*	LII-dy-4-6	LII-dy-4-6
LII-saGFP1-10-NDHFR*	LII-ins-2-3	LII-CDHFR*-saGFP11	LII-dy-4-6	LII-dy-4-6

2.2.1.2 Polymerase chain reaction (PCR)

gDNA, cDNA or plasmid DNA was used as a template for PCR reactions. Phusion polymerase was used for cloning purposes while DFS Taq Polymerase was for genotyping purposes.

Annealing temperature and elongation time were adapted respectively depending on the properties of the oligonucleotides and the length of the PCR product. If necessary, PCR products were extracted from the agarose gel and purified using NucleoSpin Gel and PCR Clean-up kit (Macherey-Nagel) according to the manufacturer's instructions. PCR conditions for each polymerase are summarized in Table 15.

Table 15: PCR conditions according to polymerase. (*) sign indicates the variables depending on the primer and product properties

Phusion Polymerase (NEB)		Reaction Conditions	
Template	1 μ l	98°C	05:00
Forward Primer (10 μ M)	1 μ l	98°C	00:30
Reverse Primer (10 μ M)	1 μ l	Annealing *	00:30
5x Reaction Buffer	4 μ l	72°C	Extension*
MgCl ₂ (100 mM)	0.5 μ l	72°C	05:00
dNTPs (10 mM each)	0.5 μ l	16°C	∞
Phusion Polymerase (2 U/ μ l)	0.2 μ l		
Water	11.8 μ l		
TOTAL	20 μ l		
Q5 Polymerase (NEB)		Reaction Conditions	
Template	1 μ l	98°C	05:00
Forward Primer (10 μ M)	1 μ l	98°C	00:30
Reverse Primer (10 μ M)	1 μ l	Annealing *	00:30
5x Reaction Buffer	4 μ l	72°C	Extension*
dNTPs (10 mM each)	0.4 μ l	72°C	02:00
Q5 Polymerase (2 U/ μ l)	0.2 μ l	16°C	∞
Water	12 μ l		
TOTAL	20 μ l		
DFS Taq Polymerase (Bioron)		Reaction Conditions	
Template	2 μ l	94°C	05:00
Forward Primer (10 μ M)	1 μ l	94°C	00:30
Reverse Primer (10 μ M)	1 μ l	Annealing *	00:30
10x Reaction Buffer	2 μ l	72°C	Extension*
MgCl ₂ (100 mM)	0.5 μ l	72°C	10:00
dNTPs (10 mM each)	0.5 μ l	16°C	∞
DFS Taq Polymerase (5 U/ μ l)	0.2 μ l		
Water	12.8 μ l		
TOTAL	20 μ l		

2.2.1.3 Sequencing

Approximately 100-200 ng of plasmid were applied to confirm the desired sequence via Sanger sequencing (Faculty of Biology Sequencing Service, Ludwig-Maximilians Universität München, Germany) with appropriate primers.

2.2.1.4 Plasmid DNA Isolation from *Escherichia coli*

A single colony was inoculated in 2 ml LB medium supplemented with appropriate antibiotics overnight. Then, plasmid DNA was isolated using the NucleoSpin Plasmid EasyPure kit (Macherey-Nagel) according to the manufacturer's instructions.

2.2.1.5 Genomic DNA Isolation from *Arabidopsis thaliana*

One small leaf of each plant was cut and collected into 2.0 ml Eppendorf tubes containing a tungsten carbide 3 mm ball bearing. Homogenization was done in 500 µl of high purity extraction buffer (0.1 M Tris HCl pH 7.5, 0.05 M NaCl, 0.05 M EDTA pH 8.0, 1% (w/v) PVP) at 13200 rpm for 3 minutes via the tissue lyser. 66 µl of 10% (w/v) SDS and 166 µl of 5M potassium acetate (pH 5.8) were added and tubes were mixed well. Then, the tubes were centrifuged for 15 minutes at 13200 rpm. The supernatant was transferred into new tubes and 0.7 vol of isopropanol was added. Tubes were mixed by inverting several times and were incubated on ice for 15 minutes. Then centrifugation for 15 minutes at 13200 rpm was done and the supernatant was removed carefully. 500 µl of 70% ethanol were added and tubes were centrifuged for 5 minutes at 13200 rpm. Ethanol was discarded gently and the pellet was dried at room temperature. 50 µl of water was used for the resuspension of the pellet.

2.2.1.6 RNA Isolation from *Arabidopsis thaliana*

Up to 80 mg of leaf material was used for RNA extraction with the RNeasy Plant Mini kit (Qiagen) according to the manufacturer's instructions. DNase digestion was performed during the RNA isolation procedure once. Afterwards, the eluted RNA was subjected to a second DNase treatment with the Ambion Turbo DNase (Thermo Fischer Scientific) according to the manufacturer's instructions.

2.2.1.7 cDNA Synthesis

Around 0.5-1.0 µg RNA was used for cDNA synthesis in 10 µl reaction volume with M-MLV reverse transcriptase (Promega) according to the manufacturer's instructions.

2.2.1.8 Site-Directed Mutagenesis

Site-directed mutagenesis primers were designed using the NEBaseChanger® version 1.3.0 tool (<http://nebasechanger.neb.com/>). Mutagenesis reaction was carried out using the Q5® Site-Directed Mutagenesis Kit (NEB) according to the manufacturer's instructions.

2.2.2 Biochemical Methods

2.2.2.1 Agarose gel electrophoresis

DNA and RNA samples were separated on 1% agarose gels supplemented with 0.5 µg/ml ethidium bromide in 1x TAE buffer at 100 V for 30 minutes. Samples were loaded onto the gel after mixing with DNA loading buffer.

2.2.2.2 Protein Overexpression from *Escherichia coli*

Transformed *Escherichia coli* BL21 strain was inoculated in LB medium and was grown until the cell density reach OD₆₀₀ of 0.6-0.8 at 37°C. Protein expression was induced with 1 mM IPTG.

2.2.2.3 Protein Purification from Plants

200 mg leaf material was homogenized with 300 µl extraction buffer (0.05 M Tris-HCl pH8, 2% LDS, 0.1 mM PMSF) using an electronic micropestle. The suspension was incubated on ice for 30 min and then centrifuged for 15 minutes at 13200 rpm and 4°C. The soluble protein-containing supernatant was transferred to another tube and protein concentration was determined via Bradford Assay. 50 mM EDTA and 10 mM DTT were added to purified proteins and stored at -20°C for long-term storage.

2.2.2.4 Protein Purification from Inclusion Bodies

Proteins were expressed and purified as inclusion bodies. To this end, the cells were pelleted by centrifugation for 15 minutes at 4000 rpm at 4°C. the pellet was resuspended in 8 x vol resuspension buffer (1x PBS, 1 mM PMSF, 1 mM beta-mercaptoethanol, 10 µg/ml Dnase I). Subsequently, the cells were disrupted by sonication and centrifuged for 20 minutes at 25000 g at 4°C. The supernatant was discarded, and the pellet was washed with 1x PBS. The supernatant was removed after centrifugation for 20 minutes at 25000 g and 4°C. Subsequently, the pellet was washed three times with wash buffer (1x PBS, 1% Triton X-100) and collected via centrifugation for 10 minutes at 25000 g and 4°C. Afterwards, the pellet was resuspended in urea buffer (1x PBS, 8 M urea) and centrifuged for 30 minutes at 25000 g and 4°C. The supernatant was used for dialysis to remove the urea from the sample. To this end, the supernatant was transferred into a dialysis membrane with a molecular weight cut-off of 14 kDa against 4 M, 2 M, 1 M and 0 M urea in 1x PBS subsequently each for 1 hour with agitation in order to refold the protein. The volume of the dialysis buffer was adjusted to 100 x the sample volume.

2.2.2.5 SDS polyacrylamide gel electrophoresis (SDS-PAGE)

Proteins were separated via SDS-PAGE with a stacking gel (5% polyacrylamide) and a separating gel (10-15% polyacrylamide). Prior to loading, proteins were boiled for 5 minutes at 95°C in an SDS loading buffer. Gels were run in SDS running buffer and either stained with coomassie staining solution or used for western blotting.

2.2.2.6 Wet Western Blot and Immunodetection of Proteins

Protein transfer from an SDS gel onto a PVDF membrane was done with the wet blotting technique. The PVDF membrane was activated with 100% methanol and Whatman papers were soaked in 1x Towbin Buffer before assembly. Blotting assembly was done accordingly: a thin sponge, three Whatman papers on the bottom, activated PVDF membrane, gel, three Whatman papers on the top and covered with a second thin sponge. The transfer was carried out in the transfer tank filled with 1x Towbin Buffer at 400 mA either for 2 hours at room temperature or overnight at 4°C. The protein transfer rate was checked by Ponceau staining. For immunodetection of proteins, the membrane was blocked for 1 hour with skimmed milk (for biotin antibody, 3% BSA; other antibodies, 3% skimmed milk) in TBST (1 x TBS, 0.05% Triton X-100). The first antibody was incubated overnight at 4°C. Afterwards, the membrane was washed three times with TBST for 10 minutes at room temperature. The secondary antibody incubation was performed for 1 hour at room temperature. Then, the membrane was subjected to a second wash step three times with TBST for 10 minutes at room temperature. Equal volumes of development solution I (100 mM Tris pH 8.5, 1% luminol, 0.44% coumaric acid) and II (100 mM Tris pH 8.5, 0.018% H₂O₂) were mixed and the membrane was incubated with the mixture for 1 minute. The signal was detected by chemiluminescence using the Image Quant LAS 400 (GE Healthcare).

2.2.2.7 Protein Extraction for LS-MS/MS Analysis

Protein extraction was adapted from (Mair et al., 2019). Briefly, 2 weeks old plants, which were grown in liquid cultures, were washed with ice-cold water 2-3 times. Plants were dried using paper towels and grounded in liquid nitrogen. Approximately 3 ml of densely packed grounded plant material was put in a 15 ml falcon tube and resuspended in 2 ml extraction buffer (50 mM Tris pH 7.5, 150 mM NaCl, 0.1% SDS, 0.5% sodium deoxycholate, 1% Triton X-100, 1 mM EGTA, 1x complete protease inhibitor (Roche), 1 mM DDT, 1 mM PMSF). Tubes were incubated on a rotor wheel for 10 minutes at 4°C. 1 µl of Lysonase (Millipore, Darmstadt, Germany) was added to the suspension and the tubes were incubated on the rotor for 15 minutes at 4°C. The

extracts were distributed into 1.5 ml Eppendorf tubes and sonicated in an ice bath 4 times for 30 seconds with 90-second breaks on ice. The protein-containing supernatant was collected via centrifugation for 15 minutes at 15000 g and 4°C. Protein samples were subjected to PD-10 Desalting Columns (GE Healthcare, VWR, Ismaning, Germany)-gravity protocol according to the manufacturer's instructions. Column equilibration was done with extraction buffer without complete protease inhibitor and PMSF. Proteins were eluted from the column with a 3.5 ml ice-cold extraction buffer. Protein concentration was determined via Bradford assay.

2.2.2.8 Redox State Analysis and TCA Precipitation of Proteins

Around 0.1-0.2 mg/ml purified protein were either incubated with 50 µM CuCl₂ (oxidation) or 10 mM DTT (reduction) for 1 hour at 20°C. Afterwards, TCA (end concentration 5%) was added to the samples and incubated on ice for 30 minutes. Samples were centrifuged for 20 minutes at a max speed at 4°C and the supernatant was removed. 100 µl of 100% acetone were added to each sample and mixed well. After 10 minutes of incubation on ice, proteins were pelleted via centrifugation for 20 minutes at 20000 g and 4°C. The supernatant was removed, and the pellet was dried at room temperature.

2.2.2.9 AMS Labeling (Gel Shift Assay)

The TCA precipitated protein pellet was dissolved in AMS buffer (10 mM AMS, 2 mM EDTA, 0.1 M Tris-HCl pH 7.0) and incubated for 1 hour at room temperature. Samples were mixed with a non-reducing SDS loading buffer and analyzed via SDS PAGE.

2.2.2.10 PEGylation of Proteins

TCA precipitated proteins were dissolved in PEGylation buffer (0.5% (w/v) SDS, 2 mM mPEG-24, 50 mM Tris-HCl pH 7.0, 100 mM NaCl) and incubated for 3 hours at room temperature. Samples were loaded onto an SDS gel after mixing with a non-reducing SDS loading buffer.

2.2.2.11 Affinity Purification of Biotinylated Proteins

According to (Mair et al., 2019), the beads to the protein ratio was adjusted to 1:80 (µl beads: µg protein) for optimum protein binding. Therefore, 10 µl of streptavidin magnetic beads (Pierce, Thermo Fischer, Braunschweig, Germany) were washed with 1 ml ice-cold extraction buffer without complete protease inhibitor and PMSF. Protein samples were added to the beads according to the determined ratio and incubated overnight at 4°C on a rotator. Beads were collected via a magnetic rack and the supernatant was kept as an unbound fraction for further analysis. Washing steps were done for 8 minutes on a rotator and the supernatant was

removed via a magnetic rack each time. The beads were washed with 1 ml ice-cold extraction buffer two times, 1 ml ice-cold 1M KCl, 1 ml ice-cold 0.1 M Na₂CO₃, 1 ml 2 M urea in 10 mM Tris-HCl pH 8.0 at room temperature and 1 ml ice-cold extraction buffer without complete protease inhibitor and PMSF two times. Beads were pelleted with a magnetic rack to remove the last wash buffer and kept at -80°C for further processing.

2.2.2.12 Sample Preparation for Mass Spectrometry Analysis

After the affinity purification, the beads were resuspended in 50 µl of 6M urea in 50 mM ammonium bicarbonate. Later, 5 µl of 0.1 M DTT were added and the tubes were incubated for 1 hour at 37°C. Tubes were cooled down on the bench to room temperature and 5 µl of 0.25 M iodoacetamide was added. The tubes were incubated for 1 hour at room temperature in the dark. Beads were diluted with 300 µl 50 mM ammonium bicarbonate (the pH should be approximately 7.5-8.0) and 15 µl trypsin (0.1 µg/µl) was added. Tubes were mixed gently and incubated overnight at 37°C. Digested peptides were collected via magnetic separation. A second washing step with 50 µl of 50 mM ammonium bicarbonate was done and the supernatant was combined with the digested peptides. Subsequently, peptide acidification was achieved by adding 50% formic acid (the pH should be approx. 2-3) to a concentration of 1%. Tubes were centrifuged for 10 minutes at max speed to remove the aggregations. Stage tips (C18-Thermo Fischer Scientific) were used for further steps. Tips were activated with 100 µl of 100% methanol and equilibrated with 100 µl of 0.5% formic acid. Acidified samples were loaded onto the tips and the flow-through was reloaded again. Later, the tips were washed with 100 µl of 0.5% formic acid. Sample elution was done with 50 µl of 80% acetonitrile, and 0.5% formic acid into new Eppendorf tubes. The desalted peptides were then dried in a speed vac and stored at -80°C until further processing.

2.2.2.13 LC-MS/MS

Proteomic analysis for TurboID constructs was performed at the Protein Analysis Unit (ZfP) of the Ludwig Maximilians University of Munich, a registered research infrastructure of the Deutsche Forschungsgemeinschaft (DFG, RI-00089). Proteomic analysis for BioID2 constructs was performed at the MSBioLMU core facility (Department Biology I, Ludwig-Maximilians-Universität München).

2.2.3 Plant Biological Methods

2.2.3.1 Plant Growth Conditions

Arabidopsis thaliana WT Columbia ecotype (Col-0) and transformed plants were either grown on soil or in half-strength MS medium in a growth chamber (16 h light/ 8h dark, 22°C, 100 $\mu\text{mol} / \text{m}^2\text{s}^{-1}$ in fluorescent light conditions). For plants grown in liquid culture, the half-strength MS liquid medium was used and cultures were placed on a shaker in a growth chamber (16 h light/ 8h dark, 22°C, 100 $\mu\text{mol} / \text{m}^2\text{s}^{-1}$ in fluorescent light conditions). Seeds were surface sterilized by washing with 70% ethanol for 2 minutes followed by 5 minutes incubation with 6% (w/v) NaOAc and 0.05% (w/v) Triton X-100 and washed three times with sterile water for 1 minute. Later, the seeds were dried under the hood and homogeneously distributed on the plate. The plates were sealed and vernalized at 4°C in the dark for 2 days. The same vernalization approach was applied for seeds sown on the soil.

2.2.3.2 *Agrobacterium tumefaciens* Transformation by the Freeze-Thaw Method

Competent *Agrobacterium tumefaciens* AGL1 or GV3101 cells (100 μl) were thawed on ice and 1 μg of plasmid was added to competent cells. Subsequently, cells were frozen in liquid nitrogen and thawed in a thermocycler for 5 minutes at 37°C. 500 μl LB medium was added and cells were incubated for 2-4 hours at 28°C. After incubation, tubes were centrifuged, and the supernatant was removed. The remaining pellet was resuspended with 100 μl LB and plated on LB plates with appropriate antibiotics. Plates were incubated for 2-3 days at 28°C.

2.2.3.3 Transient Transformation of *Nicotiana benthamiana*

Agrobacterium tumefaciens AGL1 cells were grown in 20 ml LB media with appropriate antibiotics at 28°C until they reached an OD_{600} of 0.6. Cells were pelleted via centrifugation for 5 minutes at 4000 g and resuspended in an infiltration medium (10 mM MES pH 6, 10 mM MgCl_2 , 150 μM Acetosyringon) such that OD_{600} was 1.0. The suspension was rotated for 2 hours in a horizontal shaker in the dark. 3-4 weeks old *Nicotiana benthamiana* leaves were then infiltrated from the abaxial surface. Plants were kept in the dark overnight and infiltrated leaves were incubated 2-3 days at room temperature prior to further analysis.

The helper plasmid (phage p19) was also inoculated to boost the plasmid expression. In that case, the helper plasmid containing suspension was mixed with the intended plasmid carrier suspension in a ratio of 1:1 and leaves were infiltrated.

2.2.3.4 Stable Transformation of *Arabidopsis thaliana*

Arabidopsis thaliana plants were grown until most of them started to bolt. Bolts were clipped seven days prior to transformation. 100 µl of *Agrobacterium tumefaciens* GV3103 cells were inoculated in a 5 ml LB medium with antibiotics and grown for 2 days at 28°C. Then, the precultures were transferred into a 500 ml LB medium with antibiotics and grown overnight at 28°C with 200 rpm shaking until the OD₆₀₀ reached 0.8. *Agrobacterium* cultures were centrifuged for 20 minutes at 2000 g and resuspended in 500 ml 5% (w/v) sucrose, 0.03% (v/v) silwet L-77. With gentle agitation, the flowers were dipped into the *Agrobacterium* suspension for about 10 seconds. Plants were covered with plastic a cover for two nights. After seven days, plants were dipped again according to the same protocol to achieve high transformation efficiency. Then, plants were dried out and seeds were collected for first-generation selection either on MS plates supplemented with appropriate antibiotics or on soil with herbicide spraying. Successful transformants were transferred to soil for further analysis.

2.2.3.5 Protoplast Isolation from *Nicotiana benthamiana*

Infiltrated *Nicotiana benthamiana* leaves were cut into approximately 0.3 x 1.0 cm² pieces and incubated under vacuum in 10 ml enzyme solution (1% Cellulase R10, 0.3% Mazerozym R10) made in F-PIN (5 mM KNO₃, 1.5 mM CaCl₂, 0.75 mM MgSO₄, 0.625 mM KH₂PO₄, 20 mM NH₄-succinate, 120 g/l sucrose [550 Osm], MS medium PC-vitamins [200 mg/l Myoinositol, 1 mg/l thiamin-HCl, 2 mg/l Ca-pantothenate, 2 mg/l nicotinic acid, 2 mg/l pyridoxin-HCl, 0.02 mg/l biotin, 1 mg/l 6-benzylaminopurin (BAP), 0.1 mg/l α-naphthalene acetic acid (NAA)]. After vacuum infiltration, the suspension containing leaves was incubated for 90 minutes at 40 rpm in the dark. Protoplasts were released via 1-minute rotation at 80 rpm and the suspension was filtered through a 100 µM nylon membrane into a 15 ml glass round bottom centrifugation tube. The filtered protoplasts were overlaid with 2 ml F-PCN medium (F-PIN, instead of sucrose, 80 g/l glucose [550 Osm] was added) and centrifuged for 10 minutes at 70 g (with slow deceleration and acceleration). Intact protoplasts, which were placed at the interface between the F-PIN and F-PCN buffers, were transferred into a new tube. Protoplasts were then carefully washed with 10 ml W5 buffer (125 mM NaCl, 125 mM CaCl₂, 5 mM KCl, 2 mM MES pH 5.7 [550 Osm]) and centrifuged for 10 minutes at 50 g. Pellet was resuspended in 1 ml W5 buffer.

2.2.3.6 EMS Mutagenesis

Since the EMS (Sigma-Aldrich) is carcinogenic and highly volatile, working conditions were adjusted to this situation. For this reason, a half mask (MOLDEX 7000, Mercateo, Munich, Germany), a gas filter (9400 EN14387 ABEK1, Mercateo, Munich, Germany) and long nitrile gloves 0.28 (VWR) were used. The complete mutagenesis process was performed under the fume hood. Required handling materials were incubated in 1M NaOH before usage. A 50 ml falcon tube was filled with 35 ml of double-distilled water and 70 µl of EMS was added to the falcon. The solution was gently tilted until the EMS was homogeneously dissolved. Approximately 600 mg of seeds were added into the falcon tube and incubated on a horizontal shaker for 15 hours. The EMS solution was removed into an Erlenmeyer flask which contains 50 g of solid NaOH. Seeds were then washed 12 times with 50 ml of double-distilled water and each time, the water was poured back into the Erlenmeyer flask. Seeds were dried on a Whatman paper. Mutagenized seeds were distributed in 50 x 30 or 30 x 20-sized pots.

2.2.4 Computational Analysis

2.2.4.1 General Computational Tools

Gene sequences for *AtToc75-III*, *AtTic40*, *AtTrxM2* and *AtPic1* from *Arabidopsis* were obtained from TAIR (<https://www.arabidopsis.org>) and for BioID2 and TurboID from addgene (<https://www.addgene.org>). *in silico* cloning was done via SnapGene (<https://www.snapgene.com/>).

In silico protein, 3D structure reconstruction for the Toc75-III POTRA domain was generated by using PyMol (<https://pymol.org/2>). Secondary structure analysis for the membrane-bound proteins was done via the Protter tool (<http://wlab.ethz.ch/protter/start>).

In silico protein network and gene expression profiles were generated via The Bio-Analytic Resource for Plant Biology Platform (<http://bar.utoronto.ca/eplant/>).

Graphs and statistical analysis for proteomics data were generated by using Perseus (version 1.6.12.0) (<https://maxquant.net/perseus>). Protein identification for proteomics data was done via using Uniprot Protein Database (<https://www.uniprot.org/>). Venn diagrams were generated via the Venn Diagrams tool of Van de Peer Lab from VIB-UGent (<http://bioinformatics.psb.ugent.be/webtools/Venn/>). Image analyses were done via the software ImageJ (<https://imagej.net>).

Microsoft Office 365 software programs are used for writing, statistical analyses, generation of figures, graphs and presentations (<https://www.office.com/>).

2.2.4.2 Data Analysis and Protein Enrichment of Mass Spectrometry Datasets

Protein identification and label-free quantification of proteins were made by using MaxQuant. Filtering and statistical analysis of the data sets for each experiment were generated by Perseus. The data file from MaxQuant was imported into Perseus and the LFQ intensities were set as “Main Category.” The proteins which were marked as only identified by site, reverse and potential contaminant were removed from the matrix. The LFQ values were log₂ transformed. Missing values were imputed from the normal distribution.

To identify proteins enriched in proximity labeling samples versus the WT control, unpaired two-sided Students t-tests were applied. The FDR was set to 0.05 according to the Benjamini-Hochberg approach for statistical analysis. Resulted data tables were used for further examination and identification.

3 Results

3.1 Golden Gate Cloning Validation

The transgenic plants were generated via the Golden Gate cloning method (Section **2.2.1.1 Cloning Strategy**). For this reason, each gene of interest was cloned into the Golden Gate plasmid system. Plasmids were subsequently checked with respective restriction enzyme digestion assays and validated by sequencing. Then, the plasmids were transformed to the corresponding *Arabidopsis thaliana* background as described in Section **2.2.3.4 Stable Transformation of *Arabidopsis thaliana***.

3.2 *In silico* Protein Interaction Partner Analysis of Candidate Proteins

Within the scope of this thesis, candidate proteins were selected concerning the availability, membrane anchoring properties, structural limitations, involved metabolic pathways and mutant plant phenotypes. Due to the pale green phenotype of *tic40* null mutants, *AtTic40* was preferred as a suitable protein for complementation studies. Besides, *AtTic40* is encoded by only one gene in *Arabidopsis thaliana*, making it an ideal model for avoiding functional compensation. Thus, we could obtain accurate results regarding the effect of PL tagging. Moreover, we wanted to examine *AtTrxF1* and *AtTrxM2* proteins because of the small size of the proteins, their subcellular locations, and the potential associating partners. However, the generation of *AtTrxF1* lines enabling PL failed (data not shown); therefore, the *AtTrxM2* lines were further examined. Although there is an ongoing conflict about the molecular function of *AtPic1/AtTic21*, we have added it as the negative control, accepting its function in iron regulation and will hereafter be referred to as *AtPic1* for the sake of the simplicity. Together, the interactome of three candidate proteins will broaden our knowledge about the components of protein translocation in the inner envelope membrane of the chloroplast, possible regulatory proteins and new players in several metabolic pathways.

Protein-protein interaction networks can improve the understanding of the biological processes within the cell. Depending on the published data and computer algorithms, a simple protein interaction network can be formed *in silico*. Therefore, the candidate proteins' *in silico* interaction partner analysis was performed as detailed in Section **2.2.4.1 General Computational Tools**, and the results were summarized in Table 16 concerning experimental evidence.

Table 16: *in silico* Protein Interaction Partner Analysis

Tic40 PPI Network		
Gene Accession Number	Protein Annotation	References
AT1G06950	Translocon at the inner envelope membrane of chloroplasts 110 (Tic110)	(Bédard et al., 2007; Chou et al., 2003; Stahl et al., 1999)
AT3G48870	Clp ATPase component (Hsp93III-CLPC2)	(Chou et al., 2003)
AT4G23430	NAD(P)-binding Rossmann-fold superfamily protein (Tic32)	(Hörmann et al., 2004)
AT5G50920	CLPC homologue 1 (Hsp93V)	(Kovacheva et al., 2005)
AT2G04030	Chaperone protein htpG family protein (Hsp90C)	(Inoue et al., 2013)
TrxM2 PPI Network		
Gene Accession Number	Protein Annotation	References
AT1G09420	Glucose-6-phosphate dehydrogenase 4 (G6PD4)	(Meyer et al., 2011)
AT5G35790	Plastidic glucose-6-phosphate dehydrogenase 1 (G6PD1)	(Meyer et al., 2011)
AT1G22640	Myb domain protein 3 (Myb3)	(Dreze et al., 2011)
AT5G15090	Voltage dependent anion channel 3 (VDAC3)	(Zhang et al., 2015)

The protein-protein interaction visualization was performed via The Bio-Analytic Resource for Plant Biology Platform (<http://bar.utoronto.ca/eplant/>). For each candidate protein, *AtTic40*, *AtTrxM2* and *AtPic1*, the numbers of interaction partners plotted were, seven (AT1G06950, AT3G48870, AT4G23430, AT5G50920, AT2G04030, AT5G19620, AT4G02510), five (AT1G09420, AT5G35790, AT1G22640, AT5G15090, AT2G26830) and zero (See **Appendices**). *AtTic40* and *AtTrxM2* associated proteins were sorted according to published data and relevance (Table 16). Surprisingly, there was no protein associating with *AtPic1*.

The Tic40 protein was first found to be interacting with the Tic110 protein by cross-linking analysis, subsequently followed by immunoprecipitation (Stahl et al., 1999). The Tic110-Tic40 interaction, later, was supported by biochemical cross-linking experiments (Chou et al., 2003), yeast two-hybrid and bimolecular fluorescence complementation (BiFC) assays (Bédard et al., 2007). Biochemical cross-linking has revealed that Tic40 also interacts with Hsp93III protein (Chou et al., 2003). Interestingly, co-immunoprecipitation experiments have identified the protein named Tic32, proposed to have an association with Tic40 (Hörmann et al., 2004).

Moreover, *in vivo* studies showed that Hsp93V works closely with protein import complex, possibly suggesting an interaction with Tic40 (Kovacheva et al., 2005). Later, another interaction partner, Hsp90C, was co-purified with the protein import components, including Tic40 (Inoue et al., 2013).

The interaction partners of TrxM2, G6PD1 and G6PD4 were identified via localization analyses and confirmed by yeast two-hybrid and BiFC experimental data (Meyer et al., 2011). From a high-quality proteome-wide interactome mapping, another protein, Myb3, was identified as an associating partner of TrxM2 (Dreze et al., 2011). Surprisingly, an interaction between TrxM2 and mitochondrial protein VDAC3 has been evidenced by yeast two-hybrid, BiFC and pull-down experiments (Zhang et al., 2015).

3.3 *In silico* Secondary Structure Analysis of Candidate Proteins

Proteins are dynamic molecules; thus, various factors influence their activities. It has been reported that protein tags can interfere with protein folding and alter biological activity (Booth et al., 2018; Cabantous et al., 2005). Therefore, addition of an N- or C- terminal tag requires deep investigation at the structural level. Since the TurboID is a relatively big (~35 kDa) protein (Branon et al., 2018), it is essential not to interfere with the native function of the target protein. Therefore, *in silico* analysis of *AtTic40*, *AtTrxM2* and *AtPic1* proteins was performed as described in Section **2.2.4.1 General Computational Tools**.

Transit peptides were predicted using ChloroP software (Emanuelsson et al., 1999) and excluded from the protein sequence for the membrane-bound structure prediction. It was observed that the Tic40 protein spans the membrane with a single transmembrane domain and possesses a hydrophilic domain facing the stroma (Figure 3A), whereas Pic1 protein indicates four transmembrane domains (Figure 3B). Candidate proteins have their C-terminal part facing the stroma (Figure 3). Therefore, the spatial location of the TurboID tag was confirmed to be on the stromal side of the inner chloroplast envelope.

The *AtTrxM2* is a soluble plastidial protein with the size of ~12 kDa (Fernández-Trijueque et al., 2019). Therefore, the TurboID tag was fused to the protein so as not to interfere protein's function. Next, the golden gate cloning strategy was designed according to the secondary structure analysis. Each respective plasmid was cloned according to the scheme (Table 12), and protein functionality was checked transiently and stably.

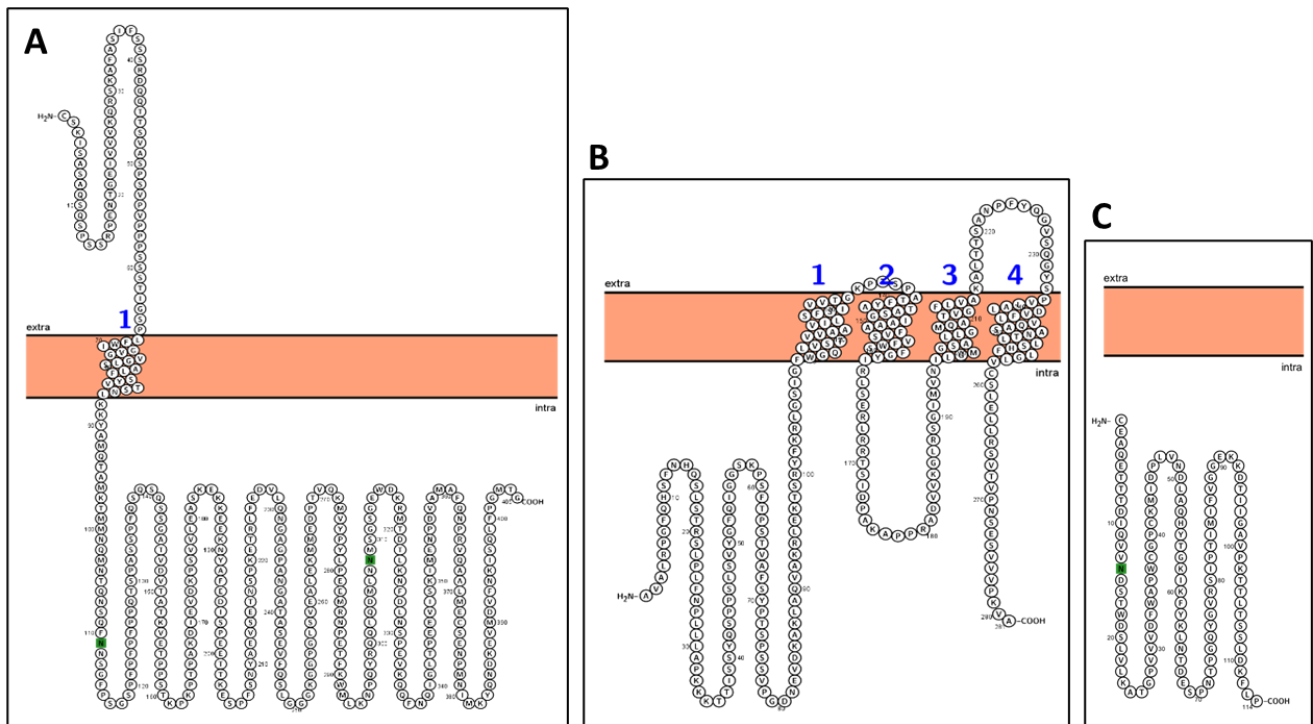


Figure 3: *in silico* secondary structure prediction of the candidate proteins. Both proteins have their C-terminal part in the stromal side. The location of the TurboID tag will be within the stroma. **(A)** Structure prediction for *AtTic40* protein. While the N-terminal part faces the intermembrane space, the C-terminal part locates within the stroma. The predicted structure shows only one intermembrane domain. **(B)** Structure prediction for *AtPic1* protein. Both C- and N- terminal domains face the stroma. There are four transmembrane domains within the depicted structure. **(C)** Structure prediction for *AtTrxM2* protein. Accordingly, the *AtTrxM2* protein appears to lack a membrane binding domain and thus tend to behave as a soluble protein.

3.4 Establishment of the Proximity Dependent Labeling in Plant Systems

Since the development of the BioID system, it has been challenging to implement this promising technology in plants for several reasons (Arora et al., 2020) (Figure 4, 5). One is that plants can produce biotin endogenously, creating background biotinylation (Arora et al., 2020). Therefore, optimization of the reaction parameters was necessary. Two biotin ligases, BioID2 (Kim et al., 2016) and TurboID (Branon et al., 2018), were used for proximity labeling and incorporated into the candidate proteins by Golden Gate DNA assembly. The biotinylation capacity of fusion proteins were initially tested with transient expression system and followed by stable expression. *Nicotiana benthamiana* leaves were used to check protein functionality transiently (Figure 6 and Supplemental Figure 1). Subsequently, it was indicated that the fusion proteins were capable of catalyzing both self and proximity biotinylation. Following this information, it is aimed to establish stable plant lines expressing the fusion proteins and promote proximity labeling by adding excess biotin. For this purpose, the WT Col-0 and homozygous Tic40 mutant (SALK_057111) seeds were transformed with respective plasmids.

Transformants were selected according to antibiotic or herbicide resistance, plasmid insertion was confirmed concerning each independent insertion, resulting seeds were pooled together, and used for further analysis (Figure 7, 8, 9, 10 and Supplemental Figure 2).

Various methods were evaluated to ensure biotin intake of the *Arabidopsis thaliana* plants. First, the transformed seeds were planted on soil and grown for at least four weeks and leaves were collected and incubated with biotin solution in a tray. Subsequently, purified total proteins were checked via western blotting, which caused insufficient biotin uptake for reaction initiation (Supplemental Figure 3A). Later, the biotin solution infiltrated the *Arabidopsis thaliana* leaves, resulting in an inadequate biotinylation reaction (Supplemental Figure 3B). These findings highlight that the soil-grown seeds cannot acquire excess biotin from the environment. Liquid cultures were used to grow *Arabidopsis thaliana* seedlings to overcome this barrier. Despite the hydrophobicity of biotin, growing plants were able to intake biotin from the liquid culture and utilize it for the biotinylation reaction. Thus, the experimental setup for the biotinylation process was built on growth in the liquid culture of the transformed seeds. Seeds were grown in the liquid culture for 14 days before biotin addition. The concentration of the biotin and the reaction time for stably transformed lines were determined as parallel to transient expression studies in *Nicotiana benthamiana* (Figure 11, 12).

Total proteins were extracted as described (Section **2.2.2.7 Protein Extraction for LS-MS/MS Analysis**), excess biotin was removed using desalting columns and biotinylated proteins were collected by streptavidin affinity purification. Since the biotin-streptavidin interaction is one of the strongest known non-covalent bonding, the complete separation of the biotinylated proteins is exceptionally challenging. Therefore, the proteins immobilized on streptavidin beads were digested into peptides with trypsin. Collected peptides were sent to mass spectrometry analysis and protein identification was performed as described (Section **2.2.4.2 Data Analysis and Protein Enrichment of Mass Spectrometry Datasets**).

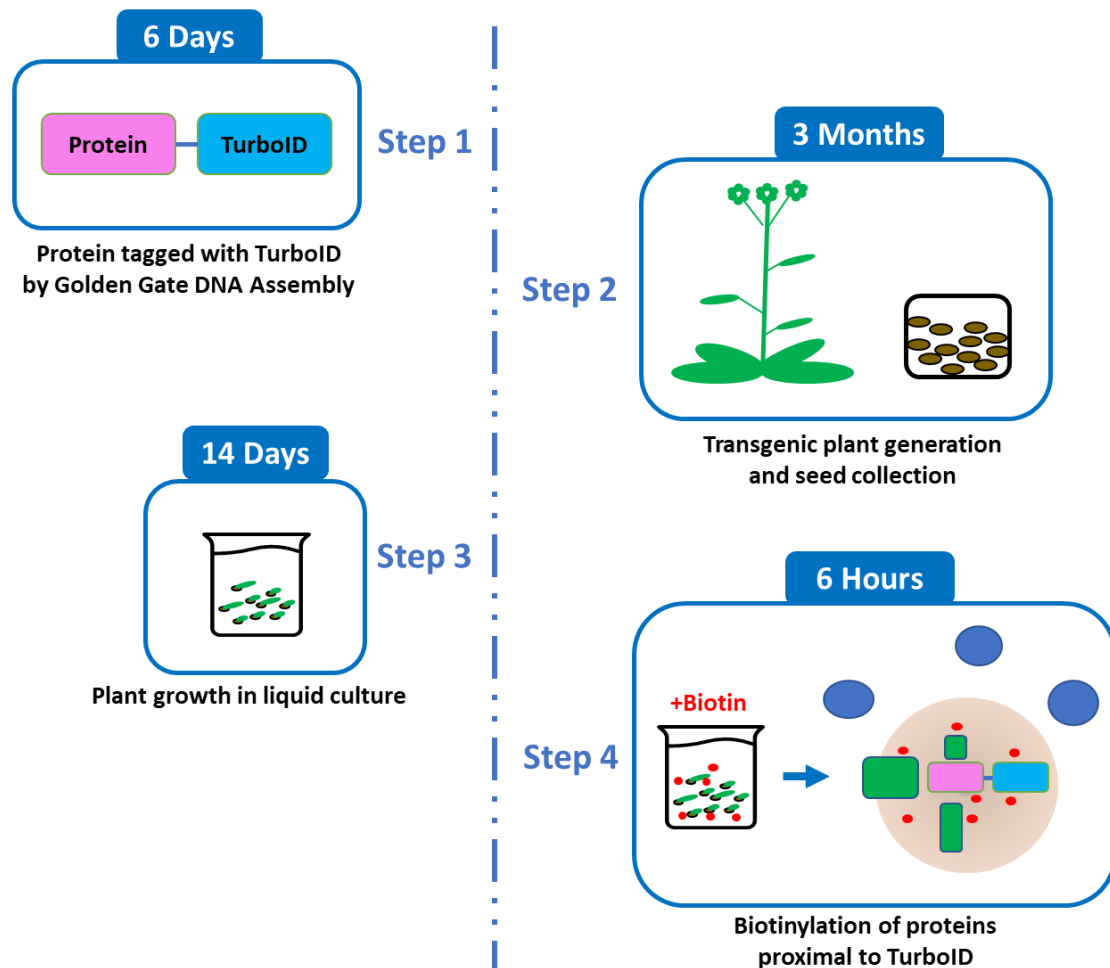


Figure 4: Experimental setup for the proximity labeling in plants. The complete setup can be divided into two subsections: **Part 1**-Transgenic plant generation and **Part 2**- Biochemical analysis of the proteins. Each part consists of 4 distinct steps. **PART 1-(Step 1)** Firstly, the sequences of candidate proteins are designated for cloning purposes and the primers are designed concerning the used plasmid system. Here, we used Golden Gate DNA assembly to create TurboID tagged proteins. **(Step 2)** Confirmed plasmids are transformed into respective *Arabidopsis thaliana* plants, successful transformants were selected according to the antibiotic/herbicide resistance, and the resulting seeds are pooled together for further analysis. **(Step 3)** Seeds are grown in the liquid culture on a shaker in the growth chamber under the 16 h light/ 8h dark, 22°C, 100 $\mu\text{mol} / \text{m}^2\text{s}^{-1}$ in fluorescent light conditions for 14 days. **(Step 4)** The biotin solution is added to 14-day-old plants in liquid culture. Then, the plants are incubated on a shaker in the same growth chamber for 6 hours to acquire a biotinylation reaction.

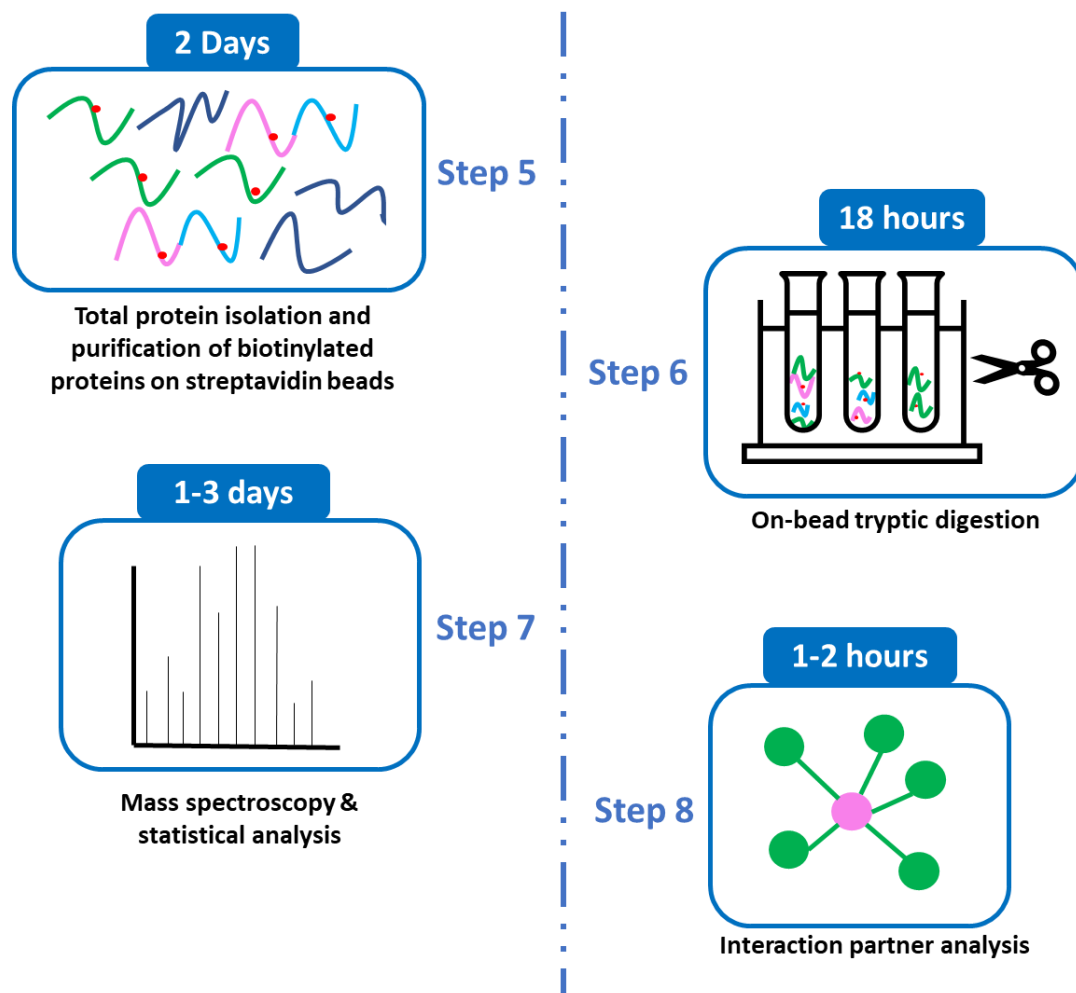


Figure 5: Experimental setup for proximity labeling in plants. PART 2-(Step 5) Total proteins are extracted and desalted to remove excess biotin. Later, biotinylated proteins are purified using streptavidin-coated magnetic beads. **(Step 6)** The magnetic beads are subjected to trypsin digestion to obtain a peptide mixture. This step contains information about the interaction partners. **(Step 7)** Peptides are prepared for mass spectrometry analysis. Then, the resulting MS data is analyzed by statistical tools to obtain a protein network. **(Step 8)** The protein network is subdivided into desired sections to create a significant interaction protein map.

3.4.1 Transient Protein Expression in *Nicotiana benthamiana* and Determination of Biotinylation Reaction Parameters

The TurboID enzyme exhibits great biotinylation outcome depending on the time (Branon et al., 2018). Therefore, enzymatic reaction parameter optimization is required. To determine the optimal reaction time, *Nicotiana benthamiana* leaves were infiltrated with the Agrobacterium carrying the TurboID constructs. After two to three days of incubation, the *Nicotiana benthamiana* leaves were again infiltrated with 500 μ M biotin (prepared as 50 μ M stock solution, dissolved in 10% DMSO). The reaction was stopped when a sample was taken for protein purification. Leaf samples were taken at 30 mins, 1 hour, 2 hours, 3 hours, 6 hours, and

18 hours for each construct. As a negative control, leaves were infiltrated with only *Agrobacterium* and incubated for two to three days. Then, leaves were injected with 500 μM biotin and after 18 hours, samples were collected.

As a result, TurboID tagged candidate proteins indicate enough biotinylation compared to the negative control (Figure 6). Each protein exhibited self biotinylation (autobiotinylation) and proximity biotinylation. Autobiotinylation bands were visible near the candidate protein sizes (TrxM2-TurboID:~56 kDa, Tic40-TurboID:~85 kDa, Pic1-TurboID:~67 kDa) and the biotinylated proteins have exhibited the smear like band formation (Figure 6). The time needed for the reaction for TrxM2 and Tic40 fusion proteins was 30 mins (Figure 6A, 6B), whereas Pic1 protein required at least 2 hours of incubation for proper biotinylation (Figure 6C). The saturation time point for the reaction was identified as 6 hours for all three proteins. *Nicotiana benthamiana* plants were infiltrated with non-transformed *Agrobacterium* and used as a negative control for proximity labeling, which resulted in almost zero biotinylation compared to tagged proteins (Figure 6). The results were confirmed that both candidate and TurboID proteins were functional. Besides, the TurboID enzyme could catalyze biotinylation reaction by adding biotin molecules to the candidate protein and the proteins in close proximity.

The transient expression of candidate proteins fused with a biotin ligase (either TurboID or BioID2) was successful in the background of *Nicotiana benthamiana* (Figure 6 and Supplemental Figure 1). Proteins were able to add biotin moieties to themselves and the neighboring proteins (Figure 6 and Supplemental Figure 1). Compared to TurboID, BioID2 tagged proteins required a more extended incubation period (18 hours) for efficient biotinylation (Supplemental Figure 1). The overall results support that the *Nicotiana benthamiana* plant model organism is suitable for *in vivo* proximity-dependent labeling studies.

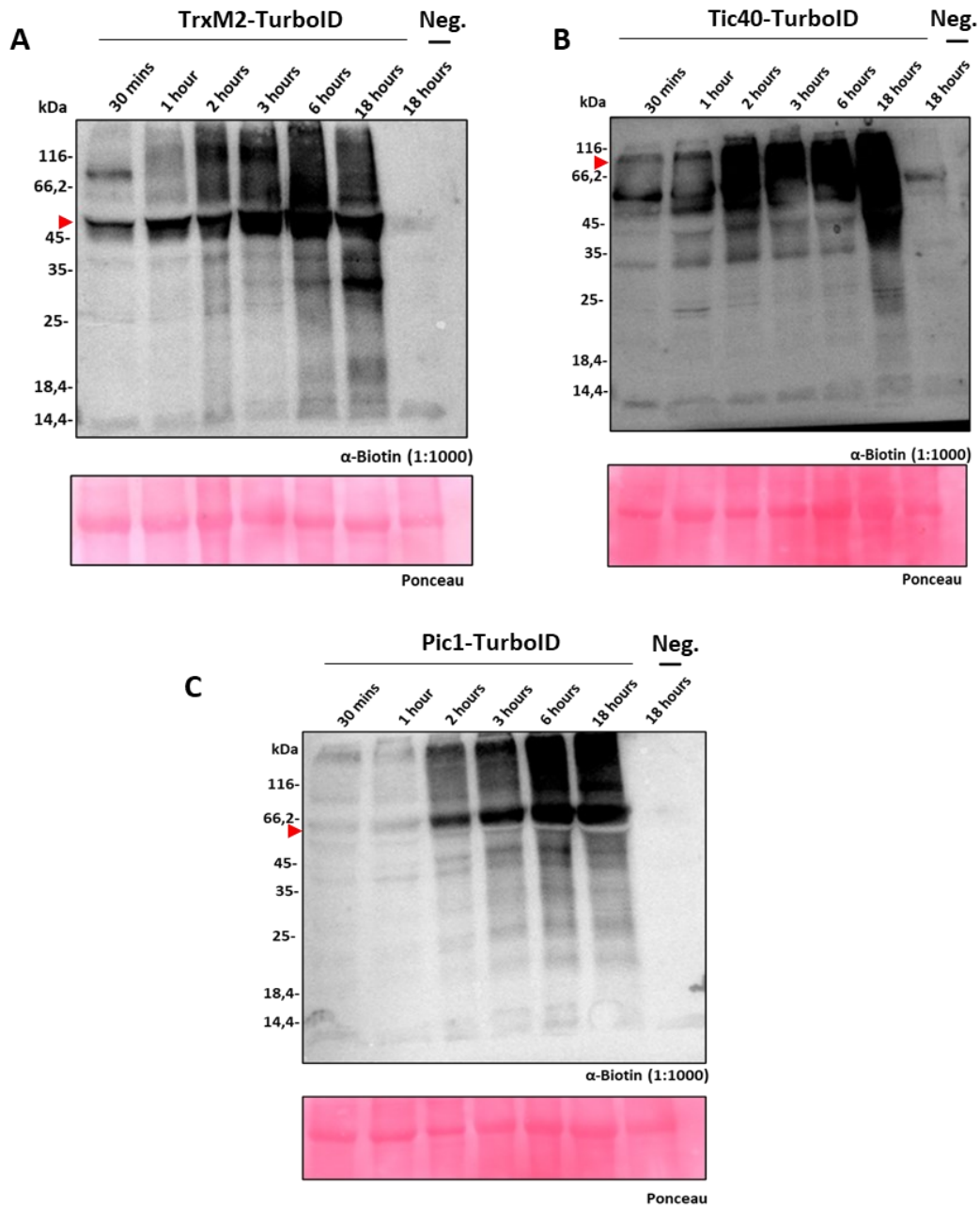


Figure 6: TurboID tagged proteins show biotinylation in *Nicotiana benthamiana*. Plasmids were transformed using *Agrobacterium*. Protein extracts were collected at the time points shown above the immunoblots (30 mins, 1 hour, 2 hours, 3 hours, 6 hours and 18 hours). As a negative control, wild type plants were incubated with the non-transformed *Agrobacterium*. Biotinylated proteins were detected with the anti-biotin antibody. Ponceau staining indicates the protein loading for each blot. Protein sizes are TrxM2-TurboID: ~56 kDa, Tic40-TurboID: ~85 kDa, Pic1-TurboID: ~67 kDa and self-biotinylated candidate proteins were indicated with the red arrow. Neg: Negative Control (A) TrxM2 fused with TurboID construct exhibits biotinylation within 30 minutes. (B) The Tic40 protein tagged with TurboID shows greater biotinylation after two hours of incubation. (C) The biotinylation rate for the Pic1-TurboID protein is relatively higher after 6 hours of incubation.

3.4.2 Generation of *Arabidopsis thaliana* Plant Lines Suitable for Proximity Dependent Labeling

Generation of stable plant lines bearing the proximity labeling plasmids were performed by using *Arabidopsis thaliana* WT Col-0 and SALK-057111 lines. To check the possible metabolic effects of the proximity labeling tag when fused to a protein, a homozygous mutant plant line (SALK-057111) was used (for the sake of simplicity, this line is hereafter called Δ Tic40 (-/-)). The genomic region of the Δ Tic40 (-/-) was depicted in Figure 7A, which was disrupted between exon 8 and exon 9 by the T-DNA insertion. The complementation was conducted using the CDS of *At*Tic40 protein followed by either BioID2 or TurboID tag, under the control of 35S promoter (Figure 7B). Thus, two different complemented lines were generated (Δ Tic40+Tic40-BioID2 & Δ Tic40+Tic40-TurboID). Transformation of the WT Col-0 were performed with plasmids containing *At*TrxF1, *At*TrxM2 CDS, *At*Tic40 CDS and *At*Pic1 CDS tagged with either BioID2 or TurboID protein, having 35S promoter in the upstream region (Figure 9 and Supplemental Figure 2). Plasmid insertion into WT Col-0 genome was confirmed via PCR product with appropriate primers designed to amplify CDS and biotin ligase region of each fusion protein (Figure 9 and Supplemental Figure 2). The seeds of each of the identified independent insertion lines were collected individually and used for proximity labeling assays.

Genotyping of the complemented Δ Tic40 (-/-) lines was performed against T-DNA insertion and the respective complementation constructs. T-DNA insertion for Δ Tic40 (-/-) was confirmed by the presence of the PCR product of LB and RP primers and the existence wild-type allele was checked by LP and RP primers (Figure 7C). Construct specific primers were used to amplify the complementation plasmids (Primer F is designed to bind exon 1 region of *At*Tic40 (*At*Tic40 C-D F1) and Primer R is to bind either the downstream region of BioID2 (BioID2 D-E R) or TurboID (TurboID D-E R)). The expected PCR product amplified by these primers confirmed the insertion of the plasmid (Figure 7C).

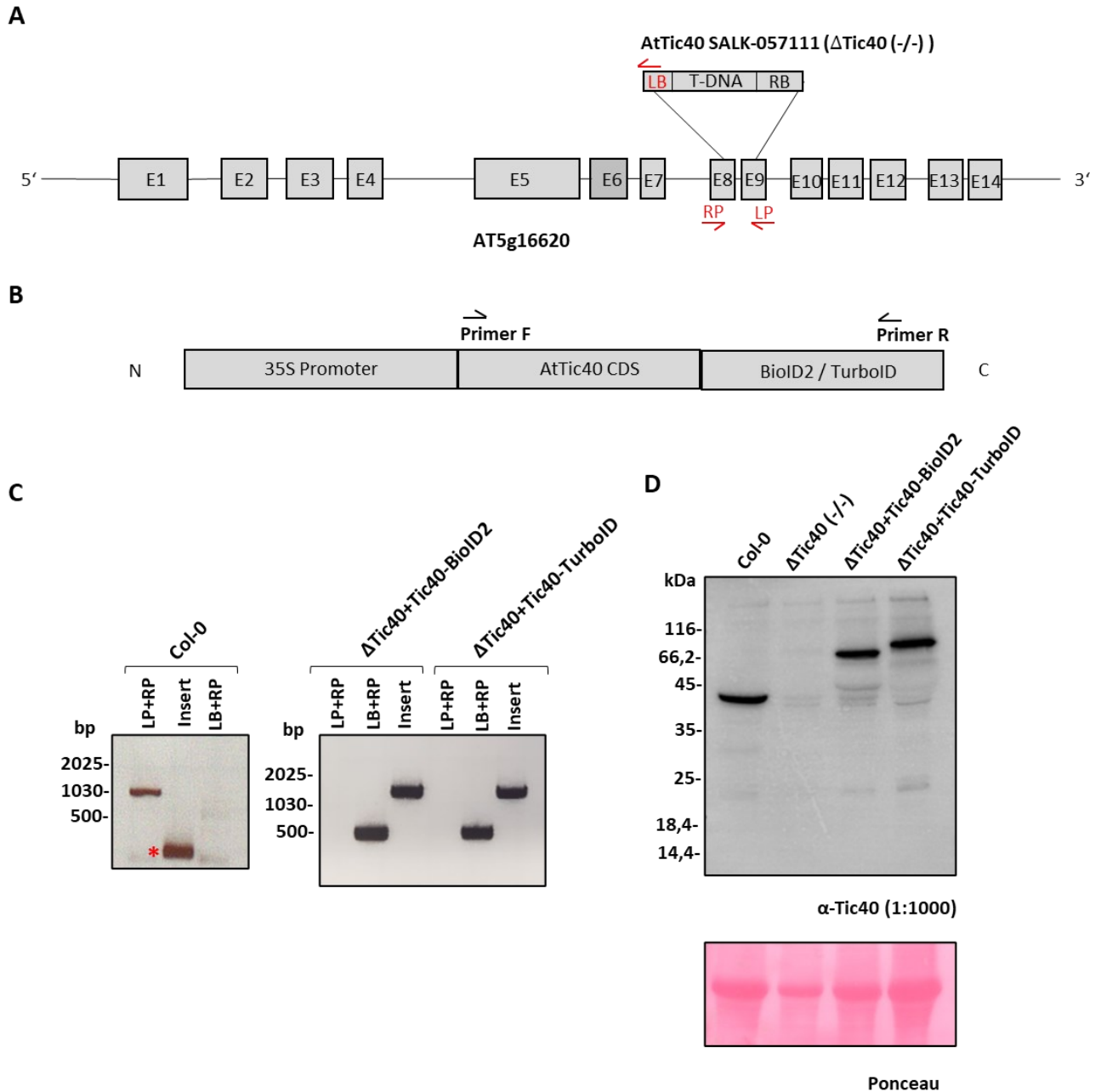


Figure 7: *AtTic40* complementation studies for proximity labeling assay. (A) Diagram of the genomic region encoding *AtTic40* as gene scheme. T-DNA insertion location of SALK-057111 line and genotyping primer binding sites are represented. Exon regions are shown by boxes labeled from E1 to E14. Introns are represented as spaces between neighboring exons. LB, RP and LP primers are listed in the Materials and Methods section as genotyping primers for *AtTic40*. **(B)** Schematic representation of the complete plasmid used for complementation studies. The coding sequence (CDS) of *AtTic40* fused either with BioID2 or TurboID under the control of 35S promoter was inserted into the genome for complementing the SALK-057111 line. The primers used to confirm the insertion are shown as Insert F and Insert R. N: N-terminus, C: C-terminus. The red asterisk (*) sign was used to depict primer dimers. **(C)** Genotyping PCR analysis. The presence of the wild type gene was checked using LP and RP primers. T-DNA insertion was checked via LB and RP primers. The presence of inserted plasmid was confirmed via genotyping primers Insert F and Insert R. The sizes of PCR products are as follows: (LP-RP): ~1000 bp, (LB-RP): ~500 bp, (Insert F-Insert R): ~1500 bp. **(D)** Immunoblot analysis of *AtTic40*

complemented lines using the antibody against Tic40, four weeks old soil-grown plant sample. Col-0 is used as the control sample. Tic40 proteins fused with BioID2/TurboID were detectable near respective sizes (Tic40-BioID2: ~77 kDa and Tic40-TurboID: ~85 kDa). The sample from Δ Tic40 (-/-) lines exhibited no band formation. Around 40 kDa, the Tic40 band was visible in the control sample. Ponceau staining shows the protein loading information.

Immunoblotting analysis was performed to confirm the protein presence within four weeks of soil-grown complemented lines. Total proteins were isolated and used for further research. WT Col-0 was used as positive control while Δ Tic40 (-/-) was negative. α -Tic40 antibody was used for the detection of Tic40 protein. Native Tic40 protein was detected near 40 kDa in the WT Col-0 sample, while none was detectable in Δ Tic40 (-/-) sample (Figure 7D). Tic40-BioID2 and Tic40-TurboID fusion proteins were detectable in the complemented lines at 77 kDa and 85 kDa, respectively (Figure 7D). Additionally, native Tic40 protein was not visible within the complemented lines (Figure 7D). Thus, the immunoblotting supports the successful complementation of Δ Tic40 (-/-) with the cDNA of *AtTic40* followed by either BioID2 or TurboID under the control of 35S promoter.

In addition to biochemical analysis of the complemented plants, physiological observations were carried out. For this reason, complemented lines were selected with related herbicide selection and grown on soil for four weeks. Both WT Col-0 and Δ Tic40 (-/-) plants were used as positive and negative controls, respectively. Complemented plants exhibited faster growth compared to Δ Tic40 (-/-) plants and they have reached a similar height as WT Col-0 plants after four weeks of the growth period in the greenhouse (Figure 8). The Δ Tic40 (-/-) plants exhibited pale green leaf formation due to the absence of Tic40 protein (Chou et al., 2003). The leaf color of the complemented lines was examined as darker than Δ Tic40 (-/-) and lighter than WT Col-0 (Figure 8B), indicating that the BioID2/TurboID tags did not dramatically affect the function of the Tic40 protein. However, it was clear that the complementation was not completely successful as the four weeks old plants did not exhibit the same phenotype as WT Col-0 (Figure 8). It was indicated that Δ Tic40+Tic40-BioID2 & Δ Tic40+Tic40-TurboID plants displayed minor abnormalities such as light green leaf color and decreased number of leaves in comparison to WT Col-0 plants (Figure 8).

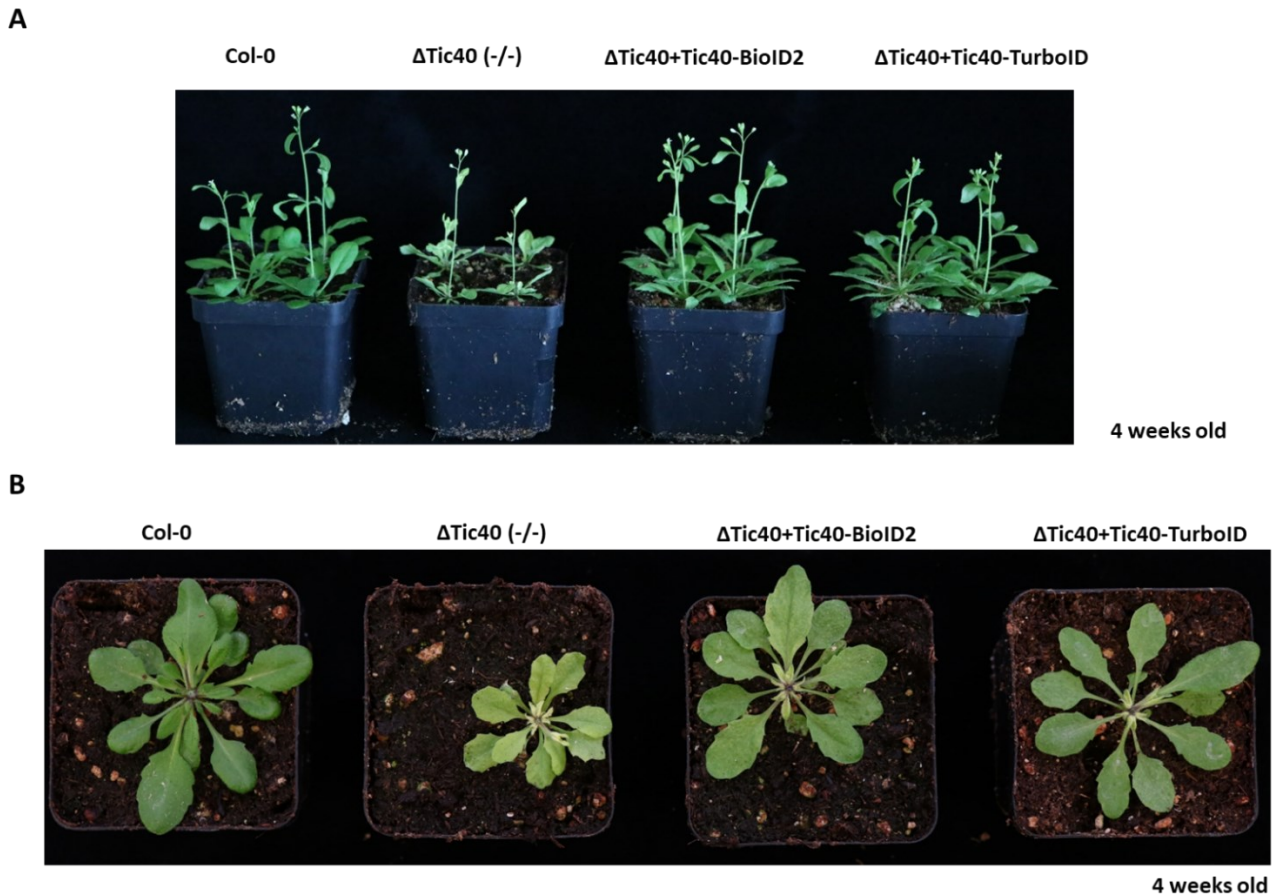


Figure 8: Representative pictures of plants grown for the soil-based phenotyping of *AtTic40* complementation studies. The phenotyping was performed after the herbicide selection of complemented lines. WT Col-0 was used as control. Homozygous *AtTic40* mutant plant (Δ Tic40 (-/-)) exhibited slow growth and pale green phenotype. The plants of complemented lines (Δ Tic40+Tic40-BioID2 & Δ Tic40+Tic40-TurboID) grew faster than the *AtTic40* mutant but relatively slower than the control. The pictures were taken of 4 weeks old plants. **(A)** Vertical depiction of the plants. Each pot consists of 4 plants of the same genotype. **(B)** Top view of the plants. One plant per genotype was represented.

As the mutant phenotype was not rescued entirely after the four weeks of the growth period (Figure 8), the possibility of obtaining false positive biotinylated proteins was estimated to be relatively increased. Therefore, candidate proteins that had been fused with the appropriate biotin ligases had been stably inserted into wild-type backgrounds. The resulting mutant seedlings were then gathered and subjected to herbicide-based selection. Following, the herbicide-resistant plants were allowed to self-pollinate and produce seeds, which were gathered and used for the proximity labeling analysis (Figure 9).

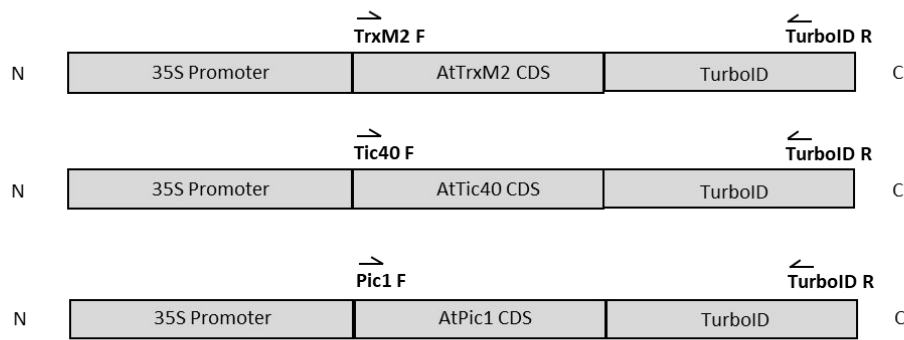
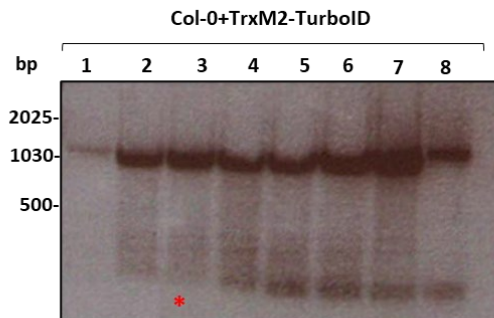
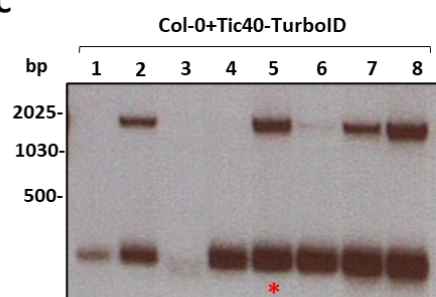
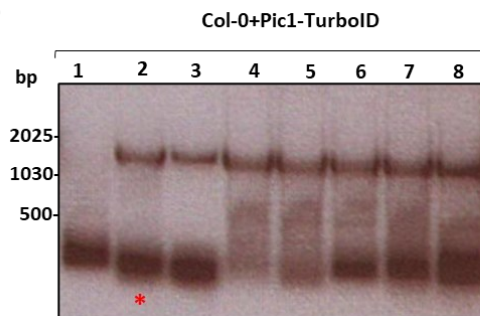
A**B****C****D**

Figure 9: Generation of *Arabidopsis thaliana* plants bearing the TurboID transformed constructs.

(A) Transformed plasmids were represented with schematic depiction. The coding sequence (CDS) of the candidate genes fused with TurboID under the control of 35S promoter was inserted into the genome of WT Col-0. The presence of the inserted plasmid was checked via primers indicated on the plasmid scheme for each candidate gene. TurboID R (TurboID D-E R) is designed to bind downstream region of the TurboID. Independent insertion lines for each fusion plasmids were used for the analysis. The **red asterisk (*)** sign was used to depict primer dimers. N: N-terminus, C: C-terminus. **(B)** Genotyping analysis of TrxM2-TurboID insertion. TrxM2 F (*AtTrxM2* C-D F) binds to upstream region of *AtTrxM2* CDS. Expected PCR product (TrxM2 F + TurboID R): ~ 1000 bp. **(C)** Genotyping analysis of Tic40-TurboID insertion. Tic40 F (*AtTic40* C-D F1) binds to upstream region of *AtTic40* CDS. Expected PCR product (Tic40 F + TurboID R): ~ 1500 bp. **(D)** Genotyping analysis of Pic1-TurboID insertion. Pic1 F (*AtPic1* C-D F1) binds to upstream region of *AtPic1* CDS. Expected PCR product (Pic1 F + TurboID R): ~ 1200 bp.

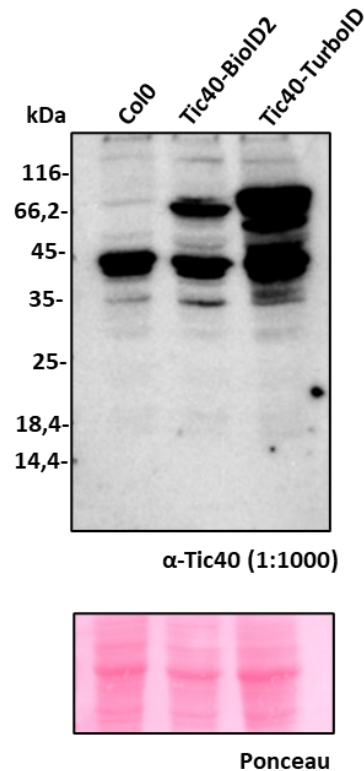


Figure 10: Immunoblot analysis of stable plant lines transformed with Tic40 protein fused with either BioID2 or TurboID. Plasmids carrying the Tic40 protein tagged with BioID2/TurboID were transformed into WT Col-0 *Arabidopsis thaliana* plants. Transformants were selected and grown in the liquid culture for 14 days. Total proteins were extracted from the plants and analyzed by western blot. Immunoblot analysis was performed using an α -Tic40 antibody. WT Col-0 was used as control. Loading information was indicated by ponceau staining. Protein sizes are: Tic40: ~40 kDa, Tic40-BioID2: ~77 kDa, Tic40-TurboID: ~85 kDa.

For a more detailed biochemical analysis, the transformed WT Col-0 plants bearing Tic40-BioID2 and Tic40-TurboID plasmids were grown in liquid culture for 14 days prior to protein extraction. Then, the total proteins were analyzed by immunoblotting using an α -Tic40 antibody. WT Col-0 samples were used as control. The antibody detected the Tic40 band in transformed lines identical to wild-type lines (Figure 10). Moreover, the tagged Tic40 protein bands were visible at the respective sizes (Figure 10). This result, therefore, supports that the wild-type transformation of plasmids containing proximity labeling tools is also suitable for further biotinylation experiments as the mutant background.

3.4.3 Determination of Biotinylation Reaction Parameters for Stable Transformed *Arabidopsis thaliana* Plant Lines

The liquid culture approach was used to determine the optimum reaction conditions for *Arabidopsis thaliana* seeds carrying the proximity labeling plasmids. For this reason, selected

seeds were grown in liquid growth culture for 14 days. The biotin concentration and the reaction time were determined concerning the data observed from *Nicotiana benthamiana* biotinylation. First, the reaction was carried out for 30 mins, 1 hour, 2 hours, 3 hours and 6 hours using 500 μ M biotin solution. Later, the reaction time was set to 6 hours and biotin concentration was changed to 50 μ M, 100 μ M, 250 μ M and 500 μ M, respectively. As discussed before, the seeds from the plasmids bearing TurboID constructs, which were transformed into WT Col-0 background, were used for the proximity labeling experiments. The reaction parameters were adjusted according to the TrxM2 and Tic40 biotinylation characteristics as Pic1 reached the saturation parameters slower (Figure 6). As a control, WT Col-0 seeds were subjected to maximum reaction conditions by utilizing 500 μ M biotin for 6 hours reaction period.

Then, the reaction was terminated by washing the seedlings with ice-cold water 2-3 times prior to protein extraction. Extracted proteins were analyzed by immunoblotting against α -biotin antibody. TrxM2 exhibited biotinylation by using 250 μ M and 500 μ M biotin solution (Figure 11A,11B), while the reaction was initiated by 100 μ M biotin for Tic40 (Figure 11C,11D). In terms of reaction time, the TrxM2 needed 6 hours for efficient biotinylation (Figure 11A), whereas 2 hours was adequate for biotinylation initiation of Tic40 (Figure 11C). However, the total amount of biotinylated proteins were significantly different between TrxM2 and Tic40 proteins.

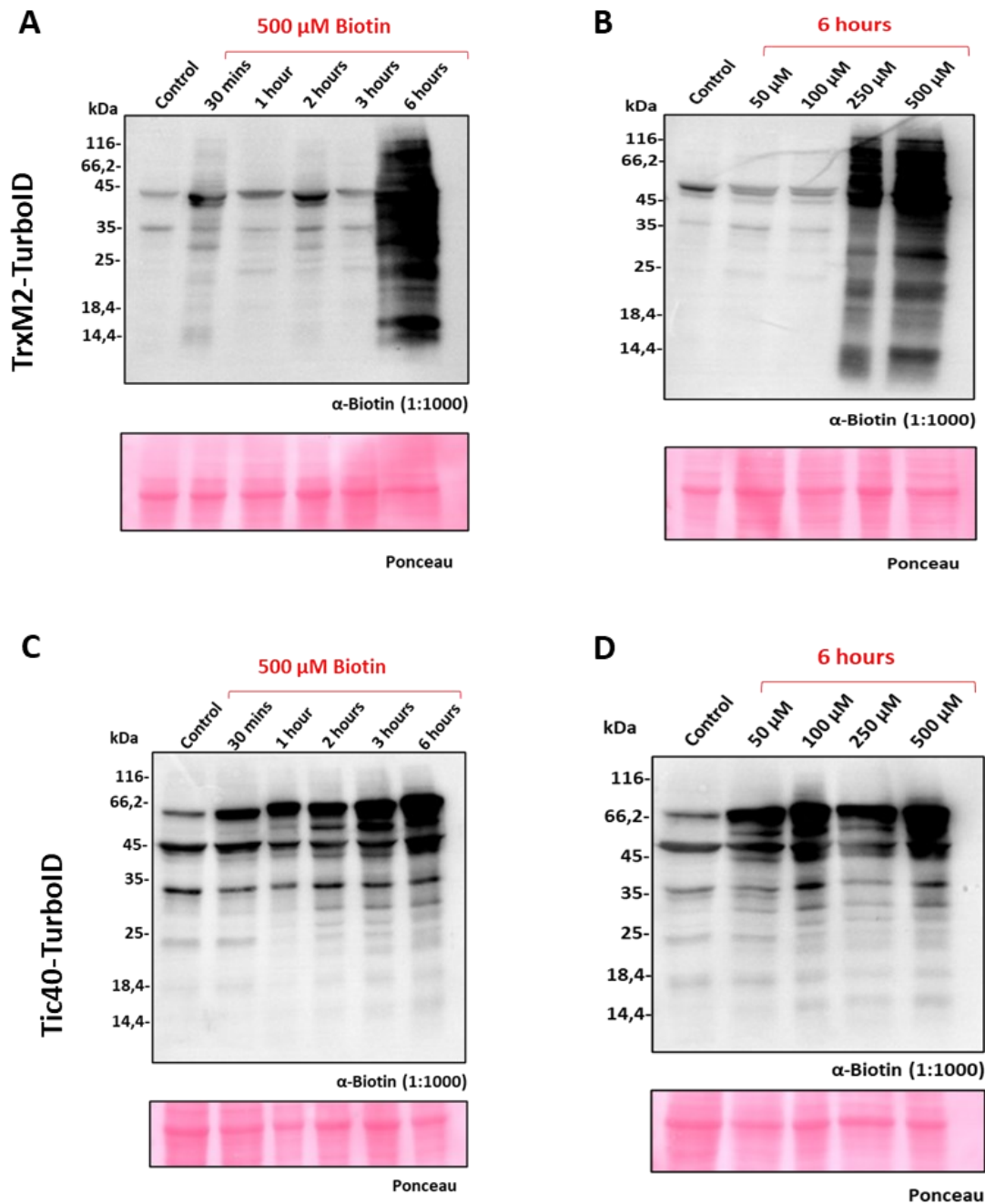


Figure 11: TurboID fused TrxM2 and Tic40 proteins indicated different biotinylation patterns depending on the biotin concentration and the reaction time. Stably transformed *Arabidopsis thaliana* seeds were grown in the liquid culture for 14 days. The biotin solution at the concentration of 500 μ M was added to the medium for the biotinylation reaction. Immunoblots were done by isolating total protein from the plants grown in liquid cultures. Untransformed WT Col-0 plants were used as control. α -Biotin antibody was used to detect biotinylated proteins. The time parameter was determined using various time points (30 mins, 1 hour, 2 hours, 3 hours, 6 hours) when the biotin concentration was set to 500 μ M. The optimal biotin concentration was determined by checking 50 μ M, 100 μ M, 250 μ M and 500 μ M concentrations while the reaction was carried out for 6 hours. Control groups were subjected to final parameters (e.g., 6 hours of reaction time using 500 μ M biotin solution). **(A)** Genotype: TrxM2-TurboID plasmid expressing in WT Col-0 background, Investigated reaction parameter: Reaction Time. **(B)** Genotype: TrxM2-TurboID plasmid expressing in WT Col-0 background,

Investigated reaction parameter: Biotin Concentration. **(C)** Genotype: Tic40-TurboID plasmid expressing in WT Col-0 background, Investigated reaction parameter: Reaction Time. **(D)** Genotype: Tic40-TurboID plasmid expressing in WT Col-0 background, Investigated reaction parameter: Biotin Concentration.

Different time points and biotin concentrations resulted in various labelling efficiencies. Biotinylation reaction by using TrxM2 as bait protein was more efficient compared to Tic40 (Figure 11A, 11B). On the other hand, Tic40 guided biotinylation of adjacent proteins was detectable on the immunoblots (Figure 11C, 11D). Concerning results, the parameters were adjusted to the 500 μ M biotin usage for 6 hours of reaction period. The reason for setting the same reaction parameters for each fusion protein was to prevent over biotinylation of the prey proteins and thus avoid misidentification by mass spectrometry. Subsequently, the proximity labeling was performed with determined parameters for the candidate proteins, TrxM2, Tic40 and Pic1. As predicted, the TrxM2 achieved great biotinylation over time, as indicated in immunoblotting results (Figure 12). Labeling of the interaction partners for Tic40 and Pic1 was relatively lower than TrxM2 (Figure 12). The endogenous biotinylation was neglected as only some bands were distinguishable in WT Col-0 samples (Figure 12). It was concluded that the optimal reaction parameters for biotin labeling were achieved, and they were reliable for further protein identification steps.

Similar approach was followed for catalyzation of BioID2 mediated proximity labeling. The reaction was carried out with 500 μ M biotin solution and stopped after 18 hours. Extracted total proteins were subjected to immunoblotting analysis, which was resulted in exhibiting biotinylated proteins (Supplemental Figure 2). Surprisingly, there was no significant biotinylation pattern difference in candidate proteins' samples compared to WT Col-0 (Supplemental Figure 2). These data suggest that the BioID2 mediated biotinylation was not achieved or the candidate proteins somehow interrupted the activity of BioID2. In any case, it was shown that the TurboID biotin ligase promotes proximity protein biotinylation more efficiently than BioID2, when the reaction was carried out at room temperature. Thus, further steps were adjusted and employed depending on TurboID mediated proximity labeling.

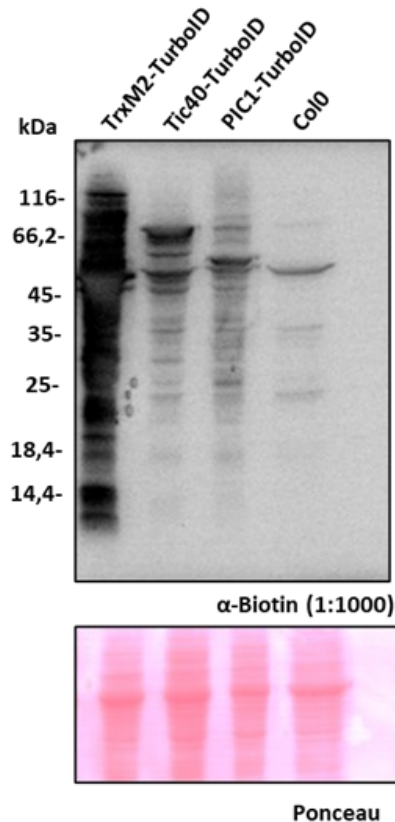


Figure 12: Stably transformed plant lines expressing candidate proteins tagged with TurboID exhibited great biotinylation over time. The biotin concentration of the reaction was 500 μ M and the reaction was stopped after 6 hours of incubation. Total proteins were extracted and used for immunoblotting. Biotinylated protein detection was achieved by using specific antibody to biotin. Smear like bands indicated the interaction partners for the candidate proteins. WT Col-0 plants were used as control. Ponceau staining shows the protein loading information.

Furthermore, the presence of candidate proteins tagged with TurboID in stable plant lines was examined by immunoblotting against α -bioID antibody (Supplemental Figure 4). TrxM2-TurboID was detected around 56 kDa clearly (Supplemental Figure 4A). The Tic40-TurboID and Pic1-TurboID bands were slightly visible, indicating the low protein abundance (Supplemental Figure 4B). Overall, these data verify that the transformation of candidate proteins tagged with proximity labeling tools was successful and expressed fusion proteins were capable of biotinylation reaction initiation.

3.4.4 Identification of Interaction Partners by TurboID Mediated Proximity Labeling

Following establishing the proper biotinylation conditions for *Arabidopsis thaliana* seeds, the next step was to analyze the labeled proteins. For this reason, BioID2 and TurboID tagged lines were utilized. BioID2 mediated biotinylation did not generate a suitable dataset for further statistical analyses. Thus, protein interactome data produced by TurboID biotinylation were

used and subjected to statistical analyses. This result further confirms that the TurboID enzyme provides reliable outcomes concerning the application in plant-based studies.

Next, stably transformed plant lines were used to identify interaction partners for candidate proteins. After 14 days of growth in the liquid culture, total proteins were isolated and subjected to affinity purification. Captured proteins were analyzed using liquid chromatography coupled to tandem mass spectrometry (LC-MS/MS). Quantification was carried out by label-free quantification by MaxQuant and Perseus was used for subsequent filtering and subsequent data analysis of identified proteins. Proteins that were not significantly enriched in the TurboID samples compared to wild type were removed to eliminate the background proteins. The dataset then resulted in 911, 890 and 333 significantly enriched proteins for TrxM2, Tic40 and Pic1, respectively. A second filtering step was applied to select the chloroplast localized proteins within the enriched ones. This approach brought high confidence candidates, 350, 332 and 125 proteins for TrxM2, Tic40 and Pic1, respectively (Supplemental Table 2, 3, 4). Proteins included in the Pic1 interactome were eliminated from TrxM2 and Tic40 interaction list as the third filtering step. During the establishment of the project, Pic1 protein was selected as the negative control group. As a result, 228 and 209 interacted proteins were identified for TrxM2 and Tic40, respectively (Figure 13A, 13B). The comparison between TrxM2 and Tic40 interactome has revealed that these two proteins were associated with 327 proteins in common (Figure 13C). The number of proteins interacting with only TrxM2 and Tic40 counted as 23 and 5, respectively and summarized in Table 17.

According to the comparison of the interactomes of the TrxM2 and Tic40, the two proteins have many associated proteins in common, however there are also proteins that are distinctive to either TrxM2 or Tic40 (Table 16, 17 and see Appendices). Proteins involving in translation, transcription, photosystem-I assembly, starch biosynthesis, photo-oxidative stress response and glycogen biosynthesis were found to be interacting with TrxM2 specifically (Table 17). Tic40 was shown to be specifically associating with the components of iron homeostasis (PIC1, FC1), ribosomal assembly factors (rpl20), carotenoid biosynthesis (LCY1) and chaperone system (BAG1) when compared to TrxM2 (Table 17). Hence, more biochemical analyses should be carried out to understand the mentioned interactomes better. The datasets could be considered an initial screening for a complex research project.

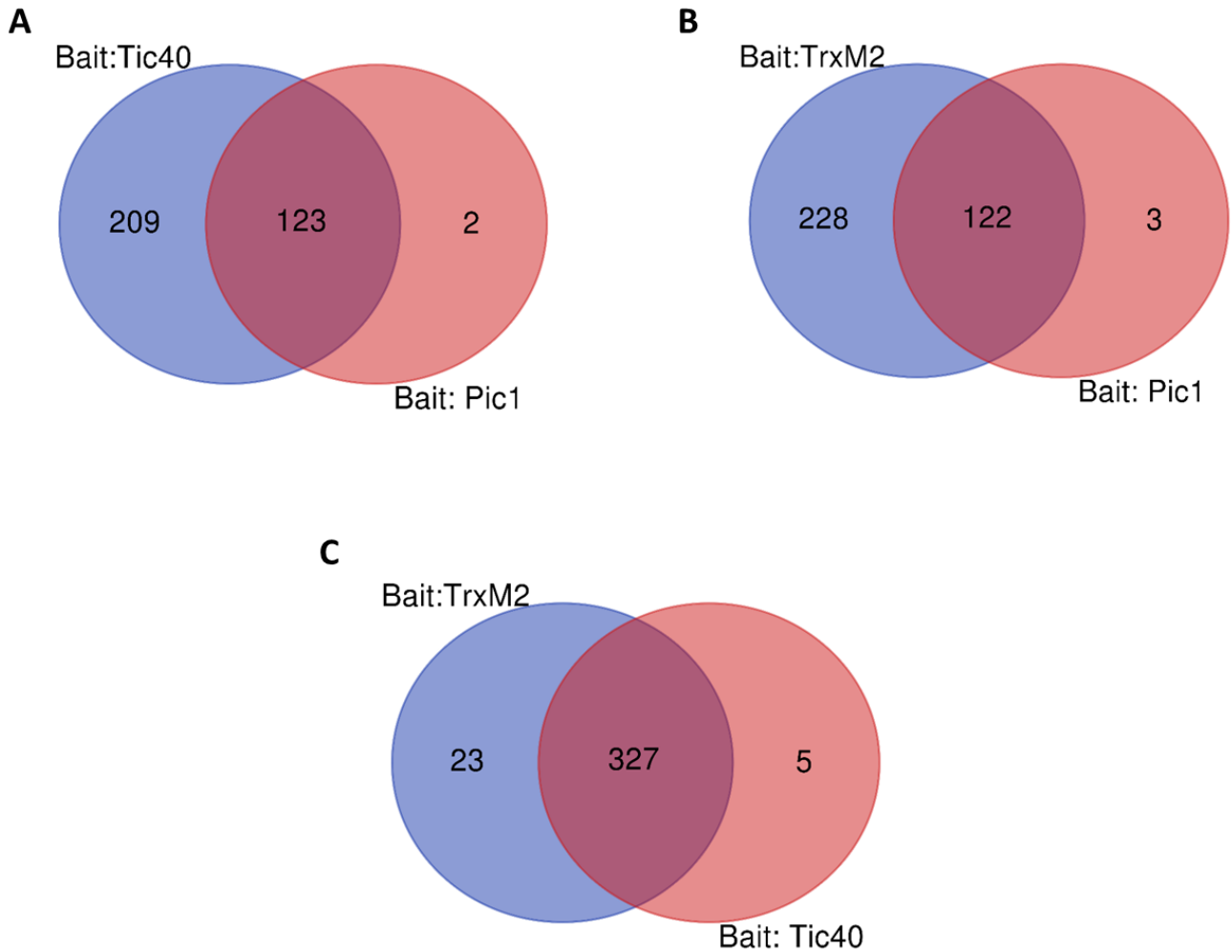


Figure 13: Venn diagram comparison of identified chloroplastic interaction partners by proximity labeling. Biotinylated proteins were identified using mass spectrometry and generated data was modified using statistical analysis tools. Chloroplast destined enriched proteins were taken into consideration for further filtering steps. Each Venn diagram depiction showed both individual and mutual associating proteins of respective bait protein. **(A)** Comparison between Tic40 and Pic1. **(B)** Comparison between TrxM2 and Pic1. **(C)** Comparison between TrxM2 and Tic40.

Table 17: Specific proteins associating/interacting with TrxM2 and Tic40, respectively. Venn diagram comparison was carried out between TrxM2 and Tic40 related proteins-chloroplast located.

Specific Preys for	Gene Name	Functional Annotation
TrxM2		
AT1G08520	CHLD	Magnesium-chelatase subunit ChLD
AT5G03420	PTST	Protein PTST homolog 3 (PROTEIN TARGETING TO STARCH homolog 3)
AT4G11010	NDPK3	Nucleoside diphosphate kinase III
ATCG00830	rpl2-A	50S ribosomal protein L2
AT2G34640	PTAC12	Protein PLASTID TRANSCRIPTIONALLY ACTIVE 12
AT2G40300	FER4	Ferritin-4
AT5G52520	OVA6	Proline--tRNA ligase (Protein OVULE ABORTION 6)
AT5G36790	PGLP1B	Phosphoglycolate phosphatase 1B
AT5G19220	ADG2	Glucose-1-phosphate adenylyltransferase large subunit 1
AT3G63190	RRF	Ribosome-recycling factor
AT5G12040	NLP3	Omega-amidase (Nitrilase-like protein 3)
AT5G44650	Y3IP1	Ycf3-interacting protein 1
AT5G30510	RPS1	30S ribosomal protein S1
ATCG00430	ndhK	NAD(P)H-quinone oxidoreductase subunit K
ATCG00170	rpoC2	DNA-directed RNA polymerase subunit beta
AT1G32900	GBSS1.8	Granule-bound starch synthase 1
ATCG00730	petD	Cytochrome b6-f complex subunit 4
AT5G22630	ADT5	Arogenate dehydratase 5
AT2G36390	SBE2.1	1,4-alpha-glucan-branching enzyme 2-1
ATCG00790	rpl16	50S ribosomal protein L16
ATCG00180	rpoC1	DNA-directed RNA polymerase subunit beta
AT4G39970		Haloacid dehalogenase-like hydrolase domain-containing protein
AT2G47390	GEP	Probable glutamyl endopeptidase
Specific Preys for		
Tic40		
AT3G10230	LYCB, LCY1	Putative lycopene beta-cyclase
AT2G15290	TIC21, PIC1	Protein TIC 21, Permease in Chloroplasts 1
ATCG00660	rpl20	50S ribosomal protein L20
AT5G26030	FC1	Ferrochelataase-1
AT3G29310	BAG1	BAG family molecular chaperone regulator 8

Data visualization through Venn diagrams and scatter plots were performed by using the chloroplast localized prey proteins (Figure 13, 14) For this reason, proteins were investigated concerning log₂ fold change and -log₁₀ p-value for each bait protein independently from each other. The proteins which have log₂ fold change ≥ 1.5 and -log₁₀ p-value < 0.05, were highlighted in the scatter plot visualization (Figure 14), hence, the probability of these proteins being partner proteins was relatively higher. Due to the autobiotinylation, the bait proteins were found to be highly abundant in their interactome datasets.

Tic110 has appeared as a common interaction protein for all bait proteins, Tic40, TrxM2 and Pic1 (Figure 14). Interestingly, Stic2, a potential suppressor of Tic40 protein (Bédard et al., 2017), was found to be interacting with both Tic40 and Pic1 (Figure 14A-14C). It has been debated for a long time that Hsp93III and Hsp93V proteins play an essential role in protein translocation by associating with Tic40 (Chou et al., 2003; Kovacheva et al., 2005; Inoue et al., 2013). However, the proteins Hsp93V and Hsp90C were identified as interaction partners for Tic40 (Supplemental Table 2), suggesting a complex interaction network. Moreover, the Tic40 interactome classifies Hsp70 as an associating protein of Tic40 and comprises many ClpP protease subunits (Supplemental Table 2).

Interestingly, none of the previously characterized interacting proteins for TrxM2 (Table 16) were detected by proximity labeling (Supplemental Table 3). Instead, Tic62, a part of redox regulon consisting of Tic32-Tic55-Tic62 (Balsera et al., 2007), was found to interact with TrxM2 (Figure 14B). Furthermore, Tic40 was identified to be associating with TrxM2, implying that they might involve in a similar biological process (Figure 14B).

There was not adequate experimental data available concerning Pic1 associating proteins. Therefore, this protein was previously considered as not interacting with the TrxM2 and Tic40. Proximity labeling revealed 125 prospective proteins associated with Pic1 (Supplemental Table 4). Notably, TrxM2, Tic40 and Stic2 were also involved in the Pic1 interactome (Figure 14C). These data suggest that more analyses were required to understand the function of the Pic1 fully. However, our data would be a starting point for such detailed characterization.

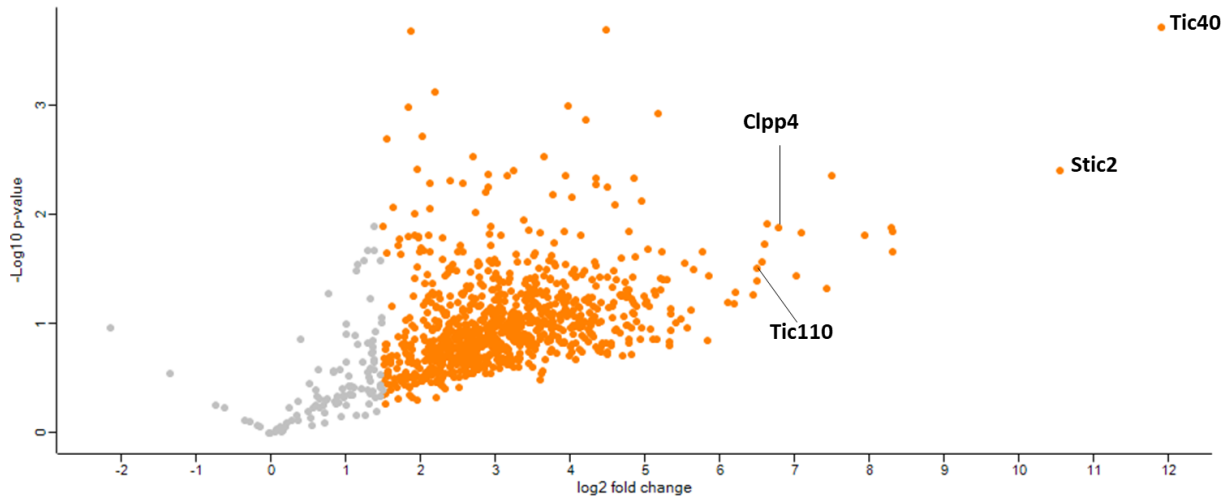
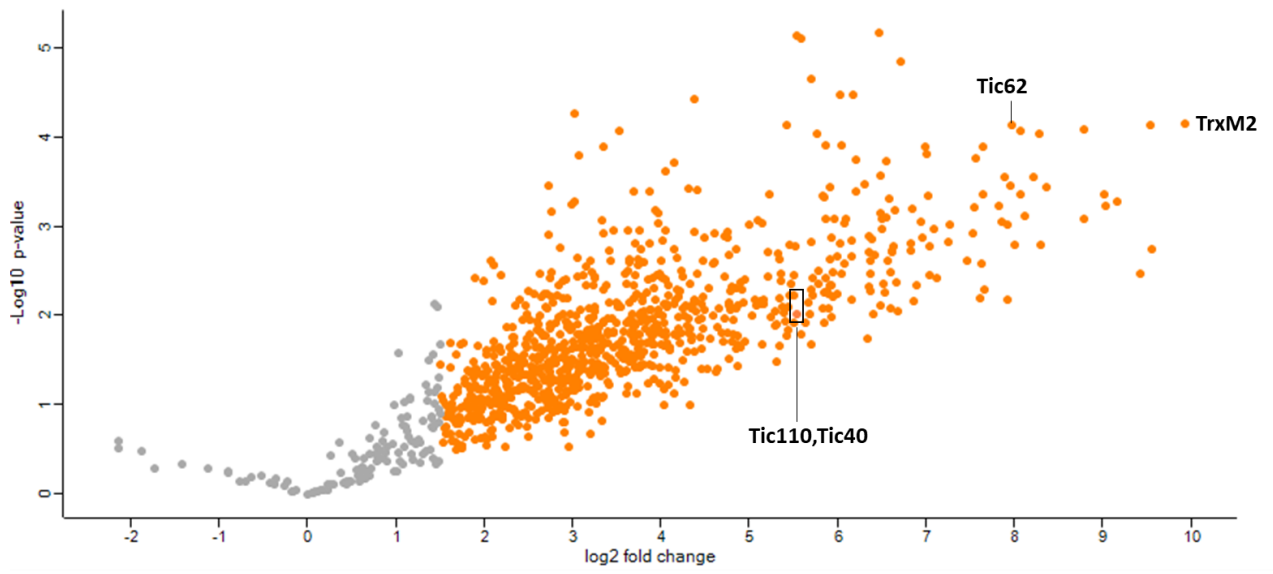
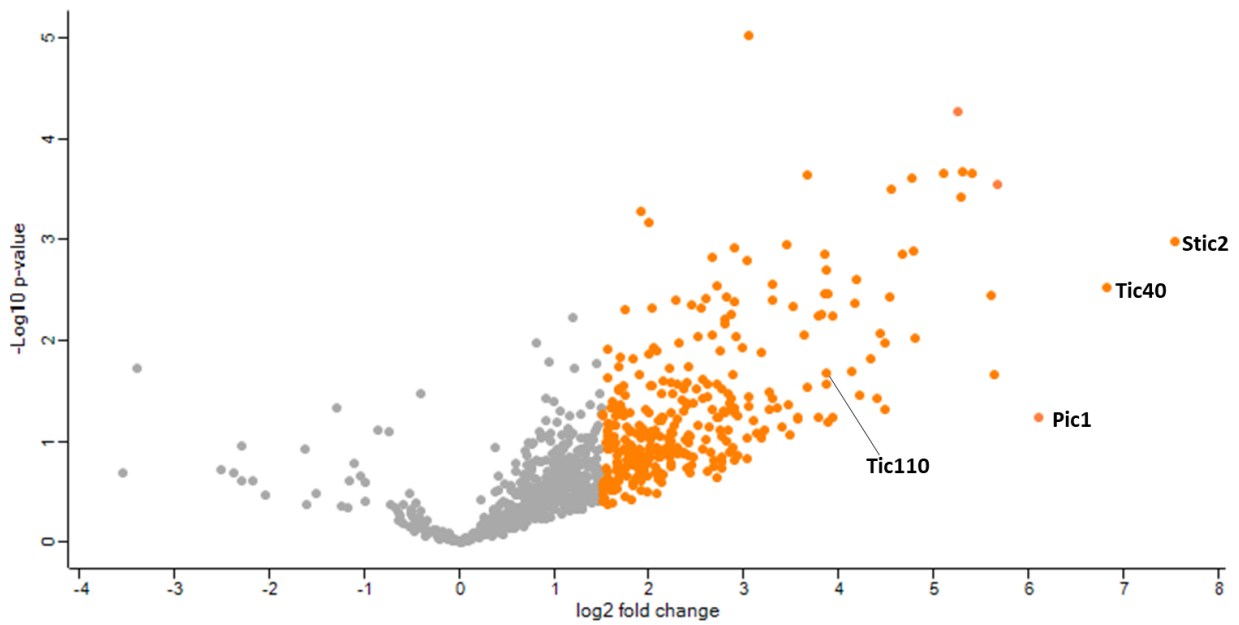
A**B****C**

Figure 14: Scatter plot visualization of prey proteins for each candidate protein (Tic40, TrxM2 and Pic1) identified by proximity labeling. Chloroplast localized prey proteins were represented in the graph as a node. The orange color was used when the preys have fold change ≥ 1.5 and p-value < 0.05 . Significant interaction partners were exhibited by their protein name next to each node. **(A)** Interactome for Tic40. **(B)** Interactome for TrxM2. **(C)** Interactome for Pic1.

Within the scope of this thesis, it is further confirmed that the yield of TurboID mediated biotin labeling is more efficient than BioID2. Besides, it was proven that membrane-bound proteins (Tic40 and Pic1) were suitable for proximity labeling by TurboID, as only nuclear proteins were previously used (Mair et al., 2019). Furthermore, our results indicated that the TurboID enzyme is applicable for organelle-based proximity labeling analysis. In conclusion, we have constituted a proximity labeling protocol and generated interactomes of three chloroplast-localized proteins (TrxM2, Tic40 and Pic1). Each generated data set contains the information of the plant cell specific organellar proteome for corresponding candidate proteins.

3.5 Establishment of the Survival Selection DHFR* Reporter Protein-Fragment Complementation Assay in Plant Species

The general route for chloroplast-destined proteins is known by the main players in the pathway. However, the intermediate interacting proteins and regulating factors are not yet identified. Thus, we aim to conduct a forward genetic screen with an *Arabidopsis thaliana* line suitable for organelle-specific selection. For this reason, the DHFR* based protein fragment complementation assay (PCA) was coupled with a split-GFP system. The two systems were combined using the golden gate plasmid assembly technique and transformed into a wild-type background. Therefore, the resulting transformants were selected concerning the plasmid segregation rate and collected seeds. A forward genetic screen was conducted by using EMS mutagenesis. The mutated seeds were further screened by survival rate in the presence of MTX. Lastly, we intend to select survival plants that indicate chloroplast deficiency on an MS medium containing plate with MTX selection.

Dihydrofolate reductase (DHFR) catalyzes the formation of tetrahydrofolate from dihydrofolate, and its activity is inhibited by methotrexate (MTX) (Michnick et al., 2010). A mutated version, namely DHFR*, was investigated to be MTX resistant. Previously, it has been shown that the *Arabidopsis thaliana* lines expressing DHFR* can proliferate on MTX-containing MS plates (Primary data from PD. Dr. Serena Schwenkert). Therefore, we aim to couple the survival-selection ability of DHFR* with organelle-specific targeting. For this reason, a split version of DHFR* was attached by a split GFP that has the self-assemble ability; hence, the

fragments of DHFR* were brought together by the interaction of two GFP parts. One fragment was attached to a chloroplast transit peptide to give the organelle-specific information, which eventually will be located in the chloroplast. The MTX resistance will be visible only in two parts close to the reconstitution of the DHFR* activity (Figure 15). Therefore, EMS mutagenesis of the seeds expressing the split GFP-split DHFR* system will ultimately lead to a deficiency in the chloroplast translocation system. This defect will lead to the accumulation of the chloroplast destined fragment in the cytosol; hence, it triggers the MTX resistance by forming the functional DHFR* enzyme. Finally, the survived plants will be further characterized by their metabolic pathways and unidentified players of chloroplast biogenesis will be discovered.

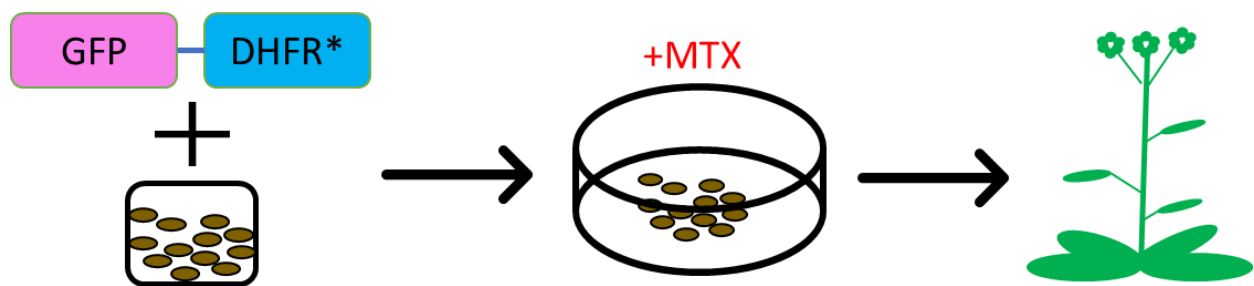


Figure 15: Schematic summary of the activity survival-selection based protein-fragment complementation assay (PCA) depending on the DHFR* reporter. A split version of DHFR* was coupled with a self-assemble split GFP fragment and cloned into a plasmid via golden gate plasmid assembly. *Arabidopsis thaliana* seeds were transformed with the plasmids bearing the constructs. The resulted transformants were able to grow on MS medium containing MTX toxin.

To assemble such PCA, each fragment was subsequently cloned into the golden gate plasmid assembly system (Table 13, 14). The main question of this technique was how the fusion of complementary reporter fragments (split-GFP and split-DHFR* fragments) could influence the activity of the fusion protein. As a proof of principle, the generated plasmids were first checked using *Nicotiana benthamiana* in terms of self-assembly. The hypothesis was that if the constructs will find each other in space and promote functional protein recovery, we could observe GFP signals in the stroma and resistant plants to MTX. To validate the localization of the plasmid carrying the respective constructs, *Nicotiana benthamiana* leaves were infiltrated with *Agrobacteria* bearing the corresponding plasmids. Then, protoplasts were isolated, and confocal microscopy was used to check the GFP and autofluorescence signals. Split constructs were able to find each other and recover the protein function; thus, the GFP signal was visible within the cytosol region of the protoplasts (Figure 16A-16B). Transit peptide caused the corresponding fragment to translocate to the stromal side of chloroplast; the two parts of the

split-GFP could not find each other. Thus, the reconstruction of the GFP protein was inhibited and the relevant signal was not detected (Figure 16C-16D).

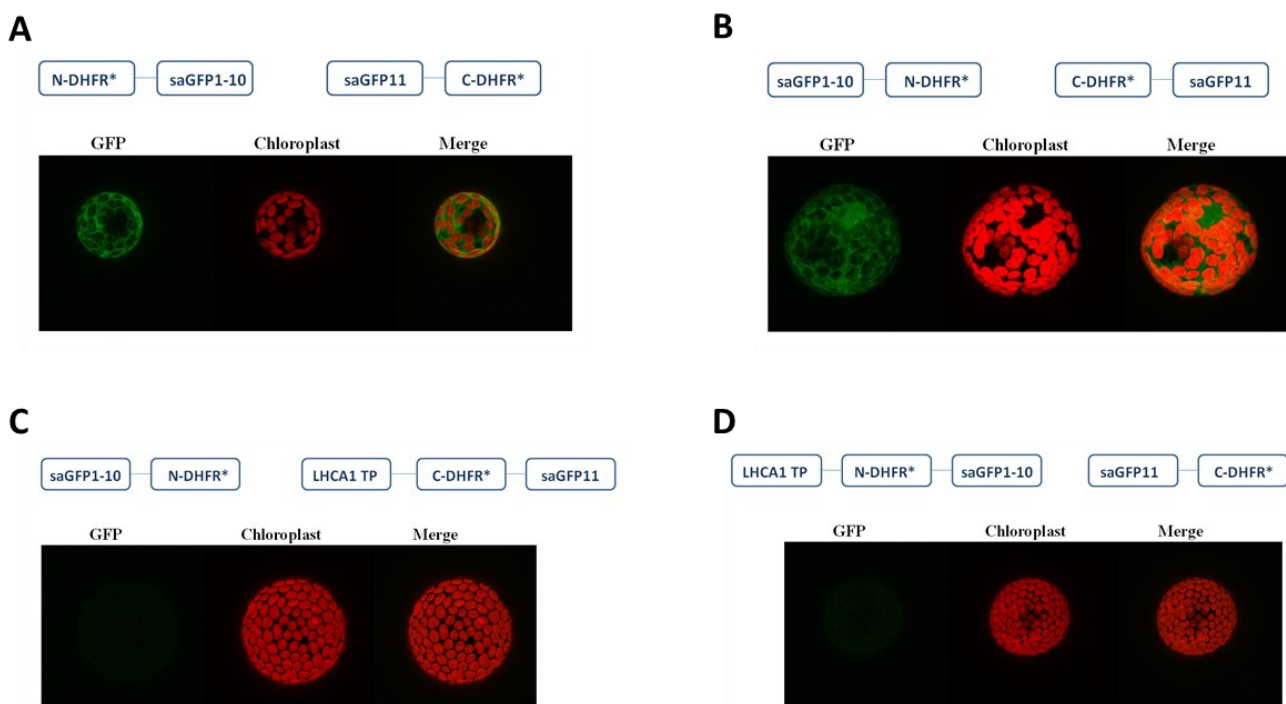


Figure 16: Plasmids bearing the fragments of DHFR* dependent PCA coupled with self-assemble GFP could promote GFP signal. Constructs were transformed to *Nicotiana benthamiana* leaves and incubated for 2-3 days. Protoplasts were isolated and analyzed with confocal microscopy. The GFP fluorescence was localized around the autofluorescence of chlorophyll from chloroplasts indicating its localization in the cytosol. The addition of transit peptide leads the corresponding part destined to the chloroplast, leading to the loss of GFP signal. The successful two different plasmid combinations were analyzed. The fragment information of each plasmid was represented above each figure. N-DHFR*: N-terminal part of DHFR* protein, saGFP1-10: self-assemble GFP protein with 1-10 domains, saGFP11: Domain 11 of self-assembly GFP protein, C-DHFR*: C-terminal part of DHFR* protein, LHCA1 TP: Transit peptide of LHCA1 protein, BASTA: Glufosinate-Ammonium **(A-B)** Fragment combinations without the transit peptide. **(C-D)** Fragment combinations with transit peptide.

Confocal microscopic analyses have revealed that the reconstruction of self-assembly GFP was successful. To check the functionality of the reconstituted DHFR* protein, small pieces of *Nicotiana benthamiana*, infiltrated with DHFR* dependent PCA fragments, were put on MTX containing MS plates. The plates were incubated in a growth chamber and the senescence rate of the leaves was recorded. Wild type *Nicotiana benthamiana* was used as control, while DHFR* FL plasmid expressing *Nicotiana benthamiana* was taken as the positive control. A significant difference between the leaves was observed after 14 days of incubation. Increasing MTX concentration has accelerated the rate of senescence, as observed in wild type (Figure 17). Fragments, including transit peptides, were deficient in DHFR*; hence, the respective leaves

turned brown faster than the positive control DHFR* FL (Figure 17). The accomplished reconstitution of DHFR* with the self-assembly GFP system has led leaves to gain resistance to MTX toxin, as their color was greener compared to wild-type and transit peptide-containing leaves (Figure 17). As expected, DHFR* FL promoted resistance to the MTX, and the leaves were observed as greener compared to the wild type (Figure 17).

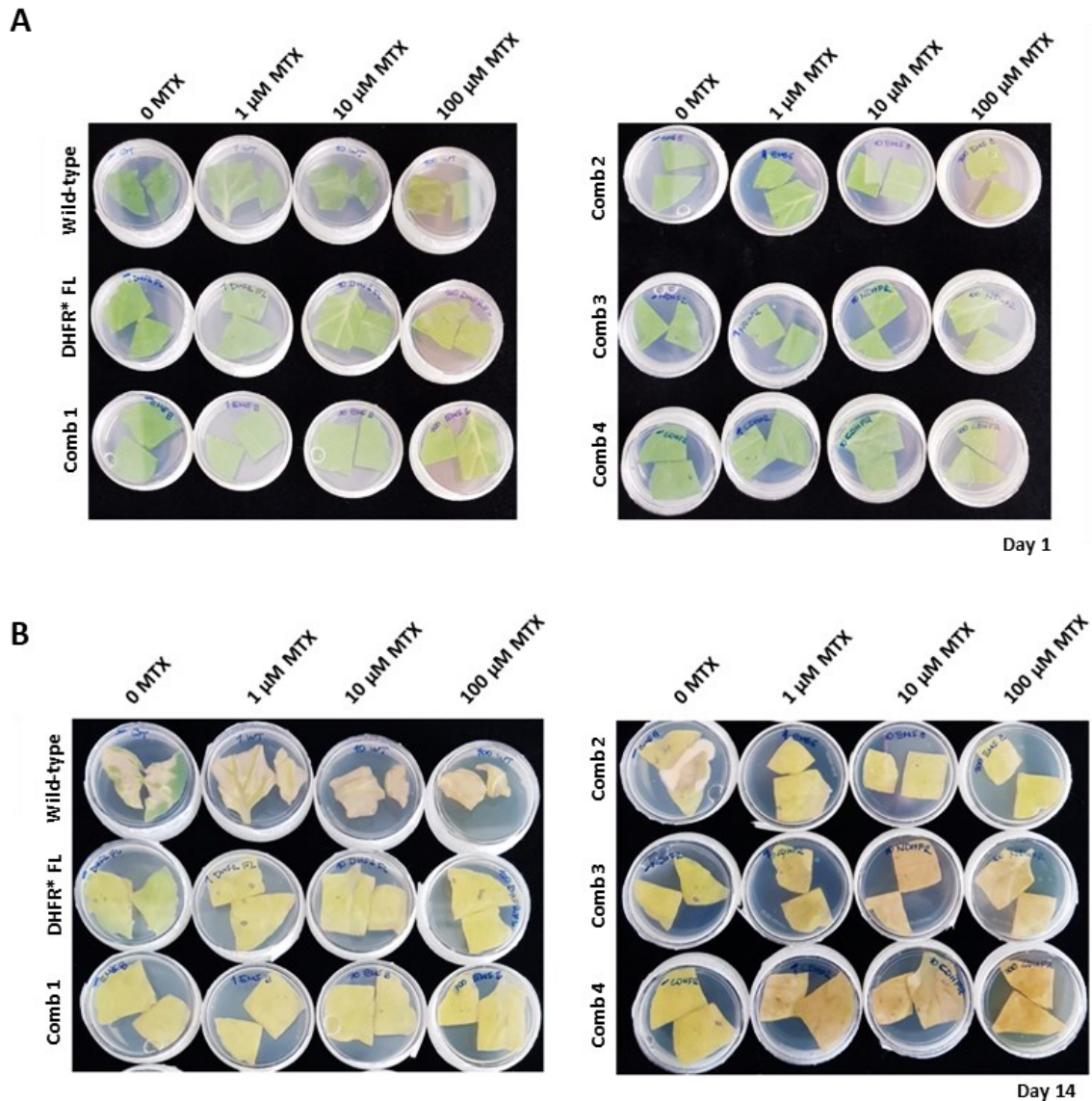


Figure 17: *Nicotiana benthamiana* leaves infiltrated with DHFR* dependent PCA constructs could resist MTX-dependent toxicity. Infiltrated leaves were disintegrated into small pieces after 2-3 days of incubation. Two pieces were put together into a 60 mm x 15 mm petri dish containing MS medium supplemented with increasing concentrations of MTX (0, 1 μ M, 10 μ M, 100 μ M MTX). The Petri dishes were incubated in a growth chamber (16 h light/ 8h dark, 22°C, 100 μ mol / m²s⁻¹ in fluorescent light conditions). The leaf senescence difference was observed after 14 days. Wild type *Nicotiana benthamiana* leaves were used as negative control and leaf pieces carrying the plasmid bearing DHFR* full length were used as the positive control. All four fragment combinations were examined individually. **Comb 1:** NDHFR*-saGFP1-10 + saGFP11-CDHFR*, **Comb 2:** saGFP1-10- NDHFR* + CDHFR*.saGFP11, **Comb 3:** LHCA1 TP-NDHFR*-saGFP1-10 + saGFP11- CDHFR*, **Comb 4:** saGFP1-10-NDHFR* + LHCA1 TP- CDHFR*.saGFP11. **(A)** Leaves before the incubation period on MTX containing

MS medium. The color of the leaves was green. **(B)** The change of leaf senescence was visible after 14 days of incubation. Transit peptide-containing leaves were exhibited brownish color as compared to DHFR* expressing ones. The increasing MTX concentration was used.

Additionally, it was observed that the wild-type leaves exhibited greater sensitivity to MTX compared to *Agrobacterium* transformed leaves. The plant immune system is the possible explanation for this reaction. The infiltration of *Agrobacterium* might trigger the wound-response pathways as the process damages the leaf tissue; hence the rapid immune response changes the structure of the plant cell wall by producing polysaccharides. Thus, it stabilizes the structure (Voigt, 2014). This response possibly gave rise to a thicker cell wall that would limit the MTX diffusion through living cells.

3.5.1 Generation of *Arabidopsis thaliana* Plant Lines Suitable for DHFR* Dependent PCA

Transient expression of the PCA fragments has proven the functional reconstitution of both GFP and DHFR* enzymes. To further confirm our DHFR* dependent PCA system hypothesis, *Arabidopsis thaliana* lines expressing corresponding plasmids were generated. For this reason, the wild-type Col-0 plants were transformed with respective plasmids. Later, the resulting seeds were selected according to the herbicide selection and the next generations were further analyzed by survival/death rate calculation on the MS plate. Lastly, the successful transformants were subjected to MTX toxin and observed throughout their development.

As a parallel to the outcome of transient expression studies, stably transformed lines were resistant to MTX toxin; thus, they continued their development and maintained green plant color (Figure 18A and Supplemental Figure 5A). Transit peptide interrupted the reformation of DHFR* enzymes; consequently, plants became vulnerable to MTX toxin and could not grow (Figure 18B and Supplemental Figure 5B). The control group of each line, grown on MTX-free MS medium, maintained normal development (Figure 18 and Supplemental Figure 5).

Due to the nature of the T-DNA insertion via *Agrobacterium*, various phenotypes will be obtained (Valentine et al., 2012). Thus, two different DHFR* fragment combinations were evaluated, and consequently, exhibited distinct growth behavior in the presence of MTX (Figure 18 and Supplemental Figure 5). Therefore, the more MTX-sensitive line was considered for further concentration determination studies.

The optimal MTX concentration determination was needed to confirm the working principle for DHFR* dependent PCA. For this reason, various amounts of MTX solution were added to the MS medium concerning the end concentration (10 nM, 100 nM, 250 nM, 500 nM, 750 nM, 1 μ M and 100 μ M). Wild type Col-0 and DHFR* FL expressing seeds were investigated; consequently, it was observed that the increasing MTX concentrations did not entirely disrupt the growth of plants having additional DHFR* FL enzyme (Figure 19A). On the other hand, any MTX addition has heavily affected the development of wild-type plants (Figure 19A). Therefore, a working concentration of 100 nM was preferred, at which wild-type plants stopped their growth.

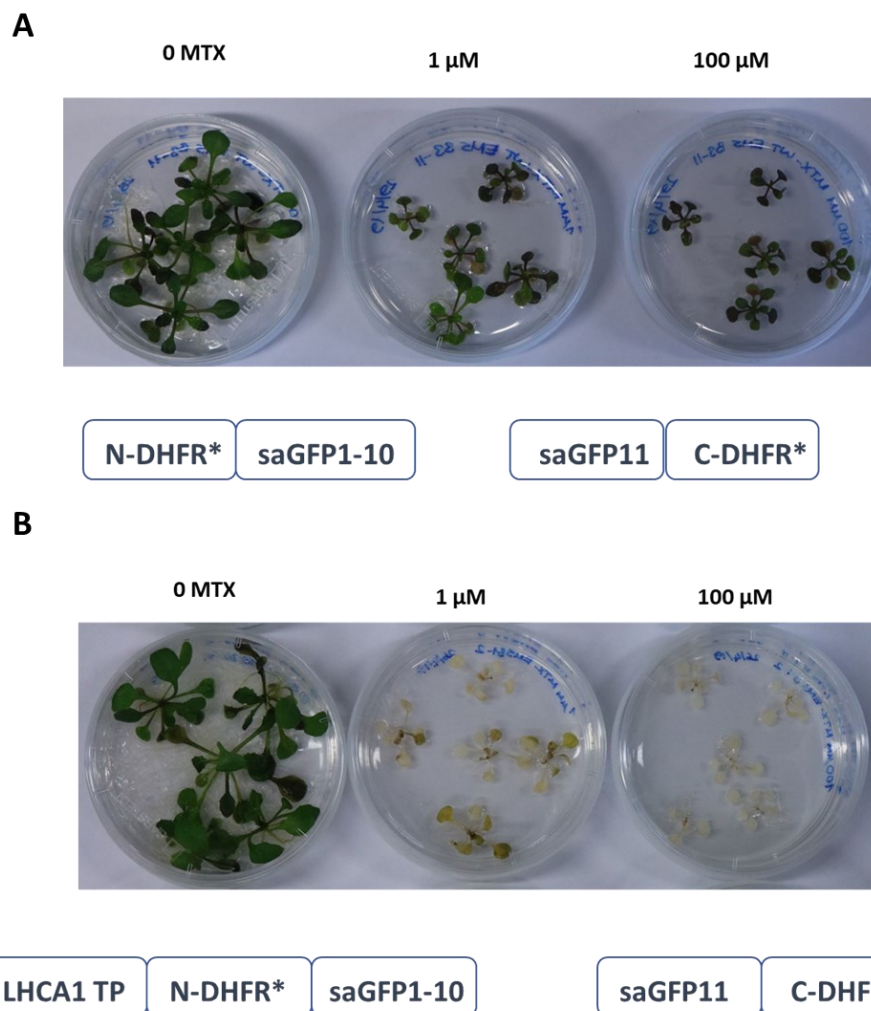


Figure 18: Reconstitution of DHFR* enzyme ensured proliferation of the stably transformed *Arabidopsis thaliana* seeds on MTX containing MS plates. Respective seeds were initially grown on MS plates containing Basta herbicide and transferred onto MTX containing Petri dishes (5 plants for each plate). The growth phenotype was recorded after 14 days of incubation. Plants were fully developed when there was no MTX present, and these plates were considered control groups. 1 μ M and 100 μ M MTX concentrations were tested. Transit peptide restricted the formation of DHFR* enzyme; thus, the coloring of the plants' leaves turned white. A plasmid combination for each phenotype was depicted below the images. **(A)** Plasmid combination without transit peptide. **(B)** Plasmid combination with transit peptide.

To confirm the correct MTX concentration, DHFR* based PCA fragments containing seeds were further subjected to the MTX at 100 nM and 1 μ M concentrations. Previously, it has been affirmed that the reconstitution of the DHFR* enzyme prevents plants from losing their proliferation ability (Figure 18A and Supplemental Figure 5A). As expected, the DHFR* enzyme reformation was adequate for the establishment of MTX resistance at even lower concentrations such as 100 nM (Figure 19B). It is important to note that DHFR* FL expressing plants exhibited greater resistance compared to reconstituted DHFR* containing lines (Figure 19). As discussed before, the low copy number of the DHFR* fragments (Valentine et al., 2012) could lead to inadequate DHFR* reassembly, consequently causing the delay in response to MTX. According to a study, *Arabidopsis thaliana* DHFR proteins have dual localization in mitochondria and cytosol (Gorelova et al., 2017). Therefore, the size of the reconstituted GFP could also influence the toxin response by disturbing the protein-protein interaction and transportation of the reassembled DHFR* to the pathway-specific regions within the cell.

Previous sections have demonstrated the applicability of the DHFR* based protein-fragment complemented assay by organelle-specific targeting: chloroplasts. Firstly, the functionality of the PCA system was confirmed without the transit peptide; later, the loss of DHFR* reassembly approved the transit peptide functioning. Our ultimate goal is to create an organelle-specific protein complementation assay, and transit peptide-containing *Arabidopsis thaliana* seeds were used for forthcoming analyses.

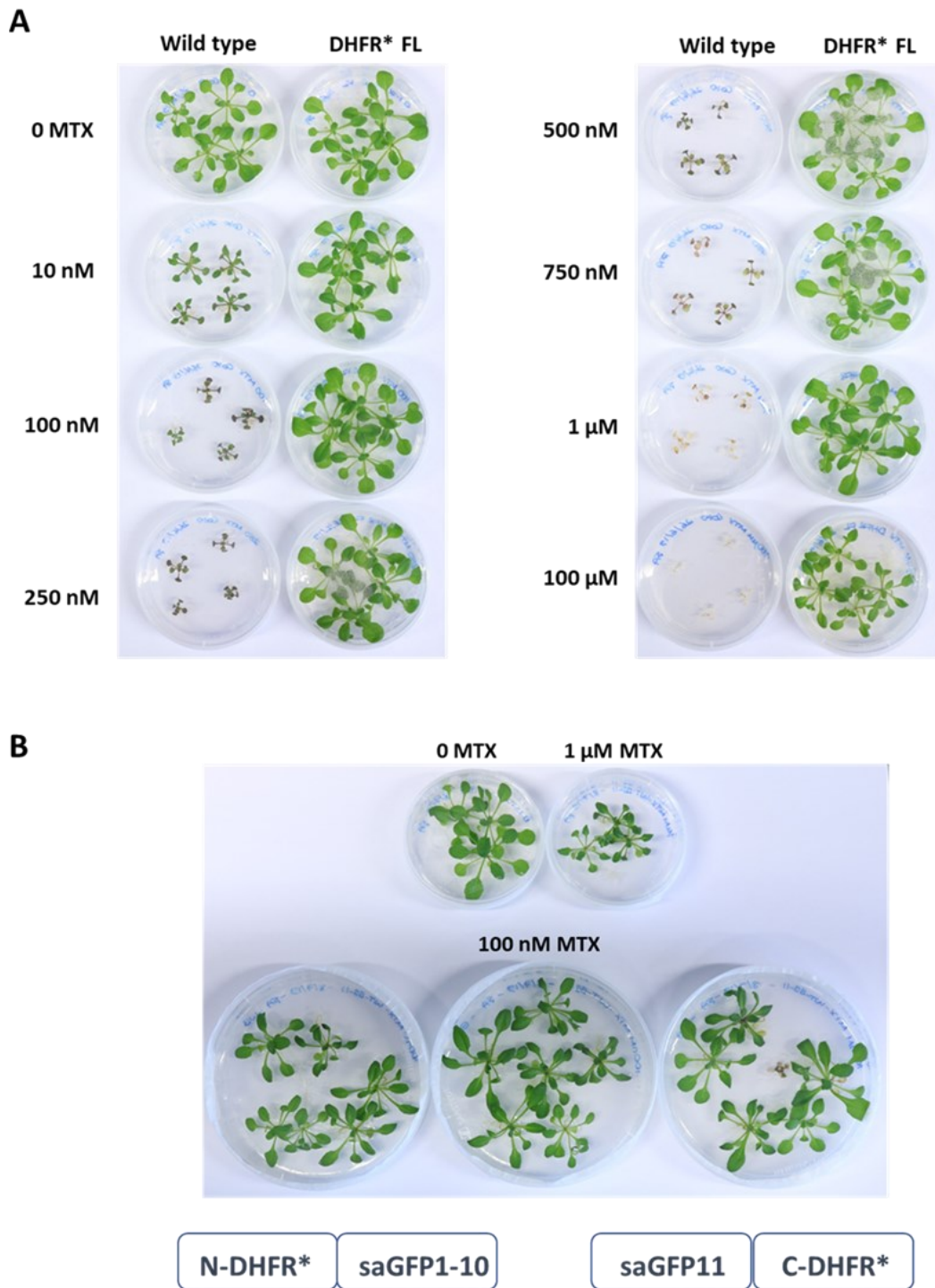


Figure 19: Optimum MTX concentration was determined concerning the selection process. Increasing concentrations of MTX were tested using DHFR* FL plasmid containing and wild-type *Arabidopsis thaliana* seeds. DHFR* expressing plants survived while wild-type remained sensitive. The growth phenotype was observed after 14 days of incubation. **(A)** Wild type and additional DHFR* FL expressing plants have behaved differently under MTX stress. Plants grown on MS plates without MTX were considered a control group. Tested MTX concentrations: 10 nM, 100 nM, 250 nM, 500 nM, 750 nM, 1 μM and 100 μM. **(B)** Seeds containing DHFR* based PCA fragments could grow under MTX stress. The Control group was grown without MTX. 1 μM and 100 nM concentrations of MTX were analyzed.

3.5.2 Insertion Line Selection for EMS Mutagenesis and MTX Plate-Based Screening

In order to check whether transit peptide expressing lines contain the respective plasmid insertion, total RNA from leaves of 14 days old plants were extracted. PCR analyses were performed subsequently after cDNA synthesis. The primers were designed to amplify the NDHFR* fragment of the construct to check the correct insertion. Various lines for each genotype were tested and several of them produced the expected PCR product with NDHFR* primers (Figure 20). As a control, primers to amplify RbCL, the large subunit of the significantly abundant protein RuBisCo in plant species (Ellis, 1979), were used. The right transformant was expected to produce PCR products with NDHFR* F+R and RbCL F+R primers (Figure 20).

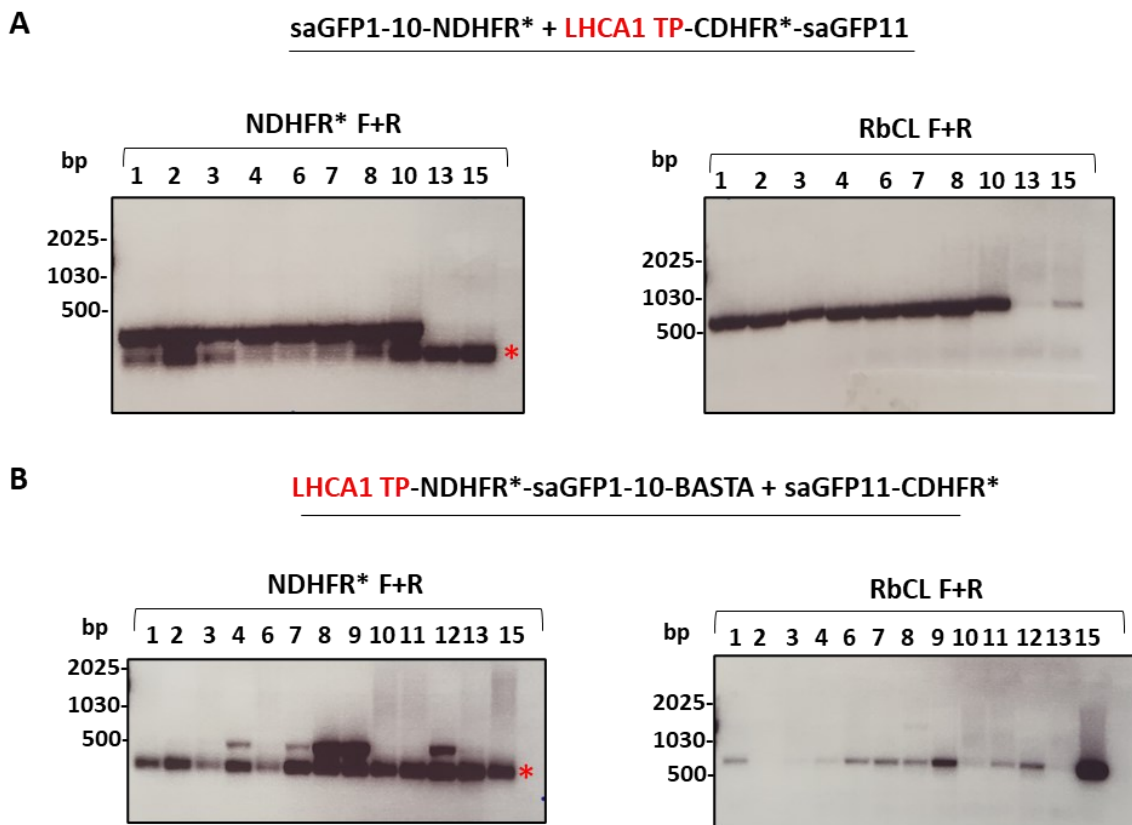


Figure 20: PCR results of DHFR* dependent PCA studies. Seeds transformed with transit peptide-containing plasmids were grown on MS plates under BASTA selection. Leaves were taken from 14 days old plants and subjected to RNA extraction. PCR analysis was performed following cDNA synthesis. Fragment combination was mentioned above the gel images. The location of the LHCA1 transit peptide within the plasmid system was highlighted in red color. The presence of inserted plasmid was confirmed via genotyping primers NDHFR* F and NDHFR* R. RbCL F and RbCL R primers were used as control. The red asterisk (*) sign was used to depict primer dimers. The sizes of PCR products are as follows: (NDHFR* F + R): ~350 bp, (RbCL F + R): ~750 bp. **(A)** Plasmid combination: saGFP1-10-NDHFR* + LHCA1 TP- CDHFR*-saGFP11 **(B)** Plasmid combination: LHCA1 TP-NDHFR*-saGFP1-10 + saGFP11- CDHFR*.

Following PCR analysis, each independent line was kept in the greenhouse to generate seeds, and the resulting seeds were stored individually. Approximately 600 mg of the seeds of one independent line were treated with EMS, an ethylating reagent, to introduce random point mutations. Next, mutagenized seeds were distributed over soil and were grown in a greenhouse research facility, where climate conditions are constantly regulated. Fully grown mutagenized *Arabidopsis thaliana* plants were retained in the greenhouse to promote self-pollination. Self-bred seeds were merged to constitute a mixture of mutagenized progenies, later subjected to MTX plate-based screening.

To identify the mutant plants, sterilized mutagenized seeds were distributed on MS plates supplemented with 100 nM MTX. Plants expressing DHFR* FL were used as the positive control, whereas wild-type Col-0 seeds were examined as negative. After 14 days of growth in a growth chamber, wild-type seeds could not germinate; accompanying, positive control demonstrated total growth (Figure 21A). The occurrence of acquiring phenotypically distinctive mutants was calculated to be 1.5 %, or roughly 3–4 mutants per 200 seeds distributed on an MS plate containing MTX. Among mutagenized progenies, various phenotypes were observed, such as growth retardation, light green and white leaf color formation, leaf phenotypic structure abnormalities (Figure 21B). Significant plants were selected over the plate and transferred either on another MS plate or soil.

Within the framework of this thesis, the main aim was to construct a molecular biology tool for DHFR* reporter-dependent protein fragment complementation assay, which enables organelle-specific selection. Thus, the corresponding plasmids were generated via golden gate DNA assembly, providing a modular platform. It has been confirmed that the reassembled split enzyme fragments function as the native protein. Later, the system was subjected to mutagenesis and the resulting mutants were analyzed throughout the selective marker-based plate screening. Mutants with specific phenotypic features were obtained and will be investigated further phenotypically and biochemically.

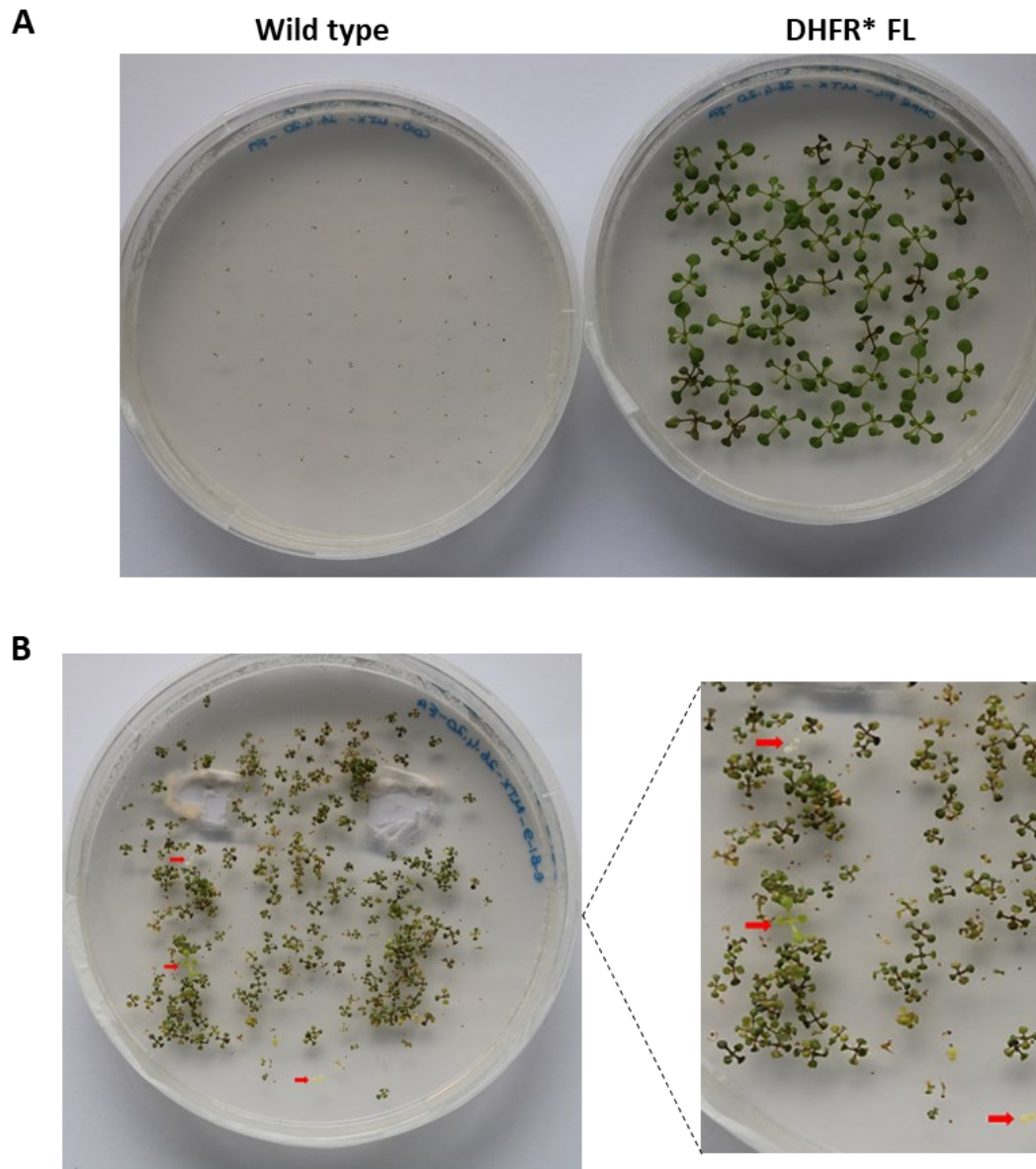


Figure 21: Functional DHFR* enables the seed to grow directly on MTX containing MS plates. Surface sterilized seeds were grown directly on 100 nM MTX containing MS plates. Functional DHFR* enables seeds to resist toxicity and continue development under MTX stress. Pictures were taken after 14 days. **(A)** Wild type *Arabidopsis thaliana* Col-0 seeds were used as negative control and seed transformed with DHFR* FL plasmid were as positive control. **(B)** EMS mutagenized seeds were distributed onto MS plates supplemented with 100 nM MTX. Various mutant plant phenotypes were indicated with a red arrow.

3.6 Analysis of Regulatory Cysteines

Although cysteine is the least abundant amino acid found in proteins, it is usually located within the functionally critical sites, mediating cofactor binding, catalytic activation, and stability regulation. Thus, the presence of cysteine residues can be directly correlated with possible inter- or intra-protein interactions. *AtToc75-III* was chosen among four Toc75-related proteins in *Arabidopsis thaliana*, as it is an essential gene and part of the significant translocation system in the outer envelope of chloroplast (Barth et al., 2022).

3.6.1 *In silico* Remodeling of *AtToc75-III* POTRA Domain

AtToc75-III is a major component of the translocation system of the chloroplast outer envelope, which acts as a translocation pore to allow the proteins to pass through the membrane (Barth et al., 2022). Apart from its pore function, *AtToc75-III* possesses a unique protein domain called POTRA. The crystal structure for *AtToc75-III* was solved by O'Neil et al. in 2017 and revealed that two adjacent cysteines within the structure suggest a possible disulfide interaction. The computational remodeling of *AtToc75-III* POTRA was performed to investigate this hypothesis further. For this reason, the original protein structure file (O'Neil et al., 2017) was rearranged accordingly and the sites where cysteines were located were visualized and distances were calculated (Figure 22). The structure of the POTRA domain consists of three central parts (P1-P2-P3) and the P2 part has three cysteines, which are C256, C300 and C359, in close vicinity to form disulfide bridges (Figure 22). Surprisingly, the recreated protein structure exhibited two additional cysteine residues: C219 and C343, quite distant from the other cysteine residues (Figure 22). However, due to their distance, these cysteines will not be considered intermolecular interaction associates.

Beyond the significance of the disulfide bridges, another important property of this interaction is the length of the bond, which can vary from 2.05 Å to 3.0 Å depending on reversibility (Sun et al., 2017). Therefore, the distance measurement between the cysteines was performed (Figure 22D). Although the proposed interacting cysteines are C256 and C300 (O'Neil et al., 2017), we included the third cysteine, C359, in our analysis. Since various factors can influence the *in vivo* protein function, we propose that the C359 has an intermediate role. Therefore, the cysteines - C256, C300, and C359 were selected to uncover further the structural and functional properties of the *AtToc75-III* POTRA domain.

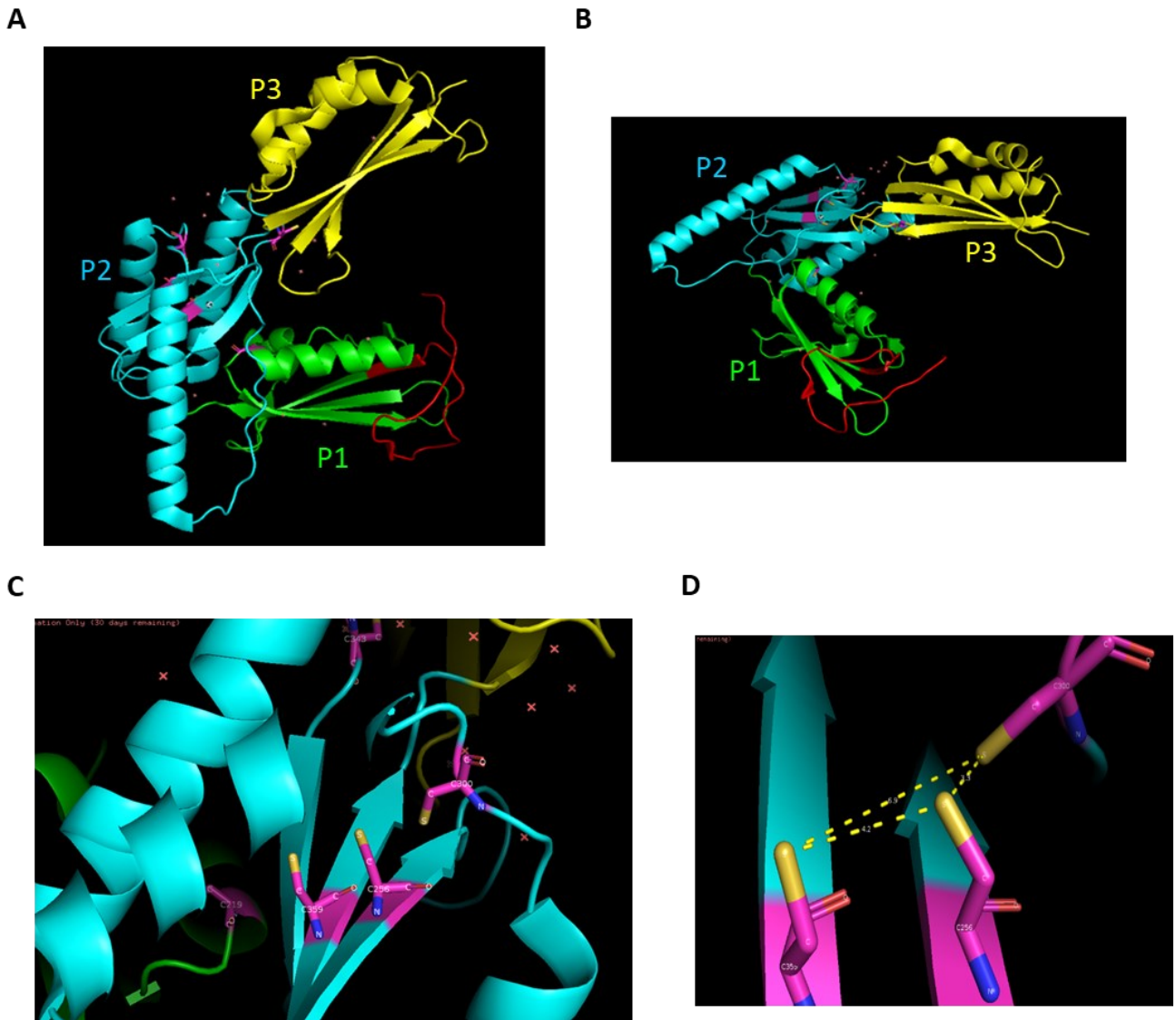


Figure 22: Remodeling of the crystal structure of *AtToc75-III* POTRA domains. Three parts of the POTRA domain were depicted. **(A, B)** Horizontal and vertical views of *AtToc75-III* POTRAs with the N-terminal linker are shown in red. P1 is shown in green, P2 is shown in cyan and P3 is shown in yellow. Cysteine residues are colored pink. **(C)** Cysteine residues in the P2 domain. C219, C256, C300, C343, C359, respectively. **(D)** Cysteine residues are close to forming disulfide bridges-C256, C300 and C359. Distances between two thiol groups; C256 - C359 = 4.2 Å, C256 - C300 = 3.3 Å, C300 - C359 = 6.9 Å. Protein remodeling based on (O’Neil et al., 2017).

3.6.2 Overexpression Profile of Native and Mutated *AtToc75-III* POTRA Domains

To check the importance of the cysteine residues (C256, C300, C359) within the POTRA domain of *AtToc75-III*, site-directed mutagenesis-cysteine to serine on the POTRA domain was performed (It is important to note that the *in vivo* experiments were carried out only with POTRA domains, not with the full-length *AtToc75-III* protein). The POTRA domain of *AtToc75-III* (codon-optimized, synthesized by Metabion AG (Martinsried, Germany)) was used as a template that was lacking the channel domain of *AtToc75-III*. Single and double cysteine mutations were inserted into each plasmid, respectively. Mutated plasmids were validated for the right mutagenesis by enzyme digestion and sequencing.

Five different mutations were introduced to each plasmid, respectively-C256S, C300S, C359S, C256S & C300S, C300S & C359S. Three single mutations and two double mutations were further analyzed. The cysteine mutations aim to disturb the disulfide bridge formation within the POTRA domain. Biochemical protein characterization mainly relies on *in vitro* expression of candidate proteins. For this reason, the native and mutated domains were over-expressed and purified. Overexpression and purification were optimized and conducted for all domains identically (Figure 23A-F). Proteins were extracted in inclusion bodies and subsequently refolded into their native form. Then, immunoblotting was done using the Toc75 antibody (Figure 23G), eventually detecting POTRA domains.

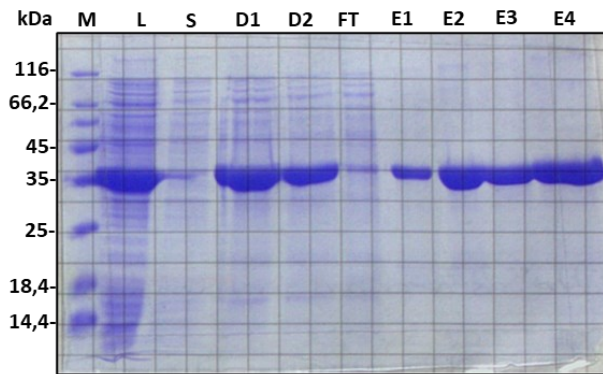
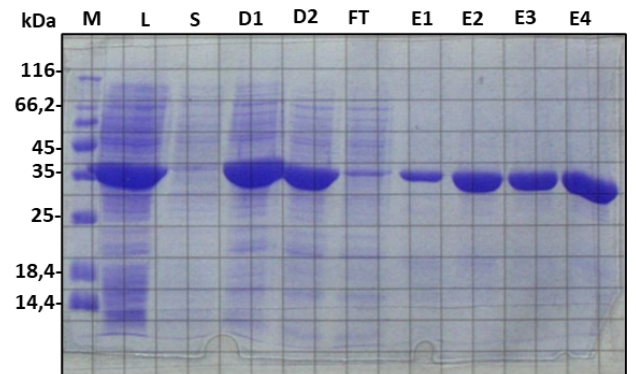
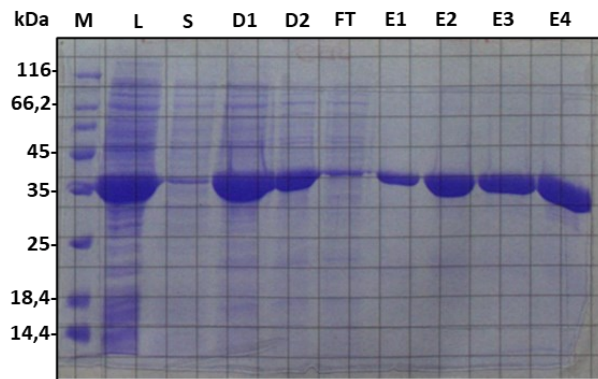
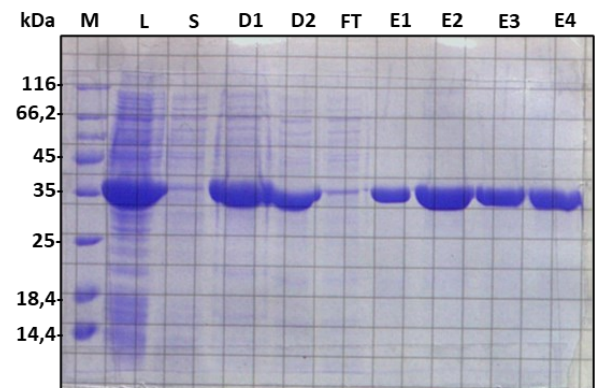
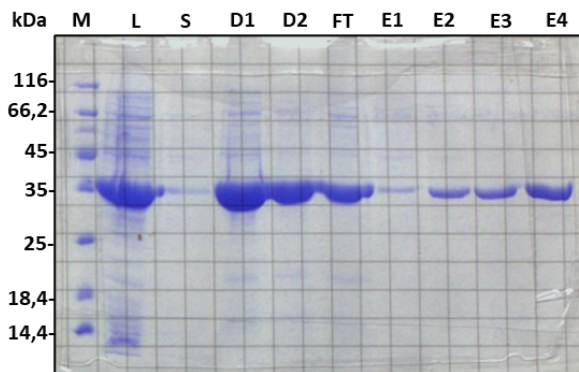
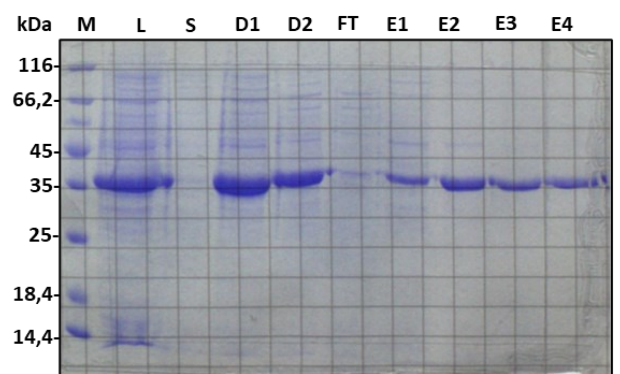
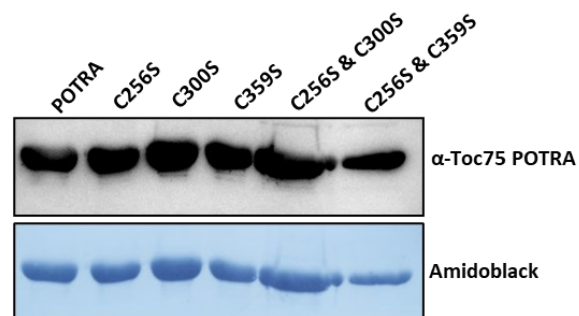
A**POTRA****B****C256S****C****C300S****D****C359S****E****C256S & C300S****F****C256S & C359S****G**

Figure 23: Overexpression and purification of native and mutated POTRA domains. Overexpressed native and mutated POTRA domains were pelleted and purified by increasing imidazole concentration. In total, five different mutations were analyzed along with the native POTRA domain. M: Marker, L: Lysate, S: Supernatant, D1: Sample taken before dialysis, D2: Sample taken after dialysis, FT: Flow through, E1: Elution with 100 mM imidazole, E2: Elution with 500 mM imidazole, E3: Elution with 1 M imidazole, E4: Elution with 2 M imidazole. **(A)** Purification of native POTRA domain. **(B)** Purification of POTRA domain bearing C256S mutation. **(C)** Purification of POTRA domain bearing C300S mutation. **(D)** Purification of POTRA domain bearing C359S mutation. **(E)** Purification of POTRA domain bearing C256S and C300S mutations. **(F)** Purification of POTRA domain bearing C256S and C359S mutations. **(G)** Purified native and mutated POTRA domain samples were collected mainly from the 500 mM imidazole purification step. Approx. 20 µg proteins were loaded onto the gel. Immunoblot analysis was performed using an α -Toc75 antibody, indicating the POTRA domains. Amidoblack staining shows the protein loading.

3.6.3 *In vitro* Examination of the Regulatory Function of the Cysteines-Oxidation and Reduction Reactions

As hypothesized before, the distances of three cysteines (C256, C300, C359) are in range to form intermolecular bonding. Since most cysteine residues are found within the redox-active sites of the proteins (Klomsiri et al., 2011), we decided to investigate the redox potential of the native and mutant purified POTRA domains. The purpose of this approach was to obtain indirect information about disulfide bonding within the protein. To determine whether these cysteines promote bonding under stimulating conditions, reducing and oxidizing reagents were used.

To examine the redox state of the purified proteins, ~0.2 mg/ml protein samples were incubated either with an oxidizing reagent (CuCl₂) or a reducing reagent (DTT). Later, TCA precipitated samples were alkylated either with AMS (~ 0.5 kDa) or mPEG-24 (~ 2 kDa). Via non-reducing SDS PAGE, the oxidized and reduced proteins were differentiated from each other by their size (e.g., 2 cysteine residues in total have 2 free sulfhydryl groups, thus reduced protein will have a size shift of 1 kDa with AMS or 4 kDa with mPEG-24 labeling). The complete procedure is explained schematically in Figure 24.

It is known that the oxidation reaction facilitates the disulfide bridge formation, whereas the reduction reaction prevents it. The AMS labeling and PEGylation reactions were carried out to confirm this change, and the gel shifts were observed. The native *AtToc75-III* POTRA domain was used as a control (Figure 25A). The non-treated control sample and oxidized control sample showed a similar size shift. The reduced control sample exhibited a significant size shift in AMS labeling and PEGylation reactions. Interestingly, single cysteine mutations (C256S, C300S, and C359S) showed the same size shift as the control group (Figure 25B, 25C, 25D).

Double mutations (C256S & C300S, C256S & C359S) continued to indicate similar size shifts as compared with control and the single mutations (Figure 25E, 25F), which indicates that the cysteine residues within the POTRA domain either do not interact with each other or the loss of them could be compensated by other amino acids within the protein.

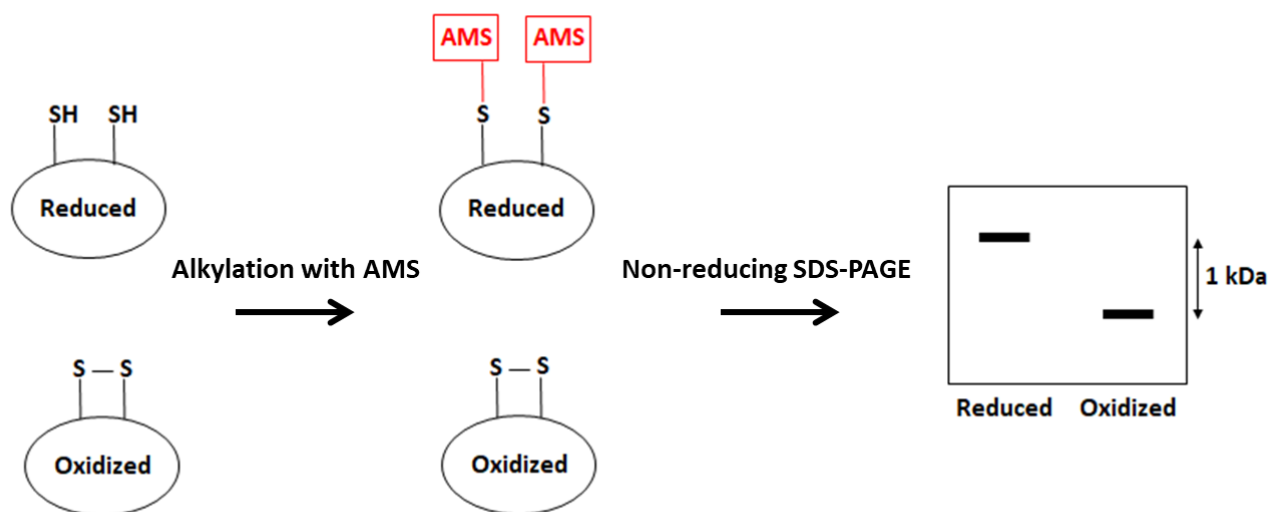


Figure 24: Schematic representation of cysteine residues' oxidative state examination. Oxidation or reduction reaction will change the intra-protein state of the cysteine residues. As a result of this reaction, the protein sample either have free cysteines or not. Via alkylation reaction, additional suitable molecules (in this case, AMS) will be covalently attached to the free cysteine molecules. This addition will eventually change the protein's molecular size, which will be visible by gel electrophoresis (Scheme based on Couturier et al., 2013; Klomsiri et al., 2011; Balsera et al., 2009c).

It is important to note that any technical difficulties encountered during or after labeling would obstruct the analysis. As a result, the experiments were repeated at least three times, and the results were accepted when at least two independent but identical experiments produced the same result. Despite the fact that SDS-PAGE analyses of the entire protein purification procedure and immunoblotting analyses of purified proteins revealed no contamination (Figure 23), analyses of labeled proteins demonstrated some contamination which might be originated from co-purified proteins (Figure 25). As a result, we conclude that the intermolecular bonding of these cysteines is not spatially favorable.

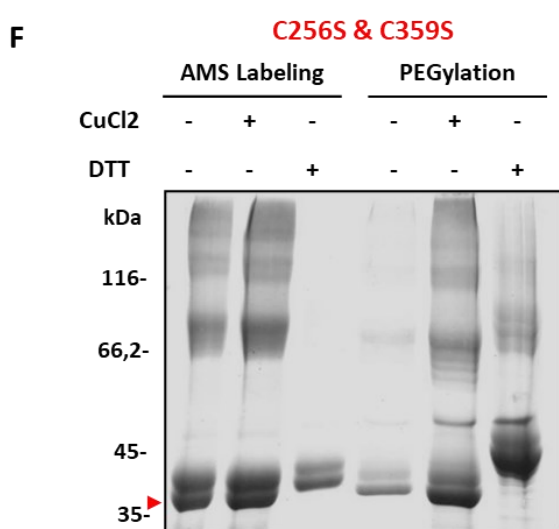
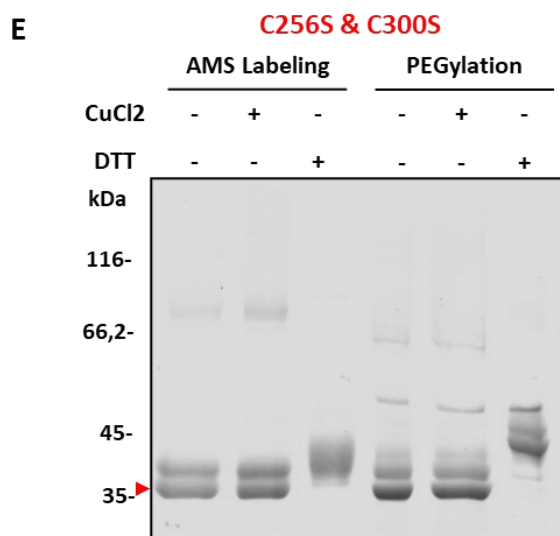
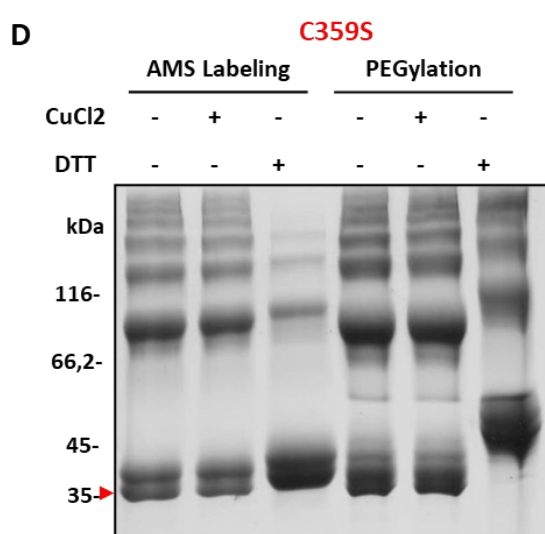
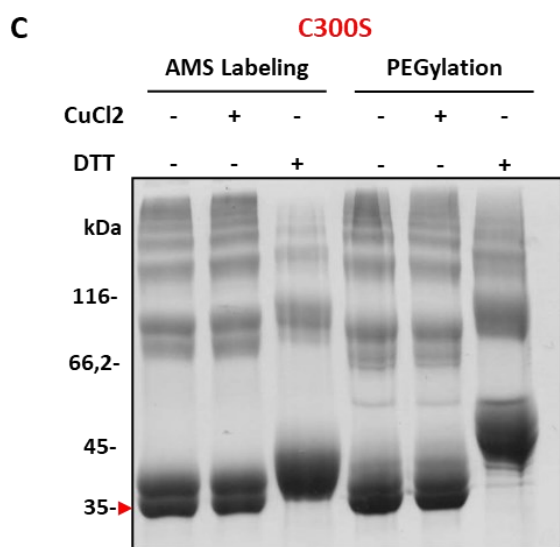
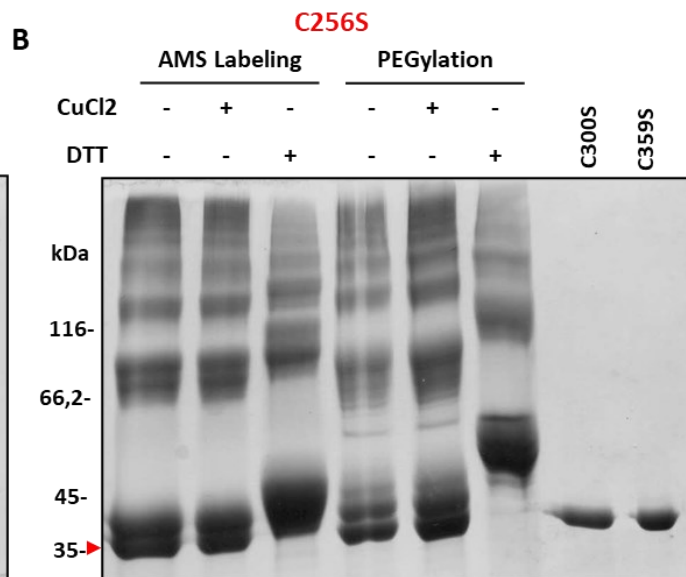
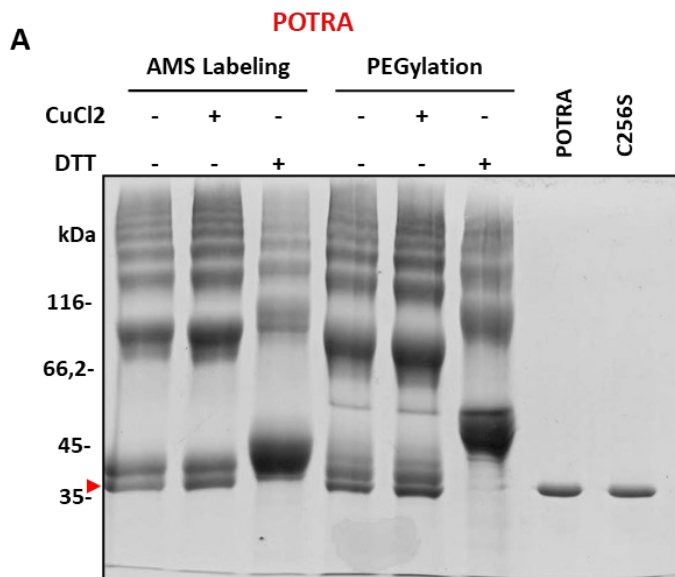


Figure 25: AMS labeling and PEGylation reactions lead to similar size shifts when compared among native and mutated *AtToc75-III* POTRA domains. Oxidation and reduction reactions were carried out in CuCl_2 and DTT, respectively. Each gel picture shows two labeling reactions: AMS and PEGylation. The first lane of each labeling shows a non-treated protein sample subjected to labeling. The second line indicates the oxidized protein sample, while the third lane is the reduced protein sample. The native *AtToc75-III* POTRA domain has a size of ~ 35 kDa. Each free cysteine will add ~ 0.5 kDa (with AMS labeling) into the total protein size and add ~ 2 kDa (with PEGylation). **Red arrow** indicates the size of the native *AtToc75-III* POTRA domain. **(A)** *AtToc75-III* POTRA domain native form. Non-treated purified protein sample *AtToc75-III* POTRA domain and bearing C256S mutation were loaded into last two lines. **(B)** *AtToc75-III* POTRA domain C256S mutation. Non-treated purified protein sample *AtToc75-III* POTRA domain bearing C300S and C359S mutation were loaded into last two lines. **(C)** *AtToc75-III* POTRA domain C300S mutation **(D)** *AtToc75-III* POTRA domain C359S mutation **(E)** *AtToc75-III* POTRA domain C256S & C300S mutations **(F)** *AtToc75-III* POTRA domain C256S and C359S mutations.

3.6.4 *In vivo* Examination of the Regulatory Cysteines in the POTRA Domain

It has been previously reported that *AtToc75-III* is an essential gene in Arabidopsis. Thus, no homozygous knock-out mutant plant line could be obtained for analysis. To study the functional role of the regulatory cysteines in the *AtToc75-III* POTRA domain, the T-DNA insertion line (SALK-015928) was complemented with the full-length *AtToc75-III* CDS and additionally with the same construct carrying a single C256S and C300S POTRA domain mutation (Figure 26B). Respective constructs were transformed into heterozygous mutants to create complementation lines by rescuing homozygous *AtToc75-III* mutants.

All complemented plants were genotyped for the original T-DNA insertion and the presence of the correct complementation construct (Figure 26C). All the complementation lines were heterozygous for the original T-DNA insertion as the PCR products for both wild-type (LP+RP) and T-DNA insertion (LB+RP) were amplified (Figure 26C). To confirm the presence of the complementation construct, construct-specific Toc75F+Toc75R primers were used. The complementation construct was amplified using the primer set, Toc75F+Toc75R (Figure 26C). As no homozygous line could be isolated upon complementation of T-DNA insertion lines using native *AtToc75-III* protein under the control of the native promoter, the embryo lethality of *AtToc75-III* could not be rescued (Figure 26C). Similarly, the mutated versions (C256S and C300S) of the *AtToc75-III* complementation construct could not rescue the homozygous lines (Figure 26C).

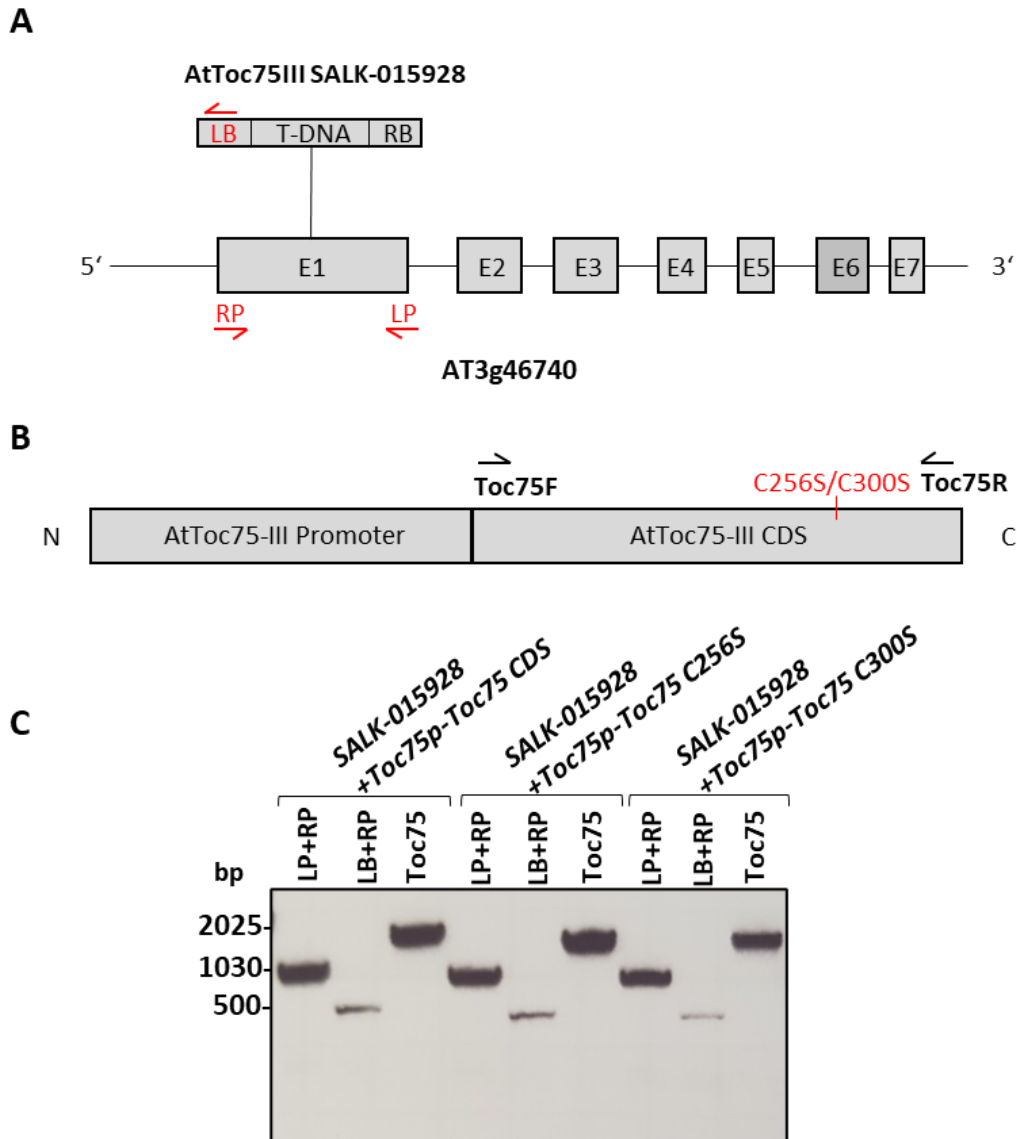


Figure 26: *AtToc75-III* complementation studies. (A) Diagram of the genomic region encoding *AtToc75-III*, gene scheme. T-DNA insertion location of SALK-015928 line and genotyping primer binding sites are represented. Boxes labeled from E1 to E7 show exon regions. Spaces between adjacent exons are represented as introns. LB: SALK LB, RP: *AtToc75III* SALK-015928 RP, LP: *AtToc75III* SALK-015928 LP **(B)** Schematic representation of the complete protein used for complementation studies. The coding sequence (CDS) of *AtToc75-III* under the control of its native promoter was inserted into the genome via *Agrobacterium* for complementing the SALK-015928 line. The primers used to confirm the insertion are shown as Toc75F and Toc75R. N: N-terminus, C: C-terminus. **(C)** Genotyping PCR analysis. WT PCR was performed using LP and RP primers. T-DNA insertion was checked via LB and RP primers. The presence of insertion was confirmed via genotyping primers Toc75F and Toc75R. The sizes of PCR products are as follows: (LP-RP): ~1000 bp, (LB-RP): ~500 bp, (Toc75F-Toc75R): ~2000 bp.

4 Discussion

4.1 Analysis of Interaction Partners Using Proximity Labeling

Protein-protein interaction analysis by proximity labeling was widely applied in various model organisms, however, the application of PL in *planta* gained insight recently with the following advances in biotin ligase variants (Supplemental Table 1). The primary PL research was established in rice (*O. sativa*) protoplasts by using the BirAG enzyme, a version of BioID that lacks the cryptic intron site (Lin et al., 2017). Later, BioID-mediated PL was implemented to study plant-pathogen interactions in *Nicotiana benthamiana* transiently (Das et al., 2019; MacHaria et al., 2019; Conlan et al., 2018) and *Arabidopsis thaliana* stably (Khan et al., 2018). Furthermore, recent studies using BioID2-based PL in stable *Arabidopsis thaliana* lines have revealed the multiple associating proteins of nuclear membrane and pore complex (Tang et al., 2020), including transmembrane-specific proteins as well as components of inner nuclear membrane protein degradation machinery (Huang et al., 2020). The development of TurboID and miniTurboID has accelerated the PL research in *planta*, including *Arabidopsis thaliana*, *Nicotiana benthamiana*, and tomato root cultures (Xu et al., 2021; Arora et al., 2020; Mair et al., 2019; Zhang et al., 2019).

Within the scope of this thesis two biotin ligase variants were used, BioID2 and TurboID. By the time of project initiation, the optimal PL conditions for TrxM2, Tic40 and Pic1 were not adjusted, thus, the reaction parameters for both PL enzymes were optimized as a first step. Although the optimal reaction temperature for both BioID and BioID2 enzymes was determined as 37°C (Kim et al., 2016; Roux et al., 2012) which may cause heat stress in plants, the PL reaction was carried out at room temperature (22-25°C) as required for normal plant growth. Adequate biotin concentration and incubation time were experimentally defined as 500 µM biotin and 18 hours for BioID2 or 6 hours for TurboID. The attachment of the PL enzyme can influence the nature of the candidate protein, thus, causing aberrant function (Ohmuro-Matsuyama et al., 2013). In parallel to this information, attempts of obtaining biotinylation through *AtTrxF1* protein tagged with BioID2 were unsuccessful, however, *AtTrxM2*, *AtTic40*, and *AtPic1* proteins exhibited biotinylation with both BioID2 and TurboID fairly. Proximity labeling via biotin ligase relies on strong biotin-avidin molecule interactions and rigorous purification of biotinylated molecules by streptavidin. Next, trypsin digestion of the peptides bound to the streptavidin molecules is followed by mass spectrometry for identification. In line with this, the mass spectrometric analysis was carried out for each

candidate protein-tagged either with BioID2 or TurboID PL enzyme. Despite having the positive immunoblot results against α -biotin antibody, BioID2 tagged proteins produced an insufficient amount of biotinylated proteins, that cannot be detected by mass spectrometry. Reasons for that could be the decreased reaction temperature for optimal BioID enzyme function and elongated reaction time causing negative results. Thus, identification of associating partners of candidate proteins was achieved by using TurboID as a biotin labeling enzyme and interactome maps were created by statistical analysis of mass spectrometry results.

The interactome data for each candidate protein was narrowed down based on the subcellular localization, explicitly to chloroplast localized proteins. Hence, this approach will reduce the involvement of aberrant interactions that may be originated during the import process of candidate proteins themselves. The detailed protein annotation and data visualization by scatter plotting were carried out with chloroplastic prey proteins. The number of identified proteins was found to be higher for the candidate proteins with increased biotinylation signal in immunoblotting analysis (Figure 12).

4.1.1 Interactome of *AtTic40*

The exact molecular function of the membrane anchoring chloroplast inner envelope membrane protein Tic40 was debated over the years. Co-chaperoning of the import process (Chou et al., 2006), protein reinsertion into the inner envelope membrane (Chiu & Li, 2008; Tripp et al., 2007) and involvement in the thylakoid biogenesis (Bédard et al., 2017) are the assigned functions of the Tic40 till today. Strikingly, PL data has confirmed that Tic40 indeed interacts directly with Tic110, Hsp70, Hsp90, Hsp93V, ClpP, and Cpn60, supporting its role in protein import (Figure 27). The two homologs of Hsp93 protein were encoded in the *Arabidopsis thaliana* genome; *AtHsp93-III*, the null mutant exhibits a similar phenotype as the wild type, whereas the absence of *AtHsp93-V* causes protein import defects by decreasing thylakoid membrane abundance (Constan et al., 2004). Only Hsp93V was detectable by PL, as it was found to be more abundant than Hsp93III (Kovacheva et al., 2005). In contrast to the proposed stromal chaperone system where Hsp93 binds to incoming preproteins by direct interaction with Tic40 (Huang et al., 2016), the Hsp70 and Hsp90 proteins were also found to be directly linked to Tic40. Together, these data support the previous hypothesis of Hsp70 being the main motor protein in preprotein propulsion along the import process and that Hsp93 is involved in the protein quality control at the later stages of the import process

(Flores-Pérez et al., 2016). Besides, the outer envelope proteins Toc75 and Toc34 were detected by PL, confirming that the preprotein form of Tic40 was recognized by the receptors of TOC complex and delivered to the channel protein Toc75 for translocation process. The overall associating partners of Tic40, particularly within the chloroplast translocation system, were visualized in the Figure 27.

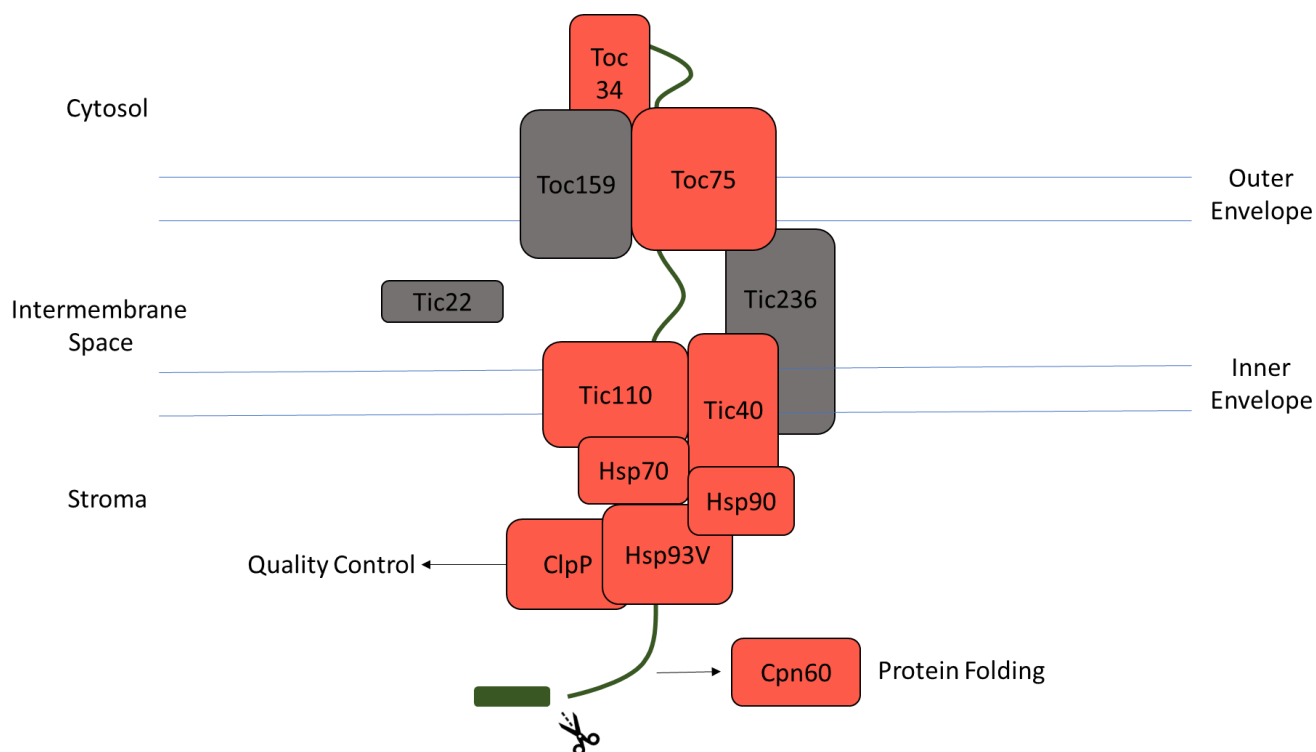


Figure 27: The PL mapped Tic40 interaction network within the chloroplast translocation system. TurboID-mediated proximity labeling confirmed that the preprotein form of Tic40 interacts with Toc34 and Toc75. Following the translocation and insertion to the inner envelope, Tic40 was found to be associated with Tic110, reassuring the current knowledge. Moreover, Hsp70 and Hsp90: stromal chaperones were identified as direct interaction partners of Tic40. Hsp93V, Clp protease, and Cpn60 were in close proximity to get biotinylated by Tic40. Proteins within the Tic40 interaction network were colored red; others were grey.

A link between Tic40 and thylakoid biogenesis was proposed as a result of the depiction of suppressors of Tic40 (Stic1 and Stic2) by a genetic screen, whereas Stic1 corresponds to Alb4 and Stic2 interacts with Alb3 and Alb4 in thylakoid protein targeting (Bédard et al., 2017). The thylakoid membrane protein Alb3 mediates both the post-translational insertion and assembly of the nuclear-encoded LHCP proteins into the thylakoid membrane and participates in the biogenesis of the plastid-encoded subunits of the photosynthetic complex (Dünschede et al., 2011). Moreover, a novel protein, LTD (LHCP Targeting Deficient) was characterized as a mediator in the transfer of the newly imported LHCP proteins from the TIC translocon to the

thylakoid membrane (Ouyang et al., 2011). Parallel to this information, Stic2, LTD, and many LHCP proteins were identified within the Tic40 interactome (Supplemental Table 2).

The interaction of Tic40 with redox regulon, despite the proposed protein Tic32 (Hörmann et al., 2004), was detected by PL to be achieved through Tic62 protein (Supplemental Table 2), which acts as a redox sensor to regulate the import process depending on the environmental stimuli (Stengel et al., 2008). In addition, Tic62's association with FNR, which catalyzes electron transport in photosynthesis-related pathways (Benz et al., 2009), strengthens the notion of Tic40 influencing thylakoid biogenesis by adjusting import pathway in response to changing stromal redox capacity. Furthermore, the Tic40 interactome map includes Pic1 protein, supporting the previous hypothesis about Tic40 mediating the membrane reinsertion of the Tic21/Pic1 protein (Chiu & Li, 2008). It is known that plants have an additional need for iron due to its function both in the electron transport chain during photosynthesis and chlorophyll biosynthesis (Rout & Sahoo, 2015). Since iron is prone to be aggregated and excess amounts lead to cytotoxicity, plants need a rapid-highly efficient system for iron uptake (Briat et al., 2010). These data suggest that, depending on the redox signaling, Tic40 might facilitate the reorganization of the thylakoidal proteins by selectively importing photosynthesis-related proteins and also promoting iron uptake by increasing the number of Pic1 proteins in the inner envelope membrane. Hence, it will alter the protein composition of the thylakoids and eventually affect their biogenesis.

Recently, a DnaJ-like chaperone ORANGE which participates in the regulation of chloroplast biogenesis and development as well as carotenoid biosynthesis was shown to possess physical interaction with Tic40, Tic110, and Tic20 (Yuan et al., 2021). Despite the experimental evidence, ORANGE protein was not present in the Tic40 interactome. It can be implied that ORANGE protein does not contain a free Lys residue within the functional form of the protein, thus, the biotin moiety addition by TurboID did not take place.

Does the Tic40 protein participate in different pathways responsible for membrane reinsertion and quality control apart from the general import pathway or the import pathway indeed is specific to the proteins responsible for thylakoid biogenesis? To tackle these questions, an in-depth biochemical analysis of the single or multiple gene mutation-bearing plants for each respective protein should be carried out. Moreover, partial complementation of the prospective mutant lines and subsequent characterization will enhance the current understanding of Tic40 function.

4.1.2 Interactome of *AtTrxM2*

Thioredoxins are a small group of proteins that can change target protein's intermolecular disulfide bridges, thereby, modulating their function and stability. TrxM2 belongs to the Trx-m family and is shown to be interacting with proteins from several metabolic pathways. For instance, TrxM2 was proposed to be responsible for redox-sensitive alternative targeting of G6PD1 and G6PD4 to the peroxisomes (Meyer et al., 2011). Instead, PL data comprises another glucose-6-phosphate dehydrogenase (G6PD), termed plastidial-G6PD2 (Supplemental Table 3), which influences plant's carbohydrate metabolism and coping mechanisms from oxidative stresses through balancing the redox poise in chloroplasts (Debnam et al., 2004). Furthermore, the nucleus localized Myb3 was determined in a computer-based interactome map as an interaction partner of TrxM2 (Dreze et al., 2011), which was undetectable by PL. Moreover, two previously classified proteins destined for different organelles; mitochondrial VDAC3 (Zhang et al., 2015) and plastidial ZE (Da et al., 2018), were present within the list of TrxM2 associating proteins, supporting the multi-localization of the TrxM2. Trx family proteins may have multiple target proteins in distinct cellular compartments, and because of their tiny size, they can easily move along the cell.

In addition to the experimentally validated TrxM2-related proteins, many others were detected by biotinylation (Supplemental Table 3). Surprisingly, components of the translocation machinery, Tic110, Tic40, Tic62, Toc34, and Toc75, were found to be included in the interactome. Previous studies have demonstrated that Tic110 has redox-active cysteines that are mostly regulated by Trxs (Balsera et al., 2009a). Strikingly, TrxM2 activity was identified to influence the metabolic pathway that contained the Stic2 protein because PL data revealed Stic2 as the most likely interaction partner (Supplemental Table 3). As was indicated above, Tic40 may affect the ratio of photosynthetic proteins in the thylakoid membrane, and it has been suggested that Stic2 functions as a suppressor of Tic40 (Bédard et al., 2017). Furthermore, TrxM2 activity has been linked to photosynthesis-related reactions on the thylakoid membrane (Nikkanen & Rintamäki, 2019). Taken all together, we propose that the environmental cues that Tic40 uses to assist thylakoid reorganization were perceived by TrxM2 and regulated by Stic2 (Figure 28). Oxidative settings will cause the TrxM2 to generate disulfide bonds, which will allow Stic2 to block Tic40. On the other hand, under normal circumstances, TrxM2-mediated disulfide bond formation will lower the activity of Stic2.

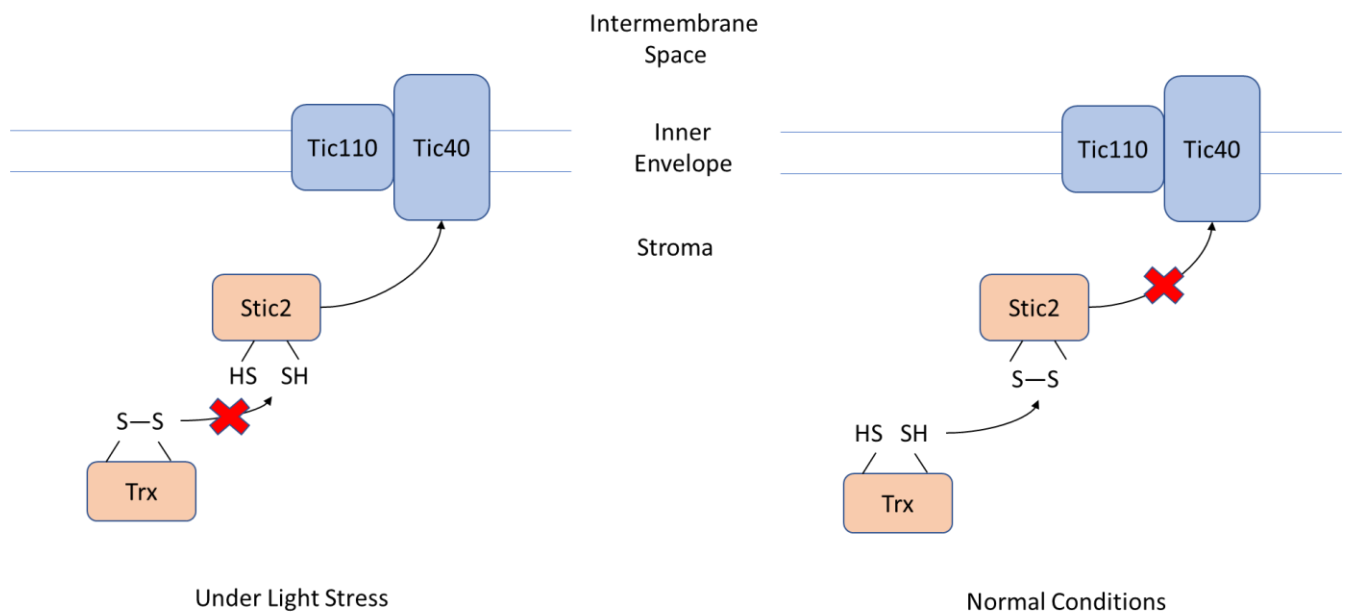


Figure 28: Proposed regulation mechanism of Tic40. TrxM2 senses redox fluctuations (oxidative or reducing) and modifies its redox status accordingly. Intermolecular disulfide bridge formation on Stic2 protein will inhibit its interaction with Tic40, thereby promoting the import of thylakoidal photosynthetic proteins. Under light stress, the Stic2 will suppress the activity of Tic40, enabling the plant actively respond to the changing conditions.

The TrxM2 does indeed have enormous flexibility owing to its ability to be present in multiple locations as well as its relatively small size, which can promote unwanted biotinylation. As a result, the related-protein list was reduced to chloroplast-destined proteins and aligned based on the interaction frequency indicated by log₂ fold change (Supplemental Table 3). The comparison of TrxM2 and Tic40 interactomes revealed alternative molecular pathways in which TrxM2 participates, such as chlorophyll biosynthesis, carbohydrate metabolism, plastid gene expression, iron storage, and pathogen response (Table 17). Taken together, these findings highlight the importance of redox regulation throughout the cell and will serve as the foundation for further research. To better understand environmental stimuli, PL-compatible plant lines will be subjected to various conditions such as fluctuating light/temperature or pathogen attack. As a result of the significant differences between the interactomes, our current understanding of Trx-mediated redox signaling will be advanced.

4.1.3 Interactome of *AtPic1*

Despite current disagreement about the Pic1 protein's exact molecular function, its involvement in iron homeostasis as a permease in the inner envelope membrane was accepted for the PL data analysis. Interestingly, Pic1 has yet to have an experimentally validated interaction partner. The NiCo (Nickel-Cobalt transporter) was thought to interact with Pic1, forming a metal translocon (Duy et al., 2011), however, the expression analysis revealed that NiCo is not involved in chloroplast iron uptake (Pham et al., 2020). Pic1 was chosen for the project because of its location in the inner membrane and non-interaction with the TIC complex, with the goal of using the PL data to identify background biotinylation caused by the protein transport process itself. Furthermore, Pic1 was reported to associate with Stic2 and Tic40 with a high degree of confidence (Supplemental Table 4), implying that Stic2 function may influence cellular iron homeostasis via altering Pic1 abundance. With the knowledge of previous PL data of candidate proteins, an additional role for Tic40 by indirectly affecting cellular iron homeostasis is suggested. Tic40 regulates Pic1 insertion into the inner envelope membrane, and its activity is regulated by Stic2, according to the proposed model (Figure 29). Furthermore, redox regulation occurs via the TrxM2-Stic2 interaction, affecting the affinity of Tic40 to Pic1, and possibly many other photosynthetic proteins. Hence, the Tic40-mediated thylakoid biogenesis will be halted in response to incoming environmental signals, allowing plants to actively respond to stressful conditions and adapt their proteome accordingly. It has long been established that the stromal iron level influences the photosynthetic capacity and the composition of the thylakoid membranes (Clemens et al., 2009; Merchant et al., 2006). Here, we present a physical link between the protein import and the thylakoid biogenesis based on the iron abundance in the stroma.

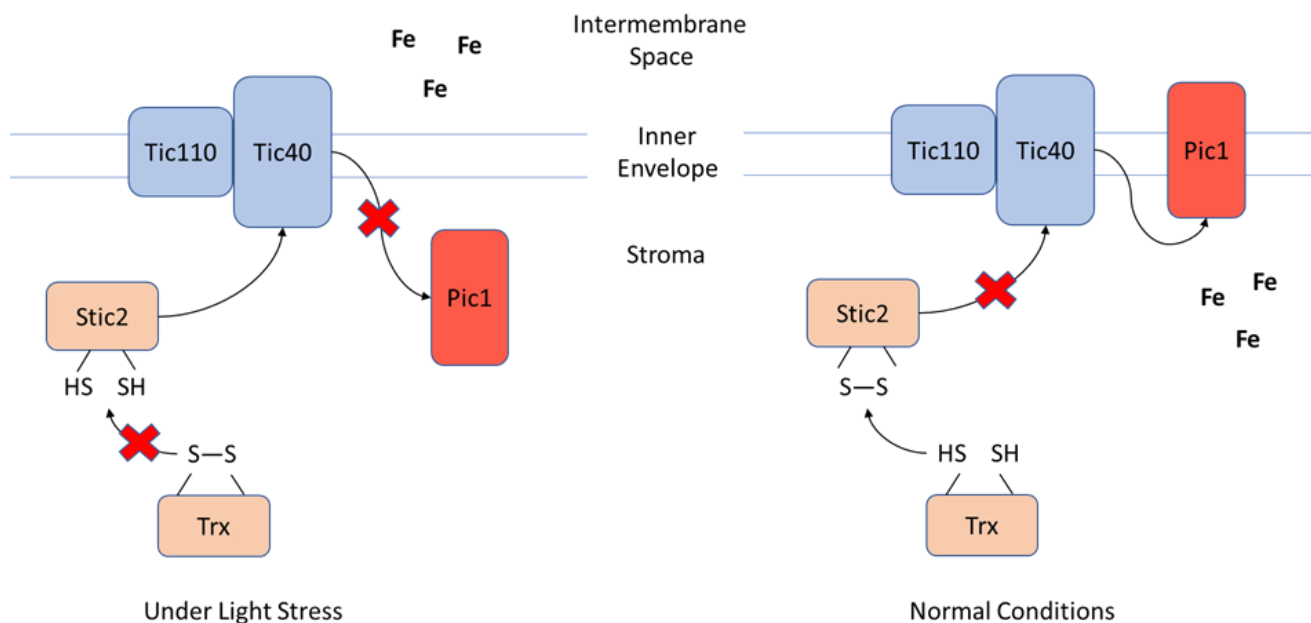


Figure 29: The potential model of Pic1 insertion into the inner envelope membrane of the chloroplast. Trx proteins detect environmental cues and inhibit Stic2, allowing Tic40 to mediate proper Pic1 membrane insertion through the channel protein Tic110. As a matter of fact, the iron level in the stroma decreases, causing a change in the photosynthetic apparatus. The normal function of Tic40, on the other hand, will contribute to Pic1 insertion on the membrane and, as a result, an increase in stromal iron levels.

PL has led to the identification of another protein, FC1 (Ferrochelatase-1) involved in heme biosynthesis, in both the Tic40 and Pic1 interactomes. FC1 catalyzes heme biosynthesis in non-photosynthetic tissues and is induced by oxidative stress in photosynthetic tissues to increase heme production (Espinosa et al., 2016). This data supports the possibility that Tic40 regulates iron homeostasis via selective protein import across membranes. A general conclusion, on the other hand, can be reached with the support of experimental evidence; thus, more research on the subject is required. In any case, contrary to popular belief, Tic40 not only acts as a co-chaperone during the import process but also actively participates in the selection of which protein is imported into the stroma.

4.2 DHFR* Reporter Based Protein Fragment Complementation Assay

Protein-protein interactions in each cell contribute to the formation of a cellular network that regulates nearly all biological processes. Thereupon, a deep understanding of these mechanisms will advance our understanding of signal transduction, cellular communication, enzymatic reactions, membrane transfer, and even disease formation. PCAs, one of the many strategies for PPI detection, enable the elucidation of PPI networks depending on the spatial distances, making them ideal for high throughput studies. Our one-of-a-kind contribution to

PCA methodology development is to combine the power of contact-dependent reporter reconstitution with an organelle-specific targeting strategy. As a result, we aimed to develop a platform that enables EMS-based forward genetic screening, particularly for mutation detection at the organelle level.

Split GFP and split DHFR* proteins were used in conjunction with the chloroplast targeting signal to create such a PCA system. Successful stable plant lines were then subjected to EMS mutagenesis to induce random point mutations, and prospective mutants with specific phenotypes were chosen using the plate-based growth supplemented with MS medium containing MTX. Later, genome sequencing approaches will be used to characterize the exact genomic location of the mutation, and molecular biological methodologies will be used to further analyze the biochemical properties of the prospective protein. Consequently, we demonstrated the feasibility of the DHFR* dependent PCA with chloroplast-specific targeting and pointed out several prospective mutants that will be studied further. As a direct result, new components of protein translocation systems, thylakoid biogenesis, photosynthetic apparatus, as well as other systems will be identified, and our perception of the molecular biology of chloroplast biogenesis will be expanded.

To summarize, survival-dependent DHFR* reporter-based PCA was effectively implemented in the laboratory. The system was given organelle-specific information via a transit peptide, designed to allow one of the fragments to relocate to the organelle. The organellar information can be adapted by changing the sequence in the cloning system, and the method could be used for a forward genetic screening. One critical point to consider before proceeding is whether two fragments could spatially find each other in the respective sub-compartment to reconstitute functional protein. For this reason, we used split-GFP fragments that possess high affinity for each other, to ensure proper fragment encounter. According to the study's design, this part could be replaced by other split proteins, and whilst DHFR* fragments should remain constant in an attempt for providing survival from MTX. Hence, the method's power is dependent on the flexibility and compatibility of the fragments, which have even at this early-stage enormous potential to characterize gene-to-function relationships.

4.3 Regulatory Cysteine Analysis

As incorporated into the protein, cysteine residues consist of a thiol group that is considered a molecular switch due to its capacity of being post-translationally oxidized or alkylated depending on the microenvironment of the surrounding protein. This conversion changes the catalytic properties of the enzymes involved in metabolism, cell signaling and stress response, etc. (Leichert et al., 2008; Le Moan et al., 2006). Thus, a complete understanding of the regulatory properties of the cysteine residues within the protein will provide a comprehensive overview of how enzymes sense environmental cues and reflect them in structural changes that eventually influence cell signaling.

Toc75, the chloroplast outer envelope channel protein, contains a POTRA domain along with three cysteine residues that have been proposed to form disulfide bridges (O'Neil et al., 2017). These cysteine residues were studied *in vivo* and *in vitro* due to the greater engagement potency of the proteins during the translocation process along the membranes. Gel shift assays were used to investigate the redox potential of cysteines under reducing and/or oxidizing conditions. However, in gel shift assays, proteins with single or double cysteine mutations did not show a noticeable difference between the changing conditions. This information suggests that the reactive cysteine sites within the Toc75 POTRA domain, if present, are either spatially located within the entire Toc75 structure so that the formation of an intermolecular disulfide bond is energetically favorable, or the mentioned cysteine residues interact with other cysteine residues in the adjacent proteins. While we are still in the early stages of identifying reactive cysteine residues, our findings could be considered preliminary. As a next step, instead of focusing solely on the POTRA domain, the entire Toc75 protein could be subjected to a redox-sensitive assay, or computational analyses could be performed to better predict the protein's native environment, yielding more accurate results. Although attempts to complement the embryo lethality of the homozygous *AtToc75-III* knock-out lines with constructs containing single cysteine mutations failed (Figure 24), this experiment can be repeated once the reactive cysteines and possible molecular mechanisms are identified. The biochemical characterization of the complemented lines will then reveal the significance of cysteines in the maintenance of cellular homeostasis.

4.4 Conclusion & Future Perspectives

Evolution from a single cell into a multicellular organism necessitated enormous adaptations, which were typically prokaryotic in origin and improved by eukaryotic additions. One of these was the development of a transport system for protein import into sub-compartments and organelles, including chloroplasts which is the main topic of this thesis. Even though the main components of the translocation system have already been identified, we sought to explore new proteins that act as regulators during the import process. State-of-the-art molecular biological techniques such as proximity labeling and protein fragment complementation assays were used to accomplish this purpose. Gradually, we attempted to address the following statements, which are listed below.

- What is the role of the Toc75 protein in *Arabidopsis thaliana* aside from its channel properties, given that it contains a POTRA domain?
- Can we develop a platform that enables forward genetic screening with the additional benefit of organelle-specific mutation-selection?
- Are there any intermediary proteins that regulate the TIC complex and may even activate additional protein sorting mechanisms?

Our findings indicate that the cysteine residues within the POTRA domain of Toc75 do not exhibit putative redox-sensitive intermolecular disulfide bonding, implying that disulfide bridges may form over the cysteine residues in between the incoming preprotein and the POTRA domain during the transport process. This interaction network may also include Tic22, which aids preprotein passage from TOC to TIC across the intermembranous space (Rudolf et al., 2013). Based on this information, disulfide interactions might play an important role in transport system regulation, preprotein stabilization, and further control of the translocation system by receiving redox signals. Without a doubt, more research on this topic is required, particularly computer-based prediction analysis of conserved cysteine residues, which will provide an overview of how to proceed in the laboratory environment. As a result, interactions between cysteine residues might be studied, and the reactive cysteines could be further characterized.

We used the MTX-survival feature of the DHFR* enzyme and the high self-affinity of the split-GFP protein to develop a platform based on PCA; thus, when these two proteins are combined in split form, the possibility of an encounter is increased. The organelle-specific information was attached to one of the split fragments via a transit peptide at the N-terminus. Incubation

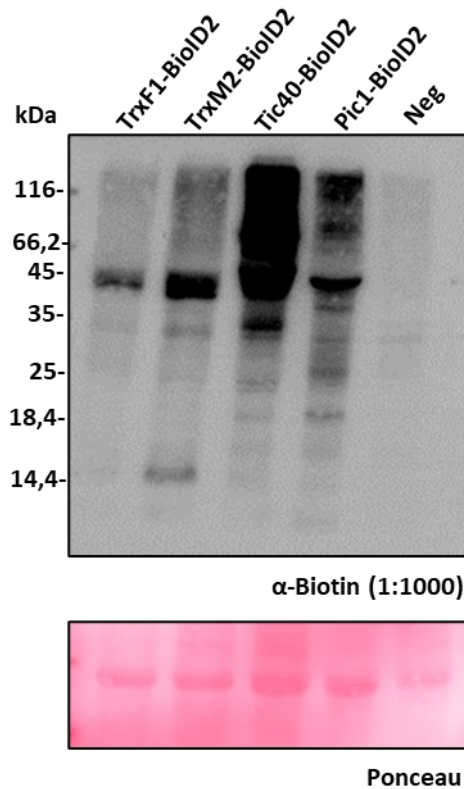
with EMS introduced random mutations, and organelle-specific mutants were obtained based on phenotype selection under MTX selectivity. In other words, defects in chloroplast import machinery will cause plants to reconstitute a functional DHFR* enzyme and promote survival; eventually, the screening will detect abnormal plant development. To summarize, we demonstrated that the reformation of active enzymes using our PCA approach is successful and capable of providing a platform for mutant selection. This platform could be used to identify several novel proteins that play important roles in organelle biogenesis, thereby improving our understanding of organelle molecular biology. As a result, we can attain a more accurate conclusion about the origin of organelles and develop solutions for metabolic disturbances that cause a variety of anomalies during the development of any organism.

Interactome studies will demonstrate the candidate protein's molecular network, resulting in the identification of several pathway involvements. In this study, *AtTic40*, *AtTrxM2*, and *AtPic1* were chosen to reveal the TIC apparatus's interaction network, and a biotin ligase-mediated proximity labeling approach was used to discover the associating proteins. The data from the molecular interaction maps revealed additional functions for each protein, forcing the current hypotheses to be reconsidered.

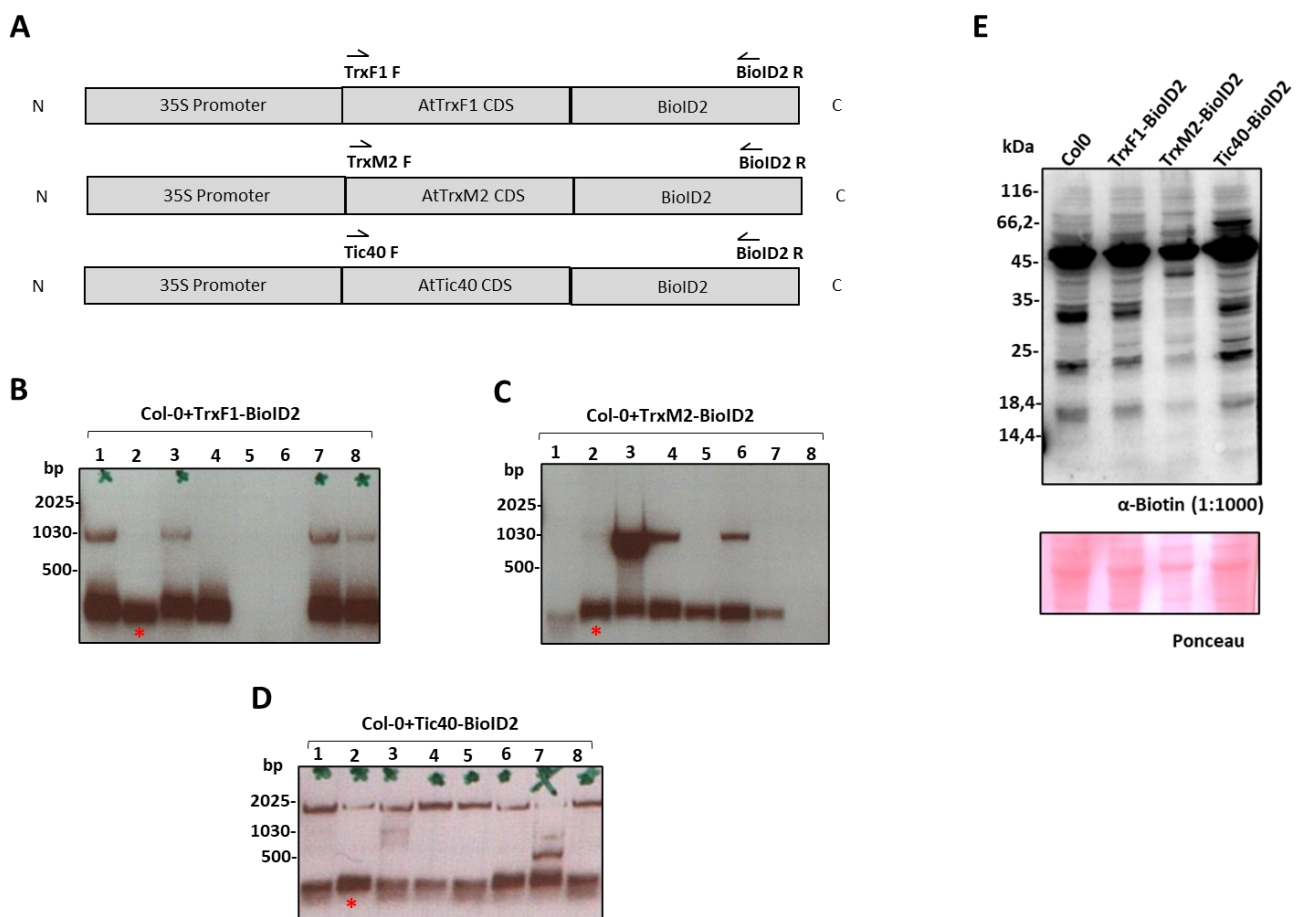
- What exactly is the Tic40's role: a cochaperone during the import process, a component to mediate preprotein quality control or a protein that actively participates in thylakoid biogenesis by selecting which proteins to import?
- Given that the inner envelope membrane contains two channel proteins, Tic110 and Tic20, could one of those proteins be specialized in the translocation of specific proteins, and the other serves as the main import channel?
- Is there a connection between the thylakoid and inner envelope membranes in sensing and responding to redox signaling via Trx family proteins?
- Is the Trx-based redox system combined with the interaction of Tic40 and Pic1 proteins involved in the regulation of stromal iron levels?

More research is clearly required to address these issues above. Overall, this information may significantly improve the current understanding of the translocation process in the chloroplast's inner envelope membrane. In the future, determining the exact roles of the system's components will be a tough challenge.

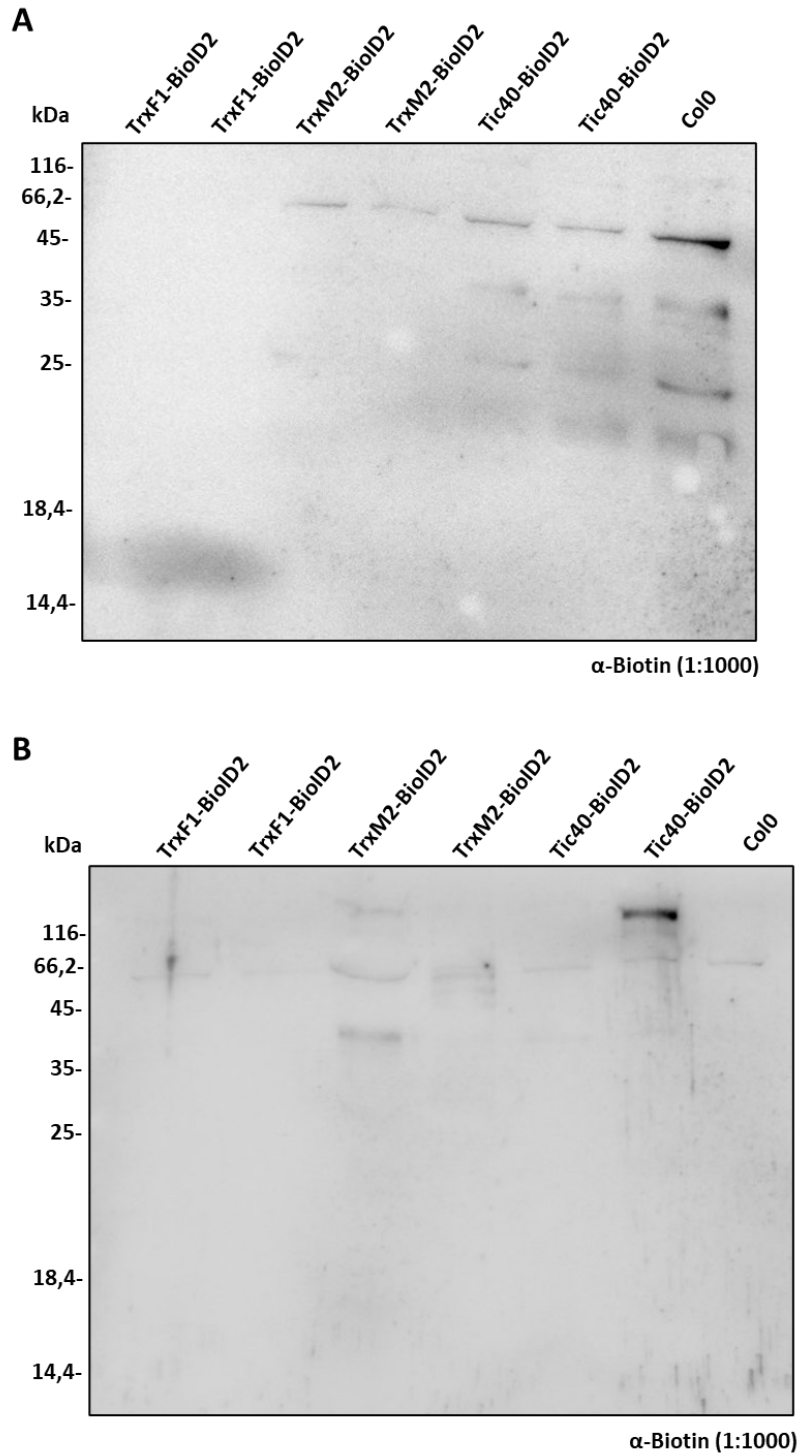
5 Supplemental Figures



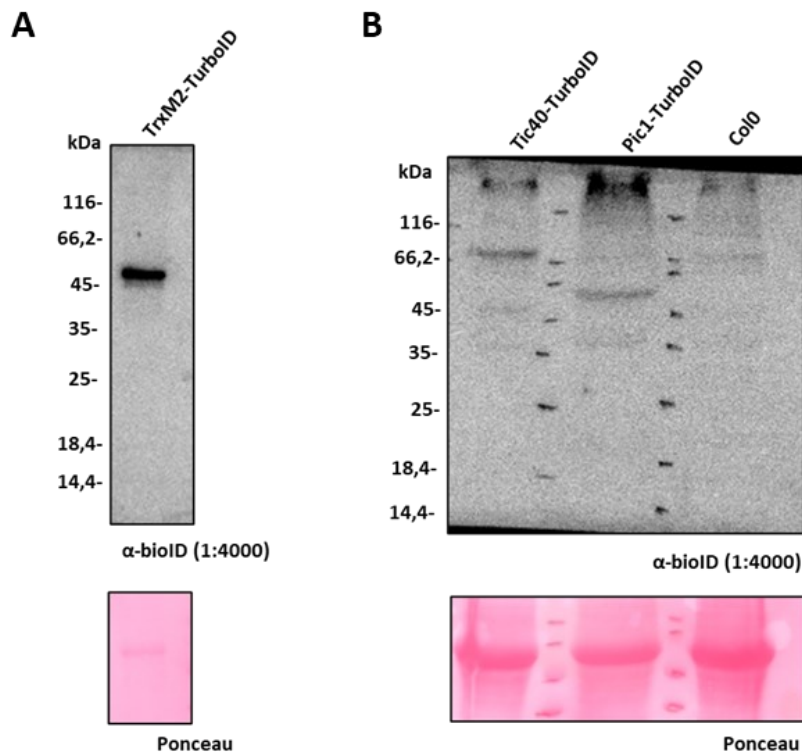
Supplemental Figure 1: BioID2 tagged candidate proteins exhibit biotinylation after 18 hours of the incubation period. Plasmids were transformed to *Nicotiana benthamiana* using Agrobacterium mediated gene transfer. Plants were incubated for two to three days prior to biotin infiltration. ~500 μ M biotin solution was infiltrated to the leaves on the same spots that were used for plasmid intake. After 18 hours of the reaction period, protein samples were extracted from the leaves and subjected to immunoblotting against α -biotin antibody. Non-transformed Agrobacterium infiltrated leaves were used as the negative control. Protein sizes are: TrxF1-BioID2: ~47 kDa, TrxM2-BioID2: ~48 kDa, Tic40-BioID2: ~77 kDa, Pic1-BioID2: ~59 kDa. Neg: Negative Control.



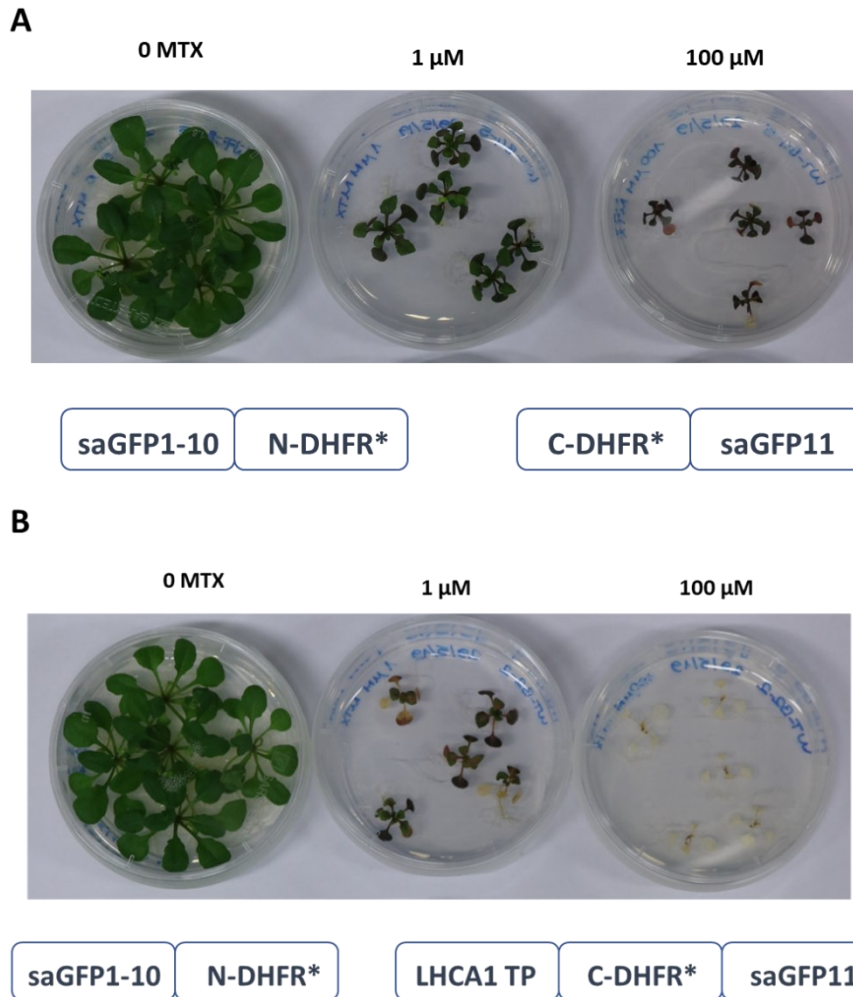
Supplemental Figure 2: Generation of stable plant lines expressing candidate proteins tagged with BioID2. Candidate proteins were transformed to WT Col-0 *Arabidopsis thaliana* plants as described in the materials and methods section. Successful transformants were selected against herbicide selection, checked concerning the plasmid insertion and grown in liquid culture for 14 days. The biotinylation reaction was initiated by adding a 500 μ M biotin solution to the medium. The reaction was stopped after 18 hours by incubation of the plants in ice-cold water. WT Col-0 seeds were used as the control group. Total proteins were extracted and subjected to immunoblotting against α -biotin. Candidate proteins: TrxF1, TrxM2, Tic40 fused with BioID2. N: N-terminus, C: C-terminus. The red asterisk (*) sign was used to depict primer dimers. **(A)** Transformed plasmids were represented with schematic depiction. The coding sequence (CDS) of the candidate genes fused with BioID2 under the control of 35S promoter was inserted into the genome of WT Col-0. The presence of the inserted plasmid was checked via primers indicated on the plasmid scheme for each candidate gene. BioID2 R (BioID2 D-E R) is designed to bind downstream region of the BioID2. Independent insertion lines for each fusion plasmids were used for the analysis. **(B)** Genotyping analysis of TrxF1-BioID2 insertion. TrxF1 F (*AtTrxF1* C-D F) binds to upstream region of *AtTrxF1* CDS. Expected PCR product (TrxF1 F + BioID2 R): \sim 1000 bp. **(C)** Genotyping analysis of TrxM2-BioID2 insertion. TrxM2 F (*AtTrxM2* C-D F) binds to upstream region of *AtTrxM2* CDS. Expected PCR product (TrxM2 F + BioID2 R): \sim 1000 bp. **(D)** Genotyping analysis of Tic40-BioID2 insertion. Tic40 F (*AtTic40* C-D F1) binds to upstream region of *AtTic40* CDS. Expected PCR product (Tic40 F + BioID2 R): \sim 1500 bp. **(E)** Immunoblot analysis of stable plant lines to detect biotinylation with α -biotin antibody. Protein sizes are: TrxF1-BioID2: \sim 47 kDa, TrxM2-BioID2: \sim 48 kDa, Tic40-BioID2: \sim 77 kDa.



Supplemental Figure 3: Immunoblot analysis of stable plant lines bearing BioID2 tag, subjected to different biotin uptake strategies. Approximately 4 weeks old soil grown plants were tested against biotin uptake either by directly incubating the leaves with biotin solution in a tray or infiltration into the leaves. Total proteins were isolated after 2 days of the biotin treatment. Immunoblotting was done against α -biotin. WT Col-0 plants were used as the control group. Candidate proteins: TrxF1, TrxM2, Tic40 fused with BioID2. **(A)** Leaves were incubated into a tray containing biotin solution. **(B)** Leaves were infiltrated with the biotin solution.



Supplemental Figure 4: Immunoblot analysis of stable plant lines suitable for proximity labeling by TurboID. Total proteins were isolated from the 14 days old plants and used for immunoblotting. α -bioID antibody was used for the detection. Ponceau staining shows the protein loading information. Expected protein sizes are TrxM2-TurboID: ~56 kDa, Tic40-TurboID: ~85 kDa, Pic1-TurboID: ~67 kDa. WT Col-0 plants were used as control. **(A)** The loaded plant genotype was: TrxM2-TurboID. **(B)** Loaded plant genotypes were: Tic40-TurboID, Pic1-TurboID and WT Col-0.



Supplemental Figure 5: Stable transformation of wild type *Arabidopsis thaliana* plants with DHFR* dependent PCA constructs could escape the toxicity of MTX. As increasing concentrations of the MTX inhibits plant growth, DHFR* enables plants to proliferate and develop further. **(A)** Stable lines expressing DHFR* fragments without the transit peptide. Fragment combinations were depicted under each figure. **(B)** Transit peptide mediates the attached fragments be subjected to the chloroplast, hence, inhibiting the DHFR* reformation. Therefore, the plants were sensitive to MTX.

6 Supplemental Tables

Supplemental Table 1: The detailed list of PL and split-PL enzymes used for PPI mapping

Enzyme	Origin	Size (kDa)	Labeling Time	Temperature (°C)	Labeling Radius (nm)	Substrate/ Cytotoxicity	Modification Sites	Organisms	References
APEX	Pea/Soybean	28	1 min	37	<20	Biotin phenol+ H ₂ O ₂ (toxic)	Tyr, Trp, Cys, His	Mammalian cells, flies	(Hung et al., 2014; Martell et al., 2012)
APEX2	Soybean	28	1 min	37	<20	Biotin phenol+ H ₂ O ₂ (toxic)	Tyr, Trp, Cys, His	Mammalian cells, bacteria, yeast, <i>Chlamydia</i>	(Lam et al., 2014)
HRP	Horseradish Peroxidase	44	5 min-2 h	37	200-300	Biotin phenol+ H ₂ O ₂ (toxic)	Tyr, Trp, Cys, His	Human, chicken cell lines	(Kotani et al., 2008)
BioID	<i>Escherichia coli</i>	35	16-24 h	37	~10	Biotin (non-toxic)	Lys	Mammalian cells, yeast, <i>Trypanosoma brucei</i> , Dictyostelium, plant cells	(Roux et al., 2012)
BioID2	<i>Aquifex aeolicus</i>	27	16-24 h	37	~10	Biotin (non-toxic)	Lys	Mammalian cells, plant cells	(Kim et al., 2016)
BASU	<i>Bacillus subtilis</i>	29	12 h	37	~10	Biotin (non-toxic)	Lys	Mammalian cells	(Ramanathan et al., 2018)
TurboID	<i>Escherichia coli</i>	35	≥10 min	25	~10	Biotin (non-toxic)	Lys	Mammalian cells, flies, worms, yeast, plant cells	(Branon et al., 2018)
miniTurboID	<i>Escherichia coli</i>	28	≥10 min	25	~10	Biotin (non-toxic)	Lys	Mammalian cells, flies, worms, yeast, plant cells	(Branon et al., 2018)

AirID	Synthetic	35	3-6 h	26	~10	Biotin (non-toxic)	Lys	Mammalian cells, wheat cell free systems	(Kido et al., 2020)
EXCELL	<i>Staphylococcus aureus</i>	24	≥30 min	37	Not available	Biotin-LPETG (non-toxic)	N-terminal Gly	Mammalian cells	(Ge et al., 2019)
PUP-IT	<i>Corynebacterium glutamicum</i>	51	24 h	37	Not available	Pup (non-toxic)	Lys	Mammalian cells	(Liu et al., 2018)
NEDDylation	Human Ubc12	21	24-36 h	37	Direct contact	NEDD8 (non-toxic)	Lys	Mammalian cells	(Hill et al., 2016)
microID	BioID2	19.7	≥1 h	25	Not available	Biotin (non-toxic)	Lys	Mammalian cells	(Zhao et al., 2021)-preprint
ultraID	BioID2	19.7	≥10 min	25	Not available	Biotin (non-toxic)	Lys	Mammalian cells	(Zhao et al., 2021)-preprint
split-HRP (G213/N214)	HRP		≥1-10 min	37	200-300	Biotin phenol+ H ₂ O ₂ (toxic)	Tyr, Trp, Cys, His	Mammalian cells	(Martell et al., 2016)
split-APEX2 (G201/L202)	APEX2		≥1 min	37	<20	Biotin phenol+ H ₂ O ₂ (toxic)	Tyr, Trp, Cys, His	Mammalian cells	(Xue et al., 2017)
split-APEX2 (E200/G201)	APEX2		≥1 min	37	<20	Biotin phenol+ H ₂ O ₂ (toxic)	Tyr, Trp, Cys, His	Mammalian cells	(Han et al., 2019)
split-BioID (E140/Q141)	BioID		≥16 h	37	~10	Biotin (non-toxic)	Lys	Mammalian cells	(De Munter et al., 2017)
split-BioID (E256/G257)	BioID		≥20 h	37	~10	Biotin (non-toxic)	Lys	Mammalian cells	(Schopp et al., 2017)
ContactID (G78/G79)	BioID		≥16 h	37	~10	Biotin (non-toxic)	Lys	Mammalian cells	(Kwak et al., 2020)
split-TurboID (L73/G74)	TurboID		≥1-4 h	25	~10	Biotin (non-toxic)	Lys	Mammalian cells	(Cho et al., 2020)

Supplemental Table 2: Complete list of potential **chloroplast** localized *AtTic40* interacting/associating proteins. Proteins were identified by proximity labeling with TurboID. Both control (WT-Col-0) and overexpression (Tic40-TurboID) groups were analyzed in three biological replicates. **Bait:** Candidate protein, **Prey:** Interaction partner proteins identified by TurboID.

No	Bait	Prey	Log2 Fold Change	Gene Name	Functional Annotation
1	Tic40	AT5G16620	11.89	TIC40	Protein TIC 40 (Translocon at the inner envelope membrane of chloroplasts 40)
2	Tic40	AT2G24020	10.54	STIC2	Nucleoid-associated protein (Suppressor of tic40 protein 2)
3	Tic40	AT1G48850	8.31	EMB1144	Chorismate synthase
4	Tic40	AT3G55250	8.28	PSA3	Photosystem I assembly factor PSA3, chloroplastic (Protein PHOTOSYSTEM I ASSEMBLY 3) (Protein PIGMENT DEFECTIVE 329)
5	Tic40	AT2G44650	7.42	CPN10-2	10 kDa chaperonin 2
6	Tic40	AT2G01140	7.09	FBA3	Fructose-bisphosphate aldolase 3 (Protein PIGMENT DEFECTIVE 345)
7	Tic40	AT1G73060	7.02	LPA3	Protein LPA3 (Protein LOW PSII ACCUMULATION 3)
8	Tic40	AT5G45390	6.78	CLPP4	ATP-dependent Clp protease proteolytic subunit 4
9	Tic40	AT5G66120	6.60	DHQS	3-dehydroquinate synthase
10	Tic40	AT5G53460	6.56	GLT1	Glutamate synthase 1 [NADH]
11	Tic40	AT1G06950	6.50	TIC110	Protein TIC110 (Translocon at the inner envelope membrane of chloroplasts 110)
12	Tic40	AT5G03900	6.50		Uncharacterized protein
13	Tic40	AT5G23010	6.45	MAM1	Methylthioalkylmalate synthase 1
14	Tic40	AT1G21600	6.21	PTAC6	PLASTID TRANSCRIPTIONALLY ACTIVE protein 6
15	Tic40	AT3G60210	6.18	CPN10-1	10 kDa chaperonin 1
16	Tic40	AT1G43800	6.10	S-ACP-DES6	Stearoyl-[acyl-carrier-protein] 9-desaturase 6
17	Tic40	AT1G50320	5.84	ATHX	Thioredoxin X
18	Tic40	AT3G05350	5.84	APP2	Aminopeptidase P2
19	Tic40	AT1G22410	5.77	DHS3	Putative 3-deoxy-D-arabino-heptulosonate 7-phosphate synthase
20	Tic40	AT1G06680	5.65	PSBP1	Oxygen-evolving enhancer protein 2-1 (23 kDa subunit of oxygen evolving system of photosystem II)
21	Tic40	AT2G43750	5.61	OASB	Cysteine synthase
22	Tic40	AT5G10920	5.56		Argininosuccinate lyase
23	Tic40	AT5G54810	5.54	TSB1	Tryptophan synthase beta chain 1
24	Tic40	AT4G38970	5.49	FBA2	Fructose-bisphosphate aldolase 2
25	Tic40	AT3G12930	5.41	IJ	Protein Iojap
26	Tic40	AT2G04030	5.35	HSP90-5	Heat shock protein 90-5
27	Tic40	AT4G30620	5.33		Nucleoid-associated protein

28	Tic40	AT4G33680	5.30	DAP	LL-diaminopimelate aminotransferase
29	Tic40	AT5G50920	5.24	CLPC1	Chaperone protein ClpC1
30	Tic40	AT1G67280	5.21		Probable lactoylglutathione lyase
31	Tic40	AT3G17810	5.21	PYD1	Dihydropyrimidine dehydrogenase (NADP(+))
32	Tic40	AT4G29840	5.13	TS1	Threonine synthase 1
33	Tic40	AT5G20720	5.10	CPN20	20 kDa chaperonin
34	Tic40	AT3G11630	5.08	BAS1	2-Cys peroxiredoxin BAS1
35	Tic40	AT1G67090	5.01	RBCS-1A	Ribulose biphosphate carboxylase small subunit 1A
36	Tic40	AT2G38040	4.84	CAC3	Acetyl-coenzyme A carboxylase carboxyl transferase subunit alpha
37	Tic40	AT5G13110	4.83	G6PD2	Glucose-6-phosphate 1-dehydrogenase 2
38	Tic40	AT2G04400	4.83	IGPS	Indole-3-glycerol phosphate synthase
39	Tic40	AT1G31330	4.81	PSAF	Photosystem I reaction center subunit III
40	Tic40	AT2G38550	4.81	FAX3	Protein FATTY ACID EXPORT 3
41	Tic40	AT2G47730	4.79	GSTF8	Glutathione S-transferase F8
42	Tic40	AT2G37860	4.79	RE, LCD1	Protein RETICULATA (Protein LOWER CELL DENSITY 1)
43	Tic40	AT5G55220	4.78	TIG	Trigger factor-like protein TIG
44	Tic40	AT3G01120	4.77	CGS1	Cystathionine gamma-synthase 1
45	Tic40	AT5G54770	4.77	THI1	Thiamine thiazole synthase
46	Tic40	AT5G04590	4.76	SIR	Assimilatory sulfite reductase (ferredoxin)
47	Tic40	AT4G21860	4.75	MSRB2	Peptide methionine sulfoxide reductase B2
48	Tic40	AT3G04790	4.74	RPI3	Probable ribose-5-phosphate isomerase 3
49	Tic40	AT1G50900	4.72	LTD, GDC1	Protein LHCP TRANSLOCATION DEFECT (Protein GRANA-DEFICIENT CHLOROPLAST 1)
50	Tic40	AT5G11880	4.70	LYSA2	Diaminopimelate decarboxylase 2
51	Tic40	AT1G29910	4.69	LHCB1.2	Chlorophyll a-b binding protein 3
52	Tic40	AT1G18500	4.67	IPMS1	2-isopropylmalate synthase 1
53	Tic40	AT1G15500	4.66	AATP2	ADP,ATP carrier protein 2
54	Tic40	AT5G22830	4.61	MRS2-11	Magnesium transporter MRS2-11
55	Tic40	AT5G16440	4.59	IPP1	Isopentenyl-diphosphate Delta-isomerase I
56	Tic40	AT2G37220	4.59	CP29B	RNA-binding protein CP29B
57	Tic40	AT1G63940	4.59	MDAR5	Monodehydroascorbate reductase
58	Tic40	AT3G58610	4.56		Ketol-acid reductoisomerase
59	Tic40	AT1G08490	4.55	NFS2	Cysteine desulfurase 1
60	Tic40	AT5G15450	4.55	CLPB3	Chaperone protein ClpB3
61	Tic40	ATCG00280	4.51	psbC	Photosystem II CP43 reaction center protein
62	Tic40	AT3G20320	4.50	TGD2	Protein TRIGALACTOSYLDIACYLGLYCEROL 2
63	Tic40	AT1G55480	4.49	MET1	Protein MET1 (PDZ domain, K-box domain, and TPR region containing protein)
64	Tic40	AT4G13200	4.48		Uncharacterized protein
65	Tic40	AT3G59890	4.43	DAPB2	4-hydroxy-tetrahydrodipicolinate

					reductase 2
66	Tic40	AT5G38410	4.41	RBCS-3B	Ribulose biphosphate carboxylase small subunit 3B
67	Tic40	AT3G46780	4.41	PTAC16	Protein PLASTID TRANSCRIPTIONALLY ACTIVE 16
68	Tic40	AT5G04740	4.41	ACR12	ACT domain-containing protein ACR12 (Protein ACT DOMAIN REPEATS 12)
69	Tic40	AT4G14070	4.39	AAE15	Long-chain-fatty-acid--[acyl-carrier-protein] ligase AEE15
70	Tic40	AT3G18890	4.33	TIC62	Protein TIC 62 (Translocon at the inner envelope membrane of chloroplasts 62)
71	Tic40	AT4G39980	4.33	DHS1	Phospho-2-dehydro-3-deoxyheptonate aldolase 1
72	Tic40	AT4G17040	4.31	CLPR4	ATP-dependent Clp protease proteolytic subunit-related protein 4
73	Tic40	AT5G23020	4.30	MAM3	Methylthioalkylmalate synthase 3
74	Tic40	AT3G44890	4.30	RPL9	50S ribosomal protein L9
75	Tic40	AT2G34590	4.29	E1-BETA-2	Pyruvate dehydrogenase E1 component subunit beta-3
76	Tic40	AT1G53670	4.29	MSRB1	Peptide methionine sulfoxide reductase B1
77	Tic40	AT4G33030	4.28	SQD1	UDP-sulfoquinovose synthase
78	Tic40	AT1G76080	4.27	CDSP32	Thioredoxin-like protein CDSP32
79	Tic40	AT5G23310	4.26	FSD3	Superoxide dismutase [Fe] 3
80	Tic40	AT4G33580	4.25	BCA5	Beta carbonic anhydrase 5
81	Tic40	AT4G39120	4.24	HISN7	Bifunctional phosphatase IMPL2 (Histidinol-phosphatase)
82	Tic40	AT3G29320	4.23	PHS1	Alpha-glucan phosphorylase 1
83	Tic40	AT3G47470	4.19	LHCA4	Chlorophyll a-b binding protein 4
84	Tic40	AT4G36810	4.19	GGPPS1	Heterodimeric geranylgeranyl pyrophosphate synthase large subunit 1
85	Tic40	AT1G31230	4.17	AKHSDH1	Bifunctional aspartokinase/homoserine dehydrogenase 1
86	Tic40	AT2G39730	4.16	RCA	Ribulose biphosphate carboxylase/oxygenase activase
87	Tic40	ATCG01120	4.16	rps15	30S ribosomal protein S15
88	Tic40	AT1G55670	4.10	PSAG	Photosystem I reaction center subunit V
89	Tic40	ATCG00680	4.08	psbB	Photosystem II CP47 reaction center protein
90	Tic40	AT4G13430	4.06	IIL1	3-isopropylmalate dehydratase large subunit
91	Tic40	AT3G06200	4.03	GK3	Guanylate kinase 3
92	Tic40	AT1G67700	4.03	HHL1	Protein HHL1 (Hypersensitive to high light 1)
93	Tic40	AT4G25130	3.98	MSR4	Peptide methionine sulfoxide reductase A4
94	Tic40	AT2G47450	3.97	CPSRP43	Signal recognition particle 43 kDa protein
95	Tic40	AT2G05990	3.97	MOD1, ENR-A	Enoyl-[acyl-carrier-protein] reductase [NADH] (Protein MOSAIC DEATH 1)
96	Tic40	AT4G09650	3.96	ATPD	ATP synthase subunit delta

97	Tic40	ATCG00800	3.94	rps3	30S ribosomal protein S3
98	Tic40	AT5G08280	3.92	HEMC	Porphobilinogen deaminase
99	Tic40	AT5G03650	3.92	SBE2.2	1,4-alpha-glucan-branching enzyme 2-2
100	Tic40	AT3G58990	3.88	SSU3	3-isopropylmalate dehydratase small subunit 3 (Isopropylmalate isomerase 1) (Isopropylmalate isomerase small subunit 3) (IPMI SSU3) (Methylthioalkylmalate isomerase small subunit) (MAM-IS)
101	Tic40	AT1G13270	3.88	MAP1B	Methionine aminopeptidase 1B
102	Tic40	AT4G16390	3.85	P67, SVR7	Pentatricopeptide repeat-containing protein (Protein SUPPRESSOR OF VARIEGATION 7)
103	Tic40	AT3G23940	3.85	DHAD	Dihydroxy-acid dehydratase
104	Tic40	AT3G58140	3.84		Phenylalanine--tRNA ligase
105	Tic40	AT1G68260	3.84	ALT3	Acyl-acyl carrier protein thioesterase ATL3
106	Tic40	AT5G49910	3.82	HSP70-7	Heat shock 70 kDa protein 7
107	Tic40	AT4G34120	3.81	CBSX2	CBS domain-containing protein CBSX2
108	Tic40	AT5G07020	3.77	MPH1	Protein MAINTENANCE OF PSII UNDER HIGH LIGHT 1
109	Tic40	AT2G14750	3.77	APK1	Adenylyl-sulfate kinase 1
110	Tic40	AT1G62750	3.76	CPEFG	Elongation factor G (Elongation factor EF-G/SCO1)
111	Tic40	AT3G59400	3.75	GUN4	Tetrapyrrole-binding protein
112	Tic40	AT5G01220	3.75	SQD2	Sulfoquinovosyl transferase SQD2 (Protein SULFOQUINOVOSYLDIACYLGLYCEROL 2)
113	Tic40	AT3G22890	3.75	APS1	ATP sulfurylase 1
114	Tic40	AT2G31810	3.75		Acetolactate synthase small subunit 2
115	Tic40	AT1G02560	3.75	CLPP5	ATP-dependent Clp protease proteolytic subunit 5
116	Tic40	AT2G37660	3.73		Uncharacterized protein
117	Tic40	AT5G26742	3.72	RH3	DEAD-box ATP-dependent RNA helicase 3
118	Tic40	AT3G53460	3.71	CP29A	29 kDa ribonucleoprotein
119	Tic40	AT1G15820	3.70	Lhcb6	Chlorophyll a-b binding protein
120	Tic40	AT3G61470	3.68	LHCA2	Photosystem I chlorophyll a/b-binding protein 2
121	Tic40	AT2G22360	3.68	DJA6	Chaperone protein dnaJ A6
122	Tic40	AT4G35630	3.68	PSAT1	Phosphoserine aminotransferase 1
123	Tic40	AT5G26030	3.67	FC1	Ferrochelatase-1
124	Tic40	AT3G27850	3.66	RPL12C	50S ribosomal protein L12-3
125	Tic40	AT3G53580	3.65	DAPF	Diaminopimelate epimerase
126	Tic40	AT1G80300	3.61	AATP1	ADP,ATP carrier protein 1
127	Tic40	AT5G48300	3.59	APS1	Glucose-1-phosphate adenylyltransferase small subunit
128	Tic40	AT5G64940	3.59	ABC1K8	Protein ACTIVITY OF BC1 COMPLEX KINASE 8
129	Tic40	AT4G03520	3.59	TRXM2	Thioredoxin M2
130	Tic40	AT5G13650	3.57	SVR3	Putative elongation factor TypA-like SVR3

131	Tic40	ATCG00780	3.56	rpl14	50S ribosomal protein L14
132	Tic40	AT3G10050	3.56	OMR1	Threonine dehydratase biosynthetic
133	Tic40	AT4G15560	3.55	DXS	1-deoxy-D-xylulose-5-phosphate synthase
134	Tic40	AT4G36910	3.55	CBSX1	CBS domain-containing protein CBSX1
135	Tic40	AT1G54630	3.52	ACP3	Acyl carrier protein 3
136	Tic40	AT3G63410	3.52	VTE3	2-methyl-6-phytyl-1,4-hydroquinone methyltransferase
137	Tic40	AT3G08640	3.51	RER3	Protein RETICULATA-RELATED 3
138	Tic40	AT4G01690	3.50	PPOX1	Protoporphyrinogen oxidase 1
139	Tic40	AT3G06350	3.50	EMB3004	Bifunctional 3-dehydroquinate dehydratase/shikimate dehydrogenase
140	Tic40	AT5G11520	3.50	ASP3	Aspartate aminotransferase 3
141	Tic40	AT2G29630	3.48	THIC	Phosphomethylpyrimidine synthase
142	Tic40	AT1G01090	3.48	PDH-E1 ALPHA	Pyruvate dehydrogenase E1 component subunit alpha-3
143	Tic40	AT5G38430	3.47	RBCS-1B	Ribulose biphosphate carboxylase small subunit 1B
144	Tic40	AT3G01180	3.45	SS2	Starch synthase 2
145	Tic40	AT1G69740	3.45	HEMB1	Delta-aminolevulinic acid dehydratase 1
146	Tic40	AT1G49970	3.44	CLPR1	ATP-dependent Clp protease proteolytic subunit-related protein 1
147	Tic40	AT2G20890	3.44	THF1	Protein THYLAKOID FORMATION 1
148	Tic40	AT5G42650	3.43	CYP74A	Allene oxide synthase (Cytochrome P450 74A)
149	Tic40	AT2G33800	3.41	rps5	30S ribosomal protein S5
150	Tic40	AT1G74470	3.40	CHLP	Geranylgeranyl diphosphate reductase
151	Tic40	AT2G22480	3.40	PFK5	ATP-dependent 6-phosphofructokinase 5 (Phosphohexokinase 5)
152	Tic40	AT4G28750	3.39	PSAE1	Photosystem I reaction center subunit IV A
153	Tic40	AT1G04620	3.38	HCAR	7-hydroxymethyl chlorophyll a reductase
154	Tic40	AT4G33510	3.36	DHS2	Phospho-2-dehydro-3-deoxyheptonate aldolase 2
155	Tic40	AT1G15390	3.36	PDF1A	Peptide deformylase 1A
156	Tic40	AT3G48560	3.36	ALS	Acetolactate synthase
157	Tic40	AT3G44720	3.35	ADT4	Arogenate dehydratase 4
158	Tic40	AT4G35250	3.33	HCF244	Protein HIGH CHLOROPHYLL FLUORESCENCE PHENOTYPE 244
159	Tic40	AT3G04550	3.32	RAF1.2	Rubisco accumulation factor 1.2
160	Tic40	AT1G55490	3.31	CPN60B1	Chaperonin 60 subunit beta 1
161	Tic40	AT2G27820	3.30	ADT3	Arogenate dehydratase 3
162	Tic40	AT4G23100	3.27	GSH1	Glutamate--cysteine ligase
163	Tic40	AT1G44575	3.26	PSBS	Photosystem II 22 kDa protein
164	Tic40	AT4G04020	3.23	PAP1	Probable plastid-lipid-associated protein 1
165	Tic40	AT1G12900	3.22	GAPA2	Glyceraldehyde-3-phosphate dehydrogenase GAPA2
166	Tic40	AT2G15620	3.22	NIR1	Ferredoxin--nitrite reductase
167	Tic40	AT3G52960	3.21	PRXIIIE	Peroxiredoxin-2E (Glutaredoxin-dependent

					peroxiredoxin)
168	Tic40	AT5G64300	3.21	RIBA1	Bifunctional riboflavin biosynthesis protein RIBA 1
169	Tic40	AT5G51070	3.20	CLPD	Chaperone protein ClpD
170	Tic40	AT1G52230	3.20	PSAH2	Photosystem I reaction center subunit VI-2
171	Tic40	AT5G42270	3.19	FTSH5	ATP-dependent zinc metalloprotease FTSH 5
172	Tic40	AT2G43100	3.17	SSU2	3-isopropylmalate dehydratase small subunit 2
173	Tic40	AT5G01600	3.17	FER1	Ferritin-1
174	Tic40	AT5G67030	3.13	ZEP, ABA1	Zeaxanthin epoxidase (Protein ABA DEFICIENT 1)
175	Tic40	ATCG00480	3.12	atpB	ATP synthase subunit beta
176	Tic40	AT5G50100	3.11		Uncharacterized protein
177	Tic40	AT4G20360	3.10	TUFA RAB8D	Elongation factor Tu (Ras-related protein Rab8D)
178	Tic40	AT2G43030	3.07	RPL3A	50S ribosomal protein L3-1
179	Tic40	AT1G09830	3.06	PUR2	Phosphoribosylamine--glycine ligase
180	Tic40	AT5G22510	3.06	INVE	Alkaline/neutral invertase E
181	Tic40	AT3G23400	3.05	PAP6	Plastid-lipid-associated protein 6
182	Tic40	AT1G77060	3.04		Carboxyvinyl-carboxyphosphonate phosphorylmutase
183	Tic40	AT2G02740	3.04	WHY3, PTAC11	Single-stranded DNA-binding protein WHY3 (Protein PLASTID TRANSCRIPTIONALLY ACTIVE 11)
184	Tic40	AT2G20260	3.03	PSAE2	Photosystem I reaction center subunit IV B
185	Tic40	AT3G54660	3.02	EMB2360	Glutathione reductase (Protein EMBRYO DEFECTIVE 2360)
186	Tic40	AT3G02630	3.01	S-ACP-DES5	Stearoyl-[acyl-carrier-protein] 9-desaturase 5
187	Tic40	AT4G24280	3.00	HSP70-6	Heat shock 70 kDa protein 6
188	Tic40	AT3G47520	2.99		Malate dehydrogenase
189	Tic40	AT3G25660	2.98	GATA	Glutamyl-tRNA(Gln) amidotransferase subunit A
190	Tic40	AT1G62640	2.97		3-oxoacyl-[acyl-carrier-protein] synthase III
191	Tic40	ATCG00500	2.97	accD	Acetyl-coenzyme A carboxylase carboxyl transferase subunit beta
192	Tic40	ATCG00160	2.96	rps2	30S ribosomal protein S2
193	Tic40	ATCG00770	2.96	rps8	30S ribosomal protein S8
194	Tic40	AT3G45140	2.95	LOX2	Lipoxygenase 2
195	Tic40	AT2G22450	2.95	RIBA2	Monofunctional riboflavin biosynthesis protein RIBA 2
196	Tic40	AT1G03130	2.93	PSAD2	Photosystem I reaction center subunit II-2
197	Tic40	AT3G25860	2.92	LTA2	Dihydrolipoyllysine-residue acetyltransferase component 4 of pyruvate dehydrogenase complex
198	Tic40	ATCG00740	2.92	rpoA	DNA-directed RNA polymerase subunit alpha

199	Tic40	AT5G52920	2.92	PKP2	Plastidial pyruvate kinase 2
200	Tic40	AT5G16290	2.89	VAT1	Acetolactate synthase small subunit 1
201	Tic40	AT4G26900	2.89	HISN4	Imidazole glycerol phosphate synthase hisHF
202	Tic40	AT4G34730	2.89		Probable ribosome-binding factor A
203	Tic40	AT3G63140	2.89	CSP41A	Chloroplast stem-loop binding protein of 41 kDa a
204	Tic40	AT1G79750	2.88	NADP-ME4	NADP-dependent malic enzyme 4
205	Tic40	ATCG00490	2.87	rbcL	Ribulose biphosphate carboxylase large chain
206	Tic40	AT3G08940	2.86	LHCB4.2	Chlorophyll a-b binding protein CP29.2 (LHCII protein 4.2)
207	Tic40	AT5G36880	2.85	ACS	Acetyl-coenzyme A synthetase
208	Tic40	AT1G75350	2.85	RPL31	50S ribosomal protein L31
209	Tic40	AT3G04870	2.83	ZDS1	Zeta-carotene desaturase
210	Tic40	AT1G14030	2.83	LSMT-L	[Fructose-bisphosphate aldolase]-lysine N-methyltransferase
211	Tic40	AT5G24020	2.80	MIND1	Putative septum site-determining protein minD homolog
212	Tic40	ATCG00130	2.80	atpF	ATP synthase subunit b
213	Tic40	AT3G16950	2.79	LPD1	Dihydrolipoyl dehydrogenase 1
214	Tic40	AT1G19800	2.79	TGD1	Protein TRIGALACTOSYLDIACYLGLYCEROL 1
215	Tic40	AT5G47870	2.78	RAD52-2	DNA repair RAD52-like protein 2
216	Tic40	AT1G03680	2.77	TRXM1	Thioredoxin M1
217	Tic40	AT4G10340	2.76	LHCB5	Chlorophyll a-b binding protein CP26 (Light-harvesting complex II protein 5)
218	Tic40	AT4G04640	2.75	ATPC1	ATP synthase gamma chain 1
219	Tic40	AT4G29060	2.74	PETs	Polyprotein of EF-Ts (150 kDa pro-protein)
220	Tic40	AT4G22240	2.73	PAP2	Probable plastid-lipid-associated protein 2
221	Tic40	AT2G35490	2.73	PAP3	Probable plastid-lipid-associated protein 3
222	Tic40	AT5G23060	2.72	CAS	Calcium sensing receptor
223	Tic40	AT4G21990	2.72	APR3, PRH26	5'-adenylylsulfate reductase 3 (Thioredoxin-independent APS reductase 3)
224	Tic40	AT5G14200	2.72	IMDH1	3-isopropylmalate dehydrogenase 1
225	Tic40	AT5G24300	2.70	SS1	Starch synthase 1
226	Tic40	AT1G68720	2.70	TADA	tRNA(adenine(34)) deaminase (tRNA adenosine deaminase arginine)
227	Tic40	AT5G04140	2.70	GLU1	Ferredoxin-dependent glutamate synthase 1
228	Tic40	AT4G18480	2.68	CHLI1	Magnesium-chelatase subunit Chl1-1
229	Tic40	AT5G27380	2.67	GSH2	Glutathione synthetase
230	Tic40	AT2G40490	2.67	HEME2	Uroporphyrinogen decarboxylase 2
231	Tic40	AT1G05190	2.65	RPL6	50S ribosomal protein L6
232	Tic40	AT3G48110	2.64	EDD1	Glycine--tRNA ligase
233	Tic40	AT3G20330	2.64	PYRB	Aspartate carbamoyltransferase
234	Tic40	AT1G61520	2.64	LHCA3	Photosystem I chlorophyll a/b-binding

					protein 3-1
235	Tic40	AT4G34350	2.63	ISPH, CLB6	4-hydroxy-3-methylbut-2-enyl diphosphate reductase (Protein CHLOROPLAST BIOGENESIS 6)
236	Tic40	AT4G18240	2.62	SS4	Probable starch synthase 4
237	Tic40	AT1G32200	2.62	ATS1	Glycerol-3-phosphate acyltransferase
238	Tic40	AT1G17745	2.61	PGDH2	D-3-phosphoglycerate dehydrogenase 2
239	Tic40	AT3G48500	2.60	PTAC10	Protein PLASTID TRANSCRIPTIONALLY ACTIVE 10
240	Tic40	AT3G54900	2.60	GRXS14	Monothiol glutaredoxin-S14
241	Tic40	AT4G04770	2.60	ABC18	UPF0051 protein ABC18 (ABC transporter I family member 8)
242	Tic40	AT2G21330	2.59	FBA1	Fructose-bisphosphate aldolase 1
243	Tic40	AT3G46740	2.58	TOC75-3	Protein TOC75-3
244	Tic40	AT2G28900	2.54	OEP16-1	Outer envelope pore protein 16-1
245	Tic40	AT3G10940	2.53	LSF2	Phosphoglucan phosphatase LSF2
246	Tic40	AT5G35630	2.53	GLN2	Glutamine synthetase
247	Tic40	AT1G79530	2.52	GAPCP1	Glyceraldehyde-3-phosphate dehydrogenase GAPCP1
248	Tic40	AT5G28500	2.52	RAF1.1	Rubisco accumulation factor 1.1
249	Tic40	ATCG00020	2.52	psbA	Photosystem II protein D1
250	Tic40	AT5G54270	2.51	LHCB3	Chlorophyll a-b binding protein 3(Light-harvesting chlorophyll B-binding protein 3)
251	Tic40	AT1G29900	2.51	CARB	Carbamoyl-phosphate synthase large chain
252	Tic40	AT2G21590	2.51		Probable glucose-1-phosphate adenylyltransferase large subunit
253	Tic40	AT3G57610	2.50	PURA	Adenylosuccinate synthetase
254	Tic40	AT1G74030	2.49	ENO1	Enolase 1
255	Tic40	ATCG00580	2.47	psbE	Cytochrome b559 subunit alpha (PSII reaction center subunit V)
256	Tic40	AT1G10760	2.46	GWD1	Alpha-glucan water dikinase 1
257	Tic40	AT3G54640	2.46	TSA1	Tryptophan synthase alpha chain
258	Tic40	AT4G39210	2.45	APL3	Glucose-1-phosphate adenylyltransferase large subunit 3
259	Tic40	AT3G48730	2.42	GSA2	Glutamate-1-semialdehyde 2,1-aminomutase 2
260	Tic40	AT3G54050	2.41	CFBP1	Fructose-1,6-bisphosphatase 1
261	Tic40	AT3G27740	2.41	CARA	Carbamoyl-phosphate synthase small chain
262	Tic40	AT1G24360	2.40		3-oxoacyl-[acyl-carrier-protein] reductase
263	Tic40	AT5G03940	2.39	CPSRP54	Signal recognition particle 54 kDa protein
264	Tic40	AT2G47400	2.37	CP12-1	Calvin cycle protein CP12-1
265	Tic40	AT5G41670	2.34	PGD3	6-phosphogluconate dehydrogenase
266	Tic40	ATCG00120	2.33	atpA	ATP synthase subunit alpha
267	Tic40	AT5G12470	2.33	RER4	Protein RETICULATA-RELATED 4
268	Tic40	AT5G64290	2.33	DIT2-1	Dicarboxylate transporter 2.1
269	Tic40	AT2G46820	2.30	CURT1B	Protein CURVATURE THYLAKOID 1B (Thylakoid membrane phosphoprotein 14

					kDa)
270	Tic40	AT5G35360	2.30	CAC2	Biotin carboxylase
271	Tic40	AT3G52150	2.29	PSRP2	30S ribosomal protein 2 (Chloroplastic small ribosomal subunit protein cS22)
272	Tic40	ATCG00570	2.28	psbF	Cytochrome b559 subunit beta (PSII reaction center subunit VI)
273	Tic40	AT4G05180	2.27	PSBQ2	Oxygen-evolving enhancer protein 3-2
274	Tic40	AT4G23890	2.26	ndhS	NAD(P)H-quinone oxidoreductase subunit S
275	Tic40	AT3G63170	2.25	FAP1	Fatty-acid-binding protein 1
276	Tic40	AT3G22960	2.25	PKP1	Plastidial pyruvate kinase 1
277	Tic40	AT4G34200	2.24	PGDH1	D-3-phosphoglycerate dehydrogenase 1
278	Tic40	AT1G42970	2.23	GAPB	Glyceraldehyde-3-phosphate dehydrogenase GAPB
279	Tic40	AT5G64050	2.23	OVA3	Glutamate--tRNA ligase
280	Tic40	ATCG01060	2.20	psaC	Photosystem I iron-sulfur center
281	Tic40	AT1G03475	2.20	CPX1	Coproporphyrinogen-III oxidase 1
282	Tic40	AT5G16715	2.20	EMB2247	Valine--tRNA ligase (Protein EMBRYO DEFECTIVE 2247)
283	Tic40	ATCG00330	2.16	rps14	30S ribosomal protein S14
284	Tic40	AT1G34430	2.15	EMB3003	Dihydrolipoyllysine-residue acetyltransferase component 5 of pyruvate dehydrogenase complex
285	Tic40	AT3G26650	2.15	GAPA1	Glyceraldehyde-3-phosphate dehydrogenase GAPA1
286	Tic40	AT3G57560	2.14	NAGK	Acetylglutamate kinase
287	Tic40	AT4G17600	2.14	LIL3.1	Light-harvesting complex-like protein 3 isotype 1
288	Tic40	AT1G32440	2.13	PKP3	Plastidial pyruvate kinase 3
289	Tic40	AT4G21210	2.12	RP1	Pyruvate, phosphate dikinase regulatory protein 1
290	Tic40	AT4G34740	2.12	ASE2	Amidophosphoribosyltransferase 2
291	Tic40	AT1G11430	2.11	MORF9, RIP9	Multiple organellar RNA editing factor 9 (RNA editing-interacting protein 9)
292	Tic40	AT1G31190	2.10	IMPL1	Phosphatase IMPL1
293	Tic40	AT3G10230	2.10	LYCB, LCY1	Putative lycopene beta-cyclase
294	Tic40	ATCG00270	2.10	psbD	Photosystem II D2 protein
295	Tic40	AT4G27070	2.09	TSB2	Tryptophan synthase beta chain 2
296	Tic40	AT5G26570	2.05	GWD3	Phosphoglucan, water dikinase
297	Tic40	AT3G26710	2.02	CCB1	Protein COFACTOR ASSEMBLY OF COMPLEX C SUBUNIT B CCB1
298	Tic40	ATCG00660	2.02	rpl20	50S ribosomal protein L20
299	Tic40	AT4G19710	2.00	AKHSDH2	Bifunctional aspartokinase/homoserine dehydrogenase 2
300	Tic40	AT2G44040	1.96	DAPB1	4-hydroxy-tetrahydrodipicolinate reductase 1
301	Tic40	AT2G15290	1.96	TIC21, CIA5, PIC1	Protein TIC 21 (Translocon at the inner envelope membrane of chloroplasts 21)

					(PERMEASE IN CHLOROPLASTS 1)
302	Tic40	AT1G74960	1.95	KAS2	3-oxoacyl-[acyl-carrier-protein] synthase II
303	Tic40	AT1G02910	1.94	LPA1	Protein LOW PSII ACCUMULATION 1
304	Tic40	AT5G47190	1.92		50S ribosomal protein L19-2
305	Tic40	AT5G01530	1.92	LHCB4.1	Chlorophyll a-b binding protein CP29.1
306	Tic40	AT3G29310	1.92	BAG1	BAG family molecular chaperone regulator 8
307	Tic40	AT1G66430	1.92		Probable fructokinase-6
308	Tic40	AT1G32060	1.92		Phosphoribulokinase
309	Tic40	AT5G06290	1.89	2-Cys Prx	Thioredoxin-dependent peroxiredoxin
310	Tic40	AT3G12780	1.89	PGK1	Phosphoglycerate kinase 1
311	Tic40	ATCG00750	1.88	rps11	30S ribosomal protein S11
312	Tic40	AT2G28000	1.86	CPN60A1	Chaperonin 60 subunit alpha 1
313	Tic40	AT5G63420	1.86	RNJ	Ribonuclease J (RNase J)
314	Tic40	AT4G27440	1.85	PORB	Protochlorophyllide reductase B
315	Tic40	AT4G04850	1.82	KEA3	K(+) efflux antiporter 3
316	Tic40	ATCG00350	1.81	psaA	Photosystem I P700 chlorophyll a apoprotein A1 (EC 1.97.1.12) (PSI-A) (PsaA)
317	Tic40	AT1G64190	1.81	PGD1	6-phosphogluconate dehydrogenase
318	Tic40	AT5G13280	1.80	AK1	Aspartate kinase 1
319	Tic40	AT5G05000	1.80	TOC34	Translocase of chloroplast 34
320	Tic40	AT2G34420	1.78		Chlorophyll a-b binding protein
321	Tic40	AT1G14410	1.73	WHY1	Single-stranded DNA-binding protein WHY1
322	Tic40	AT3G55800	1.72		Sedoheptulose-1,7-bisphosphatase
323	Tic40	AT4G11980	1.71	NUDT14	Nudix hydrolase 14
324	Tic40	ATCG00340	1.70	psaB	Photosystem I P700 chlorophyll a apoprotein A2
325	Tic40	ATCG01110	1.62	ndhH	NAD(P)H-quinone oxidoreductase subunit H
326	Tic40	AT4G04610	1.60	APR1, PRH19	5'-adenylylsulfate reductase 1 (Thioredoxin-independent APS reductase 1)
327	Tic40	AT5G01920	1.57	STN8	Serine/threonine-protein kinase STN8
328	Tic40	AT4G37925	1.57	ndhM	NAD(P)H-quinone oxidoreductase subunit M
329	Tic40	AT3G56090	1.56	FER3	Ferritin-3
330	Tic40	AT4G32520	1.56	SHM3	Serine hydroxymethyltransferase 3
331	Tic40	AT2G05100	1.55	LHCB2.1	Chlorophyll a-b binding protein 2.1
332	Tic40	AT3G06730	1.54	CITRX, TRX Z	Thioredoxin-like protein CITRX (Thioredoxin Z)

Supplemental Table 3: Complete list of potential **chloroplast** localized *AtTrxM2* interacting/associating proteins. Proteins were identified by proximity labeling with TurboID. Both control (WT-Col-0) and overexpression (TrxM2-TurboID) groups were analyzed in three biological replicates. **Bait:** Candidate protein, **Prey:** Interaction partner proteins identified by TurboID.

No	Bait	Prey	Log2 Fold Change	Gene Name	Functional Annotation
1	TrxM2	AT4G03520	9.93	TRXM2	Thioredoxin M2
2	TrxM2	AT2G24020	9.56	STIC2	Nucleoid-associated protein (Suppressor of tic40 protein 2)
3	TrxM2	AT3G01120	9.54	CGS1	Cystathionine gamma-synthase 1
4	TrxM2	AT2G44650	9.41	CPN10-2	10 kDa chaperonin 2
5	TrxM2	AT2G37660	9.15		Uncharacterized protein
6	TrxM2	AT1G67280	9.03		Probable lactoylglutathione lyase
7	TrxM2	AT2G01140	9.00	FBA3	Fructose-bisphosphate aldolase 3
8	TrxM2	AT5G20720	8.79	CPN20	20 kDa chaperonin
9	TrxM2	AT4G38970	8.78	FBA2	Fructose-bisphosphate aldolase 2
10	TrxM2	AT3G05350	8.35	APP2	Aminopeptidase P2
11	TrxM2	AT3G46780	8.29	PTAC16	Protein PLASTID TRANSCRIPTIONALLY ACTIVE 16
12	TrxM2	AT5G07020	8.28	MPH1	Protein MAINTENANCE OF PSII UNDER HIGH LIGHT 1
13	TrxM2	AT2G43750	8.11	OASB	Cysteine synthase (O-acetylserine sulfhydrylase)
14	TrxM2	AT3G11630	8.06	BAS1	2-Cys peroxiredoxin BAS1
15	TrxM2	AT1G48850	8.00	EMB1144	Chorismate synthase
16	TrxM2	AT3G18890	7.97	TIC62	Protein TIC 62 (Translocon at the inner envelope membrane of chloroplasts 62)
17	TrxM2	AT3G25860	7.95	LTA2	Dihydrolipoyllysine-residue acetyltransferase component 4 of pyruvate dehydrogenase complex
18	TrxM2	AT5G23010	7.92	MAM1	Methylthioalkylmalate synthase 1
19	TrxM2	AT4G33680	7.88	DAP	LL-diaminopimelate aminotransferase
20	TrxM2	AT2G37220	7.86	CP29B	RNA-binding protein CP29B
21	TrxM2	AT1G73060	7.65	LPA3	Protein LPA3 (Protein LOW PSII ACCUMULATION 3)
22	TrxM2	AT1G34430	7.64	EMB3003	Dihydrolipoyllysine-residue acetyltransferase component 5 of pyruvate dehydrogenase complex
23	TrxM2	AT5G55220	7.63	TIG	Trigger factor-like protein TIG
24	TrxM2	AT4G21860	7.61	MSRB2	Peptide methionine sulfoxide reductase B2
25	TrxM2	AT5G53460	7.61	GLT1	Glutamate synthase 1 [NADH]
26	TrxM2	AT2G39730	7.52	RCA	Ribulose bisphosphate carboxylase/oxygenase activase
27	TrxM2	AT1G76080	7.47	CDSP32	Thioredoxin-like protein CDSP32
28	TrxM2	AT3G55250	7.26	PSA3	Photosystem I assembly factor PSA3, chloroplastic (Protein PHOTOSYSTEM I ASSEMBLY 3) (Protein PIGMENT DEFECTIVE

					329)
29	TrxM2	AT5G66120	7.24	DHQS	3-dehydroquinate synthase
30	TrxM2	AT5G15450	7.08	CLPB3	Chaperone protein ClpB3 (ATP-dependent Clp protease ATP-binding subunit ClpB homolog 3)
31	TrxM2	AT1G22410	7.04	DHS3	Putative 3-deoxy-D-arabino-heptulosonate 7-phosphate synthase
32	TrxM2	AT5G54810	7.04	TSB1	Tryptophan synthase beta chain 1
33	TrxM2	AT2G29630	7.02	THIC	Phosphomethylpyrimidine synthase
34	TrxM2	AT4G29060	7.00	PETs	Polyprotein of EF-Ts (150 kDa pro-protein)
35	TrxM2	AT2G38040	6.99	CAC3	Acetyl-coenzyme A carboxylase carboxyl transferase subunit alpha
36	TrxM2	AT1G44575	6.96	PSBS, NPQ4	Photosystem II 22 kDa protein (Protein NONPHOTOCHEMICAL QUENCHING 4)
37	TrxM2	AT5G13110	6.88	G6PD2	Glucose-6-phosphate 1-dehydrogenase 2
38	TrxM2	AT1G67090	6.85	RBCS-1A	Ribulose bisphosphate carboxylase small subunit 1A
39	TrxM2	AT5G23020	6.83	MAM3	Methylthioalkylmalate synthase 3
40	TrxM2	AT5G01600	6.71	FER1	Ferritin-1
41	TrxM2	AT2G04030	6.68	HSP90-5	Heat shock protein 90-5
42	TrxM2	AT2G47400	6.66	CP12-1	Calvin cycle protein CP12-1
43	TrxM2	AT5G08280	6.64	HEMC	Porphobilinogen deaminase
44	TrxM2	AT2G31810	6.63		Acetolactate synthase small subunit 2
45	TrxM2	AT3G12930	6.61	IJ	Protein lojap
46	TrxM2	AT2G04400	6.60	IGPS	Indole-3-glycerol phosphate synthase
47	TrxM2	AT3G48560	6.59	ALS	Acetolactate synthase
48	TrxM2	AT5G10920	6.58		Argininosuccinate lyase, chloroplastic (EC 4.3.2.1) (Argininosuccinase)
49	TrxM2	AT4G25130	6.57	MSR4, PMSR4	Peptide methionine sulfoxide reductase A4
50	TrxM2	AT3G29320	6.54	PHS1	Alpha-glucan phosphorylase 1
51	TrxM2	AT1G17745	6.52	PGDH2	D-3-phosphoglycerate dehydrogenase 2
52	TrxM2	AT1G50900	6.50	LTD, GDC1	Protein LHCP TRANSLOCATION DEFECT (Protein GRANA-DEFICIENT CHLOROPLAST 1)
53	TrxM2	AT5G16290	6.50	VAT1	Acetolactate synthase small subunit 1
54	TrxM2	AT1G08490	6.49	NFS2	Cysteine desulfurase 1
55	TrxM2	AT2G20890	6.48	THF1	Protein THYLAKOID FORMATION 1
56	TrxM2	AT5G23310	6.47	FSD3	Superoxide dismutase [Fe] 3
57	TrxM2	AT4G34120	6.47	CBSX2	CBS domain-containing protein CBSX2
58	TrxM2	AT3G17810	6.47	PYD1	Dihydropyrimidine dehydrogenase (NADP(+))
59	TrxM2	AT4G29840	6.42	TS1	Threonine synthase 1
60	TrxM2	AT5G38410	6.40	RBCS-3B	Ribulose bisphosphate carboxylase small subunit 3B
61	TrxM2	AT1G13270	6.37	MAP1B	Methionine aminopeptidase 1B
62	TrxM2	AT3G08940	6.37	LHCB4.2	Chlorophyll a-b binding protein CP29.2

					(LHCII protein 4.2)
63	TrxM2	AT3G60210	6.36	CPN10-1	10 kDa chaperonin 1
64	TrxM2	AT4G39120	6.36	HISN7	Bifunctional phosphatase IMPL2
65	TrxM2	AT3G04790	6.35	RPI3	Probable ribose-5-phosphate isomerase 3
66	TrxM2	AT5G04740	6.34	ACR12	ACT domain-containing protein ACR12 (Protein ACT DOMAIN REPEATS 12)
67	TrxM2	ATCG01120	6.33	rps15	30S ribosomal protein S15
68	TrxM2	AT2G22480	6.21	PFK5	ATP-dependent 6-phosphofructokinase 5 (Phosphohexokinase 5)
69	TrxM2	AT2G27820	6.17	ADT3	Arogenate dehydratase 3
70	TrxM2	AT4G33580	6.16	BCA5	Beta carbonic anhydrase 5
71	TrxM2	AT1G06680	6.16	PSBP1	Oxygen-evolving enhancer protein 2-1
72	TrxM2	AT1G55670	6.15	PSAG	Photosystem I reaction center subunit V
73	TrxM2	AT4G04020	6.07	PAP1	Probable plastid-lipid-associated protein 1
74	TrxM2	AT5G45390	6.06	CLPP4	ATP-dependent Clp protease proteolytic subunit 4
75	TrxM2	AT3G16950	6.04	LPD1	Dihydrolipoyl dehydrogenase 1
76	TrxM2	AT4G13200	6.04		Uncharacterized protein
77	TrxM2	AT5G22510	6.03	INVE	Alkaline/neutral invertase E
78	TrxM2	AT5G48300	5.99	APS1	Glucose-1-phosphate adenylyltransferase small subunit
79	TrxM2	AT5G03900	5.98		Uncharacterized protein
80	TrxM2	AT3G56090	5.96	FER3	Ferritin-3
81	TrxM2	AT1G55480	5.94	MET1	Protein MET1 (PDZ domain, K-box domain, and TPR region containing protein)
82	TrxM2	AT5G50920	5.93	CLPC1	Chaperone protein ClpC1
83	TrxM2	AT4G33030	5.92	SQD1	UDP-sulfoquinovose synthase
84	TrxM2	AT3G59890	5.92	DAPB2	4-hydroxy-tetrahydrodipicolinate reductase 2
85	TrxM2	AT1G50320	5.92	ATHX	Thioredoxin X
86	TrxM2	AT3G25660	5.91	GATA	Glutamyl-tRNA(Gln) amidotransferase subunit A
87	TrxM2	ATCG00490	5.91	rbcl	Ribulose bisphosphate carboxylase large chain
88	TrxM2	AT4G28750	5.90	PSAE1	Photosystem I reaction center subunit IV A
89	TrxM2	AT5G11880	5.90	LYSA2	Diaminopimelate decarboxylase 2
90	TrxM2	AT4G01690	5.87	PPOX1	Protoporphyrinogen oxidase 1
91	TrxM2	AT3G44720	5.86	ADT4	Arogenate dehydratase 4
92	TrxM2	AT5G47870	5.86	RAD52-2	DNA repair RAD52-like protein 2
93	TrxM2	AT1G68260	5.84	ALT3	Acyl-acyl carrier protein thioesterase ATL3
94	TrxM2	ATCG00500	5.83	accD	Acetyl-coenzyme A carboxylase carboxyl transferase subunit beta
95	TrxM2	AT1G03130	5.83	PSAD2	Photosystem I reaction center subunit II-2
96	TrxM2	AT1G79750	5.83	NADP- ME4	NADP-dependent malic enzyme 4
97	TrxM2	AT1G54630	5.78	ACP3	Acyl carrier protein 3
98	TrxM2	AT2G02740	5.78	WHY3	Single-stranded DNA-binding protein WHY3

99	TrxM2	AT5G51070	5.76	CLPD	Chaperone protein ClpD
100	TrxM2	AT5G03650	5.71	SBE2.2	1,4-alpha-glucan-branching enzyme 2-2
101	TrxM2	AT2G47450	5.70	CPSRP43	Signal recognition particle 43 kDa protein
102	TrxM2	AT2G14750	5.69	APK1	Adenylyl-sulfate kinase 1
103	TrxM2	AT1G03475	5.69	CPX1	Coproporphyrinogen-III oxidase 1
104	TrxM2	AT2G21330	5.69	FBA1	Fructose-bisphosphate aldolase 1
105	TrxM2	ATCG00280	5.68	psbC	Photosystem II CP43 reaction center protein (PSII 43 kDa protein)
106	TrxM2	AT2G20260	5.67	PSAE2	Photosystem I reaction center subunit IV B
107	TrxM2	AT5G16620	5.53	TIC40	Protein TIC 40 (Translocon at the inner envelope membrane of chloroplasts 40)
108	TrxM2	ATCG00740	5.53	rpoA	DNA-directed RNA polymerase subunit alpha (PEP)
109	TrxM2	AT1G06950	5.50	TIC110	Protein TIC110 (Translocon at the inner envelope membrane of chloroplasts 110)
110	TrxM2	AT1G52230	5.45	PSAH2	Photosystem I reaction center subunit VI-2, chloroplastic (PSI-H1)
111	TrxM2	AT1G18500	5.43	IPMS1	2-isopropylmalate synthase 1
112	TrxM2	AT4G15560	5.41	DXS	1-deoxy-D-xylulose-5-phosphate synthase
113	TrxM2	AT4G39980	5.35	DHS1	Phospho-2-dehydro-3-deoxyheptonate aldolase 1
114	TrxM2	ATCG00480	5.35	atpB	ATP synthase subunit beta
115	TrxM2	AT1G43800	5.34	S-ACP-DES6	Stearoyl-[acyl-carrier-protein] 9-desaturase 6
116	TrxM2	AT3G04550	5.34	RAF1.2	Rubisco accumulation factor 1.2
117	TrxM2	AT1G03680	5.31	TRXM1	Thioredoxin M1
118	TrxM2	AT3G53460	5.29	CP29A	29 kDa ribonucleoprotein (RNA-binding protein CP29A)
119	TrxM2	AT5G04590	5.28	SIR	Assimilatory sulfite reductase (ferredoxin)
120	TrxM2	AT5G54770	5.24	THI1	Thiamine thiazole synthase
121	TrxM2	ATCG00800	5.23	rps3	30S ribosomal protein S3
122	TrxM2	ATCG00780	5.21	rpl14	50S ribosomal protein L14
123	TrxM2	AT3G59400	5.16	GUN4	Tetrapyrrole-binding protein
124	TrxM2	AT1G75350	5.15	RPL31	50S ribosomal protein L31
125	TrxM2	AT4G13430	5.14	IIL1	3-isopropylmalate dehydratase large subunit
126	TrxM2	AT1G32200	5.14	ATS1	Glycerol-3-phosphate acyltransferase
127	TrxM2	AT4G09650	5.12	ATPD	ATP synthase subunit delta
128	TrxM2	ATCG00680	5.11	psbB	Photosystem II CP47 reaction center protein (PSII 47 kDa protein)
129	TrxM2	AT3G53580	5.05	DAPF	Diaminopimelate epimerase
130	TrxM2	AT3G47470	5.02	LHCA4	Chlorophyll a-b binding protein 4
131	TrxM2	AT2G36390	4.99	SBE2.1	1,4-alpha-glucan-branching enzyme 2-1
132	TrxM2	AT2G40490	4.94	HEME2	Uroporphyrinogen decarboxylase 2
133	TrxM2	AT1G62750	4.91	CPEFG	Elongation factor G (Elongation factor EF-G/SCO1)
134	TrxM2	AT1G31330	4.89	PSAF	Photosystem I reaction center subunit III

135	TrxM2	AT1G31230	4.87	AKHSDH1	Bifunctional aspartokinase/homoserine dehydrogenase 1
136	TrxM2	AT1G63940	4.87	MDAR5, MDAR6	Monodehydroascorbate reductase
137	TrxM2	AT4G30620	4.86		Nucleoid-associated protein
138	TrxM2	AT3G58610	4.86		Ketol-acid reductoisomerase
139	TrxM2	AT4G17040	4.85	CLPR4	ATP-dependent Clp protease proteolytic subunit-related protein 4
140	TrxM2	AT3G06200	4.84	GK3	Guanylate kinase 3
141	TrxM2	AT1G53670	4.81	MSRB1	Peptide methionine sulfoxide reductase B1
142	TrxM2	AT4G05180	4.79	PSBQ2	Oxygen-evolving enhancer protein 3-2
143	TrxM2	AT4G21990	4.79	APR3, PRH26	5'-adenylylsulfate reductase 3 (Thioredoxin-independent APS reductase 3)
144	TrxM2	AT5G64300	4.77	RIBA1	Bifunctional riboflavin biosynthesis protein RIBA 1
145	TrxM2	AT3G22890	4.77	APS1	ATP sulfurylase 1
146	TrxM2	AT4G35250	4.75	HCF244	Protein HIGH CHLOROPHYLL FLUORESCENCE PHENOTYPE 244
147	TrxM2	AT5G63420	4.72	RNJ	Ribonuclease J (RNase J)
148	TrxM2	AT2G34590	4.72	E1-BETA-2	Pyruvate dehydrogenase E1 component subunit beta-3
149	TrxM2	AT5G49910	4.69	HSP70-7	Heat shock 70 kDa protein 7
150	TrxM2	AT2G47730	4.65	GSTF8	Glutathione S-transferase F8
151	TrxM2	AT1G15820	4.62	Lhcb6	Chlorophyll a-b binding protein
152	TrxM2	AT4G34350	4.61	ISPH	4-hydroxy-3-methylbut-2-enyl diphosphate reductase
153	TrxM2	AT4G04770	4.60	ABC18	UPF0051 protein ABC18
154	TrxM2	AT5G22830	4.58	MRS2-11	Magnesium transporter MRS2-11
155	TrxM2	AT1G14410	4.56	WHY1	Single-stranded DNA-binding protein WHY1
156	TrxM2	AT4G36810	4.51	GGPPS1	Heterodimeric geranylgeranyl pyrophosphate synthase large subunit 1
157	TrxM2	AT3G55800	4.48		Sedoheptulose-1,7-bisphosphatase
158	TrxM2	AT4G18480	4.47	CHL11	Magnesium-chelatase subunit Chl1-1
159	TrxM2	AT4G18240	4.47	SS4	Probable starch synthase 4
160	TrxM2	AT4G11980	4.46	NUDT14, ASPP	Nudix hydrolase 14 (ADP-sugar diphosphatase)
161	TrxM2	ATCG00340	4.43	psaB	Photosystem I P700 chlorophyll a apoprotein A2
162	TrxM2	AT1G02560	4.40	CLPP5	ATP-dependent Clp protease proteolytic subunit 5
163	TrxM2	AT1G69740	4.40	HEMB1	Delta-aminolevulinic acid dehydratase 1
164	TrxM2	AT4G36910	4.35	CBSX1, CDCP2	CBS domain-containing protein CBSX1(CBS domain-containing protein 2)
165	TrxM2	AT2G05990	4.34	MOD1, ENR-A	Enoyl-[acyl-carrier-protein] reductase [NADH] (Protein MOSAIC DEATH 1)
166	TrxM2	ATCG01110	4.34	ndhH	NAD(P)H-quinone oxidoreductase subunit H
167	TrxM2	AT5G26570	4.33	GWD3	Phosphoglucan, water dikinase

168	TrxM2	AT1G29910	4.32	LHCB1.2	Chlorophyll a-b binding protein 3
169	TrxM2	AT2G38550	4.32	FAX3	Protein FATTY ACID EXPORT 3
170	TrxM2	AT4G27440	4.31	PORB	Protochlorophyllide reductase B
171	TrxM2	AT3G06350	4.30	EMB3004	Bifunctional 3-dehydroquinone dehydratase/shikimate dehydrogenase
172	TrxM2	AT3G48500	4.27	PTAC10	Protein PLASTID TRANSCRIPTIONALLY ACTIVE 10
173	TrxM2	AT5G28500	4.25	RAF1.1	Rubisco accumulation factor 1.1
174	TrxM2	AT4G16390	4.25	P67,SVR7	Pentatricopeptide repeat-containing protein (Protein SUPPRESSOR OF VARIEGATION 7)
175	TrxM2	AT1G80300	4.21	AATP1	ADP,ATP carrier protein 1
176	TrxM2	ATCG00130	4.20	atpF	ATP synthase subunit b
177	TrxM2	AT3G01180	4.19	SS2	Starch synthase 2
178	TrxM2	AT5G01220	4.19	SQD2	Sulfoquinovosyl transferase SQD2 (Protein SULFOQUINOVOSYLDIACYLGLYCEROL 2)
179	TrxM2	AT1G01090	4.18	PDH-E1 ALPHA	Pyruvate dehydrogenase E1 component subunit alpha-3
180	TrxM2	AT2G46820	4.16	CURT1B	Protein CURVATURE THYLAKOID 1B
181	TrxM2	AT5G35360	4.15	CAC2	Biotin carboxylase
182	TrxM2	AT3G61470	4.09	LHCA2	Photosystem I chlorophyll a/b-binding protein 2
183	TrxM2	AT2G35490	4.08	PAP3, PGL40	Probable plastid-lipid-associated protein 3 (Plastoglobulin 40)
184	TrxM2	ATCG00120	4.06	atpA	ATP synthase subunit alpha
185	TrxM2	AT5G38430	4.05	RBCS-1B	Ribulose biphosphate carboxylase small subunit 1B
186	TrxM2	AT1G29900	4.05	CARB	Carbamoyl-phosphate synthase large chain
187	TrxM2	AT3G63410	4.04	VTE3, IE37	2-methyl-6-phytyl-1,4-hydroquinone methyltransferase (37 kDa inner envelope membrane protein) (Protein VITAMIN E DEFECTIVE 3)
188	TrxM2	AT4G23890	4.03	ndhS	NAD(P)H-quinone oxidoreductase subunit S
189	TrxM2	AT3G45140	4.03	LOX2	Lipoxygenase 2
190	TrxM2	AT3G58990	4.02	SSU3	3-isopropylmalate dehydratase small subunit 3
191	TrxM2	ATCG00270	4.02	psbD	Photosystem II D2 protein
192	TrxM2	ATCG00170	4.01	rpoC2	DNA-directed RNA polymerase subunit beta
193	TrxM2	AT3G54050	4.00	CFBP1	Fructose-1,6-bisphosphatase 1
194	TrxM2	AT1G09830	3.99	PUR2	Phosphoribosylamine--glycine ligase
195	TrxM2	AT5G23060	3.96	CAS	Calcium sensing receptor
196	TrxM2	AT3G23400	3.96	PAP6, PGL30.4	Plastid-lipid-associated protein 6b (Plastoglobulin 30.4)
197	TrxM2	AT1G74470	3.95	CHLP	Geranylgeranyl diphosphate reductase
198	TrxM2	AT5G42650	3.93	CYP74A	Allene oxide synthase (Cytochrome P450 74A)
199	TrxM2	AT2G21590	3.93		Probable glucose-1-phosphate

					adenylyltransferase large subunit
200	TrxM2	ATCG00020	3.92	psbA	Photosystem II protein D1
201	TrxM2	AT2G34640	3.90	PTAC12	Protein PLASTID TRANSCRIPTIONALLY ACTIVE 12
202	TrxM2	AT4G33510	3.90	DHS2	Phospho-2-dehydro-3-deoxyheptonate aldolase 2
203	TrxM2	AT5G36880	3.89	ACS	Acetyl-coenzyme A synthetase
204	TrxM2	AT5G13650	3.87	SVR3	Putative elongation factor TypA-like SVR3
205	TrxM2	AT5G24300	3.86	SS1	Starch synthase 1
206	TrxM2	AT4G26900	3.84	HISN4	Imidazole glycerol phosphate synthase hisHF
207	TrxM2	ATCG00160	3.81	rps2	30S ribosomal protein S2
208	TrxM2	AT1G55490	3.78	CPN60B1	Chaperonin 60 subunit beta 1
209	TrxM2	AT4G35630	3.77	PSAT1	Phosphoserine aminotransferase 1
210	TrxM2	AT5G42270	3.77	FTSH5	ATP-dependent zinc metalloprotease FTSH 5
211	TrxM2	AT5G54270	3.77	LHCB3	Chlorophyll a-b binding protein 3
212	TrxM2	AT1G67700	3.76	HHL1	Protein HHL1 (Hypersensitive to high light 1)
213	TrxM2	AT4G04640	3.76	ATPC1	ATP synthase gamma chain 1
214	TrxM2	AT2G37860	3.76	RE, LCD1	Protein RETICULATA, chloroplastic (Protein LOWER CELL DENSITY 1)
215	TrxM2	AT5G03940	3.75	CPSRP54	Signal recognition particle 54 kDa protein
216	TrxM2	AT3G20320	3.75	TGD2	Protein TRIGALACTOSYLDIACYLGLYCEROL 2
217	TrxM2	AT5G06290	3.73	2-Cys Prx	Thioredoxin-dependent peroxiredoxin
218	TrxM2	AT2G43100	3.72	SSU2	3-isopropylmalate dehydratase small subunit 2
219	TrxM2	ATCG00570	3.71	psbF	Cytochrome b559 subunit beta (PSII reaction center subunit VI)
220	TrxM2	AT5G11520	3.71	ASP3	Aspartate aminotransferase 3
221	TrxM2	AT3G57610	3.71	PURA	Adenylosuccinate synthetase
222	TrxM2	AT1G42970	3.70	GAPB	Glyceraldehyde-3-phosphate dehydrogenase GAPB
223	TrxM2	AT1G62640	3.68		3-oxoacyl-[acyl-carrier-protein] synthase III
224	TrxM2	AT2G40300	3.67	FER4	Ferritin-4
225	TrxM2	AT3G52960	3.66	PRXIIE	Peroxiredoxin-2E (Glutaredoxin-dependent peroxiredoxin)
226	TrxM2	AT3G44890	3.66	RPL9	50S ribosomal protein L9
227	TrxM2	AT5G67030	3.64	ZEP, ABA1	Zeaxanthin epoxidase (Protein ABA DEFICIENT 1)
228	TrxM2	AT4G34730	3.64		Probable ribosome-binding factor A
229	TrxM2	AT1G32900	3.63	GBSS1.8	Granule-bound starch synthase 1
230	TrxM2	AT3G54660	3.61	EMB2360	Glutathione reductase (Protein EMBRYO DEFECTIVE 2360)
231	TrxM2	AT5G12470	3.59	RER4	Protein RETICULATA-RELATED 4
232	TrxM2	AT5G16440	3.59	IPP1	Isopentenyl-diphosphate Delta-isomerase I
233	TrxM2	AT1G61520	3.57	LHCA3	Photosystem I chlorophyll a/b-binding protein 3-1

234	TrxM2	AT1G02910	3.53	LPA1	Protein LOW PSII ACCUMULATION 1
235	TrxM2	ATCG00180	3.53	rpoC1	DNA-directed RNA polymerase subunit beta
236	TrxM2	AT3G63140	3.50	CSP41A	Chloroplast stem-loop binding protein of 41 kDa a
237	TrxM2	AT3G48110	3.49	EDD1	Glycine--tRNA ligase
238	TrxM2	AT3G23940	3.46	DHAD	Dihydroxy-acid dehydratase
239	TrxM2	AT4G22240	3.45	PAP2	Probable plastid-lipid-associated protein 2
240	TrxM2	AT4G34200	3.44	PGDH1	D-3-phosphoglycerate dehydrogenase 1
241	TrxM2	AT4G20360	3.43	TUFA, RAB8D	Elongation factor Tu (Ras-related protein Rab8D)
242	TrxM2	AT3G58140	3.42		Phenylalanine--tRNA ligase
243	TrxM2	AT4G17600	3.42	LIL3.1	Light-harvesting complex-like protein 3 isotype 1
244	TrxM2	AT1G12900	3.41	GAPA2	Glyceraldehyde-3-phosphate dehydrogenase GAPA2
245	TrxM2	AT3G22960	3.40	PKP1	Plastidial pyruvate kinase 1
246	TrxM2	AT3G26710	3.39	CCB1	Protein COFACTOR ASSEMBLY OF COMPLEX C SUBUNIT B CCB1
247	TrxM2	AT5G12040	3.38	NLP3	Omega-amidase (Nitrilase-like protein 3)
248	TrxM2	AT3G10940	3.38	LSF2	Phosphoglucan phosphatase LSF2
249	TrxM2	AT5G22630	3.35	ADT5	Arogenate dehydratase 5
250	TrxM2	AT1G77060	3.34		Carboxyvinyl-carboxyphosphonate phosphorylmutase
251	TrxM2	AT5G35630	3.34	GLN2	Glutamine synthetase
252	TrxM2	AT4G10340	3.33	LHCB5	Chlorophyll a-b binding protein CP26
253	TrxM2	AT3G52150	3.32	PSRP2	30S ribosomal protein 2
254	TrxM2	AT5G01530	3.31	LHCB4.1	Chlorophyll a-b binding protein CP29.1 (LHCII protein 4.1)
255	TrxM2	AT4G04610	3.31	APR1, PRH19	5'-adenylylsulfate reductase 1(3'-phosphoadenosine-5'-phosphosulfate reductase homolog 19)
256	TrxM2	AT3G12780	3.30	PGK1	Phosphoglycerate kinase 1
257	TrxM2	ATCG00350	3.30	psaA	Photosystem I P700 chlorophyll a apoprotein A1
258	TrxM2	AT4G24280	3.29	HSP70-6	Heat shock 70 kDa protein 6
259	TrxM2	AT1G32440	3.27	PKP3	Plastidial pyruvate kinase 3
260	TrxM2	AT3G27850	3.24	RPL12C	50S ribosomal protein L12-3
261	TrxM2	AT5G64940	3.23	ABC1K8	Protein ACTIVITY OF BC1 COMPLEX KINASE 8 (Oxidative stress-related ABC1-like protein 1)
262	TrxM2	AT3G26650	3.22	GAPA1	Glyceraldehyde-3-phosphate dehydrogenase
263	TrxM2	AT4G14070	3.21	AAE15	Long-chain-fatty-acid--[acyl-carrier-protein] ligase AEE15
264	TrxM2	AT4G04850	3.19	KEA3	K(+) efflux antiporter 3
265	TrxM2	AT3G08640	3.17	RER3	Protein RETICULATA-RELATED 3
266	TrxM2	AT5G01920	3.15	STN8	Serine/threonine-protein kinase STN8

267	TrxM2	AT2G44040	3.13	DAPB1	4-hydroxy-tetrahydrodipicolinate reductase 1
268	TrxM2	AT1G31190	3.13	IMPL1	Phosphatase IMPL1
269	TrxM2	AT3G04870	3.12	ZDS1	Zeta-carotene desaturase
270	TrxM2	AT1G10760	3.06	GWD1	Alpha-glucan water dikinase 1
271	TrxM2	AT2G28000	3.06	CPN60A1	Chaperonin 60 subunit alpha 1
272	TrxM2	AT2G22360	3.05	DJA6	Chaperone protein dnaJ A6
273	TrxM2	AT5G04140	3.05	GLU1	Ferredoxin-dependent glutamate synthase 1
274	TrxM2	ATCG00770	3.03	rps8	30S ribosomal protein S8
275	TrxM2	AT1G15500	3.00	AATP2	ADP,ATP carrier protein 2
276	TrxM2	AT5G27380	2.99	GSH2	Glutathione synthetase
277	TrxM2	AT1G04620	2.97	HCAR	7-hydroxymethyl chlorophyll a reductase
278	TrxM2	AT5G13280	2.97	AK1	Aspartate kinase 1
279	TrxM2	AT2G47390	2.96	GEP	Probable glutamyl endopeptidase
280	TrxM2	AT4G34740	2.96	ASE2	Amidophosphoribosyltransferase 2
281	TrxM2	AT3G54900	2.94	GRXS14	Monothiol glutaredoxin-S14
282	TrxM2	AT1G49970	2.92	CLPR1	ATP-dependent Clp protease proteolytic subunit-related protein 1
283	TrxM2	AT3G06730	2.91	CITRX, TRX Z	Thioredoxin-like protein CITRX (Thioredoxin Z)
284	TrxM2	AT3G48730	2.89	GSA2	Glutamate-1-semialdehyde 2,1-aminomutase 2
285	TrxM2	AT1G11430	2.89	MORF9, RIP9	Multiple organellar RNA editing factor 9 (RNA editing-interacting protein 9)
286	TrxM2	AT3G63190	2.88	RRF	Ribosome-recycling factor
287	TrxM2	AT4G11010	2.87	NDPK3	Nucleoside diphosphate kinase III
288	TrxM2	AT2G22450	2.86	RIBA2	Monofunctional riboflavin biosynthesis protein RIBA 2
289	TrxM2	ATCG00580	2.84	psbE	Cytochrome b559 subunit alpha (PSII reaction center subunit V)
290	TrxM2	AT2G43030	2.84	RPL3A	50S ribosomal protein L3-1
291	TrxM2	AT4G39210	2.83	APL3	Glucose-1-phosphate adenylyltransferase large subunit 3
292	TrxM2	AT5G64050	2.81	OVA3	Glutamate--tRNA ligase (Protein OVULE ABORTION 3)
293	TrxM2	AT1G15390	2.80	PDF1A	Peptide deformylase 1A
294	TrxM2	AT2G34420	2.79		Chlorophyll a-b binding protein
295	TrxM2	AT4G21210	2.79	RP1	Pyruvate, phosphate dikinase regulatory protein 1
296	TrxM2	AT1G32060	2.78		Phosphoribulokinase
297	TrxM2	AT5G50100	2.78		Uncharacterized protein
298	TrxM2	AT3G54640	2.76	TSA1	Tryptophan synthase alpha chain
299	TrxM2	ATCG00730	2.75	petD	Cytochrome b6-f complex subunit 4
300	TrxM2	AT2G28900	2.73	OEP16-1	Outer envelope pore protein 16-1
301	TrxM2	AT5G44650	2.72	Y3IP1	Ycf3-interacting protein 1
302	TrxM2	AT5G26742	2.71	RH3	DEAD-box ATP-dependent RNA helicase 3

303	TrxM2	AT1G74960	2.66	KAS2	3-oxoacyl-[acyl-carrier-protein] synthase II
304	TrxM2	AT5G52920	2.65	PKP2	Plastidial pyruvate kinase 2
305	TrxM2	AT5G47190	2.64		50S ribosomal protein L19-2
306	TrxM2	AT3G47520	2.62		Malate dehydrogenase
307	TrxM2	AT5G03420	2.60	PTST	Protein PTST homolog 3 (PROTEIN TARGETING TO STARCH homolog 3)
308	TrxM2	AT5G05000	2.59	TOC34	Translocase of chloroplast 34
309	TrxM2	AT4G32520	2.59	SHM3	Serine hydroxymethyltransferase 3
310	TrxM2	AT3G27740	2.54	CARA	Carbamoyl-phosphate synthase small chain
311	TrxM2	AT2G33800	2.53	rps5	30S ribosomal protein S5
312	TrxM2	AT1G74030	2.52	ENO1	Enolase 1
313	TrxM2	AT4G23100	2.49	GSH1	Glutamate--cysteine ligase
314	TrxM2	AT1G21600	2.48	PTAC6	PLASTID TRANSCRIPTIONALLY ACTIVE protein 6
315	TrxM2	AT2G15620	2.48	NIR1	Ferredoxin--nitrite reductase
316	TrxM2	AT4G39970	2.47		Haloacid dehalogenase-like hydrolase domain-containing protein
317	TrxM2	AT1G08520	2.45	CHLD	Magnesium-chelatase subunit ChLD
318	TrxM2	AT4G37925	2.44	ndhM	NAD(P)H-quinone oxidoreductase subunit M
319	TrxM2	ATCG00830	2.44	rpl2-A	50S ribosomal protein L2
320	TrxM2	AT1G64190	2.39	PGD1	6-phosphogluconate dehydrogenase
321	TrxM2	AT3G02630	2.34	S-ACP-DES5	Stearoyl-[acyl-carrier-protein] 9-desaturase 5
322	TrxM2	AT3G10050	2.33	OMR1	Threonine dehydratase biosynthetic
323	TrxM2	AT2G05100	2.31	LHCB2.1	Chlorophyll a-b binding protein 2.1
324	TrxM2	AT5G36790	2.29	PGLP1B	Phosphoglycolate phosphatase 1B
325	TrxM2	ATCG01060	2.27	psaC	Photosystem I iron-sulfur center
326	TrxM2	AT4G27070	2.24	TSB2	Tryptophan synthase beta chain 2
327	TrxM2	ATCG00750	2.19	rps11	30S ribosomal protein S11
328	TrxM2	AT5G24020	2.14	MIND1	Putative septum site-determining protein minD homolog
329	TrxM2	AT3G57560	2.14	NAGK	Acetylglutamate kinase
330	TrxM2	AT5G52520	2.13	OVA6	Proline--tRNA ligase (Protein OVULE ABORTION 6)
331	TrxM2	AT1G79530	2.09	GAPCP1	Glyceraldehyde-3-phosphate dehydrogenase GAPCP1
332	TrxM2	AT5G14200	2.08	IMDH1	3-isopropylmalate dehydrogenase 1
333	TrxM2	AT1G19800	2.04	TGD1	Protein TRIGALACTOSYLDIACYLGLYCEROL 1
334	TrxM2	AT1G05190	2.03	RPL6	50S ribosomal protein L6
335	TrxM2	AT1G68720	2.02	TADA	tRNA(adenine(34)) deaminase, chloroplastic (TADA)
336	TrxM2	AT1G14030	2.00	LSMT-L	[Fructose-bisphosphate aldolase]-lysine N-methyltransferase
337	TrxM2	AT5G41670	1.97	PGD3	6-phosphogluconate dehydrogenase
338	TrxM2	ATCG00430	1.96	ndhK	NAD(P)H-quinone oxidoreductase subunit K
339	TrxM2	ATCG00330	1.95	rps14	30S ribosomal protein S14

340	TrxM2	AT5G30510	1.92	RPS1	30S ribosomal protein S1
341	TrxM2	AT3G46740	1.87	TOC75-3	Protein TOC75-3
342	TrxM2	AT3G63170	1.87	FAP1	Fatty-acid-binding protein 1 (
343	TrxM2	AT5G16715	1.82	EMB2247	Valine--tRNA ligase (Protein EMBRYO DEFECTIVE 2247)
344	TrxM2	AT5G19220	1.80	ADG2	Glucose-1-phosphate adenylyltransferase large subunit 1
345	TrxM2	AT5G64290	1.80	DIT2-1	Dicarboxylate transporter 2.1
346	TrxM2	AT1G66430	1.74		Probable fructokinase-6
347	TrxM2	AT3G20330	1.74	PYRB	Aspartate carbamoyltransferase
348	TrxM2	AT4G19710	1.70	AKHSDH2	Bifunctional aspartokinase/homoserine dehydrogenase 2
349	TrxM2	ATCG00790	1.61	rpl16	50S ribosomal protein L16
350	TrxM2	AT1G24360	1.54		3-oxoacyl-[acyl-carrier-protein] reductase

Supplemental Table 4: Complete list of potential **chloroplast** localized *AtPic1* interacting/associating proteins. Proteins were identified by proximity labeling with TurboID. Both control (WT-Col-0) and overexpression (*Pic1*-TurboID) groups were analyzed in three biological replicates. **Bait:** Candidate protein, **Prey:** Interaction partner proteins identified by TurboID.

No	Bait	Prey	Log2 Fold Change	Gene Name	Functional Annotation
1	Pic1	AT2G24020	7.54	STIC2	Nucleoid-associated protein (Suppressor of <i>tic40</i> protein 2)
2	Pic1	AT5G16620	6.83	TIC40	Protein TIC 40 (Translocon at the inner envelope membrane of chloroplasts 40)
3	Pic1	AT2G15290	6.09	TIC21, CIA5, PIC1	Protein TIC 21 (Translocon at the inner envelope membrane of chloroplasts 21) (PERMEASE IN CHLOROPLASTS 1)
4	Pic1	AT2G44650	5.64	CPN10-2, CPN10	10 kDa chaperonin 2 (Chloroplast chaperonin 10)
5	Pic1	AT1G48850	5.61	EMB1144	Chorismate synthase (5-enolpyruvylshikimate-3-phosphate phospholyase)
6	Pic1	AT3G55250	5.31	PSA3	Photosystem I assembly factor PSA3 (Protein PIGMENT DEFECTIVE 329)
7	Pic1	AT2G01140	4.66	FBA3	Fructose-bisphosphate aldolase 3 (Protein PIGMENT DEFECTIVE 345)
8	Pic1	AT3G60210	4.54	CPN10-1	10 kDa chaperonin 1
9	Pic1	AT5G53460	4.48	GLT1	Glutamate synthase 1 [NADH] (NADH-dependent glutamate synthase 1)
10	Pic1	AT5G03900	4.48		Uncharacterized protein
11	Pic1	AT1G22410	4.21	DHS3	Putative 3-deoxy-D-arabino-heptulosonate 7-phosphate synthase
12	Pic1	AT1G73060	4.13	LPA3	Protein LPA3 (Protein LOW PSII ACCUMULATION 3)
13	Pic1	AT4G21860	3.93	MSRB2	Peptide methionine sulfoxide reductase B2 (Peptide-methionine (R)-S-oxide reductase)
14	Pic1	AT3G46780	3.89	PTAC16	Protein PLASTID TRANSCRIPTIONALLY ACTIVE 16
15	Pic1	AT3G17810	3.87	PYD1	Dihydropyrimidine dehydrogenase (Protein PYRIMIDINE 1)
16	Pic1	AT1G06950	3.87	TIC110	Protein TIC110 (Translocon at the inner envelope membrane of chloroplasts 110)
17	Pic1	AT5G23010	3.78	MAM1	Methylthioalkylmalate synthase 1 (2-isopropylmalate synthase 3)
18	Pic1	AT3G05350	3.63	APP2	Aminopeptidase P2
19	Pic1	AT2G38550	3.57	FAX3	Protein FATTY ACID EXPORT 3
20	Pic1	AT5G13110	3.56	G6PD2	Glucose-6-phosphate 1-dehydrogenase 2
21	Pic1	AT5G54810	3.45	TSB1	Tryptophan synthase beta chain 1
22	Pic1	AT5G50920	3.40	CLPC1	Chaperone protein ClpC1 (ATP-dependent Clp protease ATP-binding subunit ClpC homolog 1)
23	Pic1	AT2G37220	3.30	CP29B	RNA-binding protein CP29B

24	Pic1	AT3G20320	3.29	TGD2	Protein TRIGALACTOSYLDIACYLGLYCEROL 2 (ABC transporter I family member 15)
25	Pic1	AT5G20720	3.27	CPN20	20 kDa chaperonin
26	Pic1	AT1G43800	3.21	S-ACP-DES6	Stearoyl-[acyl-carrier-protein] 9-desaturase 6 (Stearoyl-ACP desaturase 6)
27	Pic1	AT1G80300	3.18	AATP1	ADP,ATP carrier protein 1 (ADP/ATP translocase 1)
28	Pic1	AT1G06680	3.17	PSBP1	Oxygen-evolving enhancer protein 2-1(23 kDa subunit of oxygen evolving system of photosystem II)
29	Pic1	ATCG00280	3.17	psbC	Photosystem II CP43 reaction center protein (PSII 43 kDa protein)
30	Pic1	AT1G53670	3.05	MSRB1	Peptide methionine sulfoxide reductase B1 (Peptide-methionine (R)-S-oxide reductase)
31	Pic1	AT2G37660	3.02		Uncharacterized protein
32	Pic1	AT5G54770	3.02	THI1	Thiamine thiazole synthase (Thiazole biosynthetic enzyme)
33	Pic1	AT2G04030	3.02	HSP90-5	Heat shock protein 90-5
34	Pic1	AT2G47730	2.93	GSTF8	Glutathione S-transferase F8
35	Pic1	AT5G07020	2.90	MPH1	Protein MAINTENANCE OF PSII UNDER HIGH LIGHT 1
36	Pic1	AT1G63940	2.89	MDAR5	Monodehydroascorbate reductase
37	Pic1	AT1G67090	2.89	RBCS-1A	Ribulose biphosphate carboxylase small subunit 1A
38	Pic1	AT4G01690	2.88	PPOX1	Protoporphyrinogen oxidase 1
39	Pic1	AT2G43750	2.84	OASB	Cysteine synthase
40	Pic1	AT5G66120	2.83	DHQS	3-dehydroquinate synthase
41	Pic1	AT3G58610	2.82		Ketol-acid reductoisomerase
42	Pic1	AT2G38040	2.79	CAC3	Acetyl-coenzyme A carboxylase carboxyl transferase subunit alpha
43	Pic1	AT4G39980	2.78	DHS1	Phospho-2-dehydro-3-deoxyheptonate aldolase 1
44	Pic1	AT5G11880	2.76	LYSA2	Diaminopimelate decarboxylase 2
45	Pic1	AT5G38410	2.76	RBCS-3B	Ribulose biphosphate carboxylase small subunit 3B
46	Pic1	AT2G37860	2.75	RE, LCD1	Protein RETICULATA, chloroplastic (Protein LOWER CELL DENSITY 1)
47	Pic1	AT3G11630	2.74	BAS1	2-Cys peroxiredoxin BAS1 (Thioredoxin-dependent peroxiredoxin BAS1)
48	Pic1	AT4G38970	2.71	FBA2	Fructose-biphosphate aldolase 2
49	Pic1	AT5G26742	2.71	RH3	DEAD-box ATP-dependent RNA helicase 3
50	Pic1	AT5G42270	2.71	FTSH5	ATP-dependent zinc metalloprotease FTSH 5
51	Pic1	AT1G31330	2.67	PSAF	Photosystem I reaction center subunit III (Light-harvesting complex I 17 kDa protein)
52	Pic1	AT5G04740	2.66	ACR12	ACT domain-containing protein ACR12 (Protein ACT DOMAIN REPEATS 12)

53	Pic1	AT5G49910	2.65	HSP70-7	Heat shock 70 kDa protein 7
54	Pic1	AT2G39730	2.63	RCA	Ribulose biphosphate carboxylase/oxygenase activase
55	Pic1	AT1G15500	2.61	AATP2	ADP,ATP carrier protein 2
56	Pic1	AT1G15820	2.61	Lhcb6	Chlorophyll a-b binding protein
57	Pic1	AT1G50900	2.61	LTD, GDC1	Protein LHCP TRANSLOCATION DEFECT (Protein GRANA-DEFICIENT CHLOROPLAST 1)
58	Pic1	AT3G06200	2.57	GK3	Guanylate kinase 3
59	Pic1	AT1G50320	2.56	ATHX	Thioredoxin X
60	Pic1	AT4G30620	2.50		Nucleoid-associated protein
61	Pic1	AT1G68720	2.44	TADA	tRNA(adenine(34)) deaminase (tRNA adenosine deaminase arginine)
62	Pic1	AT1G18500	2.44	IPMS1	2-isopropylmalate synthase 1 (Methylthioalkylmalate synthase-like 4)
63	Pic1	AT3G47470	2.41	LHCA4	Chlorophyll a-b binding protein 4
64	Pic1	AT4G33680	2.40	DAP	LL-diaminopimelate aminotransferase
65	Pic1	AT4G15560	2.40	DXS	1-deoxy-D-xylulose-5-phosphate synthase
66	Pic1	AT5G04590	2.37	SIR	Assimilatory sulfite reductase (ferredoxin)
67	Pic1	AT4G25130	2.37	MSR4	Peptide methionine sulfoxide reductase A4
68	Pic1	AT3G12930	2.30	IJ	Protein lojap
69	Pic1	AT2G33800	2.29	rps5	30S ribosomal protein S5
70	Pic1	AT4G14070	2.26	AAE15	Long-chain-fatty-acid--[acyl-carrier-protein] ligase
71	Pic1	ATCG01120	2.25	rps15	30S ribosomal protein S15, chloroplastic
72	Pic1	AT2G34590	2.25	E1-BETA-2	Pyruvate dehydrogenase E1 component subunit beta-3
73	Pic1	AT1G55670	2.21	PSAG	Photosystem I reaction center subunit V
74	Pic1	AT4G33580	2.19	BCA5	Beta carbonic anhydrase 5
75	Pic1	AT4G11010	2.17	NDPK3	Nucleoside diphosphate kinase III
76	Pic1	AT3G63410	2.16	VTE3, APG1, IE37	2-methyl-6-phytyl-1,4-hydroquinone methyltransferase (37 kDa inner envelope membrane protein)
77	Pic1	AT3G04790	2.14	RPI3	Probable ribose-5-phosphate isomerase 3
78	Pic1	AT1G54630	2.13	ACP3	Acyl carrier protein 3
79	Pic1	AT2G05990	2.11	MOD1, ENR-A, ENR1	Enoyl-[acyl-carrier-protein] reductase [NADH]
80	Pic1	AT4G29840	2.10	TS1	Threonine synthase 1
81	Pic1	AT3G08940	2.09	LHCB4.2	Chlorophyll a-b binding protein CP29.2
82	Pic1	AT1G52230	2.07	PSAH2	Photosystem I reaction center subunit VI-2
83	Pic1	AT5G08280	2.05	HEMC, RUG1	Porphobilinogen deaminase
84	Pic1	AT5G10920	2.05		Argininosuccinate lyase
85	Pic1	AT5G64940	2.01	ABC1K8	Protein ACTIVITY OF BC1 COMPLEX KINASE 8
86	Pic1	ATCG00800	2.01	rps3	30S ribosomal protein S3

87	Pic1	AT5G22830	2.01	MRS2-11	Magnesium transporter MRS2-11
88	Pic1	ATCG00330	2.00	rps14	30S ribosomal protein S14
89	Pic1	AT4G13430	2.00	IIL1	3-isopropylmalate dehydratase large subunit
90	Pic1	ATCG00680	1.97	psbB	Photosystem II CP47 reaction center protein
91	Pic1	AT4G17040	1.97	CLPR4	ATP-dependent Clp protease proteolytic subunit-related protein 4
92	Pic1	ATCG00750	1.97	rps11	30S ribosomal protein S11
93	Pic1	ATCG00830	1.96	rpl2-A	50S ribosomal protein L2
94	Pic1	AT1G55490	1.96	CPN60B1	Chaperonin 60 subunit beta 1
95	Pic1	AT5G45390	1.92	CLPP4	ATP-dependent Clp protease proteolytic subunit 4
96	Pic1	AT3G48560	1.89	ALS, AHAS	Acetolactate synthase
97	Pic1	AT3G29310	1.89	BAG1	BAG family molecular chaperone regulator 8
98	Pic1	AT4G09650	1.87	ATPD	ATP synthase subunit delta
99	Pic1	AT5G26030	1.86	FC1, FC-I	Ferrochelatase-1
100	Pic1	AT4G33510	1.83	DHS2	Phospho-2-dehydro-3-deoxyheptonate aldolase 2
101	Pic1	AT3G53580	1.83	DAPF	Diaminopimelate epimerase
102	Pic1	ATCG00270	1.81	psbD	Photosystem II D2 protein
103	Pic1	AT3G01120	1.80	CGS1	Cystathionine gamma-synthase 1
104	Pic1	AT2G31810	1.78		Acetolactate synthase small subunit 2
105	Pic1	AT1G21600	1.75	PTAC6	PLASTID TRANSCRIPTIONALLY ACTIVE protein 6
106	Pic1	AT2G43030	1.73	RPL3A	50S ribosomal protein L3-1
107	Pic1	AT3G53460	1.71	CP29A, RBP29	29 kDa ribonucleoprotein
108	Pic1	AT3G47520	1.67		Malate dehydrogenase
109	Pic1	AT1G08490	1.66	NFS2	Cysteine desulfurase 1
110	Pic1	AT5G05000	1.66	TOC34	Translocase of chloroplast 34
111	Pic1	AT3G27740	1.64	CARA, VEN6	Carbamoyl-phosphate synthase small chain
112	Pic1	AT5G41670	1.63	PGD3	6-phosphogluconate dehydrogenase
113	Pic1	AT4G28750	1.62	PSAE1	Photosystem I reaction center subunit IV A
114	Pic1	AT1G31230	1.61	AKHSDH1	Bifunctional aspartokinase/homoserine dehydrogenase 1
115	Pic1	AT1G79530	1.61	GAPCP1	Glyceraldehyde-3-phosphate dehydrogenase GAPCP1
116	Pic1	AT4G17600	1.59	LIL3.1	Light-harvesting complex-like protein 3 isotype 1
117	Pic1	AT1G42970	1.58	GAPB	Glyceraldehyde-3-phosphate dehydrogenase GAPB
118	Pic1	AT5G55220	1.57	TIG	Trigger factor-like protein TIG
119	Pic1	AT3G58990	1.56	SSU3	3-isopropylmalate dehydratase small subunit 3
120	Pic1	AT4G03520	1.55	TRXM2	Thioredoxin M2

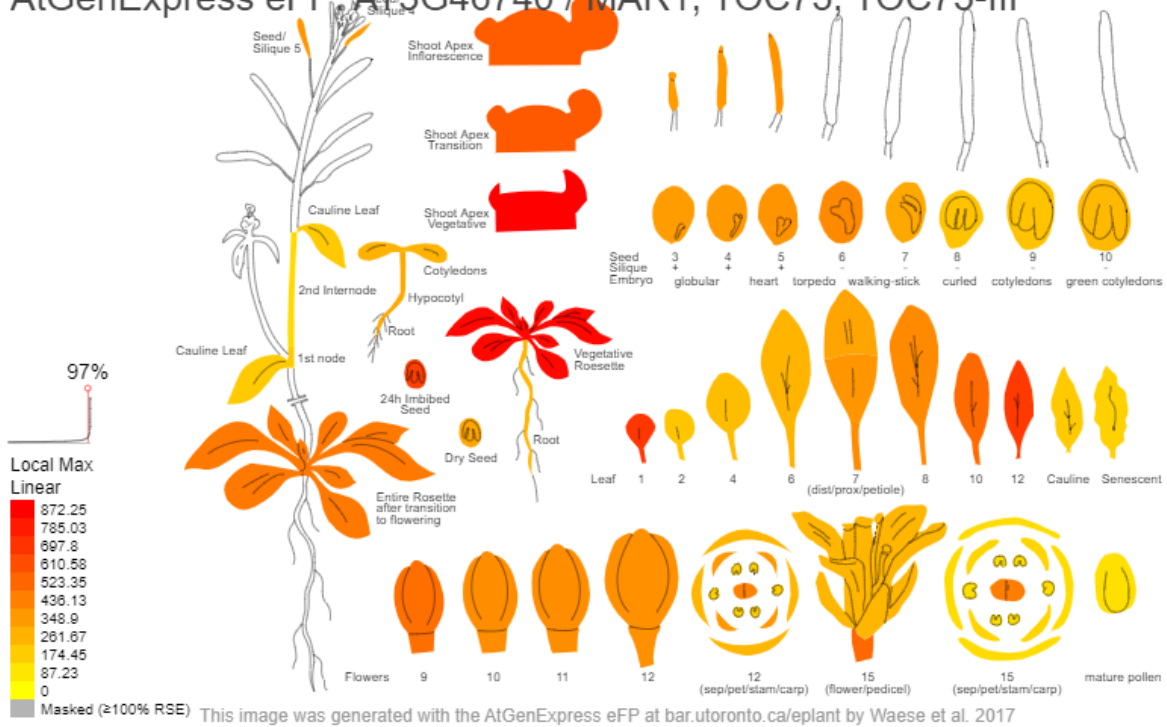
121	Pic1	AT1G01090	1.54	PDH-E1	Pyruvate dehydrogenase E1 component subunit alpha-3
122	Pic1	AT3G52960	1.54	PRXIIE	Peroxiredoxin-2E
123	Pic1	ATCG00500	1.51	accD	Acetyl-coenzyme A carboxylase carboxyl transferase subunit beta
124	Pic1	AT3G48500	1.51	PTAC10,TAC10	Protein PLASTID TRANSCRIPTIONALLY ACTIVE 10 (pTAC10)
125	Pic1	ATCG00490	1.50	rbcl	Ribulose bisphosphate carboxylase large chain

7 Appendices

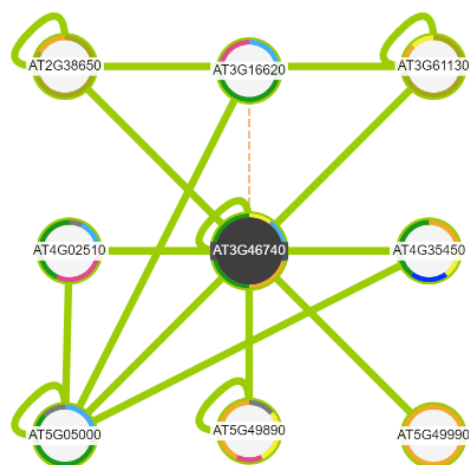
7.1 Gene Expression Profile, Protein Interaction Network and Sequence Similarity Across Plant Species

- *AtToc75-III*:

AtGenExpress eFP: AT3G46740 / MAR1, TOC75, TOC75-III

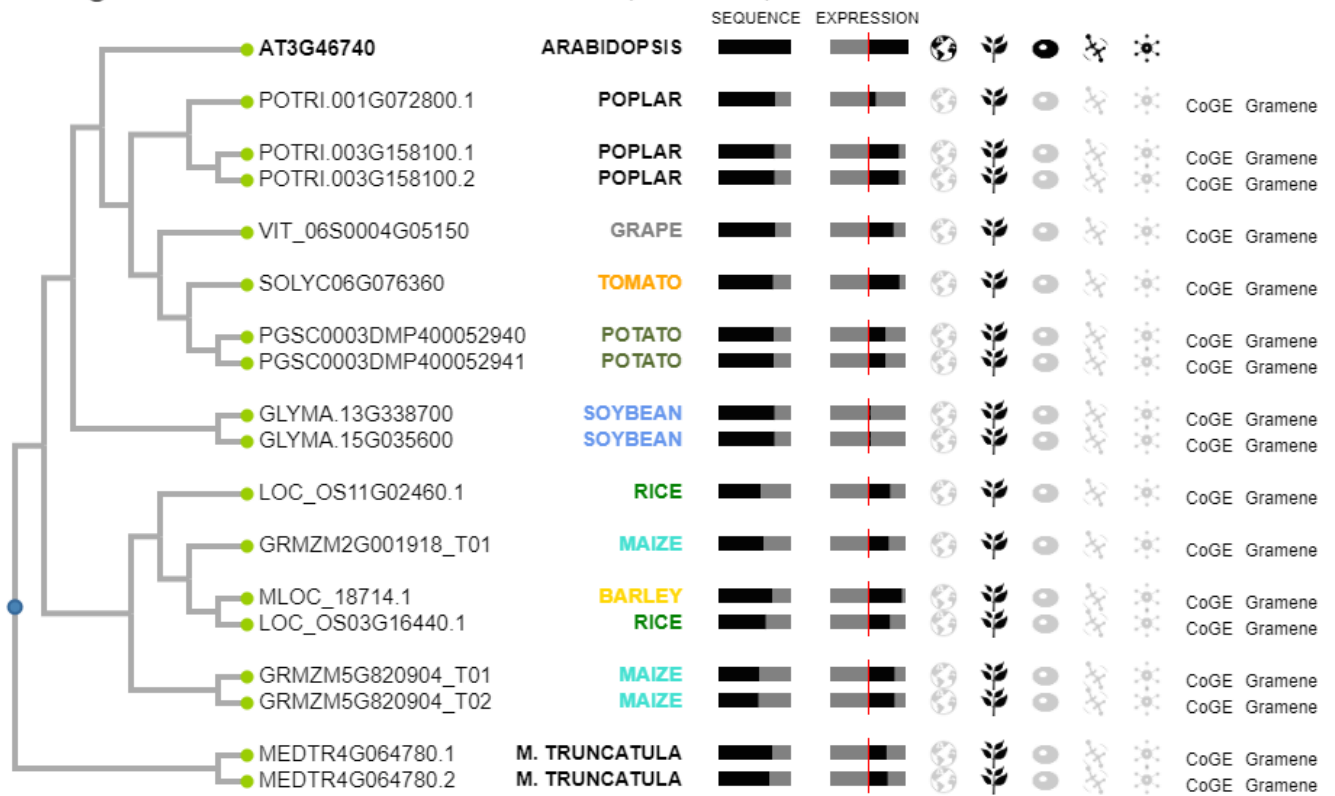


Interaction viewer: AT3G46740 / MAR1, TOC75, TOC75-III



This image was generated with the Interaction Viewer at bar.utoronto.ca/eplant by Waese et al. 2017

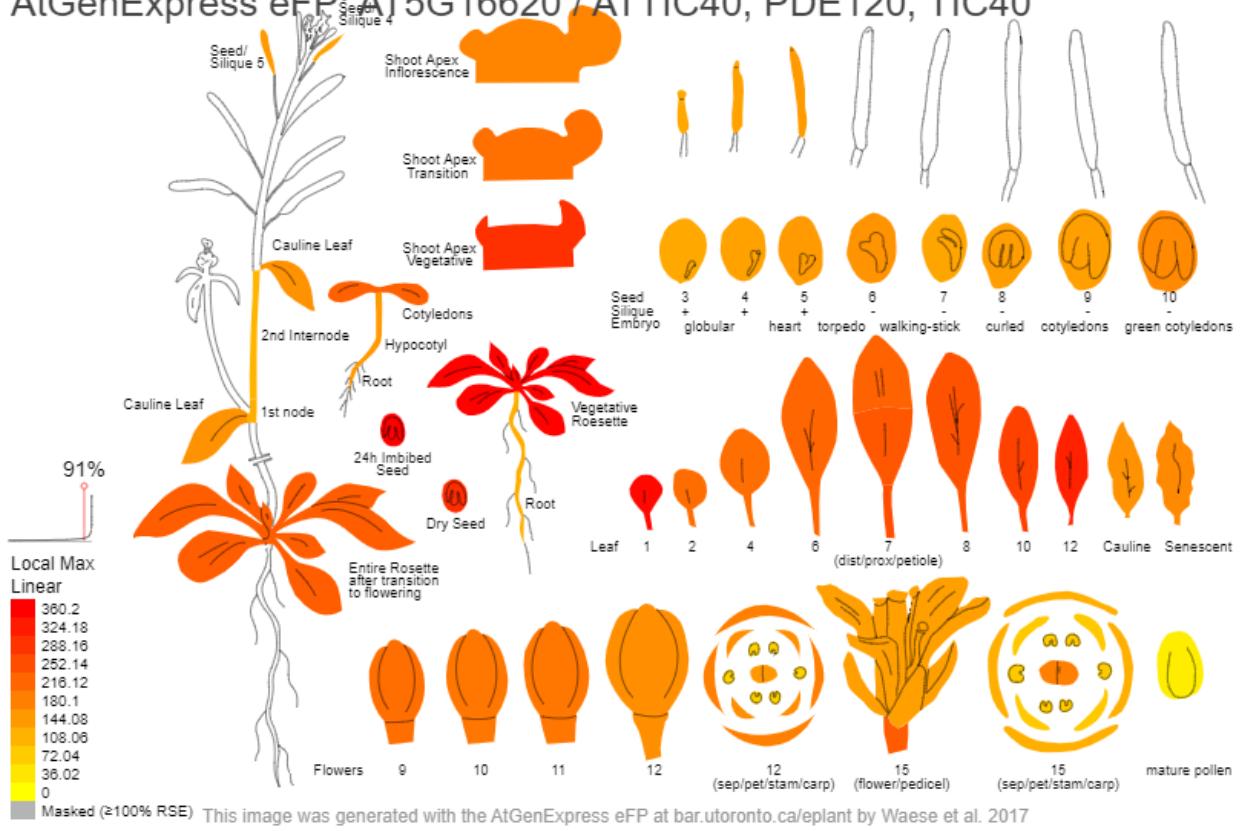
Navigator viewer: AT3G46740 / MAR1, TOC75, TOC75-III



This image was generated with the Interaction Viewer at bar.utoronto.ca/eplant by Waese et al. 2017

- **AtTic40:**

AtGenExpress eFP: AT5G16620 / ATTIC40, PDE120, TIC40

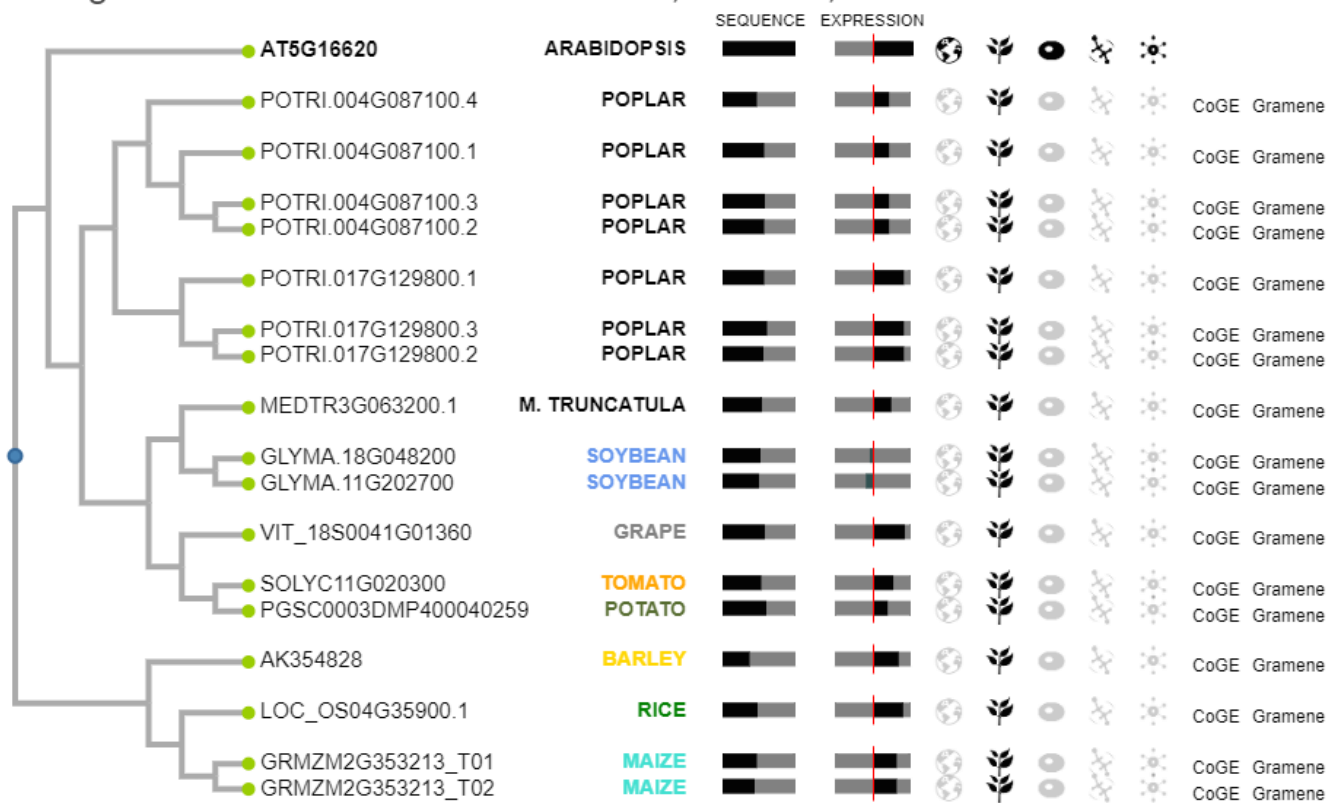


Interaction viewer: AT5G16620 / ATTIC40, PDE120, TIC40



This image was generated with the Interaction Viewer at bar.utoronto.ca/eplant by Waese et al. 2017

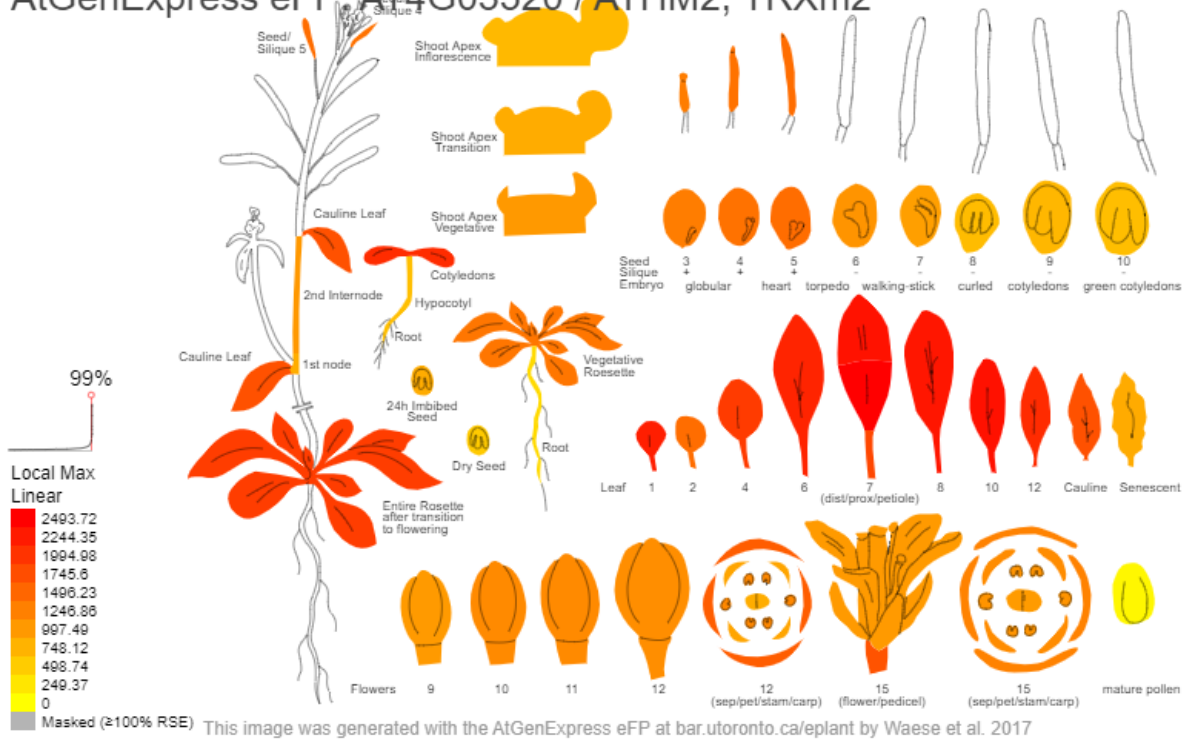
Navigator viewer: AT5G16620 / ATTIC40, PDE120, TIC40



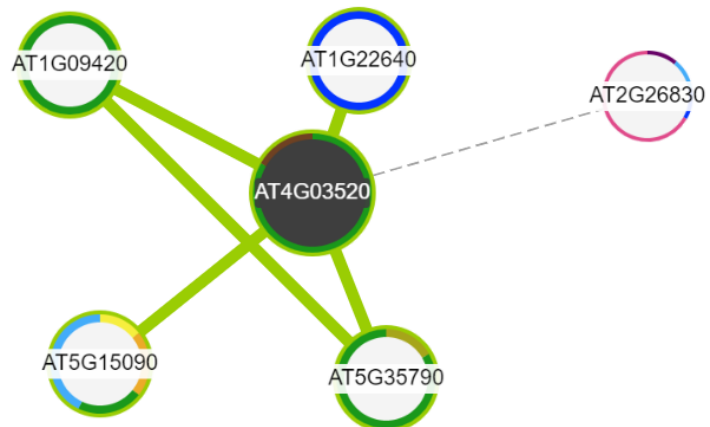
This image was generated with the Interaction Viewer at bar.utoronto.ca/eplant by Waese et al. 2017

- **AtTrxM2:**

AtGenExpress eFP: AT4G03520 / ATHM2, TRXm2



Interaction viewer: AT4G03520 / ATHM2, TRXm2



This image was generated with the Interaction Viewer at bar.utoronto.ca/eplant by Waese et al. 2017

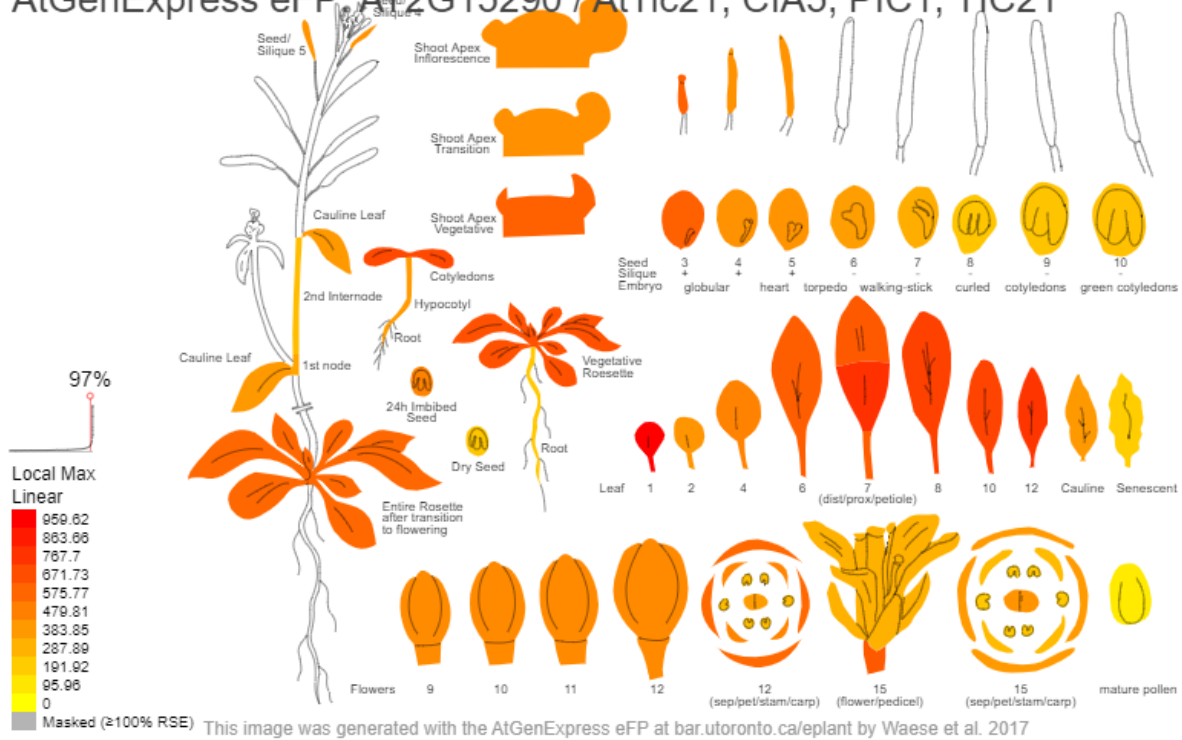
Navigator viewer: AT4G03520 / ATHM2, TRXm2



This image was generated with the Interaction Viewer at bar.utoronto.ca/eplant by Waese et al. 2017

- **AtPic1:**

AtGenExpress eFP: AT2G15290 / AtTic21, CIA5, PIC1, TIC21



Interaction Viewer: AT2G15290 / AtTic21, CIA5, PIC1, TIC21

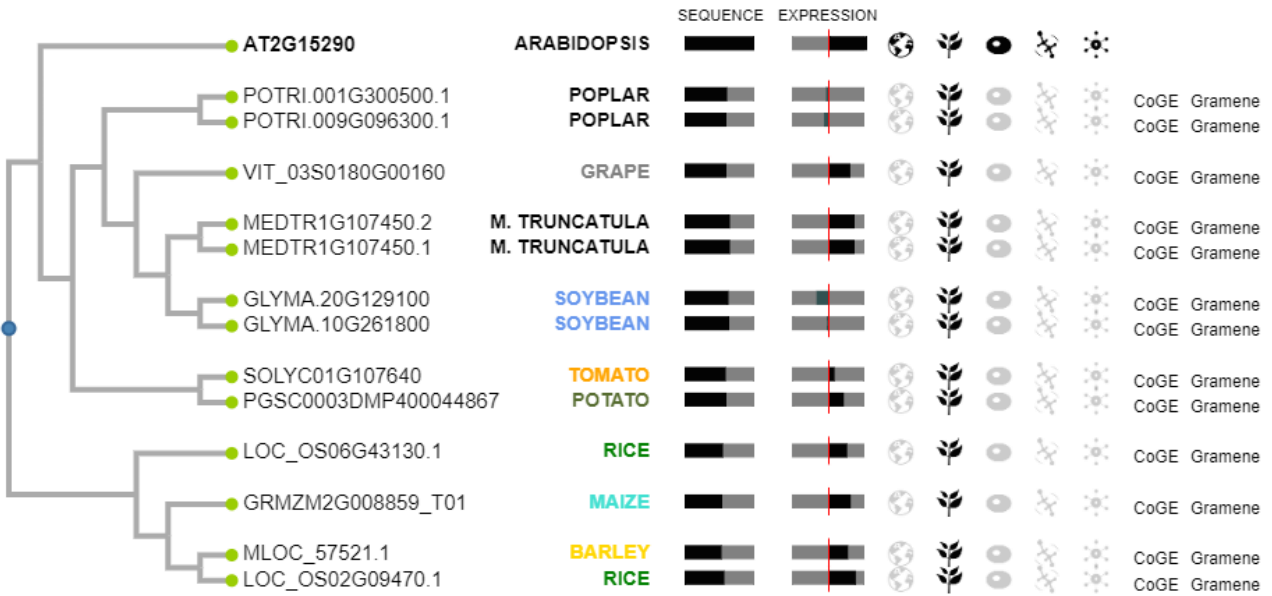
Recursive interactions not shown



No interactions found for this gene.

This image was generated with the Interaction Viewer at bar.utoronto.ca/eplant by Waese et al. 2017

Navigator viewer: AT2G15290 / AtTic21, CIA5, PIC1, TIC21



This image was generated with the Interaction Viewer at bar.utoronto.ca/eplant by Waese et al. 2017

8 References

- Arora, D., Abel, N. B., Liu, C., van Damme, P., Yperman, K., Eeckhout, D., Vu, L. D., Wang, J., Tornkvist, A., Impens, F., Korbei, B., van Leene, J., Goossens, A., de Jaeger, G., Ott, T., Moschou, P. N., & van Damme, D. (2020). Establishment of proximity-dependent biotinylation approaches in different plant model systems. *Plant Cell*, *32*(11), 3388–3407. <https://doi.org/10.1105/TPC.20.00235>
- Bacia, K., Kim, S. A., & Schwille, P. (2006). Fluorescence cross-correlation spectroscopy in living cells. *Nature Methods*, *3*(2), 83–89. <https://doi.org/10.1038/nmeth822>
- Baldwin, A., Wardle, A., Patel, R., Dudley, P., Park, S. K., Twell, D., Inoue, K., Jarvis, P., Le, L., & B, U. K. A. (2005). A Molecular-Genetic Study of the Arabidopsis Toc75 gene family. *Plant Physiology*, *138*(6), 715–733. <https://doi.org/10.1104/pp.105.063289.1>
- Balsera, M., Goetze, T. A., Kovács-Bogdán, E., Schürmann, P., Wagner, R., Buchanan, B. B., Soll, J., & Bölter, B. (2009a). Characterization of Tic110, a channel-forming protein at the inner envelope membrane of chloroplasts, unveils a response to Ca²⁺ and a stromal regulatory disulfide bridge. *Journal of Biological Chemistry*, *284*(5), 2603–2616. <https://doi.org/10.1074/jbc.M807134200>
- Balsera, M., Soll, J., & Bölter, B. (2009b). Protein import machineries in endosymbiotic organelles. *Cellular and Molecular Life Sciences*, *66*(11–12), 1903–1923. <https://doi.org/10.1007/s00018-009-8644-2>
- Balsera, M., Soll, J., & Buchanan, B. B. (2009c). Chapter 10 Protein Import in Chloroplasts. An Emerging Regulatory Role for Redox. *Advances in Botanical Research*, *52*(C), 277–332. [https://doi.org/10.1016/S0065-2296\(10\)52010-X](https://doi.org/10.1016/S0065-2296(10)52010-X)
- Balsera, M., Stengel, A., Soll, J., & Bölter, B. (2007). Tic62: A protein family from metabolism to protein translocation. *BMC Evolutionary Biology*, *7*, 1–12. <https://doi.org/10.1186/1471-2148-7-43>
- Barker, D. F., & Campbell, A. M. (1981). The birA gene of Escherichia coli encodes a biotin holoenzyme synthetase. *Journal of Molecular Biology*, *146*(4), 451–467. [https://doi.org/10.1016/0022-2836\(81\)90042-5](https://doi.org/10.1016/0022-2836(81)90042-5)
- Barth, M. A., Soll, J., & Akbaş, Ş. (2022). Prokaryotic and eukaryotic traits support the biological role of the chloroplast outer envelope. *Biochimica et Biophysica Acta (BBA) - Molecular Cell Research*, *1869*, 119224. <https://doi.org/10.1016/j.bbamcr.2022.119224>
- Bartsch, S., Monnet, J., Selbach, K., Quigley, F., Gray, J., Von Wettstein, D., Reinbothe, S., & Reinbothe, C. (2008). Three thioredoxin targets in the inner envelope membrane of chloroplasts function in protein import and chlorophyll metabolism. *Proceedings of the National Academy of Sciences of the United States of America*, *105*(12), 4933–4938. <https://doi.org/10.1073/pnas.0800378105>
- Becker, T., Jelic, M., Vojta, A., Radunz, A., Soll, J., & Schleiff, E. (2004). Preprotein recognition by the Toc complex. *EMBO Journal*, *23*(3), 520–530. <https://doi.org/10.1038/sj.emboj.7600089>
- Bédard, J., Kubis, S., Bimanadham, S., & Jarvis, P. (2007). Functional similarity between the chloroplast translocon component, Tic40, and the human co-chaperone, Hsp70-interacting protein (Hip). *Journal of Biological Chemistry*, *282*(29), 21404–21414. <https://doi.org/10.1074/jbc.M611545200>
- Bédard, J., Trösch, R., Wu, F., Ling, Q., Flores-Pérez, Ú., Töpel, M., Nawaz, F., & Jarvis, P. (2017). Suppressors of the chloroplast protein import mutant tic40 reveal a genetic link between protein import and thylakoid biogenesis. *Plant Cell*, *29*(7), 1726–1747. <https://doi.org/10.1105/tpc.16.00962>
- Benitez-Alfonso, Y., Cilia, M., San Roman, A., Thomas, C., Maule, A., Hearn, S., & Jackson, D. (2009).

Control of Arabidopsis meristem development by thioredoxin-dependent regulation of intercellular transport. *Proceedings of the National Academy of Sciences of the United States of America*, 106(9), 3615–3620. <https://doi.org/10.1073/pnas.0808717106>

- Benz, J. P., Stengel, A., Lintala, M., Lee, Y. H., Weber, A., Philippar, K., Gügel, I. L., Kaieda, S., Ikegami, T., Mulo, P., Soll, J., & Bölter, B. (2009). Arabidopsis Tic62 and ferredoxin-NADP(H) oxidoreductase form light-regulated complexes that are integrated into the chloroplast redox poise. *Plant Cell*, 21(12), 3965–3983. <https://doi.org/10.1105/tpc.109.069815>
- Binder, A., Lambert, J., Morbitzer, R., Popp, C., Ott, T., Lahaye, T., & Parniske, M. (2014). A modular plasmid assembly kit for multigene expression, gene silencing and silencing rescue in plants. *PLoS ONE*, 9(2). <https://doi.org/10.1371/journal.pone.0088218>
- Blaszczak, E., Lazarewicz, N., Sudevan, A., Wysocki, R., & Rabut, G. (2021). Protein-fragment complementation assays for large-scale analysis of protein-protein interactions. *Biochemical Society Transactions*, 49(3), 1337–1348. <https://doi.org/10.1042/BST20201058>
- Bölter, B., Soll, J., Schulz, A., Hinnah, S., & Wagner, R. (1998). Origin of a chloroplast protein importer. *Proceedings of the National Academy of Sciences of the United States of America*, 95(26), 15831–15836. <https://doi.org/10.1073/PNAS.95.26.15831>
- Booth, W. T., Schlachter, C. R., Pote, S., Ussin, N., Mank, N. J., Klapper, V., Offermann, L. R., Tang, C., Hurlburt, B. K., & Chruszcz, M. (2018). Impact of an N-terminal polyhistidine tag on protein thermal stability. *ACS Omega*, 3(1), 760–768. <https://doi.org/10.1021/acsomega.7b01598>
- Branon, T. C., Bosch, J. A., Sanchez, A. D., Udeshi, N. D., Svinkina, T., Carr, S. A., Feldman, J. L., Perrimon, N., Ting, A. Y., & Author, N. B. (2018). Efficient proximity labeling in living cells and organisms with TurboID HHS Public Access Author manuscript. *Nat Biotechnol*, 36(9), 880–887. <https://doi.org/10.1038/nbt.4201>
- Briat, J. F., Ravet, K., Arnaud, N., Duc, C., Boucherez, J., Touraine, B., Cellier, F., & Gaymard, F. (2010). New insights into ferritin synthesis and function highlight a link between iron homeostasis and oxidative stress in plants. *Annals of Botany*, 105(5), 811–822. <https://doi.org/10.1093/aob/mcp128>
- Bruce, B. D. (2000). Chloroplast transit peptides: Structure, function and evolution. *Trends in Cell Biology*, 10(10), 440–447. [https://doi.org/10.1016/S0962-8924\(00\)01833-X](https://doi.org/10.1016/S0962-8924(00)01833-X)
- Brückner, A., Polge, C., Lentze, N., Auerbach, D., & Schlattner, U. (2009). Yeast two-hybrid, a powerful tool for systems biology. *International Journal of Molecular Sciences*, 10(6), 2763–2788. <https://doi.org/10.3390/ijms10062763>
- Buchanan, S. K. (1999). Beta-Barrel proteins from bacterial function and refolding. *Current Opinion in Structural Biology*, 9, 455–461. [https://doi.org/10.1016/S0959-440X\(99\)80064-5](https://doi.org/10.1016/S0959-440X(99)80064-5)
- Cabantous, S., Terwilliger, T. C., & Waldo, G. S. (2005). Protein tagging and detection with engineered self-assembling fragments of green fluorescent protein. *Nature Biotechnology*, 23(1), 102–107. <https://doi.org/10.1038/nbt1044>
- Capitani, G., Marković-Housley, Z., DelVal, G., Morris, M., Jansonius, J. N., & Schürmann, P. (2000). Crystal structures of two functionally different thioredoxins in spinach chloroplasts. *Journal of Molecular Biology*, 302(1), 135–154. <https://doi.org/10.1006/jmbi.2000.4006>
- Chapman-Smith, A., & Cronan, J. E. (1999). Molecular biology of biotin attachment to proteins. *Journal of Nutrition*, 129(2), 477–484. <https://doi.org/10.1093/jn/129.2.477s>
- Chen, X., Smith, M. D., Fitzpatrick, L., & Schnell, D. J. (2002). In vivo analysis of the role of atTic20 in

- protein import into chloroplasts. *Plant Cell*, 14(3), 641–654. <https://doi.org/10.1105/tpc.010336>
- Chen, Y.-L., Chen, L.-J., Chu, C.-C., Huang, P.-K., Wen, J.-R., & Li, H.-M. (2018). TIC236 links the outer and inner membrane translocons of the chloroplast. *Nature*. <https://doi.org/10.1038/s41586-018-0713-y>
- Chen, Y. L., Chen, L. J., & Li, H. M. (2016). Polypeptide transport-associated domains of the Toc75 channel protein are located in the intermembrane space of chloroplasts. *Plant Physiology*, 172(1), 235–243. <https://doi.org/10.1104/pp.16.00919>
- Chibani, K., Pucker, B., Dietz, K. J., & Cavanagh, A. (2021). Genome-wide analysis and transcriptional regulation of the typical and atypical thioredoxins in *Arabidopsis thaliana*. *FEBS Letters*, 595(21), 2715–2730. <https://doi.org/10.1002/1873-3468.14197>
- Chigri, F., Hörmann, F., Stamp, A., Stammers, D. K., Bölter, B., Soll, J., & Vothknecht, U. C. (2006). Calcium regulation of chloroplast protein translocation is mediated by calmodulin binding to Tic32. *Proceedings of the National Academy of Sciences of the United States of America*, 103(43), 16051–16056. <https://doi.org/10.1073/pnas.0607150103>
- Chiu, C. C., & Li, H. M. (2008). Tic40 is important for reinsertion of proteins from the chloroplast stroma into the inner membrane. *Plant Journal*, 56(5), 793–801. <https://doi.org/10.1111/J.1365-3113X.2008.03638.X>
- Cho, K. F., Branon, T. C., Rajeev, S., Svinkina, T., Udeshi, N. D., Thoudam, T., Kwak, C., Rhee, H. W., Lee, I. K., Carr, S. A., & Ting, A. Y. (2020). Split-TurboID enables contact-dependent proximity labeling in cells. *Proceedings of the National Academy of Sciences of the United States of America*, 117(22). <https://doi.org/10.1073/pnas.1919528117>
- Chou, M. L., Chu, C. C., Chen, L. J., Akita, M., & Li, H. M. (2006). Stimulation of transit-peptide release and ATP hydrolysis by a cochaperone during protein import into chloroplasts. *Journal of Cell Biology*, 175(6), 893–900. <https://doi.org/10.1083/jcb.200609172>
- Chou, M. L., Fitzpatrick, L. M., Tu, S. L., Budziszewski, G., Potter-Lewis, S., Akita, M., Levin, J. Z., Keegstra, K., & Li, H. M. (2003). Tic40, a membrane-anchored co-chaperone homolog in the chloroplast protein translocon. *EMBO Journal*, 22(12), 2970–2980. <https://doi.org/10.1093/emboj/cdg281>
- Chrétien, A. È., Gagnon-Arsenault, I., Dubé, A. K., Barbeau, X., Després, P. C., Lamothe, C., Dion-Côté, A. M., Lagüe, P., & Landry, C. R. (2018). Extended Linkers Improve the Detection of Protein-protein Interactions (PPIs) by Dihydrofolate Reductase Protein-fragment Complementation Assay (DHFR PCA) in Living Cells. *Molecular and Cellular Proteomics*, 17(2), 373–383. <https://doi.org/10.1074/mcp.TIR117.000385>
- Clemens, S., Naumann, B., & Hippler, M. (2009). Proteomics of metal mediated protein dynamics in plants - Iron and cadmium in the focus. *Frontiers in Bioscience*, 14(5), 1955–1969. <https://doi.org/10.2741/3355>
- Conlan, B., Stoll, T., Gorman, J. J., Saur, I., & Rathjen, J. P. (2018). Development of a rapid in planta bioid system as a probe for plasma membrane-Associated immunity proteins. *Frontiers in Plant Science*, 871. <https://doi.org/10.3389/fpls.2018.01882>
- Constan, D., Froehlich, J. E., Rangarajan, S., & Keegstra, K. (2004). A stromal Hsp100 protein is required for normal chloroplast development and function in *Arabidopsis*. *Plant Physiology*, 136(3), 3605–3615. <https://doi.org/10.1104/PP.104.052928>
- Courteille, A., Vesa, S., Sanz-Barrio, R., Cazalé, A. C., Becuwe-Linka, N., Farran, I., Havaux, M., Rey, P., & Rumeau, D. (2013). Thioredoxin m4 controls photosynthetic alternative electron pathways in *Arabidopsis*. *Plant Physiology*, 161(1), 508–520. <https://doi.org/10.1104/pp.112.207019>

- Da, Q., Sun, T., Wang, M., Jin, H., Li, M., Feng, D., Wang, J., Wang, H. Bin, & Liu, B. (2018). M-type thioredoxins are involved in the xanthophyll cycle and proton motive force to alter NPQ under low-light conditions in *Arabidopsis*. *Plant Cell Reports*, 37(2), 279–291. <https://doi.org/10.1007/s00299-017-2229-6>
- Das, P. P., Macharia, M. W., Lin, Q., & Wong, S. M. (2019). In planta proximity-dependent biotin identification (BioID) identifies a TMV replication co-chaperone NbSGT1 in the vicinity of 126 kDa replicase. *Journal of Proteomics*, 204, 103402. <https://doi.org/10.1016/j.jprot.2019.103402>
- De Munter, S., Görnemann, J., Derua, R., Lesage, B., Qian, J., Heroes, E., Waelkens, E., Van Eynde, A., Beullens, M., & Bollen, M. (2017). Split-BioID: a proximity biotinylation assay for dimerization-dependent protein interactions. *FEBS Letters*, 591(2), 415–424. <https://doi.org/10.1002/1873-3468.12548>
- de Vries, J., & Archibald, J. M. (2017). Endosymbiosis: Did Plastids Evolve from a Freshwater Cyanobacterium? *Current Biology*, 27(3), R103–R105. <https://doi.org/10.1016/j.cub.2016.12.006>
- Debnam, P. M., Fernie, A. R., Leisse, A., Golding, A., Bowsher, C. G., Grimshaw, C., Knight, J. S., & Emes, M. J. (2004). Altered activity of the P2 isoform of plastidic glucose 6-phosphate dehydrogenase in tobacco (*Nicotiana tabacum* cv. Samsun) causes changes in carbohydrate metabolism and response to oxidative stress in leaves. *Plant Journal*, 38(1), 49–59. <https://doi.org/10.1111/j.1365-313X.2004.02017.x>
- Dixon, A. S., Schwinn, M. K., Hall, M. P., Zimmerman, K., Otto, P., Lubben, T. H., Butler, B. L., Binkowski, B. F., MacHleidt, T., Kirkland, T. A., Wood, M. G., Eggers, C. T., Encell, L. P., & Wood, K. V. (2016). NanoLuc Complementation Reporter Optimized for Accurate Measurement of Protein Interactions in Cells. *ACS Chemical Biology*, 11(2), 400–408. <https://doi.org/10.1021/acschembio.5b00753>
- Dreze, M., Carvunis, A.-R., Charlotiaux, B., Galli, M., Pevzner, S. J., Tasan, M., Ahn, Y.-Y., Balumuri, P., Barabási, A.-L., Bautista, V., Braun, P., Byrdsong, D., Chen, H., Chesnut, J. D., Cusick, M. E., Dangl, J. L., de los Reyes, C., Dricot, A., Duarte, M., ... Yazaki, J. (2011). Evidence for Network Evolution in an *Arabidopsis* Interactome Map. *Science*, 333(6042), 601–607. <https://doi.org/10.1126/science.1203877>
- Dunham, W. H., Mullin, M., & Gingras, A. C. (2012). Affinity-purification coupled to mass spectrometry: Basic principles and strategies. *Proteomics*, 12(10), 1576–1590. <https://doi.org/10.1002/pmic.201100523>
- Dünschede, B., Bals, T., Funke, S., & Schünemann, D. (2011). Interaction studies between the chloroplast signal recognition particle subunit cpSRP43 and the full-length translocase Alb3 reveal a membrane-embedded binding region in Alb3 protein. *Journal of Biological Chemistry*, 286(40), 35187–35195. <https://doi.org/10.1074/jbc.M111.250746>
- Duy, D., Stübe, R., Wanner, G., & Philippar, K. (2011). The chloroplast permease PIC1 regulates plant growth and development by directing homeostasis and transport of iron. *Plant Physiology*, 155(4), 1709–1722. <https://doi.org/10.1104/pp.110.170233>
- Duy, D., Wanner, G., Meda, A. R., Von Wirén, N., Soll, J., & Philippar, K. (2007). PIC1, an ancient permease in *Arabidopsis* chloroplasts, mediates iron transport. *Plant Cell*, 19(3), 986–1006. <https://doi.org/10.1105/tpc.106.047407>
- Dyall, S. D., Brown, M. T., & Johnson, P. J. (2004). Ancient Invasions: From Endosymbionts to Organelles. *Science*, 304(5668), 253–257. <https://doi.org/10.1126/science.1094884>
- Eckart, K., Eichacker, L., Sohr, K., Schleiff, E., Heins, L., & Soll, J. (2002). A Toc75-like protein import channel is abundant in chloroplasts. *EMBO Reports*, 3(6), 557–562.

<https://doi.org/10.1093/embo-reports/kvf110>

- Ellis, R. J. (1979). The most abundant protein in the world. *Trends in Biochemical Sciences*, 4(11), 241–244. [https://doi.org/10.1016/0968-0004\(79\)90212-3](https://doi.org/10.1016/0968-0004(79)90212-3)
- Emanuelsson, O., Nielsen, H., & Heijne, G. Von. (1999). ChloroP, a neural network-based method for predicting chloroplast transit peptides and their cleavage sites. In *Protein Science* (Vol. 8, Issue 5). <https://doi.org/10.1110/ps.8.5.978>
- Endo, T., Kawamura, K., & Nakai, M. (1992). The chloroplast-targeting domain of plastocyanin transit peptide can form a helical structure but does not have a high affinity for lipid bilayers. In *European Journal of Biochemistry* (Vol. 207, Issue 2). <https://doi.org/10.1111/j.1432-1033.1992.tb17094.x>
- Ertel, F., Mirus, O., Bredemeier, R., Moslavac, S., Becker, T., & Schleiff, E. (2005). The evolutionarily related β -barrel polypeptide transporters from *Pisum sativum* and *Nostoc PCC7120* contain two distinct functional domains. *Journal of Biological Chemistry*, 280(31), 28281–28289. <https://doi.org/10.1074/jbc.M503035200>
- Espinás, N. A., Kobayashi, K., Sato, Y., Mochizuki, N., Takahashi, K., Tanaka, R., & Masuda, T. (2016). Allocation of heme is differentially regulated by ferrochelatase isoforms in *Arabidopsis* cells. *Frontiers in Plant Science*, 7(AUG2016). <https://doi.org/10.3389/fpls.2016.01326>
- Fernández-Trijueque, J., Serrato, A. J., & Sahrawy, M. (2019). Proteomic analyses of thioredoxins f and m *arabidopsis thaliana* mutants indicate specific functions for these proteins in plants. *Antioxidants*, 8(3). <https://doi.org/10.3390/ANTIOX8030054>
- Filiz, E., & Aydın Akbudak, M. (2020). Investigation of PIC1 (permease in chloroplasts 1) gene's role in iron homeostasis: bioinformatics and expression analyses in tomato and sorghum. *BioMetals*, 33(1), 29–44. <https://doi.org/10.1007/s10534-019-00228-x>
- Flores-Pérez, Ú., Bédard, J., Tanabe, N., Lympieropoulos, P., Clarke, A. K., & Jarvis, P. (2016). Functional analysis of the Hsp93/ClpC chaperone at the chloroplast envelope. *Plant Physiology*, 170(1), 147–162. <https://doi.org/10.1104/pp.15.01538>
- Förster, T. (1948). Zwischenmolekulare Energiewanderung und Fluoreszenz. In *Annalen der Physik* (Vol. 437, Issues 1–2, pp. 55–75). <https://doi.org/10.1002/andp.19484370105>
- Friso, G., Giacomelli, L., Ytterberg, A. J., Peltier, J. B., Rudella, A., Sun, Q., & Van Wijk, K. J. (2004). In-Depth Analysis of the Thylakoid Membrane Proteome of *Arabidopsis thaliana* Chloroplasts: New Proteins, New Functions, and a Plastid Proteome Database. *Plant Cell*, 16(2), 478–499. <https://doi.org/10.1105/tpc.017814>
- Ge, Y., Chen, L., Liu, S., Zhao, J., Zhang, H., & Chen, P. R. (2019). Enzyme-Mediated Intercellular Proximity Labeling for Detecting Cell-Cell Interactions [Rapid-communication]. *Journal of the American Chemical Society*, 141(5), 1833–1837. <https://doi.org/10.1021/jacs.8b10286>
- Genevros, S., Steeghs, L., Roholl, P., Letesson, J. J., & Van der Ley, P. (2003). The Omp85 protein of *Neisseria meningitidis* is required for lipid export to the outer membrane. In *EMBO Journal* (Vol. 22, Issue 8, pp. 1780–1789). <https://doi.org/10.1093/emboj/cdg174>
- Glaser, S., Van Dooren, G. G., Agrawal, S., Brooks, C. F., McFadden, G. I., Striepen, B., & Higgins, M. K. (2012). Tic22 is an essential chaperone required for protein import into the apicoplast. *Journal of Biological Chemistry*, 287(47), 39505–39512. <https://doi.org/10.1074/jbc.M112.405100>
- Goloubinoff, P., Christeller, J. T., Gatenby, A. A., & Lorimer, G. H. (1989). Reconstitution of active dimeric ribulose biphosphate carboxylase from an unfolded state depends on two chaperonin proteins and Mg-ATP. *Nature*, 342(6252), 884–889. <https://doi.org/10.1038/342884a0>

- Gong, X., Guo, C., Terachi, T., Cai, H., & Yu, D. (2015). Tobacco PIC1 Mediates Iron Transport and Regulates Chloroplast Development. *Plant Molecular Biology Reporter*, *33*(3), 401–413. <https://doi.org/10.1007/s11105-014-0758-5>
- Gorelova, V., De Lepeleire, J., Van Daele, J., Pluim, D., Mei, C., Cuypers, A., Leroux, O., Rébeillé, F., Schellens, J. H. M., Blancquaert, D., Stove, C. P., & Van Der Straeten, D. (2017). Dihydrofolate reductase/thymidylate synthase fine-tunes the folate status and controls redox homeostasis in plants. *Plant Cell*, *29*(11), 2831–2853. <https://doi.org/10.1105/tpc.17.00433>
- Gray, M. W. (2017). Lynn Margulis and the endosymbiont hypothesis: 50 years later. *Molecular Biology of the Cell*, *28*(10), 1285–1287. <https://doi.org/10.1091/mbc.E16-07-0509>
- Gross, J., & Bhattacharya, D. (2009a). Mitochondrial and plastid evolution in eukaryotes: An outsiders' perspective. In *Nature Reviews Genetics* (Vol. 10, Issue 7). Cambridge Univ. Press. <https://doi.org/10.1038/nrg2610>
- Gross, J., & Bhattacharya, D. (2009b). Revaluating the evolution of the Toc and Tic protein translocons. *Trends in Plant Science*, *14*(1), 13–20. <https://doi.org/10.1016/j.tplants.2008.10.003>
- Gross, L. E., Klinger, A., Spies, N., Ernst, T., Flinner, N., Simm, S., Ladig, R., Bodensohn, U., & Schleiff, E. (2021). Insertion of plastidic b-barrel proteins into the outer envelopes of plastids involves an intermembrane space intermediate formed with Toc75-V/OEP80. *Plant Cell*, *33*(5), 1657–1681. <https://doi.org/10.1093/plcell/koab052>
- Han, Y., Branon, T. C., Martell, J. D., Boassa, D., Shechner, D., Ellisman, M. H., & Ting, A. (2019). Directed Evolution of Split APEX2 Peroxidase. *ACS Chemical Biology*, *14*(4), 619–635. <https://doi.org/10.1021/acscchembio.8b00919>
- Heins, L., Mehrle, A., Hemmler, R., Wagner, R., Kuchler, M., Hörmann, F., Sveshnikov, D., & Soll, J. (2002). The preprotein conducting channel at the inner envelope membrane of plastids. *EMBO Journal*, *21*(11), 2616–2625. <https://doi.org/10.1093/emboj/21.11.2616>
- Hill, Z. B., Pollock, S. B., Zhuang, M., & Wells, J. A. (2016). Direct Proximity Tagging of Small Molecule Protein Targets Using an Engineered NEDD8 Ligase. *Journal of the American Chemical Society*, *138*(40), 13123–13126. <https://doi.org/10.1021/JACS.6B06828>
- Hinnah, S. C., Wagner, R., Sveshnikova, N., Harrer, R., & Soll, J. (2002). The chloroplast protein import channel Toc75: Pore properties and interaction with transit peptides. *Biophysical Journal*, *83*(2), 899–911. [https://doi.org/10.1016/S0006-3495\(02\)75216-8](https://doi.org/10.1016/S0006-3495(02)75216-8)
- Hirsch, S., Muckel, E., Heemeyer, F., Von Heijne, G., & Soll, J. (1994). A receptor component of the chloroplast protein translocation machinery. *Science*, *266*(5193), 1989–1992. <https://doi.org/10.1126/science.7801125>
- Hörmann, F., Kuchler, M., Sveshnikov, D., Oppermann, U., Li, Y., & Soll, J. (2004). Tic32, an essential component in chloroplast biogenesis. *Journal of Biological Chemistry*, *279*(33), 34756–34762. <https://doi.org/10.1074/jbc.M402817200>
- Hsu, C. Y., Chou, M. L., Wei, W. C., Chung, Y. C., Loo, X. Y., & Lin, L. F. (2022). Chloroplast Protein Tic55 Involved in Dark-Induced Senescence through AtbHLH/AtWRKY-ANAC003 Controlling Pathway of Arabidopsis thaliana. *Genes*, *13*(2). <https://doi.org/10.3390/genes13020308>
- Huang, A., Tang, Y., Shi, X., Jia, M., Zhu, J., Yan, X., Chen, H., & Gu, Y. (2020). Proximity labeling proteomics reveals critical regulators for inner nuclear membrane protein degradation in plants. *Nature Communications*, *11*(1). <https://doi.org/10.1038/s41467-020-16744-1>
- Huang, P. K., Chan, P. T., Su, P. H., Chen, L. J., & Li, H. M. (2016). Chloroplast Hsp93 directly binds to

transit peptides at an early stage of the preprotein import process. *Plant Physiology*, 170(2), 857–866. <https://doi.org/10.1104/pp.15.01830>

- Hung, V., Zou, P., Rhee, H. W., Udeshi, N. D., Cracan, V., Svinkina, T., Carr, S. A., Mootha, V. K., & Ting, A. Y. (2014). Proteomic Mapping of the Human Mitochondrial Intermembrane Space in Live Cells via Ratiometric APEX Tagging. *Molecular Cell*, 55(2), 332–341. <https://doi.org/10.1016/j.molcel.2014.06.003>
- Inoue, H., Li, M., & Schnell, D. J. (2013). An essential role for chloroplast heat shock protein 90 (Hsp90C) in protein import into chloroplasts. *Proceedings of the National Academy of Sciences of the United States of America*, 110(8), 3173–3178. <https://doi.org/10.1073/pnas.1219229110>
- Inoue, K., & Potter, D. (2004). The chloroplastic protein translocation channel Toc75 and its paralog OEP80 represent two distinct protein families and are targeted to the chloroplastic outer envelope by different mechanisms. *Plant Journal*, 39(3), 354–365. <https://doi.org/10.1111/j.1365-313X.2004.02135.x>
- Jacquot, J. P., Gelhaye, E., Rouhier, N., Corbier, C., Didierjean, C., & Aubry, A. (2002). Thioredoxins and related proteins in photosynthetic organisms: Molecular basis for thiol dependent regulation. *Biochemical Pharmacology*, 64(5–6), 1065–1069. [https://doi.org/10.1016/S0006-2952\(02\)01177-2](https://doi.org/10.1016/S0006-2952(02)01177-2)
- Kalanon, M., & McFadden, G. I. (2008). The chloroplast protein translocation complexes of *Chlamydomonas reinhardtii*: A bioinformatic comparison of Toc and Tic components in plants, green algae and red algae. *Genetics*, 179(1), 95–112. <https://doi.org/10.1534/genetics.107.085704>
- Kalocsay, M. (2019). APEX peroxidase-catalyzed proximity labeling and multiplexed quantitative proteomics. *Methods in Molecular Biology*, 2008, 41–55. https://doi.org/10.1007/978-1-4939-9537-0_4
- Karlin-Neumann, G. A., & Tobin, E. M. (1986). Transit peptides of nuclear-encoded chloroplast proteins share a common amino acid framework. *The EMBO Journal*, 5(1), 9–13. <https://doi.org/10.1002/j.1460-2075.1986.tb04170.x>
- Kessler, F., Blobel, G., Patel, H. A., & Schnell, D. J. (1994). Identification of two GTP-binding proteins in the chloroplast protein import machinery. *Science*, 266(5187), 1035–1039. <https://doi.org/10.1126/science.7973656>
- Khan, M., Youn, J. Y., Gingras, A. C., Subramaniam, R., & Desveaux, D. (2018). In planta proximity dependent biotin identification (BioID). *Scientific Reports*, 8(1), 2–9. <https://doi.org/10.1038/s41598-018-27500-3>
- Kido, K., Yamanaka, S., Nakano, S., Motani, K., Shinohara, S., Nozawa, A., Kosako, H., Ito, S., & Sawasaki, T. (2020). Airid, a novel proximity biotinylation enzyme, for analysis of protein–protein interactions. *ELife*, 9. <https://doi.org/10.7554/eLife.54983>
- Kikuchi, S., Bédard, J., Hirano, M., Hirabayashi, Y., Oishi, M., Imai, M., Takase, M., Ide, T., & Nakai, M. (2013). Uncovering the protein translocon at the chloroplast inner envelope membrane. *Science*, 339(6119), 571–574. <https://doi.org/10.1126/science.1229262>
- Kikuchi, S., Hirohashi, T., & Nakai, M. (2006). Characterization of the preprotein translocon at the outer envelope membrane of chloroplasts by blue native PAGE. *Plant and Cell Physiology*, 47(3), 363–371. <https://doi.org/10.1093/pcp/pcj002>
- Kikuchi, S., Oishi, M., Hirabayashi, Y., Lee, D. W., Hwang, I., & Nakai, M. (2009). A 1.1-Megadalton translocation complex containing tic20 and tic21 mediates chloroplast protein import at the inner envelope membrane. *Plant Cell*, 21(6), 1781–1797. <https://doi.org/10.1105/tpc.108.063552>

- Kim, D. I., Birendra, K. C., Zhu, W., Motamedchaboki, K., Doye, V., & Roux, K. J. (2014). Probing nuclear pore complex architecture with proximity-dependent biotinylation. *Proceedings of the National Academy of Sciences of the United States of America*, *111*(24), 2453–2461. <https://doi.org/10.1073/pnas.1406459111>
- Kim, D. I., Jensen, S. C., Noble, K. A., KC, B., Roux, K. H., Motamedchaboki, K., & Roux, K. J. (2016). An improved smaller biotin ligase for BioID proximity labeling. *Molecular Biology of the Cell*, *27*(8), 1188–1196. <https://doi.org/10.1091/mbc.E15-12-0844>
- Klomsiri, C., Karplus, P. A., & Poole, L. B. (2011). Cysteine-based redox switches in enzymes. *Antioxidants and Redox Signaling*, *14*(6), 1065–1077. <https://doi.org/10.1089/ars.2010.3376>
- Knopp, M., Garg, S. G., Handrich, M., & Gould, S. B. (2020). Major Changes in Plastid Protein Import and the Origin of the Chloroplastida. *IScience*, *23*(3), 100896. <https://doi.org/10.1016/j.isci.2020.100896>
- Ko, K., Budd, D., Wu, C., Seibert, F., Kourtz, L., & Ko, Z. W. (1995). Isolation and characterization of a cDNA clone encoding a member of the Com44/Cim44 envelope components of the chloroplast protein import apparatus. *Journal of Biological Chemistry*, *270*(48), 28601–28608. <https://doi.org/10.1074/jbc.270.48.28601>
- Kotani, N., Gu, J., Isaji, T., Udaka, K., Taniguchi, N., & Honke, K. (2008). Biochemical visualization of cell surface molecular clustering in living cells. *Proceedings of the National Academy of Sciences of the United States of America*, *105*(21), 7405–7409. <https://doi.org/10.1073/pnas.0710346105>
- Kouranov, A., Chen, X., Fuks, B., & Schnell, D. J. (1998). Tic20 and Tic22 are new components of the protein import apparatus at the chloroplast inner envelope membrane. *Journal of Cell Biology*, *143*(4), 991–1002. <https://doi.org/10.1083/jcb.143.4.991>
- Kouranov, A., & Schnell, D. J. (1997). Analysis of the interactions of preproteins with the import machinery over the course of protein import into chloroplasts. *Journal of Cell Biology*, *139*(7), 1677–1685. <https://doi.org/10.1083/jcb.139.7.1677>
- Kovacheva, S., Bédard, J., Patel, R., Dudley, P., Twell, D., Ríos, G., Koncz, C., & Jarvis, P. (2005). In vivo studies on the roles of Tic110, Tic40 and Hsp93 during chloroplast protein import. *Plant Journal*, *41*(3), 412–428. <https://doi.org/10.1111/j.1365-313X.2004.02307.x>
- Küchler, M., Decker, S., Hörmann, F., Soll, J., & Heins, L. (2002). Protein import into chloroplasts involves redox-regulated proteins. *EMBO Journal*, *21*(22), 6136–6145. <https://doi.org/10.1093/emboj/cdf621>
- Kwak, C., Shin, S., Park, J. S., Jung, M., My Nhung, T. T., Kang, M. G., Lee, C., Kwon, T. H., Park, S. K., Mun, J. Y., Kim, J. S., & Rhee, H. W. (2020). Contact-ID, a tool for profiling organelle contact sites, reveals regulatory proteins of mitochondrial-associated membrane formation. *Proceedings of the National Academy of Sciences of the United States of America*, *117*(22). <https://doi.org/10.1073/pnas.1916584117>
- Lam, S. S., Martell, J. D., Kamer, K. J., Deerinck, T. J., Ellisman, M. H., Mootha, V. K., & Ting, A. Y. (2014). Directed evolution of APEX2 for electron microscopy and proximity labeling. *Nature Methods*, *12*(1), 51–54. <https://doi.org/10.1038/nmeth.3179>
- Le Moan, N., Clement, G., Le Maout, S., Tacnet, F., & Toledano, M. B. (2006). The *Saccharomyces cerevisiae* proteome of oxidized protein thiols: Contrasted functions for the thioredoxin and glutathione pathways. *Journal of Biological Chemistry*, *281*(15), 10420–10430. <https://doi.org/10.1074/jbc.M513346200>
- Lee, D. W., & Hwang, I. (2019). Protein import into chloroplasts via the Tic40-dependent and -

independent pathways depends on the amino acid composition of the transit peptide. *Biochemical and Biophysical Research Communications*, 518(1), 66–71. <https://doi.org/10.1016/j.bbrc.2019.08.009>

- Leichert, L. I., Gehrke, F., Gudiseva, H. V., Blackwell, T., Ilbert, M., Walker, A. K., Strahler, J. R., Andrews, P. C., & Jakob, U. (2008). Quantifying changes in the thiol redox proteome upon oxidative stress in vivo. *Proceedings of the National Academy of Sciences of the United States of America*, 105(24), 8197–8202. <https://doi.org/10.1073/pnas.0707723105>
- Lin, Q., Zhou, Z., Luo, W., Fang, M., Li, M., & Li, H. (2017). Screening of proximal and interacting proteins in rice protoplasts by proximity-dependent biotinylation. *Frontiers in Plant Science*, 8, 749. <https://doi.org/10.3389/fpls.2017.00749>
- Lindman, S., Hernandez-Garcia, A., Szczepankiewicz, O., Frohm, B., & Linse, S. (2010). In vivo protein stabilization based on fragment complementation and a split GFP system. *Proceedings of the National Academy of Sciences of the United States of America*, 107(46), 19826–19831. <https://doi.org/10.1073/pnas.1005689107>
- Liu, Q., Zheng, J., Sun, W., Huo, Y., Zhang, L., Hao, P., Wang, H., & Zhuang, M. (2018). A proximity-tagging system to identify membrane protein–protein interactions. *Nature Methods*, 15(9), 715–722. <https://doi.org/10.1038/s41592-018-0100-5>
- Ma, Y., Kouranov, A., LaSala, S. E., & Schnell, D. J. (1996). Two components of the chloroplast protein import apparatus, IAP86 and IAP75, interact with the transit sequence during the recognition and translocation of precursor proteins at the outer envelope. *Journal of Cell Biology*, 134(2), 315–327. <https://doi.org/10.1083/jcb.134.2.315>
- MacHaria, M. W., Tan, W. Y. Z., Das, P. P., Naqvi, N. I., & Wong, S. M. (2019). Proximity-dependent biotinylation screening identifies NbHYPK as a novel interacting partner of ATG8 in plants. *BMC Plant Biology*, 19(1). <https://doi.org/10.1186/s12870-019-1930-8>
- Mair, A., & Bergmann, D. C. (2022). Advances in enzyme-mediated proximity labeling and its potential for plant research. *Plant Physiology*, 188(2), 756–768. <https://doi.org/10.1093/plphys/kiab479>
- Mair, A., Xu, S. L., Branon, T. C., Ting, A. Y., & Bergmann, D. C. (2019). Proximity labeling of protein complexes and cell type specific organellar proteomes in Arabidopsis enabled by TurboID. *ELife*, 8. <https://doi.org/10.7554/eLife.47864>
- Martell, J. D., Deerinck, T. J., Sancak, Y., Poulos, T. L., Mootha, V. K., Sosinsky, G. E., Ellisman, M. H., & Ting, A. Y. (2012). Engineered ascorbate peroxidase as a genetically encoded reporter for electron microscopy. *Nature Biotechnology*, 30(11), 1143–1148. <https://doi.org/10.1038/nbt.2375>
- Martell, J. D., Yamagata, M., Deerinck, T. J., Phan, S., Kwa, C. G., Ellisman, M. H., Sanes, J. R., & Ting, A. Y. (2016). A split horseradish peroxidase for the detection of intercellular protein-protein interactions and sensitive visualization of synapses. *Nature Biotechnology*, 34(7), 774–780. <https://doi.org/10.1038/nbt.3563>
- Martin, W., & Herrmann, R. G. (1998). Gene transfer from organelles to the nucleus: How much, what happens, and why? *Plant Physiology*, 118(1), 9–17. <https://doi.org/10.1104/pp.118.1.9>
- May, T., & Soll, J. (2000). 14-3-3 Proteins Form a Guidance Complex With Chloroplast Precursor Proteins in Plants. *Plant Cell*, 12(1), 53–63. <https://doi.org/10.2307/3871029>
- Merchant, S. S., Allen, M. D., Kropat, J., Moseley, J. L., Long, J. C., Tottey, S., & Terauchi, A. M. (2006). Between a rock and a hard place: Trace element nutrition in Chlamydomonas. *Biochimica et Biophysica Acta - Molecular Cell Research*, 1763(7), 578–594. <https://doi.org/10.1016/j.bbamcr.2006.04.007>

- Meyer, T., Hölscher, C., Schwöppe, C., & Von Schaewen, A. (2011). Alternative targeting of Arabidopsis plastidic glucose-6-phosphate dehydrogenase G6PD1 involves cysteine-dependent interaction with G6PD4 in the cytosol. *Plant Journal*, *66*(5), 745–758. <https://doi.org/10.1111/j.1365-313X.2011.04535.x>
- Meyer, Y., Buchanan, B. B., Vignols, F., & Reichheld, J. P. (2009). Thioredoxins and glutaredoxins: Unifying elements in redox biology. *Annual Review of Genetics*, *43*, 335–367. <https://doi.org/10.1146/annurev-genet-102108-134201>
- Michnick, S. W., Ear, P. H., Landry, C., Malleshaiah, M. K., & Messier, V. (2010). A toolkit of protein-fragment complementation assays for studying and dissecting large-scale and dynamic protein-protein interactions in living cells. In *Methods in Enzymology* (2nd ed., Vol. 470, Issue C). Elsevier Inc. [https://doi.org/10.1016/S0076-6879\(10\)70014-8](https://doi.org/10.1016/S0076-6879(10)70014-8)
- Michnick, S. W., Ear, P. H., Manderson, E. N., Remy, I., & Stefan, E. (2007). Universal strategies in research and drug discovery based on protein-fragment complementation assays. *Nature Reviews Drug Discovery*, *6*(7), 569–582. <https://doi.org/10.1038/nrd2311>
- Nikkanen, L., & Rintamäki, E. (2019). Chloroplast thioredoxin systems dynamically regulate photosynthesis in plants. *Biochemical Journal*, *476*(7), 1159–1172. <https://doi.org/10.1042/BCJ20180707>
- Nikkanen, L., Toivola, J., & Rintamäki, E. (2016). Crosstalk between chloroplast thioredoxin systems in regulation of photosynthesis. *Plant Cell and Environment*, *39*(8), 1691–1705. <https://doi.org/10.1111/pce.12718>
- O’Neil, P. K., Richardson, L. G. L., Paila, Y. D., Piszczek, G., Chakravarthy, S., Noinaj, N., & Schnell, D. (2017). The POTRA domains of Toc75 exhibit chaperone-like function to facilitate import into chloroplasts. *Proceedings of the National Academy of Sciences*, *114*(24), E4868–E4876. <https://doi.org/10.1073/pnas.1621179114>
- Ohmuro-Matsuyama, Y., Chung, C. I., & Ueda, H. (2013). Demonstration of protein-fragment complementation assay using purified firefly luciferase fragments. *BMC Biotechnology*, *13*. <https://doi.org/10.1186/1472-6750-13-31>
- Okegawa, Y., & Motohashi, K. (2015). Chloroplastic thioredoxin m functions as a major regulator of Calvin cycle enzymes during photosynthesis in vivo. *Plant Journal*, *84*(5), 900–913. <https://doi.org/10.1111/tpj.13049>
- Ouyang, M., Li, X., Ma, J., Chi, W., Xiao, J., Zou, M., Chen, F., Lu, C., & Zhang, L. (2011). LTD is a protein required for sorting light-harvesting chlorophyll-binding proteins to the chloroplast SRP pathway. *Nature Communications*, *2*(1). <https://doi.org/10.1038/ncomms1278>
- Paila, Y. D., Richardson, L. G. L., Inoue, H., Parks, E. S., McMahon, J., Inoue, K., & Schnell, D. J. (2016). Multi-functional roles for the polypeptide transport associated domains of Toc75 in chloroplast protein import. *ELife*, *5*(MARCH2016). <https://doi.org/10.7554/eLife.12631>
- Pang, P., Meathrel, K., & Ko, K. (1997). A component of the chloroplast protein import apparatus functions in bacteria. *Journal of Biological Chemistry*, *272*(41), 25623–25627. <https://doi.org/10.1074/jbc.272.41.25623>
- Patel, R., Hsu, S. C., Bédard, J., Inoue, K., & Jarvis, P. (2008). The Omp85-related chloroplast outer envelope protein OEP80 is essential for viability in Arabidopsis. *Plant Physiology*, *148*(1), 235–245. <https://doi.org/10.1104/pp.108.122754>
- Perry, S. E., & Keegstra, K. (1994). Envelope membrane proteins that interact with chloroplastic precursor proteins. *Plant Cell*, *6*(1), 93–105. <https://doi.org/10.1105/tpc.6.1.93>

- Pfleger, K. D. G., Seeber, R. M., & Eidne, K. A. (2006). Bioluminescence resonance energy transfer (BRET) for the real-time detection of protein-protein interactions. *Nature Protocols*, *1*(1), 337–345. <https://doi.org/10.1038/nprot.2006.52>
- Pham, H. D., Pólya, S., Müller, B., Szenthe, K., Sági-Kazár, M., Bánkúti, B., Bánáti, F., Sárvári, É., Fodor, F., Tamás, L., Philippar, K., & Solti, Á. (2020). The developmental and iron nutritional pattern of PIC1 and NiCo does not support their interdependent and exclusive collaboration in chloroplast iron transport in *Brassica napus*. *Planta*, *251*(5), 96. <https://doi.org/10.1007/s00425-020-03388-0>
- Qbadou, S., Becker, T., Mirus, O., Tews, I., Soll, J., & Schleiff, E. (2006). The molecular chaperone Hsp90 delivers precursor proteins to the chloroplast import receptor Toc64. *EMBO Journal*, *25*(9), 1836–1847. <https://doi.org/10.1038/sj.emboj.7601091>
- Ramanathan, M., Majzoub, K., Rao, D. S., Neela, P. H., Zarnegar, B. J., Mondal, S., Roth, J. G., Gai, H., Kovalski, J. R., Siprashvili, Z., Palmer, T. D., Carette, J. E., & Khavari, P. A. (2018). RN A-protein interaction detection in living cells. *Nature Methods*, *15*(3), 207–212. <https://doi.org/10.1038/nmeth.4601>
- Ravet, K., Touraine, B., Boucherez, J., Briat, J. F., Gaymard, F., & Cellier, F. (2009). Ferritins control interaction between iron homeostasis and oxidative stress in *Arabidopsis*. *Plant Journal*, *57*(3), 400–412. <https://doi.org/10.1111/j.1365-313X.2008.03698.x>
- Remy, I., & Michnick, S. W. (2007). Application of protein-fragment complementation assays in cell biology. *BioTechniques*, *42*(2), 137–145. <https://doi.org/10.2144/000112396>
- Reumann, S., Davila-Aponte, J., & Keegstra, K. (1999). The evolutionary origin of the protein-translocating channel of chloroplastic envelope membranes: Identification of a cyanobacterial homolog. *Proceedings of the National Academy of Sciences of the United States of America*, *96*(2), 784–789. <https://doi.org/10.1073/pnas.96.2.784>
- Rhee, H. W., Zou, P., Udeshi, N. D., Martell, J. D., Mootha, V. K., Carr, S. A., & Ting, A. Y. (2013). Proteomic mapping of mitochondria in living cells via spatially restricted enzymatic tagging. *Science*, *339*(6125), 1328–1331. <https://doi.org/10.1126/science.1230593>
- Richly, E., & Leister, D. (2004). An improved prediction of chloroplast proteins reveals diversities and commonalities in the chloroplast proteomes of *Arabidopsis* and rice. *Gene*, *329*(1–2), 11–16. <https://doi.org/10.1016/j.gene.2004.01.008>
- Richter, S., & Lamppa, G. K. (1998). A chloroplast processing enzyme functions as the general stromal processing peptidase. *Proceedings of the National Academy of Sciences of the United States of America*, *95*(13), 7463–7468. <https://doi.org/10.1073/pnas.95.13.7463>
- Romei, M. G., & Boxer, S. G. (2019). Split Green Fluorescent Proteins: Scope, Limitations, and Outlook. *Annual Review of Biophysics*, *48*, 19–44. <https://doi.org/10.1146/annurev-biophys-051013-022846>
- Rout, G. R., & Sahoo, S. (2015). Role of Iron in Plant Growth and Metabolism. *Reviews in Agricultural Science*, *3*(0), 1–24. <https://doi.org/10.7831/ras.3.1>
- Roux, K. J., Kim, D. I., Raida, M., & Burke, B. (2012). A promiscuous biotin ligase fusion protein identifies proximal and interacting proteins in mammalian cells. *Journal of Cell Biology*, *196*(6), 801–810. <https://doi.org/10.1083/jcb.201112098>
- Rudolf, M., MacHettira, A. B., Groß, L. E., Weber, K. L., Bolte, K., Bionda, T., Sommer, M. S., Maier, U. G., Weber, A. P. M., Schleiff, E., & Tripp, J. (2013). In vivo function of Tic22, a protein import component of the intermembrane space of chloroplasts. *Molecular Plant*, *6*(3), 817–829. <https://doi.org/10.1093/mp/sss114>

- Sánchez-Baracaldo, P., & Cardona, T. (2020). On the origin of oxygenic photosynthesis and Cyanobacteria. *New Phytologist*, 225(4), 1440–1446. <https://doi.org/10.1111/nph.16249>
- Sánchez-Pulido, L., Devos, D., Genevrois, S., Vicente, M., & Valencia, A. (2003). POTRA: A conserved domain in the FtsQ family and a class of β -barrel outer membrane proteins. In *Trends in Biochemical Sciences* (Vol. 28, Issue 10, pp. 523–526). Elsevier Current Trends. <https://doi.org/10.1016/j.tibs.2003.08.003>
- Schnell, D. J., Kessler, F., & Blobel, G. (1994). Isolation of components of the chloroplast protein import machinery. *Science*, 266(5187), 1007–1012. <https://doi.org/10.1126/science.7973649>
- Schopp, I. M., Amaya Ramirez, C. C., Debeljak, J., Kreibich, E., Skribbe, M., Wild, K., & Béthune, J. (2017). Split-BioID a conditional proteomics approach to monitor the composition of spatiotemporally defined protein complexes. *Nature Communications*, 8. <https://doi.org/10.1038/ncomms15690>
- Schulz, G. E. (2002). The structure of bacterial outer membrane proteins. *Biochimica et Biophysica Acta - Biomembranes*, 1565(2), 308–317. [https://doi.org/10.1016/S0005-2736\(02\)00577-1](https://doi.org/10.1016/S0005-2736(02)00577-1)
- Serrato, A. J., Rojas-González, J. A., Torres-Romero, D., Vargas, P., Mérida, Á., & Sahrawy, M. (2021). Thioredoxins m are major players in the multifaceted light-adaptive response in *Arabidopsis thaliana*. *Plant Journal*, 108(1), 120–133. <https://doi.org/10.1111/tpj.15429>
- Sommer, M. S., Daum, B., Gross, L. E., Weis, B. L. M., Mirus, O., Abram, L., Maier, U. G., Kühlbrandt, W., & Schleiff, E. (2011). Chloroplast Omp85 proteins change orientation during evolution. In *Proceedings of the National Academy of Sciences of the United States of America* (Vol. 108, Issue 33, pp. 13841–13846). <https://doi.org/10.1073/pnas.1108626108>
- Stahl, T., Glockmann, C., Soll, J., & Heins, L. (1999). Tic40, a new “old” subunit of the chloroplast protein import translocon. *Journal of Biological Chemistry*, 274(52), 37467–37472. <https://doi.org/10.1074/jbc.274.52.37467>
- Stengel, A., Benz, J. P., Buchanan, B. B., Soll, J., & Bölder, B. (2009). Preprotein import into chloroplasts via the toc and tic complexes is regulated by redox signals in *pisum sativum*. *Molecular Plant*, 2(6), 1181–1197. <https://doi.org/10.1093/mp/ssp043>
- Stengel, A., Benz, P., Balsera, M., Soll, J., & Bölder, B. (2008). TIC62 redox-regulated translocon composition and dynamics. *Journal of Biological Chemistry*, 283(11), 6656–6667. <https://doi.org/10.1074/jbc.M706719200>
- Sun, M., Wang, Y., Zhang, Q., Xia, Y., Ge, W., & Guo, D. (2017). Prediction of reversible disulfide based on features from local structural signatures. *BMC Genomics*, 18(1). <https://doi.org/10.1186/S12864-017-3668-8>
- Sveshnikova, N., Grimm, R., Soll, J., & Schleiff, E. (2000). Topology studies of the chloroplast protein import channel Toc75. *Biological Chemistry*, 381(8), 687–693. <https://doi.org/10.1515/BC.2000.089>
- Tang, Y., Huang, A., & Gu, Y. (2020). Global profiling of plant nuclear membrane proteome in *Arabidopsis*. *Nature Plants*, 6(7), 838–847. <https://doi.org/10.1038/s41477-020-0700-9>
- Teixeira, P. F., & Glaser, E. (2013). Processing peptidases in mitochondria and chloroplasts. *Biochimica et Biophysica Acta - Molecular Cell Research*, 1833(2), 360–370. <https://doi.org/10.1016/j.bbamcr.2012.03.012>
- Teng, Y. S., Su, Y. S., Chen, L. J., Lee, Y. J., Hwang, I., & Li, H. M. (2006). Tic21 is an essential translocon component for protein translocation across the chloroplast inner envelope membrane. *Plant Cell*, 18(9), 2247–2257. <https://doi.org/10.1105/tpc.106.044305>

- Thormählen, I., Zupok, A., Rescher, J., Leger, J., Weissenberger, S., Groysman, J., Orwat, A., Chatel-Innocenti, G., Issakidis-Bourguet, E., Armbruster, U., & Geigenberger, P. (2017). Thioredoxins Play a Crucial Role in Dynamic Acclimation of Photosynthesis in Fluctuating Light. *Molecular Plant*, *10*(1), 168–182. <https://doi.org/10.1016/j.molp.2016.11.012>
- Timmis, J. N., Ayliff, M. A., Huang, C. Y., & Martin, W. (2004). Endosymbiotic gene transfer: Organelle genomes forge eukaryotic chromosomes. *Nature Reviews Genetics*, *5*(2), 123–135. <https://doi.org/10.1038/nrg1271>
- Tranel, P. J., Froehlich, J., Goyal, A., & Keegstra, K. (1995). A component of the chloroplastic protein import apparatus is targeted to the outer envelope membrane via a novel pathway. *EMBO Journal*, *14*(11), 2436–2446. <https://doi.org/10.1002/j.1460-2075.1995.tb07241.x>
- Tripp, J., Inoue, K., Keegstra, K., & Froehlich, J. E. (2007). A novel serine/proline-rich domain in combination with a transmembrane domain is required for the insertion of AtTic40 into the inner envelope membrane of chloroplasts. *Plant Journal*, *52*(5), 824–838. <https://doi.org/10.1111/j.1365-313X.2007.03279.x>
- Trösch, R., & Jarvis, P. (2011). The stromal processing peptidase of chloroplasts is essential in Arabidopsis, with knockout mutations causing embryo arrest after the 16-cell stage. *PLoS ONE*, *6*(8). <https://doi.org/10.1371/journal.pone.0023039>
- Valentine, M. E., Wolyniak, M. J., & Rutter, M. T. (2012). Extensive Phenotypic Variation among Allelic T-DNA Inserts in Arabidopsis thaliana. *PLoS ONE*, *7*(9), 1–5. <https://doi.org/10.1371/journal.pone.0044981>
- Voigt, C. A. (2014). Callose-mediated resistance to pathogenic intruders in plant defense-related papillae. *Frontiers in Plant Science*, *5*(APR), 1–6. <https://doi.org/10.3389/fpls.2014.00168>
- von Heijne, G., Steppuhn, J., & Hermann, R. G. (1989). Domain structure of mitochondrial and chloroplast targeting peptides. In *European Journal of Biochemistry* (Vol. 180, Issue 3). <https://doi.org/10.1111/j.1432-1033.1989.tb14679.x>
- Voulhoux, R., Bos, M. P., Geurtsen, J., Mols, M., & Tommassen, J. (2003). Role of a highly conserved bacterial protein in outer membrane protein assembly. *Science*, *299*(5604), 262–265. <https://doi.org/10.1126/science.1078973>
- Waegemann, K., & Soll, J. (1991). Characterization of the protein import apparatus in isolated outer envelopes of chloroplasts. In *The Plant Journal* (Vol. 1, Issue 2, pp. 149–158). <https://doi.org/10.1111/j.1365-313X.1991.00149.x>
- Wang, P., Liu, J., Liu, B., Feng, D., Da, Q., Wang, P., Shu, S., Su, J., Zhang, Y., Wang, J., & Wang, H. Bin. (2013). Evidence for a role of chloroplastic m-type thioredoxins in the biogenesis of photosystem II in arabidopsis. *Plant Physiology*, *163*(4), 1710–1728. <https://doi.org/10.1104/pp.113.228353>
- Wienk, H. L. J., Czisch, M., & De Kruijff, B. (1999). The structural flexibility of the preferredoxin transit peptide. In *FEBS Letters* (Vol. 453, Issue 3). [https://doi.org/10.1016/S0014-5793\(99\)00653-5](https://doi.org/10.1016/S0014-5793(99)00653-5)
- Wu, C., Seibert, F. S., & Ko, K. (1994). Identification of chloroplast envelope proteins in close physical proximity to a partially translocated chimeric precursor protein. *Journal of Biological Chemistry*, *269*(51), 32264–32271. [https://doi.org/10.1016/s0021-9258\(18\)31630-2](https://doi.org/10.1016/s0021-9258(18)31630-2)
- Wu, T., Malinverni, J., Ruiz, N., Kim, S., Silhavy, T. J., & Kahne, D. (2005). Identification of a multicomponent complex required for outer membrane biogenesis in Escherichia coli. *Cell*, *121*(2), 235–245. <https://doi.org/10.1016/j.cell.2005.02.015>
- Xu, F., Jia, M., Li, X., Tang, Y., Jiang, K., Bao, J., & Gu, Y. (2021). Exportin-4 coordinates nuclear shuttling of

TOPLESS family transcription corepressors to regulate plant immunity. *Plant Cell*, 33(3), 697–713. <https://doi.org/10.1093/plcell/koaa047>

- Xue, M., Hou, J., Wang, L., Cheng, D., Lu, J., Zheng, L., & Xu, T. (2017). Optimizing the fragment complementation of APEX2 for detection of specific protein-protein interactions in live cells. *Scientific Reports*, 7(1). <https://doi.org/10.1038/s41598-017-12365-9>
- Yuan, H., Pawlowski, E. G., Yang, Y., Sun, T., Thannhauser, T. W., Mazourek, M., Schnell, D., & Li, L. (2021). Arabidopsis ORANGE protein regulates plastid pre-protein import through interacting with Tic proteins. *Journal of Experimental Botany*, 72(4), 1059–1072. <https://doi.org/10.1093/jxb/eraa528>
- Zhang, M., Takano, T., Liu, S., & Zhang, X. (2015). Arabidopsis mitochondrial voltage-dependent anion channel 3 (AtVDAC3) protein interacts with thioredoxin m2. *FEBS Letters*, 589(11), 1207–1213. <https://doi.org/10.1016/j.febslet.2015.03.034>
- Zhang, Y., Song, G., Lal, N. K., Nagalakshmi, U., Li, Y., Zheng, W., Huang, P. jui, Branon, T. C., Ting, A. Y., Walley, J. W., & Dinesh-Kumar, S. P. (2019). TurboID-based proximity labeling reveals that UBR7 is a regulator of N NLR immune receptor-mediated immunity. *Nature Communications*, 10(1). <https://doi.org/10.1038/s41467-019-11202-z>
- Zhao, X., Bitsch, S., Kubitz, L., Schmitt, K., Deweid, L., Roehrig, A., Barazzzone, E. C., Valerius, O., Kolmar, H., & Béthune, J. (2021). ultraID: a compact and efficient enzyme for proximity-dependent biotinylation in living cells. *BioRxiv*, 2021.06.16.448656. <https://www.biorxiv.org/content/10.1101/2021.06.16.448656v1%0Ahttps://www.biorxiv.org/content/10.1101/2021.06.16.448656v1.abstract>
- Zimorski, V., Ku, C., Martin, W. F., & Gould, S. B. (2014). Endosymbiotic theory for organelle origins. *Current Opinion in Microbiology*, 22, 38–48. <https://doi.org/10.1016/j.mib.2014.09.008>

9 Acknowledgment

First and foremost, I would like to express my sincerest gratitude to Prof. Dr. Jürgen Soll for providing me with the opportunity to join his laboratory group.

I would like to express my deep appreciation to Dr. Christopher Carrie for his continuous support during my master's and doctorate projects. Additionally, I want to thank Dr. Bettina Bölter and Dr. Serena Schwenkert for initiating the project. Furthermore, I want to thank my TAC members Prof. Dr. Christof Osman and Dr. Jörg Meurer, for their insightful discussions and suggestions.

DFG funded research consortium, CRC/Transregio 175 The Green Hub: Central Coordinator of Acclimation in Plants, is recognized for great collaboration, conferences, workshops, scientific training, and funding. The advanced training opportunities provided by the Graduate School of Life Science Munich are cordially acknowledged. Lastly, Ludwig Maximilian University of Munich is praised for providing an exclusive scientific platform. I believe that every moment I spend in LMU will have a unique place in my heart.

I am extremely grateful to everyone at AG Soll for their kindness and assistance. Both positive and negative experiences will be remembered fondly in the future.

Training as a scientist requires an absolute passion for science and outstanding mentorship to deal with exceptional circumstances. I was and continue to be fortunate to be inspired by great scientists, for which I will be forever grateful.

My journey has been enriched by the diversity of the people I've met, many of whom I am proud to call friends. Thank you for the wonderful memories, journeys, spontaneous vacations, encouragement, and support!

Lastly, I would like to express my special gratitude to my family. Canım annem ve babam; uzun ve meşakkatli olan bu süreçte benim hep yanımda olup, cesaretlendiğiniz için çok teşekkür ederim. Sizlerin sevgisi ve desteğiyle daha nice başarılarla imza atmak dileğiyle!

2022, August

Şebnem Akbaş